UNIVERSITY OF CALIFORNIA,
IRVINE

Thermal Density Functional Theory, Ensemble Density Functional Theory, and Potential Functional Theory for Warm Dense Matter

DISSERTATION

submitted in partial satisfaction of the requirements
for the degree of

DOCTOR OF PHILOSOPHY

in Chemistry

by

Aurora Pribram-Jones

Dissertation Committee:
Professor Kieron Burke, Chair
Professor Filipp Furche
Professor Ioan Andricioaei

2015

TABLE OF CONTENTS

LIST OF FIGURES

LIST OF TABLES

ACKNOWLEDGMENTS

I have been fortunate to have an incredible mentor in my advisor, Kieron Burke. His guidance and support have been invaluable in navigating the seas of DFT and life in general. I had no idea what I was getting into when I accepted that first cup of coffee.

My colleagues in the Burke Group have provided tutelage, hilarity, perspective, and fraternity (and TeX templates). Life would not have been the same without them. Similarly, Filipp Furche and his group bring balance to the Electronic Structure Group, and I am especially grateful for Filipp's guidance, teaching, and skepticism.

I am thankful for the hard work and many life-hours that my major collaborators, Attila Cangi and Zenghui Yang, have put into our work together. Thank you for putting up with my incessant questioning and unending paper edits.

Anyone interested in WDM needs friends in the national labs, and I have been lucky to have Mike Desjarlais and Frank Graziani as my guides into that world. My future would look entirely different without them.

Lori Bassman and the Laspas have taught me the joys of high entropy. Thanks for accepting a useless theorist into your world of alloys.

Many thanks to the administrators and support staff of the UCI Chemistry Department, particularly Jenny Du, without whom, nothing would ever get done.

There are a huge number of friends and family members in the Legion that has gotten me to this point: the Grosses, Goodsteins, Winkelsteins, Pribrams, and Joneses, not to mention the Fishers, the Quinns, some Williamsons, a Cokenias, a Rek, a Landi, a Moore, a Shaikh, heaps of Mudders, and a Popebear. But there are a few in particular who stand out.

My comrade, Josette Marrero: Your humor and honesty made me feel less alone. I am lucky to have gone to graduate school with family.

My brother, Tommy: Your dedication to our family and my freedom is more than anyone deserves, and I'll never be able to thank you enough.

My partner, David: I could never have predicted you, and you are beyond this world's imagination. Your belief in me is staggering and humbling. Thank you for everything.

mb&c.

And little Avra, who changed everything. Thank you for turning this joint upside down and sharing your first meals with laptops, equations, coffee, and proofreading.

I am grateful to the DOE Computational Graduate Fellowship and the Krell Institute for four full years of funding (DE-FG02-97ER25308) and the UCI Chancellor's Fellowship for partial support of my first two years.

I am indebted to publishers for allowing me to use the following work in this thesis:

⟨Ch. 2⟩ A. Pribram-Jones, D. A. Gross, and K. Burke, "DFT: A Theory Full of Holes?" *Ann. Rev. Phys. Chem.* **66**, 283–304 (2015). Reproduced by permission of Annual Review.

⟨Ch. 3⟩ A. Pribram-Jones, S. Pittalis, E.K.U. Gross, and K. Burke, "Thermal Density Functional Theory in Context," in *Frontiers and Challenges in Warm Dense Matter*, Lecture Notes in Computational Science and Engineering No. 96, edited by F. Graziani, M.P. Desjarlais, R. Redmer, and S.B. Trickey (Springer, 2014) Chap. 2, pp. 25–60. Reproduced by permission of Springer via the Copyright Clearance Center.

⟨Ch. 4⟩ A. Pribram-Jones, Z.-H. Yang, J.R. Trail, K. Burke, R.J. Needs, and C.A. Ullrich, "Excitations and benchmark ensemble density functional theory for two electrons," *J. Chem. Phys.* **140**, 18A541 (2014). Reproduced by permission of the AIP Publishing LLC.

⟨Ch. 5⟩ Z.-H. Yang, J.R. Trail, A. Pribram-Jones, K. Burke, R.J. Needs, and C.A. Ullrich, "Exact and approximate Kohn-Sham potentials in ensemble density-functional theory," *Phys. Rev. A* **90**, 042501, (2014). Reproduced by permission of the American Physical Society.

⟨Ch. 7⟩ A. Cangi and A. Pribram-Jones, "An Efficient Formalism for Warm Dense Matter Simulations," *Under review with PRB*, (2015). Reproduced by permission of the American Physical Society, if accepted.

CURRICULUM VITAE

Aurora Pribram-Jones

Education

Univeristy of California Irvine, 2015

Ph.D., Chemistry

Non-Empirical Thermal Density Functional Theory

Advisor: Kieron Burke

Harvey Mudd College, 2009

B.S., Chemistry

Thesis: *Binary Liquid Mixtures and Bulk Chirality: Two New Explorations of the 2,7-Diacyl Fluorenes*

Advisor: Gerald R. Van Hecke

Foothill College, 2005

A.S., Biology/Chemistry/Mathematics, *High Honors*

Projects and Positions

Graduate Student Researcher

Burke Research Group, University of California Irvine, 2009–2015

Finite-temperature density functional theory, development of ab initio methods for warm dense matter

Ensemble density functional theory: formalism, benchmarks, and new approximations

Independent Collaboration

With Attila Cangi (Max Planck Institute, Halle, Germany), 2012–2015

Finite-temperature potential functional theory for warm dense matter

Visiting Fellow and Mentor

Laspa Fellowship, University of New South Wales, 2014

Quantum molecular dynamics simulation of novel high entropy alloys

Differential scanning calorimetry for thermodynamics of novel high entropy alloys

Researcher and Mentor

Laspa Fellowship, Harvey Mudd College, 2013–2015

Quantum molecular dynamics simulation of novel high entropy alloys

Graduate Student Intern

High Energy Density Physics Theory, Sandia National Laboratories, 2013–2015

Release isentropes for shocked aluminum from quantum molecular dynamics

Undergraduate Researcher

Van Hecke Research Group, Harvey Mudd College, 2006–2009

The 2,7-diacyl fluorenes: a library for the systematic study of structure and function

Publications

1. Knudson, M.D.; Desjarlais, M.P.; Pribram-Jones, A. Adiabatic release measurements in aluminum between 400-1200 GPa: Characterization of aluminum as a shock standard in the multimegabar regime. *Phys. Rev. B*, **91**, 224105 (2015).

2. Cangi, A.; Pribram-Jones, A. Bypassing the malfunction junction in warm dense matter simulations. *under review, Phys. Rev. B*, arxiv:1411.1532.

3. Pribram-Jones, A.; Gross, David A.; Burke, K. DFT: A Theory Full of Holes? *Ann. Rev. Phys. Chem.*, **66**, 283-304 (2015), *invited article.*

4. Yang, Z.-H.; Trail, J.R.; Burke, K.; Needs, R.J.; Ullrich, C.A. Exact and approximate Kohn-Sham potentials in ensemble density-functional theory. *Phys. Rev. A*, **90**, 042501 (2014).

5. Pribram-Jones, A.; Yang, Z.-H.; Trail, J.R.; Burke, K.; Needs, R.J.; Ullrich, C.A. Excitations and benchmark ensemble density functional theory for two electrons. *J. Chem. Phys.*, **140**, 18A541 (2014).

6. Pribram-Jones, A.; Pittalis, S.; Gross, E.K.U.; Burke, K. Thermal Density Functional Theory in Context. In: *Frontiers and Challenges in Warm Dense Matter* (F. Graziani, M. P. Desjarlais, R. Redmer, and S. B. Trickey, eds.), vol. 96 of *Lecture Notes in Computational Science and Engineering*, pp. 25–60, Springer International Publishing, 2014.

Invited Presentations

8. Pribram-Jones, A. An efficient formalism for warm dense matter simulations. DOE Computational Science Graduate Fellowship Annual Program Review, July 2015.

7. Pribram-Jones, A. Improving density functional theory for warm dense matter. Lawrence Finalist Seminar, Lawrence Livermore National Laboratory, February 2015.

6. Pribram-Jones, A. Bridging the gap for warm dense matter simulations. NSF Institute for Pure and Applied Mathematics, Computational Methods in High Energy Density Plasmas Reunion Conference II, December 2014.

5. Pribram-Jones, A. Thermal Density Functional Theory: An Introduction and Recent Progress. Dynamic Materials Meeting, High Energy Density Physics Division, Sandia National Laboratories, February 2014.

4. Pribram-Jones, A. Excited States and Ensemble Density Functional Theory. NSF Institute for Pure and Applied Mathematics, Computational Methods in High Energy Density Plasmas Reunion Conference I, December 2013.

3. Pribram-Jones, A. The quantum simulation working group: comparison of high energy density physics simulation methods. NSF Institute for Pure and Applied Mathematics, Computational Methods in High Energy Density Plasmas Culminating Workshop, June 2012.

2. Pribram-Jones, A. Finite Temperature Density Functional Theory. Heavy Ion Fusion Division/Virtual National Laboratory Weekly Seminar, Lawrence Berkeley National Laboratory, February 2012.

1. Pribram-Jones, A. Finite Temperature Density Functional Theory. Center for Applied Scientific Computing Seminar, Lawrence Livermore National Laboratory, January 2012.

Contributed Presentations

5. Pribram-Jones, A.; Burke K. Adiabatic Connection and Virial Theorem for Ensemble Density Functional Theory, March Meeting 2014: Recent Advances in Density Functional Theory III.

4. Pribram-Jones, A. Tools for Thermal Density Functional Theory. Institute for Pure and Applied Mathematics: Semiclassical Foundations of Density Functional Theory, 2013, Poster Session; Time-Dependent Density Functional Theory Gordon Research Seminar and Gordon Research Conference, 2013, Poster Session.

3. Pribram-Jones, A.; Burke, K. Temperature dependence of Thomas-Fermi errors. American Chemical Society, Spring Meeting 2012: Quantum Chemistry Methodology Session.

2. Pribram-Jones, A.; Burke, K. Temperature dependence of Thomas-Fermi errors. American Physical Society, March Meeting 2012: DFT for Chemical Physics Focus Session.

1. Pribram-Jones, A. Binary Liquid Mixtures and Bulk Chirality: Two New Explorations of the 2,7-Diacyl Fluorenes. Harvey Mudd College Presentation Days, Senior Thesis Presentations, May 2009.

Presentations to the General Public

Pribram-Jones, A. Gossamer Threads and Gingko Leaves: Three Years of Hidden Twists in Undergraduate Research. Harvey Mudd College Parents Day Student Research Presentation, February 2009.

Selected Honors, Awards, & Fellowships

Lawrence Postdoctoral Fellow, Lawrence Livermore National Laboratory, 2015

University of California Presidential Postdoctoral Fellow, UC Berkeley, 2015

E.K.C. Lee Award, UC Irvine Department of Chemistry, 2015

Outstanding Contributions to the Department, UC Irvine School of Physical Sciences, 2015

UCI Lauds and Laurels, Outstanding Graduate Student, 2015

Department of Energy Computational Science Graduate Fellowship, 2011–2015

Award for Contributions to UC Irvine Chemistry Department Teaching Program, 2012

National Science Foundation Graduate Research Fellowship, 2011

National Science Foundation Travel Award, 2011

UC Irvine Chancellor's Fellowship, 2009–2011

Harald V. Johnson Award for Effective Communication of Chemistry, 2009

Faculty nomination to Sigma Xi, Claremont Colleges Chapter, 2009

Harvey Mudd College Dean's List, 2005, 2008

Harvey Mudd Scholarship, 2005–2009

Harvey Mudd College Broccoli Scholar, 2007–2008

NSF-REU Travel Award, 2006

California Mathematics Council Community Colleges Foundation Scholarship, 2005

Teaching Experience

University of California Irvine, Department of Chemistry

Guest Lectures

Chemistry and Materials Physics Program, Math for Chemists, Summer 2014

Linear Vector Spaces

Chemistry and Materials Physics Program, Theoretical Chemistry Lab Rotation, Summer 2011

Introduction to Molecular Dynamics for Proteins

Fundamentals of Quantum Mechanics, Fall 2010

Mathematics for Beginning Quantum Mechanics
The Hydrogen Atom: Part 1

Chemistry and Material Physics Program, Theoretical Chemistry Lab Rotation, Summer 2010

Introduction to Density Functional Theory and Mathematica

Teaching Assistant

Graduate Courses:

Time-Dependent Density Functional Theory, Spring 2015
Math for Chemists, Summer 2014
Fundamentals of Quantum Mechanics, Fall 2010
Classical Mechanics and Electromagnetism, Fall 2010

Undergraduate Courses:

General Chemistry Laboratory, Spring 2010
Organic Chemistry Laboratory, Fall 2009–Winter 2010

Harvey Mudd College, Department of Chemistry

Teaching and Laboratory Assistant, 2006–2008

Undergraduate Courses:

Group Theory, Quantum Chemistry, and Spectroscopy
Physical Chemistry
Physical Chemistry Laboratory

Foothill College, Physical Sciences, Math, and Engineering Division

Math Center Tutor, 2004–2005

Courses: Arithmetic, Algebra, Geometry, Precalculus, Finite Math, Business Calculus, Introductory Calculus, Integral Calculus, Multivariable Calculus, Linear Algebra

Grader, 2004–2005

Courses: Algebra, Precalculus, Finite Math

Workshops and Educational Programs

NSF Institute for Pure and Applied Mathematics, UCLA

Visiting Scholar and Core Participant, *Computational Methods in High Energy Density Plasmas Long Program, March through June 2012.*

CECAM Workshop, Atlantic Center for Atomistic Modeling, University College Dublin

How to Speed Up Progress and Reduce Empiricism in Density Functional Theory, 2011

NSF Institute for Pure and Applied Mathematics, UCLA

Visiting Scholar and Core Participant, *Navigating Chemical Compound Space for Materials and Bio Design Long Program, 2011*

Outreach

*Indicates significant interaction with undergraduate and/or high school students.

2013–2014: Laspa Fellowship, Harvey Mudd College. Co-advisor and mentor to two undergraduate computational researchers in physics and engineering.*

2011–2014: Harvey Mudd College Mentoring Program. Mentor to undergraduate over three-year period.*

2010–2013: Harvey Mudd College Alumni Association Board of Governors. Elected member of Alumni Board. Member of Events and Fundd Committees. Chair of Student-Alumni Outreach Committee and organizer of first annual HMC Career Forum attended by over 200 students and alumni.*

2010–2011: Mentor to two physical science undergraduates through UCI Physical Sciences Mentoring Program.*

2010–2011: Member of Iota Sigma Pi Outreach Team serving Santa Ana and surrounding communities (hands-on demonstrations at community centers, Ask-A-Scientist nights in elementary schools).

2010–2011: Member of UCI Chemistry Outreach Team.*

2008: Coordinator for volunteer Pomona High School tutoring program.*

2007–2008: Saturday Tutor for Harvey Mudd College Upward Bound.*

Service Activities

2014–15: DECADE Student Council Representative, School of Physical Sciences

2014: Session Chair, Recent Advances in Density Functional Theory V, APS March Meeting

2012–14: Co-Organizer and Mentor, UC Irvine Physical Sciences Graduate Fellowship Workshop

2011: Harvey Mudd College Vice President and Dean of Faculty Search Committee

2008: Harvey Mudd College Vice President for Student Affairs and Dean of Students Search Committee

ABSTRACT OF THE DISSERTATION

Thermal Density Functional Theory, Ensemble Density Functional Theory, and Potential Functional Theory for Warm Dense Matter

By

Aurora Pribram-Jones

Doctor of Philosophy in Chemistry

University of California, Irvine, 2015

Professor Kieron Burke, Chair

Warm dense matter (WDM) is a high energy phase between solids and plasmas, with characteristics of both. It is present in the centers of giant planets, within the earth's core, and on the path to ignition of inertial confinement fusion. The high temperatures and pressures of warm dense matter lead to complications in its simulation, as both classical and quantum effects must be included. One of the most successful simulation methods is density functional theory-molecular dynamics (DFT-MD). Despite great success in a diverse array of applications, DFT-MD remains computationally expensive and it neglects the explicit temperature dependence of electron-electron interactions known to exist within exact DFT.

Finite-temperature density functional theory (FT DFT) is an extension of the wildly successful ground-state DFT formalism via thermal ensembles, broadening its quantum mechanical treatment of electrons to include systems at non-zero temperatures. Exact mathematical conditions have been used to predict the behavior of approximations in limiting conditions and to connect FT DFT to the ground-state theory. An introduction to FT DFT is given within the context of ensemble DFT and the larger field of DFT is discussed for context.

Ensemble DFT is used to describe ensembles of ground-state and excited systems. Exact conditions in ensemble DFT and the performance of approximations depend on ensemble

weights. Using an inversion method, exact Kohn-Sham ensemble potentials are found and compared to approximations. The symmetry eigenstate Hartree-exchange approximation is in good agreement with exact calculations because of its inclusion of an ensemble derivative discontinuity. Since ensemble weights in FT DFT are temperature-dependent Fermi weights, this insight may help develop approximations well-suited to both ground-state and FT DFT.

A novel, highly efficient approach to free energy calculations, finite-temperature potential functional theory, is derived, which has the potential to transform the simulation of warm dense matter. As a semiclassical method, it connects the normally disparate regimes of cold condensed matter physics and hot plasma physics. This orbital-free approach captures the smooth classical density envelope and quantum density oscillations that are both crucial to accurate modeling of materials where temperature and pressure effects are influential.

Part I

Introduction

Chapter 1

Motivation and Section Summaries

1.1 The Malfunction Junction

Warm dense matter (WDM) has been characterized as the "malfunction junction" because of the inadequacy of traditional condensed matter and classical plasma descriptions of its complicated state[179]. In these systems with temperatures over 10^3 K and condensed matter densities, theoretical treatments must incorporate quantum effects, strong correlation, and partial ionization[80, 179]. The reliability of phase diagrams for WDM is crucial for modeling the core structures of planets like Jupiter, Saturn, and the Earth itself. These cores determine planetary magnetic fields and bear the signature of historical astronomical events. Further, WDM can help us examine how the planets within and beyond our solar system were formed and how that formation determined their current state[179].

Good predictions of WDM melt properties and thermal conductivity also contribute to the development of inertial confinement fusion (ICF), whereby a hot, compressed sphere of fuel is used to initiate a fusion reaction[5]. The ignition process requires that the fuel and capsule pass through WDM conditions toward those of even higher temperatures and pressures. This

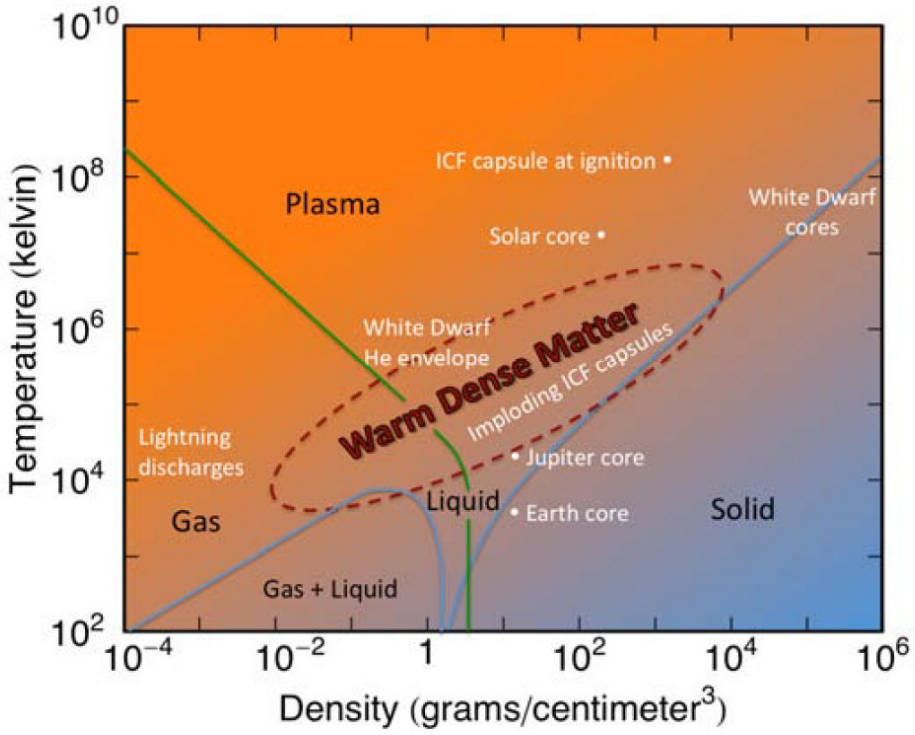

Figure 1.1: WDM occurs at temperatures over 10^3 K and pressures between 10^5 and 10^9 atm. The blue region in the lower right indicates the dominance of quantum effects, while the orange region in the upper left indicates dominant classical effects. WDM bridges many regions, with no one effect dominating its behavior[179].

transition must be controlled through accurate theoretical models for both fuel and capsule materials, as inhomogeneity developed at any point during ignition can potentially quench the budding reaction. This accuracy can only be achieved over the entire range of ignition conditions through careful consideration of a model's limiting behaviors[179].

In the last decade, the predictive power of WDM simulations has skyrocketed[81, 101, 123, 128, 167, 213]. In Ref. [167], inclusion of electron thermal statistics in quantum-classical simulations resulted in a new phase diagram for high energy density water that was supported by experimental results from the Z Machine at Sandia National Laboratories. This led to new predictions of structural characteristics of Neptune. A few years later[213], researchers

predicted Hugoniot states of shocked xenon using similar methods, which were again verified by experiments on Z. Despite these and other great successes, current WDM computational methods suffer from important drawbacks. Inclusion of electron thermal statistics, as in the first example, captures hugely important temperature effects, but there are still missing thermal effects in its treatment of electronic interactions[206].

Simulation of WDM materials is a priority[36, 179] because of these and other contributions to geochemistry, planetary science, and fusion efforts. Simulations are crucial for experimental design, prediction of material properties, and analysis of experimental results. They are of particular value due to the difficult and expensive nature of WDM experiments. In Ref. [179], one of the specific research priorities identified was development of a comprehensive theory for WDM. The work described in this dissertation provides insight into how WDM's high temperatures influence their equally important quantum mechanical behavior, and it lays the foundation of a promising comprehensive theoretical method specifically suited to WDM.

1.2 Density Functional Theory-Molecular Dynamics

Since not all WDM experiments are conducive to taking reliable or isolated measurements at such extreme conditions, density functional theory-molecular dynamics (DFT-MD)[31, 104, 134, 135, 136] is often used to predict material properties. DFT-MD uses DFT, a quantum mechanical method[17, 99], to calculate the forces used in molecular dynamics simulations for the generation of ion distributions in the material. This mixed quantum-classical method has been very successful[128, 167], but it is hugely expensive, misses some temperature effects, and its accuracy cannot be systematically improved using standard approaches. This is largely due to its reliance on Kohn-Sham DFT.

Kohn-Sham DFT is an iterative method of calculating energies of an interacting electronic system using a noninteracting system with the same density[132]. Exact expressions are known for all but a small piece of the energy in Kohn-Sham DFT, called the exchange-correlation (XC) energy:

$$E_{\mathrm{XC}}[n] = E[n] - T_{\mathrm{S}}[n] - U[n], \tag{1.1}$$

where E is the total electronic energy, T_{S} is the non-interacting kinetic energy, U is the classical electrostatic energy, and square brackets indicate that these are functionals of the single-particle electronic density, $n(\mathbf{r})$. Numerous approximations for this piece exist at zero temperature[18, 22], and these zero-temperature functionals are often used for finite-temperature DFT (FT DFT) at this time. FT DFT combines statistical mechanical ensembles of energy states with the methods of energy minimization used in DFT[169]. This move to include statistical equilibrium demands use of a finite-temperature XC functional in the exact theory[206]. This shortcoming in current practice is coupled with incredible computational demands. Kohn-Sham DFT at WDM conditions includes huge numbers of high-energy states that are fractionally occupied[120]. In order to find the kinetic energy of these states, massive eigensystems must be solved at each time step at great computational expense.

1.3 Overview of the Dissertation

My work focuses on the electronic structure step of WDM simulations, unraveling the structure of density functional theory applied to thermal ensembles. I begin in Chapter 2 with a casual introduction to DFT's underlying logic and its history, while Chapter 3 gives a detailed technical introduction to ground-state and thermal DFT. Chapters 4 and 5 use simple-yet-meaningful model systems to address questions related to why some approxima-

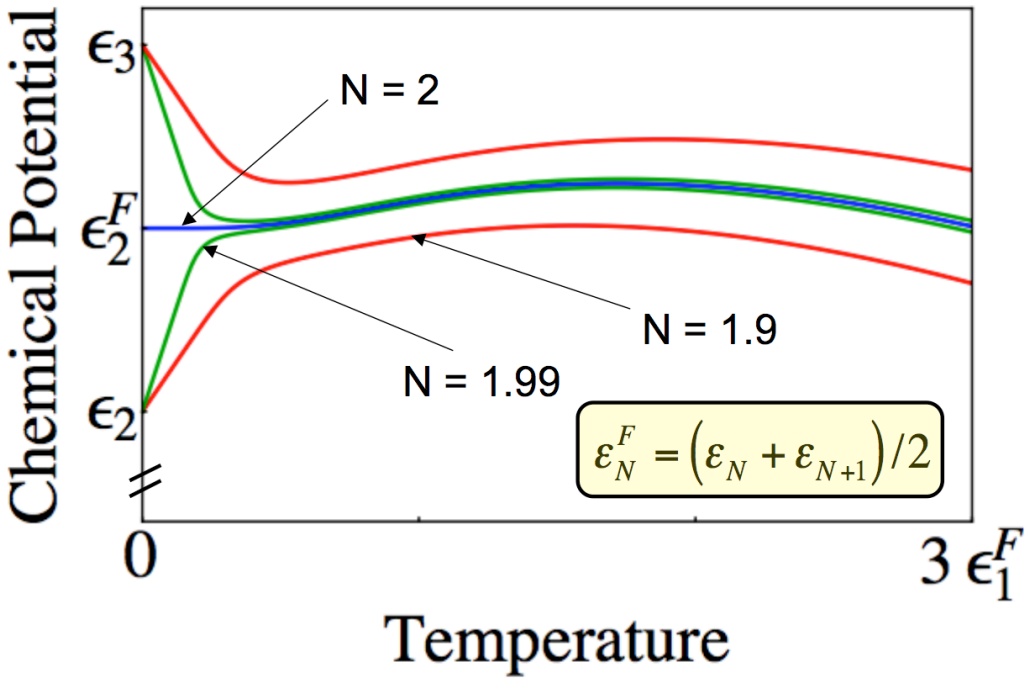

Figure 1.2: Though the zero-temperature chemical potential is discontinuous, this discontinuity is smoothed as temperatures increase. Here, N is the number of electrons in a unit-width infinite well, and ϵ_N^F is the Fermi energy of N electrons.

tions work well for ensembles, thermal or otherwise. Finally, in Chapters 6 and 7, I introduce a way to bypass the malfunction junction by skirting KS-DFT altogether. An overview of these chapters is given below.

1.3.1 Chapter 3: Thermal DFT

A primary focus of my thesis work has been on finite-temperature DFT, an extension of the ground-state formalism via thermal ensembles[169, 206]. Much of my work has focused on the exact theory and the derivation of exact mathematical conditions. These conditions can help us analyze approximations, where we expect them to fail, and their behavior in limiting conditions[152, 153]. Examining the exact theory also lets us connect finite-temperature DFT to the ground-state theory. For instance, in Fig. 1.2, the chemical potential develops a

discontinuity as temperatures drop to zero, even for non-interacting particles in an incredibly simple potential. These types of connections between finite-temperature DFT and limiting conditions are crucial for developing DFT methods that will span the many physical regimes bridged by WDM.

1.3.2 Chapters 4 and 5: Ensemble DFT

Ensemble DFT[85, 86, 159] is used to describe ensembles of ground-state and excited systems. Ensembles are constructed by taking a collection of ground and excited states for a given Hamiltonian. Ensemble energies and densities are weighted sums of the eigenvalues and densities of these states, with lower-energy states being weighted more heavily than higher-energy states. Its main use is its efficient extraction of excitation energies, which was the focus of two papers that we have published in the past year[207, 257]. Of particular interest to us is how exact conditions and the performance of approximations are dependent on the ensemble weights, which we investigated by examining essentially exact Kohn-Sham potentials.

Because FT DFT is a form of ensemble DFT with a particular weighting[206], my interest in ensembles is not just for the extraction of excitation energies. The symmetry eigenstate Hartree-exchange approximation (SEHX) that we examine in our publications may be useful in a finite-temperature context as well. SEHX has shown good agreement with exact calculations because of its inclusion of an ensemble derivative discontinuity[257]. This discontinuity is defined as the difference between the Kohn-Sham potentials of an ensemble with small ensemble weights and of the ensemble with ensemble weight going to zero[150]. This can be related to the weight-derivative of the XC energy:

$$\Delta v_{\mathrm{XC}}(\mathbf{r}) = \lim_{\mathtt{w}\to 0} \partial E_{\mathrm{HXC},\mathtt{w}}[n]/\partial \mathtt{w}|_{n=n_{\mathtt{w}}}. \tag{1.2}$$

Since ensemble weights in FT DFT are temperature-dependent Fermi weights, this and other insights into ensemble DFT may help us develop approximations well-suited to both ground-state and FT DFT.

1.3.3 Chapters 6 and 7: Finite Temperature PFT

As mentioned earlier, Kohn-Sham DFT is a clever way to solve a fully interacting, quantum-mechanical electronic system by mapping it to a non-interacting system. This introduces a new problem: although we know the non-interacting kinetic energy exactly, to find it we must solve a computationally expensive eigenvalue problem to find eigenstates called orbitals. In our recently submitted paper[29], we use the mapping to a non-interacting system without having to solve the expensive eigenvalue problem.

At zero-temperature, one solution to this problem is potential functional theory (PFT)[26, 28]. In this method, one flips DFT on its head and uses functionals of the potential instead of functionals of the density. Instead of using the Kohn-Sham eigenfunctions to generate kinetic energies, PFT uses a coupling-constant formalism to generate kinetic energies. We have developed a finite-temperature extension of PFT, called FT PFT, that uses similar logic to write a formally exact expression for the non-interacting free energy[29]. Since this is an exact relationship, once we write down an approximation to the finite-temperature density, we have a corresponding approximation to this free energy that introduces no additional errors. This may seem like we are just switching one problem for another: approximating a density instead of an energy. However, because we have systematic semiclassical methods at our disposal[9, 27, 30], approximating a density to higher accuracy is potentially a much easier problem in practice.

To demonstrate the accuracy of our method, we provide a numerical demonstration. We used a path integral formulation to approximate the density via a series approximation

to the density that contains both the smooth, average density from classical physics and the important density oscillations from quantum mechanics. This sum converges more and more quickly as the temperature increases. Becoming more efficient at higher temperatures while still including quantum corrections at all temperatures means FT PFT is uniquely suited to problems in warm dense matter. There, high temperatures make orbital-based methods very expensive and high pressures make quantum oscillations crucially important for accurate simulations. Since the already inexpensive method becomes more efficient as temperatures rise, this should eliminate the computational Kohn-Sham DFT bottleneck in DFT-MD simulations while maintaining their accurate free energies.

1.3.4 Caveat

Many of these chapters come from papers published for different audiences. As such, some of the notation is inconsistent between chapters. Please refer to the definitions given within each chapter to prevent confusion.

Part II

Context and Overview of DFT

Chapter 2

DFT: A Theory Full of Holes?

written with David A. Gross and Kieron Burke. Published in *Ann. Rev. Phys. Chem.* **66**, 283–304 (2015).

Abstract: *This article is a rough, quirky overview of both the history and present state of the art of density functional theory. The field is so huge that no attempt to be comprehensive is made. We focus on the underlying exact theory, the origin of approximations, and the tension between empirical and non-empirical approaches. Many ideas are illustrated on the exchange energy and hole. Features unique to this article include how approximations can be systematically derived in a non-empirical fashion and a survey of warm dense matter.*

2.1 What is this article about?

The popularity of density functional theory (DFT) as an electronic structure method is unparalleled, with applications that stretch from biology[254] to exoplanets[129]. However, its quirks of logic and diverse modes of practical application have led to disagreements

on many fronts and from many parties. Developers of DFT are guided by many different principles, while applied practitioners (a.k.a. users) are suspicious of DFT for reasons both practical (*how can I pick a functional with so many choices?*[208]) and cultural (*with so many choices, why would I call this first-principles?*).

A modern DFT calculation[22] begins with the purchase of a computer, which might be as small as a laptop, and a quantum chemical code. Next, a basis set is chosen, which assigns predetermined functions to describe the electrons on each atom of the molecule being studied. Finally, a DFT approximation to something called the exchange-correlation energy (XC) is chosen, and the code starts running. For each guess of the nuclear positions, the code calculates an approximate energy[22]. A geometry optimization should find the minimum energy configuration. With variations on this theme[43, 185], one can read out all molecular geometries, dissociation energies, reaction barriers, vibrational frequencies, etc. A modern desktop may do a calculation for a 100-atom system within a day. A careful user will repeat the most important parts of the calculation with bigger basis sets, to check that answers don't change significantly.

2.2 Where does DFT come from?

Although DFT's popularity has skyrocketed since applications to chemistry became useful and routine, its roots stretch back much further[18, 110, 258].

2.2.1 Ye olde DFT

Developed without reference to the Schrödinger equation[219], Thomas-Fermi (TF) theory[60, 61, 240] was the first DFT. It is pure DFT, relying only on the electronic density, $\rho(\mathbf{r})$, as input. The kinetic energy was approximated as that of a uniform electron gas, while the

repulsion of the electrons was modeled with the classical electrostatic Coulomb repulsion, again depending only on the electronic density as an input.

2.2.2 Mixing in orbitals

John Slater was a master of electronic structure whose work foreshadowed the development of DFT. In particular, his X_α method[227] approximates the interactions of electrons in ground-state systems and improved upon Hartree-Fock (HF) [67, 94], one of the simplest ways to capture the Pauli exclusion principle. One of Slater's great insights was the importance of *holes*, a way of describing the depressed probability of finding electrons close to one another. Ahead of his time, Slater's X_α included focus on the hole, satisfied exact conditions like sum rules, and considered of the degree of localization present in the system of interest.

2.2.3 A great logical leap

Although Slater's methods provided an improvement upon HF, it was not until 1964 that Hohenberg and Kohn formulated their famous theorems[99], which now serve as the foundation of DFT:

(i) the ground-state properties of an electronic system are completely determined by $\rho(\mathbf{r})$, and

(ii) there is a one-to-one correspondence between the external potential and the density.

We write this by splitting the energy into two pieces:

$$E_{\text{elec}}[density] = F[density] + NucAtt, \tag{2.1}$$

where E_{elec} is the total energy of the electrons, F is the sum of their exact quantum kinetic

and electron-electron repulsion energies, and $NucAtt$ is their attraction to the nuclei in the molecule being calculated. Square brackets [ ] denote some (very complex) dependence on the one-electron density, $\rho(\mathbf{r})$, which gives the relative probability of finding an electron in a small chunk of space around the point $\mathbf{r}$. F is the same for all electronic systems, and so is called universal. For any given molecule, your computer simply finds $\rho(\mathbf{r})$ that minimizes E_{elec} above. Compare this to the variational principle in regular quantum mechanics. Instead of spending forever searching lots of wavefunctions that depend on all $3N$ electronic coordinates, you just search over one-electron densities, which have only 3 coordinates (and spin).

The pesky thing about the Hohenberg-Kohn theorems, however, is that they tell us such things exist without telling us how to find them. This means that to actually use DFT, we must approximate $F[density]$. We recognize that the old TF theory did precisely this, with very crude approximations for the two main contributions to F:

$$F[density] \sim \int d^3r\, \rho^{5/3}(\mathbf{r}) + CoulRep, \qquad (TF) \tag{2.2}$$

where we've not bothered with constants, etc. The first term is an approximation to the kinetic energy as a simple integral over the density. It is a local approximation, since the contribution at any point comes from only the density at that point. The other piece is the self-repulsion among electrons, which is simply modeled as the classical electrostatic repulsion, often called their Hartree energy or the direct Coulomb energy. Such simple approximations are typically good to within about 10% of the electronic energy, but bonds are a tiny fraction of this, and so are not accurate in such a crude theory[237].

2.2.4 A great calculational leap

Kohn and Sham proposed rewriting the universal functional in order to approximate only a small piece of the energy. They mapped the interacting electronic system to a fake non-

interacting system with the same $\rho(\mathbf{r})$. This requires changing the external potential, so these aloof, non-interacting electrons produce the same density as their interacting cousins. The universal functional can now be broken into new pieces. Where in the interacting system, we had kinetic energy and electron-electron interaction terms, in the Kohn-Sham (KS) system, we write the functional

$$F = OrbKE + CoulRep + XC \tag{2.3}$$

where $OrbKE$ is the kinetic energy of the fake KS electrons. XC contains all the rest, which includes both kinetic and potential pieces. Although it is small compared to the total, 'nature's glue' [140] is critical to getting chemistry and physics right. The X part is (essentially) the Fock exchange from a HF calculation, while C is the correlation energy, i.e., that part that traditional methods such as coupled cluster usually get very accurately[10].

When you minimize this new expression for the energy, you find a set of orbital equations, the celebrated KS equations. They are almost identical to Hartree-Fock equations, and this showed that Slater's idea could be made exact (if the exact functional were known). The genius of the KS scheme is that, because it calculates orbitals and gives their kinetic energy, only XC, a small fraction of the total energy, needs to be approximated as a density functional. The KS scheme usually produces excellent self-consistent densities, even with simple approximations like LDA, but approximate potentials for this non-interacting KS system are typically very different from the exact KS potential (Fig. 2.1).

2.2.5 Popular approximations for XC

Despite the overwhelming number of approximations available in the average DFT code, most calculations rely on a few of the most popular approximations. The sequence of these

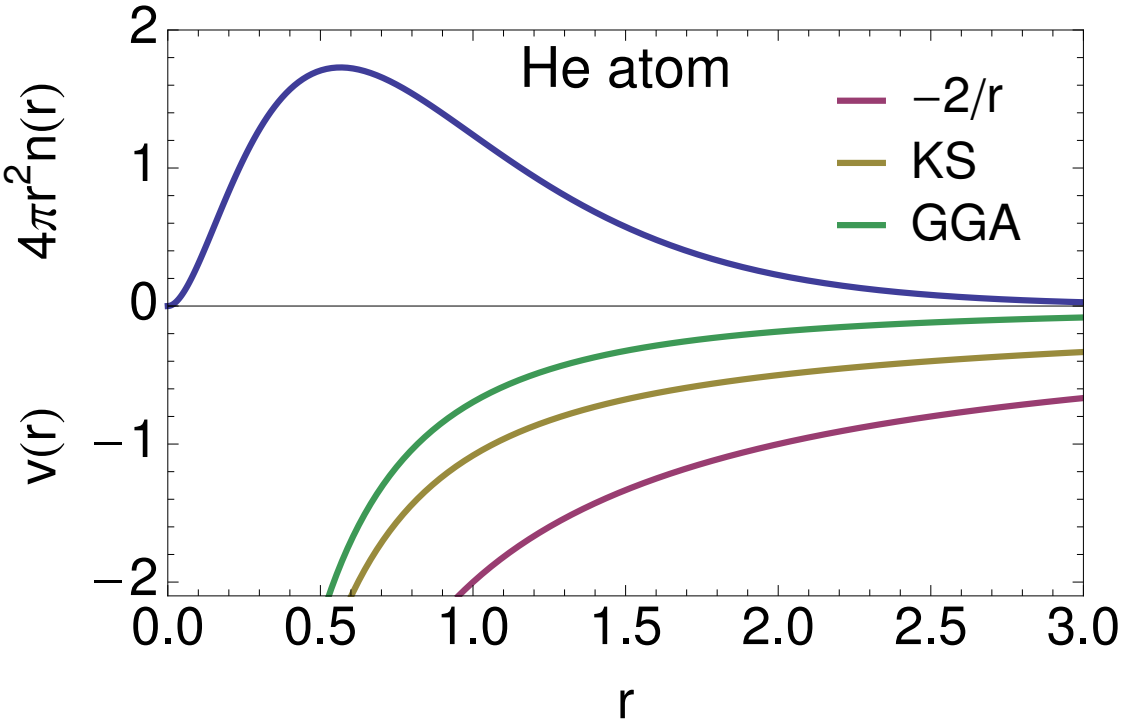

Figure 2.1: Radial densities and potentials for the He atom (energies in Hartree, distances in Bohr). The pink line is $-2/r$, the attraction of real electrons to the nucleus. The yellow is the *exact* KS potential. Two fake electrons in the $1s$ orbital of this potential have the same ground-state density as real He. The green is the potential of a typical approximation which, although inaccurate, yields a highly accurate density.

approximations is

$$\begin{aligned} XC &\sim XC^{\text{unif}}(\rho) && (LDA) \\ &\sim XC^{\text{GGA}}(\rho, |\nabla\rho|) && (GGA) \\ &\sim a(X - X^{\text{GGA}}) + XC^{\text{GGA}} && (hybrid) \end{aligned} \tag{2.4}$$

The first was the third major step from the mid-60s and was invented in the KS paper[132]. It was the mainstay of solid-state calculations for a generation, and remains popular for some specific applications even today. It is (almost) never used in quantum chemistry, as it typically overbinds by about 1eV/bond. The local density approximation (LDA)[132] assumes that the XC energy depends on the density at each position only, and that dependence is the same as in a uniform electron gas.

Adding another level of complexity leads to the more accurate generalized gradient approximations (GGAs)[13, 192], which use information about both the density and its gradient at each point. Hybrid approximations mix a fraction (a) of exact exchange with a GGA[14]. These maneuvers beyond the GGA usually increase the accuracy of certain properties with an affordable increase in computational cost[197]. (Meta-GGAs try to use a dependence on the KS kinetic energy density to avoid calculating the Fock exchange of hybrids[195, 234], which can be very expensive for solids.)

Fig. 2.2 shows that the two most popular functionals, PBE[112, 194] and B3LYP[14, 145], comprise a large fraction of DFT citations each year (about 2/3), even though they are now cited only about half the time they are used. PBE is a GGA, while B3LYP is a hybrid[14]. As a method tied to Hartree-Fock, quantum chemists' old stomping grounds, and one with typically higher accuracy than PBE, B3LYP is more often a chemist's choice. PBE's more systematic errors, mathematical rationale, and lack of costly exact exchange, have made it

most popular in solid-state physics and materials science. In reality, both are used in both fields and many others as well.

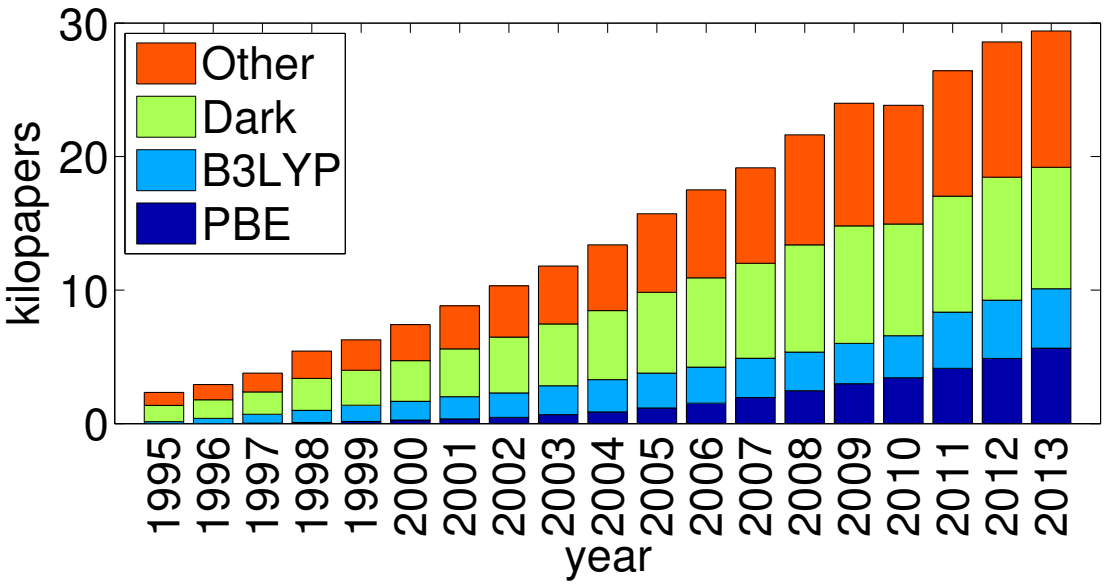

Figure 2.2: The number of DFT citations has exploded (as have *ab initio* methods). PBE is the number of citations of Ref. [194], and B3LYP of Ref. [14]. *Dark* indicates papers using either of these approximations without citing the original papers, while *other* is all other DFT papers. All numbers are estimates. Contrast with Fig. 1 of Ref. [18], which missed almost 2/3 of these.

2.2.6 Cultural wars

The LDA was defined by Kohn and Sham in 1965; there is no controversy about how it was designed. On the other hand, adding complexity to functional approximations demands choices about how to take the next step. Empirical functional developers fit their approximations to sets of highly accurate reference data on atoms and molecules. Non-empirical developers use exact mathematical conditions on the functional and rely on reference systems like the uniform and slowly-varying electron gases. The PBE GGA is the most popular non-empirical approximation, while the most popular empirical functional approximation is the B3LYP hybrid. Modern DFT conferences usually include debates about the morality of

this kind of empiricism.

Both philosophies have been incredibly successful, as shown by their large followings among developers and users, but each of these successes is accompanied by failures. No single approximation works well enough for every property of every material of interest. Many users sit squarely and pragmatically in the middle of the two factions, taking what is best from both of their accomplishments and insights. Often, empiricists and non-empiricists find themselves with similar end products, a good clue that something valuable has been created with the strengths of both.

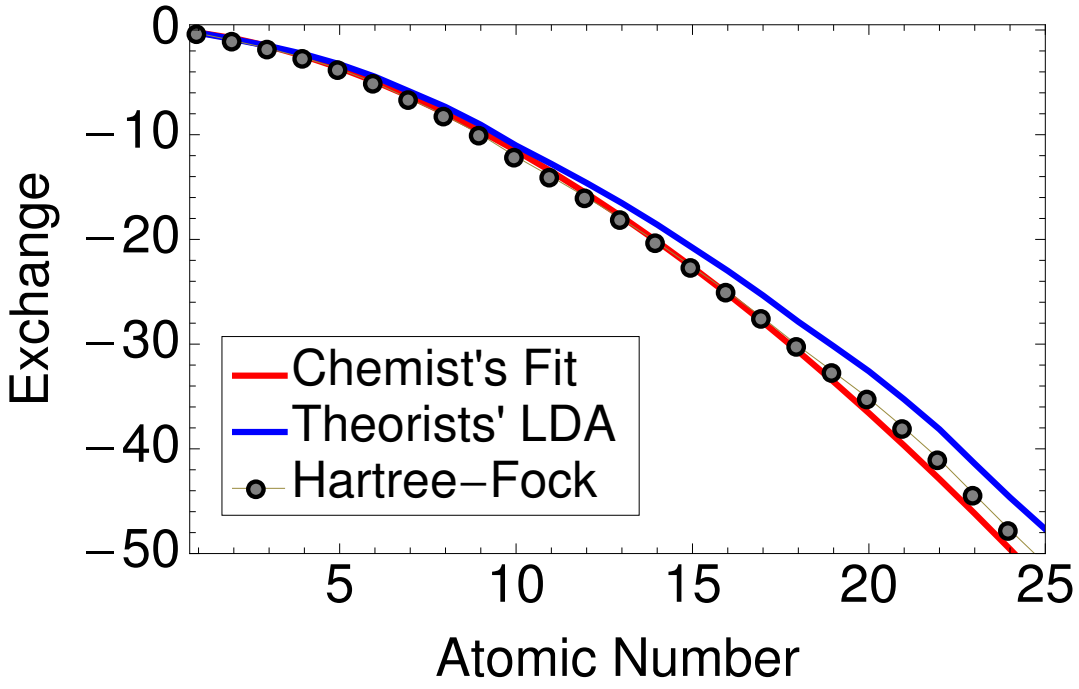

Figure 2.3: Exchange energy (in Hartrees) of atoms from a HF calculation as a function of Z, atomic number, and two LDA X calculations, one with the theoretical asymptote, the other fitted.

To illustrate this idea, we give a brief allegory from an alternative universe. Since at least the 1960s, accurate HF energies of atoms have been available due to the efforts of Charlotte Froese Fischer and others[65, 66]. A bright young chemistry student plots these X energies as a function of Z, the atomic number, and notices they behave roughly as $Z^{5/3}$, as in Fig.

2.3. She's an organic chemistry student, and mostly only cares about main-group elements, so she fits the curve by choosing a constant to minimize the error on the first 18 elements, finding $E_{\rm x} = -0.25Z^{5/3}$. Much later, she hears about KS DFT, and the need to approximate the XC energy. A little experimentation shows that if

$$X^{\rm opt} = C_0 \int d^3r \; \rho^{4/3}(\mathbf{r}), \tag{2.5}$$

this goes as $Z^{5/3}$ when Z is large, and choosing $C_0 = -0.80$ makes it agree with her fit.

In our alternate timeline, a decade later, Paul Dirac, a very famous physicist, proves[40] that for a uniform gas, $C_0 = A_{\rm x} = -(3/4)(3/\pi)^{1/3} = -0.738$. Worse still, Julian Schwinger proves[222] that inserting the TF density into Dirac's expression becomes exact as $Z \to \infty$, so that $E_{\rm x} \to -0.2201Z^{5/3}$. Thus theirs is the 'correct' LDA for X, and our brave young student should bow her head in shame.

Or should she? If we evaluate the mean absolute errors in exchange for the first 20 atoms, her functional is significantly better than the 'correct' one[92]. If lives depend on the accuracy for those 20 atoms, which would you choose[1]?

This simple fable contains the seeds of our actual cultural wars in DFT derivations:

(i) An intuitive, inspired functional need not wait for an official derivation. One parameter might be extracted by fitting, and later derived.

(ii) A fitted functional will usually be more accurate than the derived version for the cases where it was fitted. The magnitude of the errors will be smaller, but less systematic.

[1] In fact, sadly, the young chemist is unable to find a permanent position, and she ends up selling parametrized functionals for food on the streets. On the other hand, the physicists all celebrate their triumph over empiricism with a voyage on a brand new ship, which has been designed with materials whose properties have been calculated using DFT. Because the local approximation, as given above, underestimates the magnitude of the exchange energy, the brittle transition temperature is overestimated. When the new ship sails through icy waters, its hull is weakened and damaged by an iceberg, so all of them drown. (The interested reader may find more information on the ductile-to-brittle transition in Ref. [220] and other works by Kaxiras.)

(iii) The fitted functional will miss universal properties of a derived functional. We see in Sec. 2.6 that the correct LDA for exchange is a universal limit of *all* systems, not just atoms.

(iv) If you want to add the next correction to LDA, starting with the wrong constant will make life very difficult (see Sec. 2.6).

2.3 What's at the forefront?

2.3.1 Accurate Gaps

Calculating accurate energy gaps and self-interaction errors are notorious difficulties within DFT[64]. Self-interaction error (SIE) stems from spurious interaction of an electron with itself in the Coulomb repulsion term. Orbital-dependent methods often cure most of the SIE problem, but they can be expensive to run. The 'gap problem' in DFT often stems from treating the KS HOMO-LUMO gap as the fundamental gap, but the difference in the HOMO and LUMO of the KS system is not the same as the difference between the ionization potential and the electron affinity[64]. Ad hoc methods are often used to correct DFT gaps, but these methods require expensive additional calculations, empirical knowledge of your system, or empirical tuning. However, it has recently been shown that some classes of self-interaction error are really just errors due to poor potentials leading to poorer densities [124, 125]. Such errors are removed by using more accurate densities (Fig. 2.4).

2.3.2 Range-separated hybrids

Range-separated hybrids[98] improve fundamental gaps calculated via the DFT HOMO-LUMO gap[138]. Screened range-separated hybrids can even achieve gap renormalization present when moving between gas-phase molecules and molecular crystals[210]. The basic

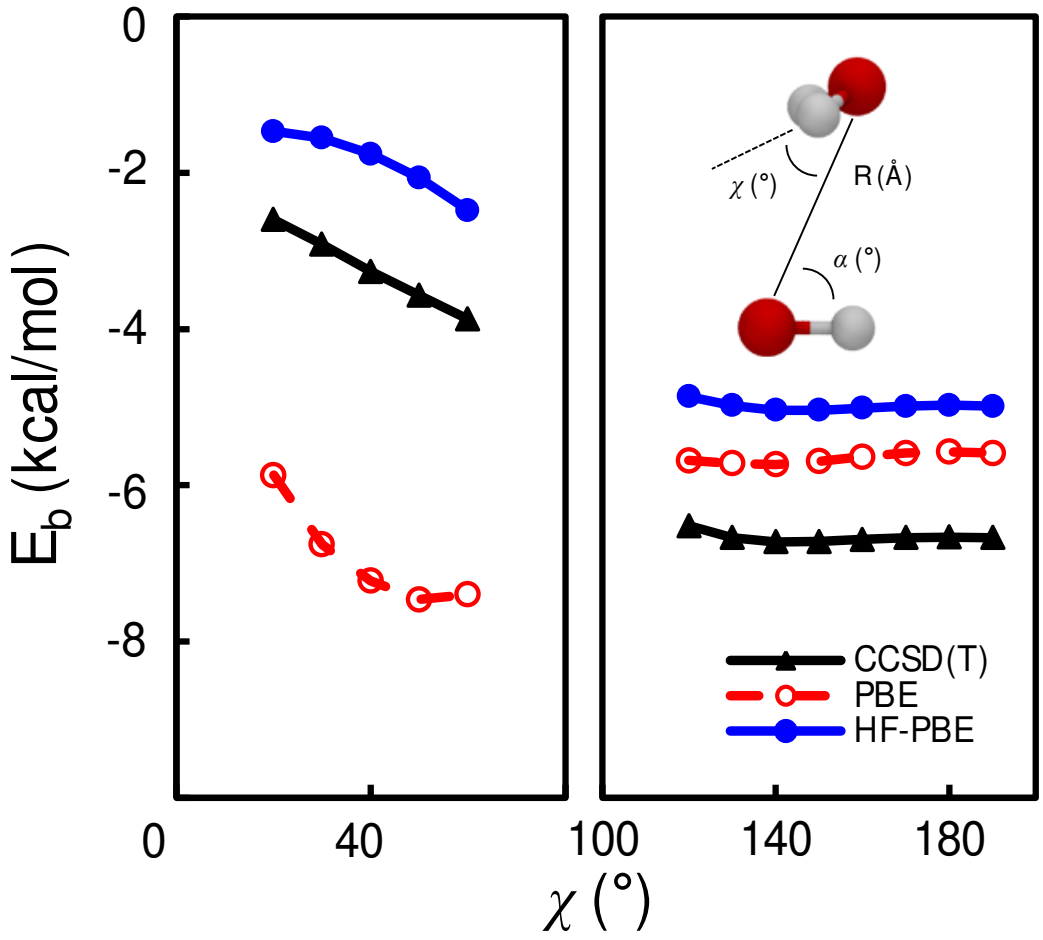

Figure 2.4: When a DFT calculation is *abnormally* sensitive to the potential, the density can go bad. Usually, DFT approximate densities are better than HF[7], as in Fig 1. Here, self-consistent PBE results for $OH - H_2O$ interactions yield the wrong geometry, but PBE on HF-densities fixes this[125].

range-separated hybrid scheme separates the troublesome Coulomb interaction into long-range and short-range pieces. The screened version enforces exact conditions to determine where this separation occurs and incorporates the dielectric constant as an adaptive parameter. This technique takes into account increased screening as molecules form solids, resulting in reduced gaps critical for calculations geared toward applications in molecular electronics.

2.3.3 Weak Interactions

Another of DFT's classic failings is its poor treatment of weak interactions[84, 109]. Induced dipoles and the resulting dispersion interactions are not captured by the most popular approximations of Eq. 2.4. This prevents accurate modeling of the vast majority of biological systems, as well as a wide range of other phenomena, such as surface adsorption and molecular crystal packing. GGAs and hybrids are unable to model the long-range correlations occurring between fluctuations induced in the density. The non-empirical approach based on the work of Langreth and Lundqvist[2, 39, 146, 230] and the empirical DFT-D of Grimme[83, 114] have dominated the advances in this area, along with the more recent, less empirical approach of Tkatchenko and Scheffler[241, 259].

2.4 Reducing cost: Is less more?

No matter how much progress is made in improving algorithms to reduce the computational cost of DFT calculations, there will always be larger systems of interest, and even the fastest calculations become prohibitively expensive. The most glaring example is molecular dynamics (MD) simulation in biochemistry. With classical force fields, these can be run for nano- to milli-seconds, with a million atoms, with relative ease. But when bonds break, a quantum treatment is needed, and the first versions of these were recognized in last year's

Nobel prize in chemistry[122, 147, 251]. These days, many people run Car-Parrinello MD[31, 104], with DFT calculations inside their MD, but this reduces tractable system sizes to a few hundred atoms.

Because of this, there remains a great deal of interest in finding clever ways to keep as much accuracy as needed while simplifying computational steps. One method for doing so involves circumventing the orbital-dependent KS step of traditional DFT calculations. Alternatively, one can save time by only doing those costly steps (or even more expensive procedures) on a system's most important pieces, while leaving the rest to be calculated using a less intensive method. The key to both approaches is to achieve efficiency without sacrificing precious accuracy.

2.4.1 Removing the orbitals

Orbital-free methods[43, 115, 117, 118, 229, 250] like TF reduce computational costs, but are often not accurate enough to compete with KS DFT calculations. Current methods search for a similar solution, by working on non-interacting kinetic energy functionals that allow continued use of existing XC functionals[130]. (An intriguing alternative is to use the potential as the basic variable [26, 28] – see Secs. 2.6 and 2.7.)

2.4.2 Embedding

Partitioning and embedding are similar procedures, in which calculations on isolated pieces of a molecule are used to gain understanding of the molecule as a whole[158]. One might want to separate out molecular regions to look more closely at pieces of high interest or to find a better way to approximate the overall energy with density functionals. Parsing a molecule into chunks can also allow for entirely new computational approaches not possible

when dealing with the molecule as a whole.

Partition DFT[47] is an exact embedding method based on density partitioning[34, 35]. Because it uses ensemble density functionals[85, 207], it can handle non-integer electron numbers and spins[233]. Energy of the fragments is minimized using effective potentials consisting of a fragment's potential and a global partition potential that maintains the correct total density. This breakdown into fragment and partition energies allows approximations good for localized systems to be used alongside those better for the extended effects associated with the partition potential.

While partition DFT uses DFT methods to break up the system, projector-based wavefunction-theory-in-DFT embedding techniques combine wavefunction and DFT methods[8, 161]. This multiscale approach leverages the increased accuracy of some wavefunction methods for some bonds, where high accuracy is vital, without extending this computational cost to the entire system. Current progress in this field has been toward the reduction of the errors introduced by the mismatch of methods between subsystems. This type of embedding has been recently applied to heterolytic bond cleavage and conjugated systems[75]. Density matrix embedding theory on lattices[126] and its extension to full quantum mechanical chemical systems[127] use ideas from the density matrix renormalization group (DMRG)[252, 253], a blazingly fast way to exactly solve low-dimensional quantum mechanics problems. This shifts the interactions between fragments to a quantum bath instead of dealing with them through a partition potential.

2.5 What is the underlying theory behind DFT approximations?

Given the Pandora's box of approximate functionals, many found by fitting energies of systems, most users imagine DFT as an empirical hodgepodge. Ultimately, if we end up with a different functional for every system, we will have entirely defeated the idea of first-principles calculations. However, prior to the mid-90s, many decades of theory were developed to better understand the local approximation and how to improve on it[109]. Here we summarize the most relevant points.

The joint probability of finding one electron in a little chunk of space around point A and another in some other chunk of space around point B is called the pair probability density. The exact quantum repulsion among electrons is then

$$ElecRep = \frac{1}{2}\int dA \int dB \, \frac{P(A,B)}{|\mathbf{r}_A - \mathbf{r}_B|}. \tag{2.6}$$

But we can also write

$$P(A,B) = \rho(A)\,\rho_{\rm cond}(A,B). \tag{2.7}$$

where $\rho(A)$ is the density at $\mathbf{r}_A$ and $\rho_{\rm cond}(A,B)$ is the probability of finding the second electron at B, *given* that there's one at A. (If you ignore the electron at A, this is just $\rho(B)$, and Eq. 2.6 gives the Coulomb repulsion in Eqs. 2.2 and 2.3). We write this conditional probability as

$$\rho_{\rm cond}(A,B) = \rho(B) + \rho_{\rm XC}(A,B). \tag{2.8}$$

where $\rho_{\rm XC}(A,B)$ is called the hole around A. It is mostly negative and represents a missing

electron (it integrates to -1), since the conditional probability integrates to $N-1$. With a little math trick (called the adiabatic connection[87, 143]), we can fold the kinetic correlation into the hole so that

$$XC = \frac{1}{2}\int dA \int dB \, \frac{\rho(A)\,\rho_{\rm XC}(A,B)}{|\mathbf{r}_A - \mathbf{r}_B|}. \tag{2.9}$$

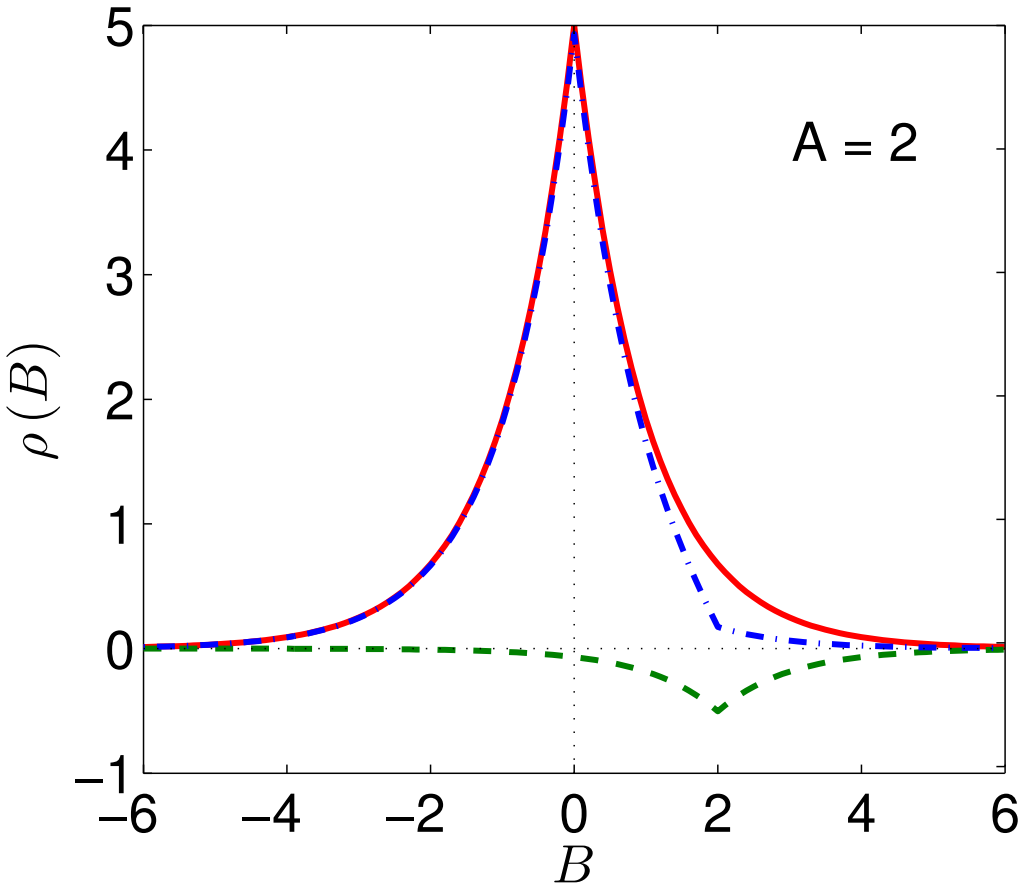

Figure 2.5: Cartoon of a one-dimensional 10-electron density (solid red), the conditional density (dot-dashed blue) given an electron at $A = 2$, and its hole density (dashed green).

Because the XC hole tends to follow an electron around, i.e., be centered on A as in Fig. 2.5, its shape is roughly a simple function of $\rho(A)$. If one approximates the hole by that of a uniform gas of density $\rho(A)$, Eq. 2.9 above yields the LDA for the XC energy. So the LDA approximation for XC can be thought of as approximating the hole by that of a uniform

gas[52, 109].

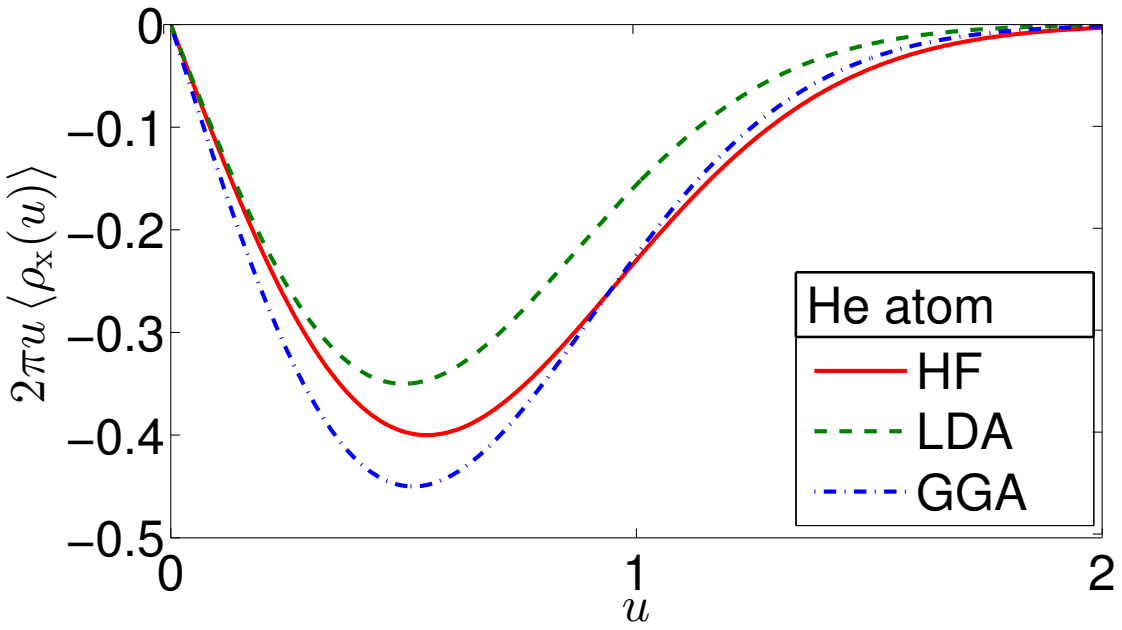

Figure 2.6: Representation of system-averaged radial exchange holes for the helium atom[54], weighted by the Coulomb repulsion, so that the area equals the X energy. The LDA hole (dashed green) is not deep enough, reflecting the LDA underestimate of the magnitude of the X energy. The GGA hole (dot-dashed blue) is substantially better, but a little too deep.

But while the XC is roughly approximated by LDA, the energy density at each point in a system is not, especially in systems of low symmetry. But from Eq. 2.9, the energy depends only on the *average* of the XC hole over the system, and Fig. 2.6 shows such a system-averaged hole for the He atom. (Integrate over A and the angular parts of B in Eq. (2.9).) The LDA hole is not deep enough, and neither is the LDA energy. This is the effect that leads to LDA overbinding of molecules.

2.5.1 GGA Made Briefer

The underlying idea behind the Perdew series of GGAs was to improve on the LDA hole[11]. Adding gradient corrections to the hole violates certain sum rules (negativity of the X hole and integration to -1, and integration to 0 for the correlation hole), so the real-space cutoff

procedure was designed to restore these conditions. This is an effective resummation of the gradient expansion, producing the numerical GGA. The popular functional PBE was derived from imposing exact conditions on a simple form[112, 194], but should be believed because it mimics the numerical GGA. In Fig. 2.6, we show how the GGA hole roughly improves on LDA, reducing typical energy errors by a factor of three.

GGAs don't only show how important good hole models can be. They also demonstrate that good approximations can satisfy different exact conditions, so picking which to satisfy is non-trivial. For instance, B88[13], PW91[113, 193], and PBE[112, 194] give similar values for exchange energy when densities do not get too small or vary too quickly. However, once they do, each behaves very differently. Each approximation was sculpted to satisfy different exact conditions in this limit. Becke decided a good energy density for exponential electronic densities was important. Perdew first thought that a particular scaling behavior was important[21], then that satisfying a certain bound was better[194]. Without a systematic way to improve our approximations, these difficult choices guide our progress. But starting from a model for the XC hole is an excellent idea, as such a model can be checked against the exact XC hole[25].

2.5.2 XDM

A recent, parameter-free approach to capturing dispersion is the exchange-hole dipole moment (XDM) method[15, 16, 108, 182], where perturbation theory yields a multipole-multipole interaction, and quantum effects are included through the dipole moment of the electron with its exchange hole. Using these in concert with atomic polarizabilities and dipole moments generates atomic pair dispersion coefficients that are within 4% of reference C_6 values[12]. Such a model has the advantage over the more popular methods of Sec. 2.3 because its assertions about the hole can be checked.

2.5.3 RPA and other methods

Originally put forth in the 1950s as a method for the uniform electron gas, the random phase approximation (RPA) can be viewed as a simplified wavefunction method or a nonlocal density functional approach that uses both occupied and unoccupied KS states to approximate the correlation energy. RPA correlation performs extremely well for noncovalent, weak interactions between molecules and yields the correct dissociation limit of H_2[70], two of the major failures of traditional DFT approximations[33].

Though computational expense once hindered its wide use, resolution-of-identity implementations[58, 72] have improved its efficiency, making RPA accessible to researchers interested in large molecular systems. RPA gives good dissociation energy for catalysts involving the breaking of transition-metal-ligand and carbon-carbon bonds in a system of over 100 atoms[57]. Though RPA handles medium- and long-range interactions very well, its trouble with short-range correlations invites development of methods that go 'beyond RPA.' RPA used in quantum chemistry usually describes only the particle-hole channel of the correlation, but another recent approach to RPA is the particle-particle RPA (pp-RPA)[247]. pp-RPA is missing some correlation, which causes errors in total energies of atoms and small molecules. This nearly cancels out in reaction energy calculations and yields fairly accurate binding energies[189].

RPA and variations on it will likely lead to methods that work for both molecules and solids, and their computational cost will be driven down by algorithmic development. However, RPA is likely to remain substantially more expensive than a GGA calculation for the indefinite future. While it may rise to fill an important niche in quantum chemistry, producing comparably accurate energetics to modern functionals without any empiricism, such methods will not *replace* DFT as the first run for many calculations. Moreover, as with almost all 'better' methods than DFT, there appears to be no way to build in the good performance

of older DFT approximations.

2.6 Is there a systematic approach to functional approximation?

A huge intellectual gap in DFT development has been in the theory behind the approximations. This, as detailed above, has allowed the rise of empirical energy fitting. Even the most appealing non-empirical development seems to rely on picking and choosing which exact conditions the approximation should satisfy. Lately, even Perdew has resorted to one or two parameters in the style of Becke[111, 231], in order to construct a meta-GGA. Furthermore, up until the mid 1990s, many good approximations were developed as approximations to the XC hole, which could then be tested and checked for simple systems.

However, in fact, there *is* a rigorous way to develop density functional approximations. Its mathematical foundations were laid down 40 years ago by Lieb and Simon[154, 155, 157]. They showed the fractional error in the energy in any TF calculation vanishes as $Z \to \infty$, keeping $N = Z$. Their original proof is for atoms, but applies to any molecule or solid, once the nuclear positions are scaled by $Z^{1/3}$ also. Their innocuous statement is in fact very profound. This very complicated many-body quantum problem, in the limit of *large* numbers of electrons, has an almost trivial (approximate) solution. And although the world finds TF theory too inaccurate to be useful, and performs KS calculations instead, the equivalent statement (not proven with rigor) is that the fractional error in the LDA for XC vanishes as $Z \to \infty$. XC, like politics, is entirely local in this limit.

These statements explain many of the phenomena we see in modern DFT:

(i) LDA is *not* just an approximation that applies for uniform or slowly varying systems, but

is instead a universal limit of *all* electronic systems.

(ii) LDA is the leading term in an asymptotic expansion in powers of $\hbar$, i.e., semiclassical. Such expansions are notoriously difficult to deal with mathematically.

(iii) The way in which LDA yields an ever smaller error as Z grows is very subtle. The leading corrections are of several origins. Often the dominant error is a lack of spatial quantum oscillations in the XC hole. However, as Z grows, these oscillations get faster, and so their net effect on the XC energy becomes smaller. Thus, even as Z grows, LDA should not yield accurate energy densities everywhere in a system (and its potential is even worse, as in Fig. 2.1), but the integrated XC energy will become ever more accurate.

(iv) The basic idea of the GGA as the leading correction to LDA makes sense. The leading corrections to the LDA hole should exist as very sophisticated functionals of the potential, but whose energetic effects can be captured by simple approximations using the density gradient. This yields improved net energetics, but energy densities might look even worse, especially in regions of high gradients, such as atomic cores.

Next, we continue the allegory from Sec. 2.2.6. To do so, we subtract the LDA X energy from our accurate ones, so we can see the next correction, and plot this, per electron, in Fig. 2.7. Now, a bright young chemist has heard about the GGA, cooks up an intuitive correction to LDA, and fits one parameter to the noble gas values. Later, some physicists derive a different GGA, which happens to also give the correct value. Later still, a derivation of the correction for large Z is given, which can be used to determine the parameter (and turns out to match the empirical value within 10%). The only difference from the original allegory is that this is all true. The chemist was Axel Becke; his fitted functional is B88[13]. The derived functional is PBE[194], and the derivation of the parameter in B88 is given in Ref. [46].

This true story both validates Becke's original procedure and the semiclassical approach to

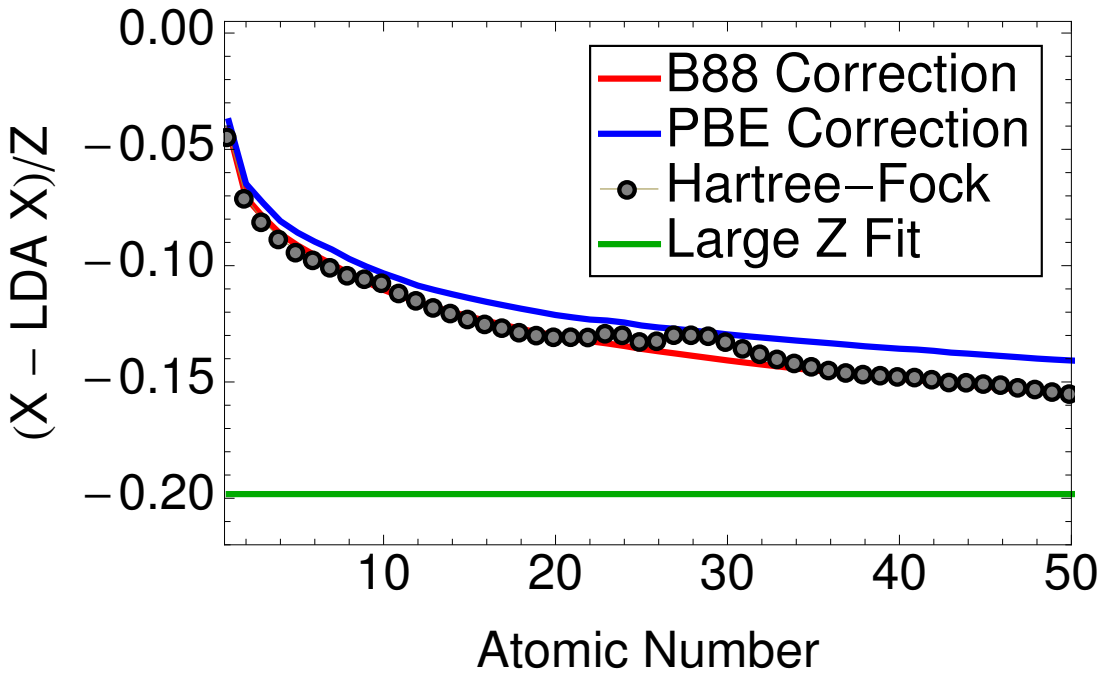

Figure 2.7: The non-local exchange energy (exchange minus LDA X) per electron of atoms with atomic number Z (compare with Fig. 2.3). The PBE functional tends to the theoretical limit ($Z \to \infty$) (horizontal green line), but B88 is more accurate for $Z < 50$ because of fitting[46].

density functional approximation. Note that even the correction is evaluated on the TF density to find the limiting behavior. The PBE exchange functional also yields the leading the correction to the exchange energy of atoms. By throwing this away and restoring the (different) gradient expansion for slowly-varying gases, PBEsol was created[55].

2.6.1 Semiclassical approximations

New approximations driven by semiclassical research can be divided into density approaches and potential approaches. In the density camp, we find innovations like the approximations by Armiento and Mattsson[4, 165, 166], which incorporate surface conditions through their semiclassical approach. In the potential functional camp, we find highly accurate approximations to the density, which automatically generate approximations to non-interacting kinetic energies[26, 27, 28]. Since these approaches use potential functionals, they are orbital-free and incredibly efficient, but only apply in one dimension (see also Sec. 2.7). Current research is focused on extension to three dimensions, semiclassical approximations in the presence of classical turning points, as well as semiclassical approximations to exchange and correlation energies.

2.7 Warm dense matter: A hot new area?

Though we do not live at icy absolute zero, most chemistry and physics happens at low enough temperatures that electrons are effectively in their ground state. Most researchers pretend to be at zero temperature for their DFT work with impunity. But some people, either those working at high enough temperatures and pressures or those interested in low-energy transitions, can't ignore thermal effects. Those of us caught up in these warmer pursuits must tease out where temperature matters for our quantum mechanical work.

Mermin proved a finite-temperature version of the Hohenberg-Kohn theorem in 1965[169], and the finite-temperature LDA was shown in the original KS paper[132]. However, many people continue to rely on the zero-temperature approximations, though they populate states at higher energy levels using finite-temperature weightings. Better understanding and modeling of the finite-temperature XC hole could lead to improvement in some of the finer details of these calculations, like optical and electronic properties[206].

2.7.1 WDM and MD

One area that has seen great recent progress with DFT is the study of warm dense matter (WDM)[80, 180]. WDM is intermediate to solids and plasmas, inhabiting a world where both quantum and classical effects are important. It is found deep within planetary interiors, during shock physics experiments, and on the path to ignition of inertial confinement fusion. Lately, use of DFT MD has been a boon to researchers working to simulate these complicated materials[101, 123, 128, 167, 213]. Most of these calculations are performed using KS orbitals with thermal occupations, ignoring any temperature dependence of XC, in hopes that the kinetic and Coulomb energies will capture most of the thermal effects. Agreement with experiment has been excellent, though there is great interest in seeing if temperature-dependent XC approximations affects these results.

2.7.2 Exact conditions

Exact conditions have been derived[45, 56, 202, 206] for finite-temperature systems that seem very similar to their ground-state counterparts. However, a major difference in thermal systems is that when one squeezes or compresses the length scale of the system, one sees an accompanying scaling of the temperature. This is further reflected in the thermal adiabatic connection, which connects the non-interacting KS system to the interacting system through

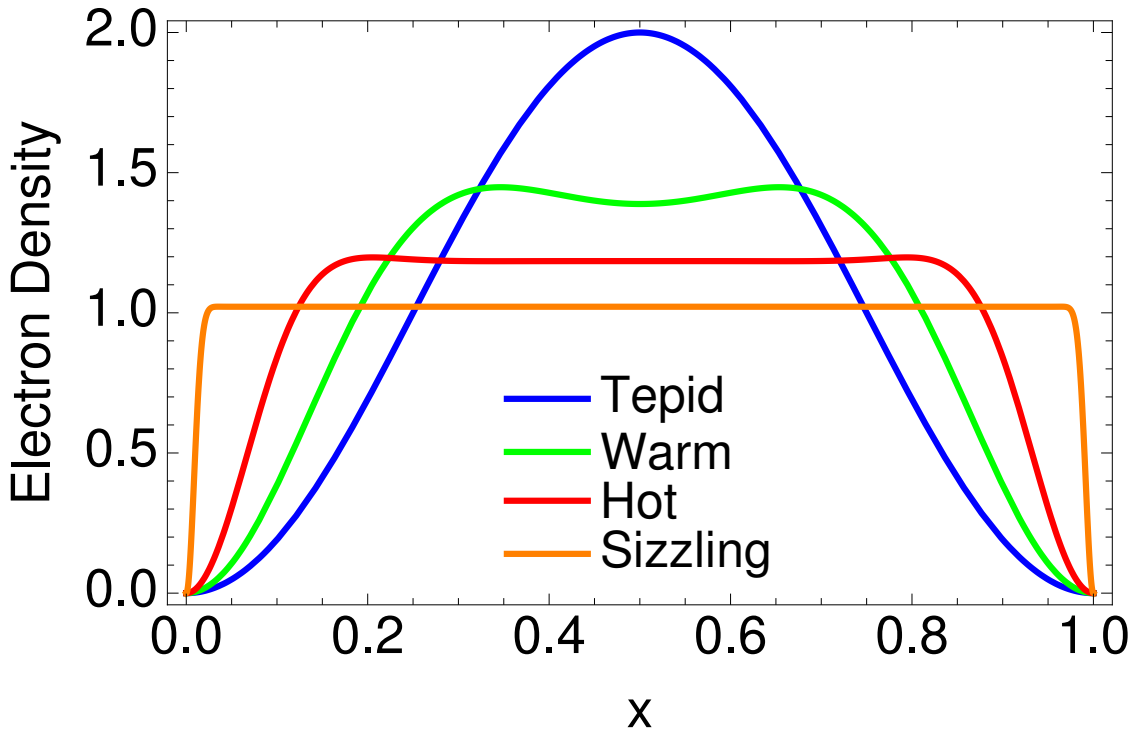

Figure 2.8: The density of a single electron in a flat box spreads toward the infinite walls as temperatures rise.

scaling of the electron-electron interaction. At zero temperature, this allows us to write the XC energy in terms of the potential alone, as long as it is accompanied by appropriate squeezing or stretching of the system's length scale (see Sec. 2.5). With the temperature-coordinate scaling present in thermal ensembles, the thermal adiabatic connection requires not only length scaling, but also the correct temperature scaling.

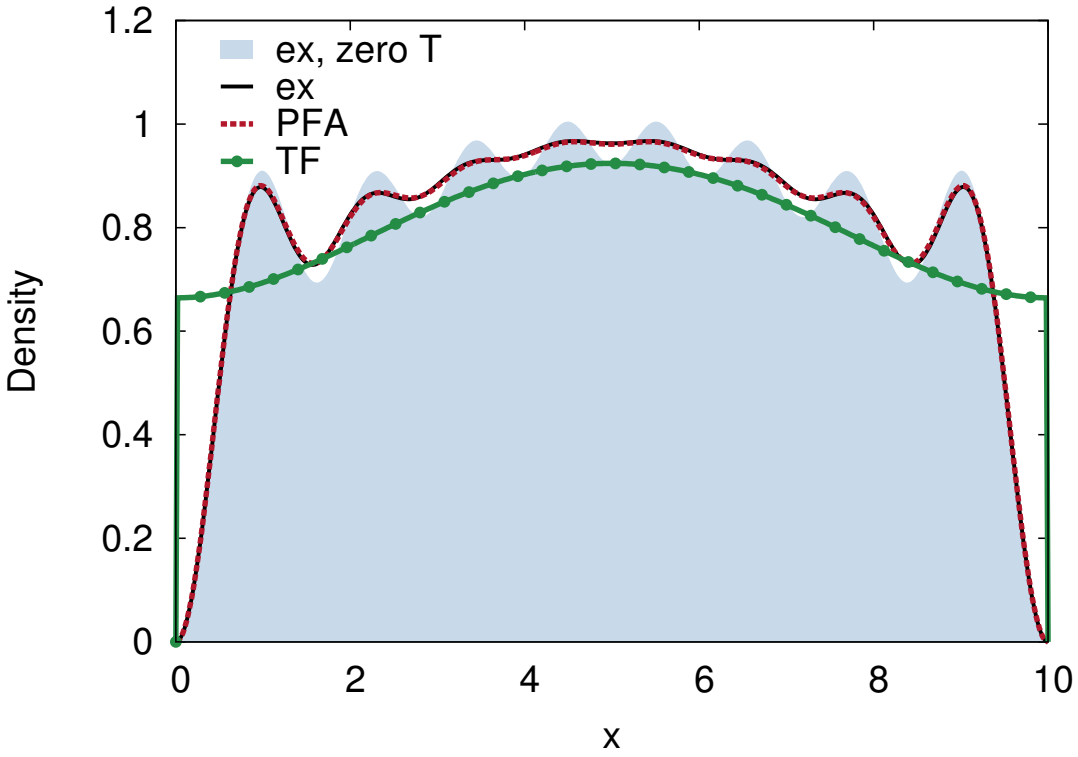

Figure 2.9: Eight electrons in the potential $-2\sin^2(\pi x/10)$ in a 1d box. At zero temperature (gray), the density exhibits sharp quantum oscillations, which wash out as the temperature increases (black). This effect is much weaker near the edges. TF is used in many warm simulations, but (green) misses all oscillations, vital for accurate chemical effects. The orbital-free, finite-temperature potential functional approximation of Ref. [29] is almost exact here (red).

2.7.3 OF Methods

Orbital-free methods, discussed in Sec. 2.4, are of particular interest in the WDM community. Solving the KS equations with many thermally populated orbitals is repeated over and

over in DFT MD, leading to prohibitive cost as temperatures rise. The focus on free energies for thermal ensembles has led to two different approaches to orbital-free approximations. One approach uses two separate forms for kinetic and entropic contributions[45]. Following this path, one can either make approximations empirically[121] or non-empirically[116]. Another approach enforces a particular type of response in the uniform gas limit[226]. If one wishes to approximate the kentropy[206] as a whole, one can use temperature-dependent potential functional theory to generate highly accurate approximations from approximate densities generated semiclassically or stochastically[6, 29]. Fig. 2.9 shows the accuracy of a semiclassical density approximation, which captures the quantum oscillations missed by Thomas-Fermi and still present as temperatures rise.

2.8 What can we guess about the future?

The future of DFT remains remarkably bright. As Fig. 2.2 shows, the number of applications continues to grow exponentially, with three times as much activity than previously realized (Fig. 1 of [18]). While empiricism has generated far too many possible alternatives, the standard well-derived approximations continue to dominate.

To avoid losing insight, it is important to further develop the systematic path to approximations, which eschews all empiricism and expands the functional in powers of $\hbar$, Planck's constant. This will ultimately tell us what we can and cannot do with local-type approximations. There is huge room for development in this area, and any progress could impact all those applications.

Meanwhile, new areas have been (e.g. weak interactions) or are being developed (warm dense matter). New methods, such as using Bayesian statistics for error analysis[168] or machine learning for finding functionals[228, 229], are coming on line. Such methods will not suffer the

limitations of local approximations, and should be applicable to strongly correlated electronic systems, an arena where many of our present approximations fail. We have little doubt that DFT will continue to thrive for decades to come.

APJ thanks the U.S. Department of Energy (DE-FG02-97ER25308), and KB thanks the National Science Foundation (CHE-1112442). We are grateful to Cyrus Umrigar for data on the helium atom and to Min-Cheol Kim for Fig. 2.4 and Attila Cangi for Fig. 2.9.

Part III

Introduction to Thermal DFT

Chapter 3

Thermal Density Functional Theory in Context

written with Stefano Pittalis, E.K.U. Gross, and Kieron Burke. Published in Frontiers and Challenges in Warm Dense Matter, *Lecture Notes in Computational Science and Engineering* **96**, Frank Graziani, Michael P. Desjarlais, Ronald Redmer, and Samuel B. Trickey, *eds.*, Springer International Publishing, 25–60 (2014), *ibid.* **113**, 1601(E) (2013).

Abstract: *This chapter introduces thermal density functional theory, starting from the ground-state theory and assuming a background in quantum mechanics and statistical mechanics. We review the foundations of density functional theory (DFT) by illustrating some of its key reformulations. The basics of DFT for thermal ensembles are explained in this context, as are tools useful for analysis and development of approximations. We close by discussing some key ideas relating thermal DFT and the ground state. This review emphasizes thermal DFT's strengths as a consistent and general framework.*

3.1 Introduction

The subject matter of high-energy-density physics is vast [180], and the various methods for modeling it are diverse [81, 167, 218]. The field includes enormous temperature, pressure, and density ranges, reaching regimes where the tools of plasma physics are appropriate [5]. But, especially nowadays, interest also stretches down to warm dense matter (WDM), where chemical details can become not just relevant, but vital [128]. WDM, in turn, is sufficiently close to zero-temperature, ground-state electronic structure that the methods from that field, especially Kohn-Sham density functional theory (KS DFT) [123, 213], provide a standard paradigm for calculating material-specific properties with useful accuracy.

It is important to understand, from the outset, that the logic and methodology of KS-DFT is at times foreign to other techniques of theoretical physics. The procedures of KS-DFT appear simple, yet the underlying theory is surprisingly subtle. Consequently, progress in developing useful approximations, or even writing down formally correct expressions, has been incredibly slow. As the KS methodology develops in WDM and beyond, it is worth taking a few moments to wrap one's head around its logic, as it does lead to one of the most successful paradigms of modern electronic structure theory [18].

This chapter sketches how the methodology of KS DFT can be generalized to warm systems, and what new features are introduced in doing so. It is primarily designed for those unfamiliar with DFT to get a general understanding of how it functions and what promises it holds in the domain of warm dense matter. Section 2 is a general review of the basic theorems of DFT, using the original methodology of Hohenberg-Kohn [99] and then the more general Levy-Lieb construction [148, 156]. In Section 3, we discuss approximations, which are always necessary in practice, and several important exact conditions that are used to guide their construction. In Section 4, we review the thermal KS equations [169] and some relevant statistical mechanics. Section 5 summarizes some of the most important exact conditions for

thermal ensembles [45, 202]. Last, but not least, in Section 6 we review some recent results that generalize ground-state exact scaling conditions and note some of the main differences between the finite-temperature and the ground-state formulation.

3.2 Density functional theory

A reformulation of the interacting many-electron problem in terms of the electron density rather than the many-electron wavefunction has been attempted since the early days of quantum mechanics [60, 61, 240]. The advantage is clear: while the wavefunction for interacting electrons depends in a complex fashion on all the particle coordinates, the particle density is a function of only three spatial coordinates.

Initially, it was believed that formulating quantum mechanics solely in terms of the particle density gives only an approximate solution, as in the Thomas-Fermi method [60, 61, 240]. However, in the mid-1960s, Hohenberg and Kohn [99] showed that, for systems of electrons in an external potential, all the properties of the many-electron ground state are, in principle, exactly determined by the ground-state particle density alone.

Another important approach to the many-particle problem appeared early in the development of quantum mechanics: the single-particle approximation. Here, the two-particle potential representing the interaction between particles is replaced by some effective, one-particle potential. A prominent example of this approach is the Hartree-Fock method [67, 94], which includes only exchange contributions in its effective one-particle potential. A year after the Hohenberg-Kohn theorem had been proven, Kohn and Sham [132] took a giant leap forward. They took the ground state particle density as the basic quantity and showed that both exchange and correlation effects due to the electron-electron interaction can be treated through an effective single-particle Schrödinger equation. Although Kohn and Sham wrote

their paper using the local density approximation, they also pointed out the exactness of that scheme if the exact exchange-correlation functional were to be used (see Section 3.2.3). The KS scheme is used in almost all DFT calculations of electronic structure today. Much development in this field remains focused on improving approximations to the exchange-correlation energy (see Section 3.3).

The Hohenberg-Kohn theorem and Kohn-Sham scheme are the basic elements of modern density-functional theory (DFT) [17, 18, 23]. We will review the initial formulation of DFT for non-degenerate ground states and its later extension to degenerate ground states. Alternative and refined mathematical formulations are then introduced.

3.2.1 Introduction

The non-relativistic Hamiltonian[1] for N interacting electrons[2] moving in a static potential $v(\mathbf{r})$ reads (in atomic units)

$$\hat{H} = \hat{T} + \hat{V}_{ee} + \hat{V} := -\frac{1}{2}\sum_{i=1}^{N}\nabla_i^2 + \frac{1}{2}\sum_{\substack{i,j=1 \\ i\neq j}}^{N}\frac{1}{|\mathbf{r}_i - \mathbf{r}_j|} + \sum_{i=1}^{N} v(\mathbf{r}_i). \tag{3.1}$$

Here, $\hat{T}$ is the total kinetic-energy operator, $\hat{V}_{ee}$ describes the repulsion between the electrons, and $\hat{V}$ is a local (multiplicative) scalar operator. This includes the interaction of the electrons with the nuclei (considered within the Born-Oppenheimer approximation) and any other external scalar potentials.

The eigenstates, $\Psi_i(\mathbf{r}_1, ..., \mathbf{r}_N)$, of the system are obtained by solving the eigenvalue problem

[1] See Refs. [221] or [217] for quantum mechanical background that is useful for this chapter.
[2] In this work, we discuss only spin-unpolarized electrons.

$$\hat{H}\Psi_i(\mathbf{r}_1, ..., \mathbf{r}_N) = E_i\Psi_i(\mathbf{r}_1, ..., \mathbf{r}_N), \tag{3.2}$$

with appropriate boundary conditions for the physical problem at hand. Eq. (3.2) is the time-independent Schrödinger equation. We are particularly interested in the ground state, the eigenstate with lowest energy, and assume the wavefunction can be normalized.

Due to the interactions among the electrons, $\hat{V}_{ee}$, an explicit and closed solution of the many-electron problem in Eq. (3.2) is, in general, not possible. But because accurate prediction of a wide range of physical and chemical phenomena requires inclusion of electron-electron interaction, we need a path to accurate approximate solutions.

Once the number of electrons with Coulombic interaction is given, the Hamiltonian is determined by specifying the external potential. For a given $v(\mathbf{r})$, the total energy is a functional of the many-body wavefunction $\Psi(\mathbf{r}_1, ..., \mathbf{r}_N)$

$$E_v[\Psi] = \langle\Psi|\hat{T} + \hat{V}_{ee} + \hat{V}|\Psi\rangle \ . \tag{3.3}$$

The energy functional in Eq. (3.3) may be evaluated for any N-electron wavefunction, and the Rayleigh-Ritz variational principle ensures that the ground state energy, E_v, is given by

$$E_v = \inf_{\Psi} E_v[\Psi], \tag{3.4}$$

where the infimum is taken over all normalized, antisymmetric wavefunctions. The Euler-Lagrange equation expressing the minimization of the energy is

$$\frac{\delta}{\delta\Psi}\left\{E_v[\Psi] - \mu\left[\langle\Psi|\Psi\rangle - 1\right]\right\} = 0, \tag{3.5}$$

where the functional derivative is performed over $\Psi \in \mathcal{L}^2(\mathbb{R}^{3N})$ (defined as in Ref. [50]). Relation (3.5) again leads to the many-body Schrödinger equation and the Lagrangian multiplier μ can be identified as the chemical potential.

We now have a procedure for finding approximate solutions by restricting the form of the wavefunctions. In the Hartree-Fock (HF) approximation, for example, the form of the wavefunction is restricted to a single Slater determinant. Building on the HF wavefunction, modern quantum chemical methods can produce extremely accurate solutions to the Schrödinger equation [224]. Unfortunately, wavefunction-based approaches that go beyond HF usually are afflicted by an impractical growth of the numerical effort with the number of particles. Inspired by the Thomas-Fermi approach, one might wonder if the role played by the wavefunction could be played by the particle density, defined as

$$n(\mathbf{r}) := \langle \Psi | \sum_{i=1}^{N} \delta(\hat{\mathbf{r}} - \hat{\mathbf{r}}_i) | \Psi \rangle = N \int d\mathbf{r}_2 ... \int d\mathbf{r}_N \Big| \Psi(\mathbf{r}, \mathbf{r}_2, ..., \mathbf{r}_N) \Big|^2, \tag{3.6}$$

from which

$$\int d^3r \; n(\mathbf{r}) = N. \tag{3.7}$$

In that case, one would deal with a function of only three spatial coordinates, regardless of the number of electrons.

3.2.2 Hohenberg-Kohn theorem

Happily, the two-part Hohenberg-Kohn (HK) Theorem assures us that the electronic density alone is enough to determine all observable quantities of the systems. These proofs cleverly connect specific sets of densities, wavefunctions, and potentials, exposing a new framework for the interacting many-body problem.

Let $\mathbf{P}$ be the set of external potentials leading to a *non-degenerate* ground state for N electrons. For a given potential, the corresponding ground state, Ψ, is obtained through the solution of the Schrödinger equation:

$$v \quad \longrightarrow \quad \Psi, \quad \text{with} \quad v \in \mathbf{P}. \tag{3.8}$$

Wavefunctions obtained this way are called interacting v-representable. We collect these ground state wavefunctions in the set $\mathbf{W}$. The corresponding particle densities can be computed using definition (3.6):

$$\Psi \quad \longrightarrow \quad n, \quad \text{with} \quad \Psi \in \mathbf{W}. \tag{3.9}$$

Ground state particle densities obtained this way are also called interacting v-representable. We denote the set of these densities as $\mathbf{D}$.

First part

Given a density $n \in \mathbf{D}$, the first part of the Hohenberg-Kohn theorem states that the wavefunction $\Psi \in \mathbf{W}$ leading to n is unique, apart from a constant phase factor. The proof is carried out by *reductio ad absurdum* and is illustrated in Figure 3.1.

Consider two different wavefunctions in $\mathbf{W}$, Ψ_1 and Ψ_2, that differ by more than a constant phase factor. Next, let n_1 and n_2 be the corresponding densities computed by Eq. (3.6). Since, by construction, we are restricting ourselves to non-degenerate ground states, Ψ_1 and Ψ_2 must come from two different potentials. Name these v_1 and v_2, respectively.

Assume that these different wavefunctions yield the same density:

$$\Psi_1 \neq \Psi_2 \quad \text{but} \quad n_1(\mathbf{r}) = n_2(\mathbf{r}). \tag{3.10}$$

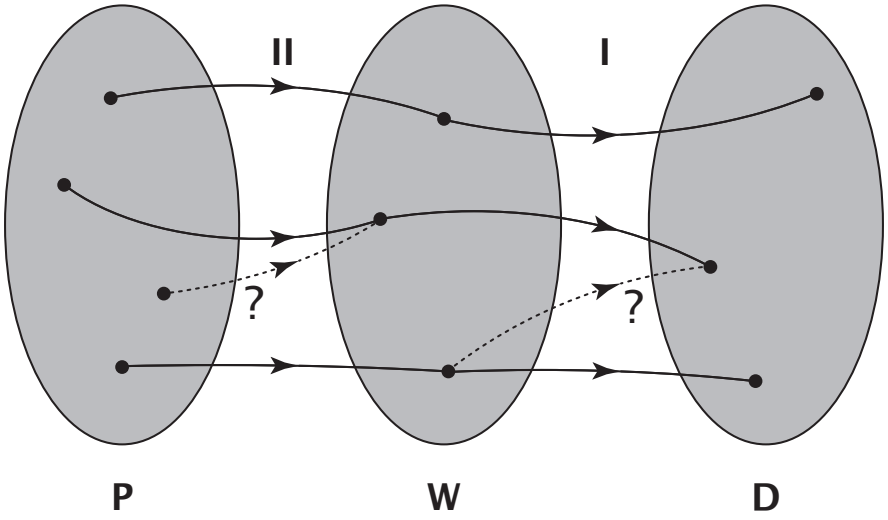

Figure 3.1: The Hohenberg-Kohn proves the one-to-one mappings between potentials and ground-state wavefunctions and between ground-state wavefunctions and ground-state densities. The dotted lines indicated by question marks show the two-to-one mappings disproved by Hohenberg and Kohn [43, 50].

Application of the Rayleigh-Ritz variational principle yields the inequality

$$\langle \Psi_1 | \hat{H}_1 | \Psi_1 \rangle < \langle \Psi_2 | \hat{H}_1 | \Psi_2 \rangle, \tag{3.11}$$

from which we obtain

$$E_1 < \langle \Psi_2 | \hat{H}_2 + (\hat{V}_1 - \hat{V}_2) | \Psi_2 \rangle = E_2 + \int d^3r \; n_1(\mathbf{r}) \left[v_1(\mathbf{r}) - v_2(\mathbf{r}) \right]. \tag{3.12}$$

Reversing the role of systems 1 and 2 in the derivation, we find

$$E_2 < \langle \Psi_1 | \hat{H}_1 + (\hat{V}_2 - \hat{V}_1) | \Psi_1 \rangle = E_1 + \int d^3r \; n_2(\mathbf{r}) \left[v_2(\mathbf{r}) - v_1(\mathbf{r}) \right]. \tag{3.13}$$

The assumption that the two densities are equal, $n_1(\mathbf{r}) = n_2(\mathbf{r})$, and addition of the inequalities (3.12) and (3.13) yields

$$E_1 + E_2 < E_1 + E_2, \tag{3.14}$$

which is a contradiction. We conclude that the foregoing hypothesis (3.10) was wrong, so $n_1 \neq n_2$. Thus each density is the ground-state density of, at most, one wavefunction. This mapping between the density and wavefunction is written

$$n \; \longrightarrow \; \Psi, \text{ with } n \in \mathbf{D} \text{ and } \Psi \in \mathbf{W}. \tag{3.15}$$

Second part

Having specified the correspondence between density and wavefunction, Hohenberg and Kohn then consider the potential. By explicitly inverting the Schrödinger equation,

$$\sum_{i=1}^{N} v(\mathbf{r}_i) = E - \frac{\left(\hat{T} + \hat{V}_{ee}\right) \Psi(\mathbf{r}_1, \mathbf{r}_2, ..., \mathbf{r}_N)}{\Psi(\mathbf{r}_1, \mathbf{r}_2, ..., \mathbf{r}_N)}, \tag{3.16}$$

they show the elements Ψ of $\mathbf{W}$ also determine the elements v of $\mathbf{P}$, apart from an additive constant.

We summarize this second result by writing

$$\Psi \longrightarrow v, \text{ with } \Psi \in \mathbf{W} \text{ and } v \in \mathbf{P}. \tag{3.17}$$

Consequences

Together, the first and second parts of the theorem yield

$$n \longrightarrow v + const, \quad \text{with } n \in \mathbf{D} \text{ and } v \in \mathbf{P}, \tag{3.18}$$

that the ground state particle density determines the external potential up to a trivial additive constant. This is the first HK theorem.

Moreover, from the first part of the theorem it follows that any ground-state observable is a functional of the ground-state particle density. Using the one-to-one dependence of the wavefunction, $\Psi[n]$, on the particle density,

$$\langle \Psi | \hat{O} | \Psi \rangle = \langle \Psi[n] | \hat{O} | \Psi[n] \rangle = O[n]. \tag{3.19}$$

For example, the following functional can be defined:

$$E_{v,\mathrm{HK}}[n] := \langle \Psi[n] | \hat{T} + \hat{V}_{ee} + \hat{V} | \Psi[n] \rangle = F_{\mathrm{HK}}[n] + \int d^3r \; n(\mathbf{r}) v(\mathbf{r}), \tag{3.20}$$

where v is a given external potential and n can be any density in $\mathbf{D}$. Note that

$$F_{\mathrm{HK}}[n] := \langle \Psi[n] | \hat{T} + \hat{V}_{ee} | \Psi[n] \rangle \tag{3.21}$$

is independent of v. The second HK theorem is simply that $F_{\mathrm{HK}}[n]$ is independent of $v(\mathbf{r})$. This is therefore a universal functional of the ground-state particle density. We use the subscript, HK, to emphasize that this is the original density functional of Hohenberg and Kohn.

Let n_0 be the ground-state particle density of the potential v_0. The Rayleigh-Ritz variational principle (3.4) immediately tells us

$$E_{v_0} = \min_{n \in \mathbf{D}} E_{v_0,\mathrm{HK}}[n] = E_{v_0,\mathrm{HK}}[n_0]. \tag{3.22}$$

We have finally obtained a variational principle based on the particle density instead of the computationally expensive wavefunction.

Extension to degenerate ground states

The Hohenberg-Kohn theorem can be generalized by allowing $\mathbf{P}$ to include local potentials having *degenerate* ground states [43, 148, 249], . This means an entire subspace of wavefunctions can correspond to the lowest eigenvalue of the Schrödinger equation (3.2). The sets $\mathbf{W}$ and $\mathbf{D}$ are enlarged accordingly, to include all the additional ground-state wavefunctions and particle densities.

In contrast to the non-degenerate case, the solution of the Schrödinger equation (3.2) now establishes a mapping from **P** to **W** which is one-to-many (see Figure 3.2). Moreover, different degenerate wavefunctions can have the same particle density. Equation (3.6), therefore, establishes a mapping from **W** to **D** that is many-to-one. However, any one of the degenerate ground-state densities still determines the potential uniquely.

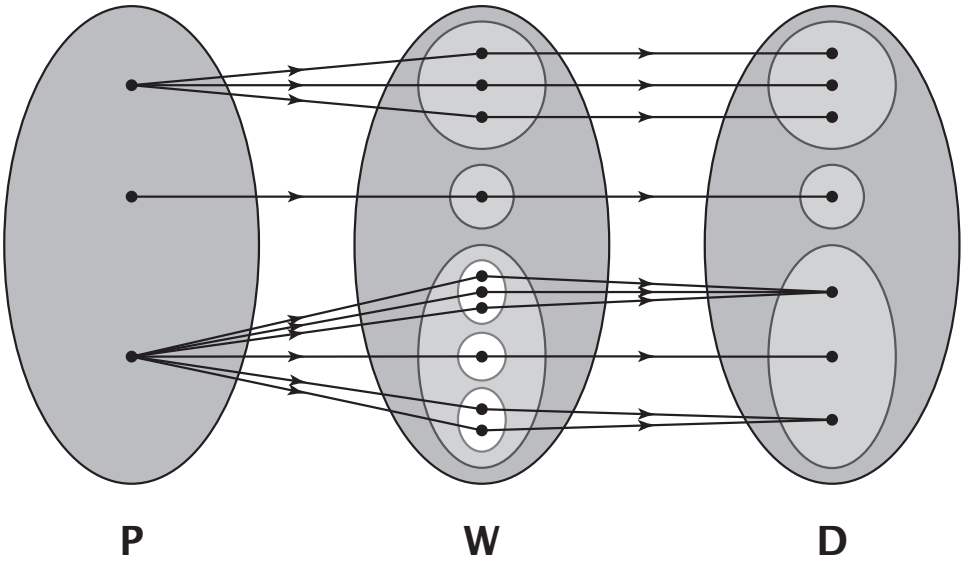

Figure 3.2: The mappings between sets of potentials, wavefunctions, and densities can be extended to include potentials with degenerate ground states. This is seen in the one-to-many mappings between **P** and **W**. Note also the many-to-one mappings from **W** to **D** caused by this degeneracy [43, 74].

The first part of the HK theorem needs to be modified in light of this alteration of the mapping between wavefunctions and densities. To begin, note that two degenerate subspaces, sets of ground states of two different potentials, are disjoint. Assuming that a common eigenstate Ψ can be found, subtraction of one Schrödinger equation from the other yields

$$(\hat{V}_1 - \hat{V}_2)\Psi = (E_1 - E_2)\Psi. \tag{3.23}$$

For this identity to be true, the eigenstate Ψ must vanish in the region where the two potentials differ by more than an additive constant. This region has measure greater than zero. Eigenfunctions of potentials in $\mathbf{P}$, however, vanish only on sets of measure zero [42]. This contradiction lets us conclude that v_1 and v_2 cannot have common eigenstates. We then show that ground states from two different potentials always have different particle densities using the Rayleigh-Ritz variational principle as in the non-degenerate case.

However, two or more degenerate ground state wavefunctions can have the same particle density. As a consequence, neither the wavefunctions nor a generic ground state property can be determined uniquely from knowledge of the ground state particle density alone. This demands reconsideration of the definition of the universal F_{HK} as well. Below, we verify that the definition of F_{HK} does not rely upon one-to-one correspondence among ground state wavefunctions and particle densities.

The second part of the HK theorem in this case proceeds as in the original proof, with each ground state in a degenerate level determining the external potential up to an additive constant. Combining the first and second parts of the proof again confirms that any element of $\mathbf{D}$ determines an element of $\mathbf{P}$, up to an additive constant. In particular, any one of the degenerate densities determines the external potential. Using this fact and that the total energy is the same for all wavefunctions in a given degenerate level, we define F_{HK}:

$$F_{\mathrm{HK}}[n] := E\left[v[n]\right] - \int d^3r \; v[n](\mathbf{r})n(\mathbf{r}). \tag{3.24}$$

This implies that the value of

$$F_{\mathrm{HK}}[n] = \langle \Psi_0 \to n | \hat{T} + \hat{V}_{ee} | \Psi_0 \to n \rangle \tag{3.25}$$

is the same for all degenerate ground-state wavefunctions that have the same particle density. The variational principle based on the particle density can then be formulated as before in

Eq. (3.22).

3.2.3 Kohn-Sham scheme

The exact expressions defining F_{HK} in the previous section are only formal ones. In practice, F_{HK} must be approximated. Finding approximations that yield usefully accurate results turns out to be an extremely difficult task, so much so that pure, orbital-free approximations for F_{HK} are not pursued in most modern DFT calculations. Instead, efficient approximations can be constructed by introducing the Kohn-Sham scheme, in which a useful decomposition of F_{HK} in terms of other density functionals is introduced. In fact, the Kohn-Sham decomposition is so effective that effort on orbital-free DFT utilizes the Kohn-Sham structure, but not its explicitly orbital-dependent expressions.

Consider the Hamiltonian of N non-interacting electrons

$$\hat{H}_s = \hat{T} + \hat{V} := -\frac{1}{2}\sum_{i=1}^{N}\nabla_i^2 + \sum_{i=1}^{N} v(\mathbf{r}_i). \tag{3.26}$$

Mimicking our procedure with the interacting system, we group external local potentials in the set $\mathbf{P}$. The corresponding non-interacting ground state wavefunctions Ψ_s are then grouped in the set $\mathbf{W^s}$, and their particle densities n_s are grouped in $\mathbf{D^s}$. We can then apply the HK theorem and define the non-interacting analog of F_{HK}, which is simply the kinetic energy:

$$T_s[n_s] := E\left[v[n_s]\right] - \int d^3r\ v[n_s](\mathbf{r})n_s(\mathbf{r}). \tag{3.27}$$

Restricting ourselves to non-degenerate ground states, the expression in Eq. (3.27) can be

rewritten to stress the one-to-one correspondence among densities and wavefunctions:

$$T_s[n_s] = \langle \Psi_s[n_s] | \hat{T} | \Psi_s[n_s] \rangle \ . \tag{3.28}$$

We now introduce a fundamental assumption: for each element n of $\mathbf{D}$, a potential v_s in $\mathbf{P^s}$ exists, with corresponding ground-state particle density $n_s = n$. We call v_s the Kohn-Sham potential. In other words, interacting v-representable densities are also assumed to be non-interacting v-representable. This maps the interacting problem onto a non-interacting one.

Assuming the existence of v_s, the HK theorem applied to the class of non-interacting systems ensures that v_s is unique up to an additive constant. As a result, we find the particle density of the interacting system by solving the non-interacting eigenvalue problem, which is called the Kohn-Sham equation:

$$\hat{H}_s \Phi = E \Phi. \tag{3.29}$$

For non-degenerate ground states, the Kohn-Sham ground-state wavefunction is a single Slater determinant. In general, when considering degenerate ground states, the Kohn-Sham wavefunction can be expressed as a linear combination of several Slater determinants [51, 156]. There also exist interacting ground states with particle densities that can only be represented by an ensemble of non-interacting particle densities [59, 183, 184, 215, 244]. We will come back to this point in Section 3.2.5.

Here we continue by considering the simplest cases of non-degenerate ground states. Eq. (3.29) can be rewritten in terms of the single-particle orbitals as follows:

$$\left[-\frac{1}{2}\nabla^2 + v_s(\mathbf{r}) \right] \varphi_i(\mathbf{r}) = \epsilon_i \varphi_i(\mathbf{r}) \ . \tag{3.30}$$

The single-particle orbitals $\varphi_i(\mathbf{r})$ are called Kohn-Sham orbitals and Kohn-Sham wavefunctions are Slater determinants of these orbitals. Via the Kohn-Sham equations, the orbitals are implicit functionals of $n(\mathbf{r})$. We emphasize that – although in DFT the particle density is the only basic variable – the Kohn-Sham orbitals are proper fermionic single-particle states. The ground-state Kohn-Sham wavefunction is obtained by occupying the N eigenstates with lowest eigenvalues. The corresponding density is

$$n(\mathbf{r}) = \sum_{i=1}^{N} n_i |\varphi_i(\mathbf{r})|^2, \tag{3.31}$$

with n_i the i^{th} occupation number.

In the next section, we consider the consequences of introducing the Kohn-Sham system in DFT.

Exchange-correlation energy functional

A large fraction of $F_{\text{HK}}[n]$ can be expressed in terms of kinetic and electrostatic energy. This decomposition is given by

$$F_{\text{HK}}[n] = T_s[n] + U[n] + E_{xc}[n] \ . \tag{3.32}$$

The first term is the kinetic energy of the Kohn-Sham system,

$$T_s[n] = -\frac{1}{2} \sum_{i=1}^{N} \int \mathrm{d}^3 r \ \varphi_i^*(\mathbf{r}) \nabla^2 \varphi_i(\mathbf{r}) \ . \tag{3.33}$$

The second is the Hartree energy (a.k.a. electrostatic self-energy, a.k.a. Coulomb energy),

$$U[n] = \frac{1}{2} \int \int d^3 r d^3 r' \ \frac{n(\mathbf{r}) n(\mathbf{r}')}{|\mathbf{r} - \mathbf{r}'|} \ . \tag{3.34}$$

The remainder is defined as the exchange-correlation energy,

$$E_{xc}[n] := F_{\mathrm{HK}}[n] - T_s[n] - U[n] \ . \tag{3.35}$$

For systems having more than one particle, E_{xc} accounts for exchange and correlation energy contributions. Comparing Eqs. (3.32) and (3.20), the total energy density functional is

$$E_{v,\mathrm{HK}}[n] = T_s[n] + U[n] + E_{xc}[n] + \int d^3r \ n(\mathbf{r})v(\mathbf{r}). \tag{3.36}$$

Consider now the Euler equations for the interacting and non-interacting system. Assuming the differentiability of the functionals (see Section 3.2.5), these necessary conditions for having energy minima are

$$\frac{\delta F_{\mathrm{HK}}}{\delta n(\mathbf{r})} + v(\mathbf{r}) = 0 \tag{3.37}$$

and

$$\frac{\delta T_s}{\delta n(\mathbf{r})} + v_s(\mathbf{r}) = 0, \tag{3.38}$$

respectively. With definition (3.32), from Eqs. (3.37) and (3.38), we obtain

$$v_s(\mathbf{r}) = v_H[n](\mathbf{r}) + v_{xc}[n](\mathbf{r}) + v(\mathbf{r}). \tag{3.39}$$

Here, $v(\mathbf{r})$ is the external potential acting upon the interacting electrons, $v_H[n](\mathbf{r})$ is the Hartree potential,

$$v_H[n](\mathbf{r}) = \int d^3r' \frac{n(\mathbf{r}')}{|\mathbf{r} - \mathbf{r}'|} = \frac{\delta U}{\delta n(\mathbf{r})}, \tag{3.40}$$

and $v_{xc}[n](\mathbf{r})$ is the exchange-correlation potential,

$$v_{xc}[n](\mathbf{r}) = \frac{\delta E_{xc}[n]}{\delta n(\mathbf{r})}. \tag{3.41}$$

Through the decomposition in Eq. (3.32), a significant part of F_{HK} is in the explicit form of $T_s[n] + U[n]$ without approximation. Though often small, the E_{xc} density functional still represents an important part of the total energy. Its exact functional form is unknown, and it therefore must be approximated in practice. However, good and surprisingly efficient approximations exist for E_{xc}.

We next consider reformulations of DFT, which allow analysis and solution of some important technical questions at the heart of DFT. They also have a long history of influencing the analysis of properties of the exact functionals.

3.2.4 Levy's formulation

An important consequence of the HK theorem is that the Rayleigh-Ritz variational principle based on the wavefunction can be replaced by a variational principle based on the particle density. The latter is valid for all densities in the set $\mathbf{D}$, the set of v-representable densities. Unfortunately, v-representability is a condition which is not easily verified for a given function $n(\mathbf{r})$. Hence it is highly desirable to formulate the variational principle over a set of densities characterized by simpler conditions. This was provided by Levy [148] and later reformulated and extended by Lieb [156]. In this and the sections that follow, Lebesgue and Sobolev spaces are defined in the usual way [50, 209].

First, the set $\mathbf{W}$ is enlarged to $\mathbf{W_N}$, which includes all possible antisymmetric and normalized N-particle wavefunctions Ψ. The set $\mathbf{W_N}$ now also contains N-particle wavefunctions which are *not* necessarily ground-state wavefunctions to some external potential v, though

it remains in the same Sobolev space [50] as $\mathbf{W}$: $\mathcal{H}^1(\mathbb{R}^{3N})$. Correspondingly, the set $\mathbf{D}$ is replaced by the set $\mathbf{D_N}$. $\mathbf{D_N}$ contains the densities generated from the N-particle antisymmetric wavefunctions in $\mathbf{W_N}$ using Eq. (3.6):

$$\mathbf{D_N} = \left\{ n \mid n(\mathbf{r}) \geq 0, \int d^3r \; n(\mathbf{r}) = N, n^{1/2}(\mathbf{r}) \in \mathcal{H}^1(\mathbb{R}^3) \right\}. \tag{3.42}$$

The densities of $\mathbf{D_N}$ are therefore called N-representable. Harriman's explicit construction [93] shows that any integrable and positive function $n(\mathbf{r})$ is N-representable.

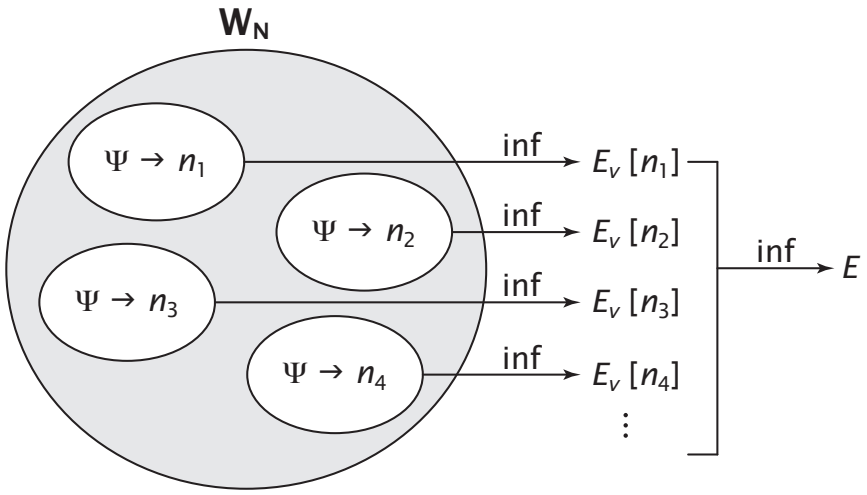

Figure 3.3: This diagram shows the two-step minimization of Levy's constrained search. The first infimum search is over all wavefunctions corresponding to a certain density n_i. The second search runs over all of the densities [74, 185].

Levy reformulated the variational principle in a constrained-search fashion (see Figure 3.3):

$$E_v = \inf_{n \in \mathbf{D_N}} \left\{ \inf_{\Psi \to n | \Psi \in \mathbf{W_N}} \langle \Psi | \hat{T} + \hat{V}_{ee} | \Psi \rangle + \int d^3r \; n(\mathbf{r}) v(\mathbf{r}) \right\}. \tag{3.43}$$

In this formulation, the search inside the braces is constrained to those wavefunctions which yield a given density n – therefore the name "constrained search". The minimum is then found by the outer search over all densities. The potential $v(\mathbf{r})$ acts like a Lagrangian multiplier to satisfy the constraint on the density at each point in space. In this formulation, F_{HK} is replaced by

$$F_{\mathrm{LL}}[n] := \inf_{\Psi \to n} \langle \Psi | \hat{T} + \hat{V}_{ee} | \Psi \rangle, \quad \text{with } \Psi \in \mathbf{W_N} \text{ and } n \in \mathbf{D_N} \; . \tag{3.44}$$

The functional E_{HK} can then be replaced by

$$E_{v,\mathrm{LL}}[n] := F_{\mathrm{LL}}[n] + \int d^3r \; n(\mathbf{r}) v(\mathbf{r}), \quad \text{with } n \in \mathbf{D_N}. \tag{3.45}$$

If, for a given v_0, the corresponding ground-state particle density, n_0, is inserted, then

$$E_{v_0,\mathrm{LL}}[n_0] = E_{v_0,\mathrm{HK}}[n_0] = E_{v_0}, \tag{3.46}$$

from which

$$F_{\mathrm{LL}}[n] = F_{\mathrm{HK}}[n], \quad \text{for all } n \; \in \; \mathbf{D} \; . \tag{3.47}$$

Furthermore, if any other particle density is inserted, we obtain

$$E_{v_0,\mathrm{LL}}[n] \geq E_{v_0}, \quad \text{for} \;\; n \neq n_0 \;\; \text{and } n \in \mathbf{D_N}. \tag{3.48}$$

In this approach, the degenerate case does not require particular care. In fact, the corre-

spondences between potentials, wavefunctions and densities are not explicitly employed as they were in the previous Hohenberg-Kohn formulation. However, the N-representability is of secondary importance in the context of the Kohn-Sham scheme. There, it is still necessary to assume that the densities of the interacting electrons are non-interacting v-representable as well. We discuss this point in more detail in the next section.

Though it can be shown that the $F_{\mathrm{LL}}[n]$ infimum is a minimum [156], the functional's lack of convexity causes a serious problem in proving the differentiability of F_{LL} [156]. Differentiability is needed to define an Euler equation for finding $n(\mathbf{r})$ self-consistently. This is somewhat alleviated by the Lieb formulation of DFT (see below).

3.2.5 Ensemble-DFT and Lieb's formulation

In the remainder of this section, we are summarizing more extensive and pedagogical reviews that can be found in Refs. [50], [43], and [248]. Differentiability of functionals is, essentially, related to the convexity of the functionals. Levy and Lieb showed that the set $\mathbf{D}$ is not convex [156]. In fact, there exist combinations of the form

$$n(\mathbf{r}) = \sum_{k=1}^{M} \lambda_k n_k(\mathbf{r}), \;\; \lambda_k = 1 \;\; (0 \leq \lambda_k \leq 1), \tag{3.49}$$

where n_k is the density corresponding to degenerate ground state Ψ_k, that are not in $\mathbf{D}$ [149, 156].

A convex set can be obtained by looking at ensembles. The density of an ensemble can be defined through the (statistical, or von Neuman) density operator

$$\hat{D} = \sum_{k=1}^{M} \lambda_k |\Psi_k\rangle\langle\Psi_k|, \quad \text{with} \;\; \sum_{k=1}^{M} \lambda_k = 1 \;\; (0 \leq \lambda_k \leq 1) \; . \tag{3.50}$$

The expectation value of an operator $\hat{O}$ on an ensemble is defined as

$$O := \mathrm{Tr}\left\{\hat{D}\hat{O}\right\}, \tag{3.51}$$

where the symbol "Tr" stands for the trace taken over an arbitrary, complete set of orthonormal N-particle states

$$\mathrm{Tr}\{\hat{D}\hat{O}\} := \sum_k \langle\Phi_k|(\hat{D}\hat{O})|\Phi_k\rangle. \tag{3.52}$$

The trace is invariant under unitary transformations of the complete set for the ground-state manifold of the Hamiltonian $\hat{H}$ [see Eq.(3.50)]. Since

$$\mathrm{Tr}\left\{\hat{D}\hat{O}\right\} = \sum_{k=1}^{M} \lambda_k \langle\Psi_k|\hat{O}|\Psi_k\rangle, \tag{3.53}$$

the energy obtained from a density matrix of the form (3.50) is the total ground-state energy of the system.

Densities of the form (3.49) are called ensemble v-representable densities, or E-V-densities. We denote this set of densities as $\mathbf{D_{EV}}$. Densities that can be obtained from a single wavefunction are said to be pure-state (PS) v-representable, or PS-V-densities. The functional F_{HK} can then be extended as [216]

$$F_{\mathrm{EHK}}[n] := Tr\left\{\hat{D}\left(\hat{T} + \hat{V}_{ee}\right)\right\}, \quad \text{with } n \in \mathbf{D_{EV}} \tag{3.54}$$

where $\hat{D}$ has the form (3.50) and is any density matrix giving the density n. However, the set $\mathbf{D_{EV}}$, just like $\mathbf{D}$, is difficult to characterize. Moreover, as for F_{HK} and F_{LL}, a proof of the differentiability of F_{EHK} (and for the non-interacting versions of the same functional) is not available.

In the Lieb formulation, however, differentiability can be addressed to some extent [89, 90, 156] . In the work of Lieb, $\mathbf{P}$ is restricted to $\mathbf{P} = \mathcal{L}^{\mathbf{3/2}}(\mathbb{R}^{\mathbf{3}}) + \mathcal{L}^{\infty}(\mathbb{R}^{\mathbf{3}})$ and wavefunctions are required to be in

$$\mathbf{W_N} = \{\Psi \mid ||\Psi|| = 1, T[\Psi] \leq \infty\} . \tag{3.55}$$

The universal functional is defined as

$$F_{\mathrm{L}}[n] := \inf_{\hat{D} \to n \in \mathbf{D_N}} Tr\left\{\hat{D}\left(\hat{T} + \hat{V}_{ee}\right)\right\}, \tag{3.56}$$

and it can be shown that the infimum is a minimum [156]. Note that in definition (3.56), $\hat{D}$ is a generic density matrix of the form

$$\hat{D} = \sum_k \lambda_k |\Psi_k\rangle\langle\Psi_k|, \quad \text{with } \sum_k \lambda_k = 1 \quad (0 \leq \lambda_k \leq 1) , \tag{3.57}$$

where $\Psi_k \in \mathbf{W_N}$. The sum is not restricted to a finite number of degenerate ground states as in Eq. (3.50). This minimization over a larger, less restricted set leads to the statements

$$F_{\mathrm{L}}[n] \leq F_{\mathrm{LL}}[n], \quad \text{for } n \in \mathbf{D_N}, \tag{3.58}$$

and

$$F_{\mathrm{L}}[n] = F_{\mathrm{LL}}[n] = F_{\mathrm{HK}}[n], \quad \text{for } n \in \mathbf{D} . \tag{3.59}$$

$F_{\mathrm{L}}[n]$ is defined on a convex set, and it is a convex functional. This implies that $F_{\mathrm{L}}[n]$ is differentiable at any ensemble v-representable densities and nowhere else [156]. Minimizing

the functional

$$E_{\mathrm{L}}[n] := F_{\mathrm{L}}[n] + \int d^3r \; n(\mathbf{r})v(\mathbf{r}) \tag{3.60}$$

with respect to the elements of $\mathbf{D_{EV}}$ by the Euler-Lagrange equation

$$\frac{\delta F_{\mathrm{L}}}{\delta n(\mathbf{r})} + v(\mathbf{r}) = 0 \tag{3.61}$$

is therefore well-defined on the set $\mathbf{D_{EV}}$ and generates a valid energy minimum.

We finally address, although only briefly, some important points about the Kohn-Sham scheme and its rigorous justification. The results for F_{L} carry over to $T_{\mathrm{L}}[n]$. That is, the functional

$$T_{\mathrm{L}}[n] = \inf_{\hat{D}\to n} Tr\left\{\hat{D}\hat{T}\right\}, \quad \text{with } n \in \mathbf{D_N} \tag{3.62}$$

is differentiable at any non-interacting ensemble v-representable densities and nowhere else. We can gather all these densities in the set $\mathbf{D^s_{EV}}$. Then, the Euler-Lagrange equation

$$\frac{\delta T_{\mathrm{L}}}{\delta n(\mathbf{r})} + v_s(\mathbf{r}) = 0 \tag{3.63}$$

is well defined on the set $\mathbf{D^s_{EV}}$ only. One can then redefine the exchange-correlation functional as

$$E_{xc,\mathrm{L}}[n] = F_{\mathrm{L}}[n] - T_{\mathrm{L}}[n] - U[n], \tag{3.64}$$

and observe that the differentiability of $F_{\mathrm{L}}[n]$ and $T_{\mathrm{L}}[n]$ implies the differentiability of $E_{xc}[n]$ only on $\mathbf{D_{EV}} \cap \mathbf{D^s_{EV}}$. The question as to the size of the latter set remains. For densities defined on a discrete lattice (finite or infinite) it is known [105] that $\mathbf{D_{EV}} = \mathbf{D^s_{EV}}$. Moreover,

in the continuum limit, $\mathbf{D_E}$ and $\mathbf{D_E^s}$ can be shown to be dense with respect to one another [89, 90, 156]. This implies that any element of $\mathbf{D_{EV}}$ can be approximated, with an arbitrary accuracy, by an element of $\mathbf{D_{EV}^s}$. But, whether or not the two sets coincide remains an open question.

3.3 Functional Approximations

Numerous approximations to E_{xc} exist, each with its own successes and failures [18]. The simplest is the local density approximation (LDA), which had early success with solids[132]. LDA assumes that the exchange-correlation energy density can be approximated locally with that of the uniform gas. DFT's popularity in the chemistry community skyrocketed upon development of the generalized gradient approximation (GGA) [192]. Inclusion of density gradient dependence generated sufficiently accurate results to be useful in many chemical and materials applications.

Today, many scientists use hybrid functionals, which substitute a fraction of single-determinant exchange for part of the GGA exchange [13, 14, 145]. More recent developments in functional approximations include meta-GGAs [197], which include dependence on the kinetic energy density, and hyper-GGAs [197], which include exact exchange as input to the functional. Inclusion of occupied and then unoccupied orbitals as inputs to functionals increases their complexity and computational cost; the idea that this increase is coupled with an increase in accuracy was compared to Jacob's Ladder [197]. The best approximations are based on the exchange-correlation hole, such as the real space cutoff of the LDA hole that ultimately led to the GGA called PBE [112, 194]. An introduction to this and some other exact properties of the functionals follows in the remainder of this section.

Another area of functional development of particular importance to the warm dense matter

community is focused on orbital-free functionals [43, 115, 117, 119, 250]. These approximations bypass solution of the Kohn-Sham equations by directly approximating the non-interacting kinetic energy. In this way, they recall the original, pure DFT of Thomas-Fermi theory [60, 61, 240]. While many approaches have been tried over the decades, including fitting techniques from computer science [229], no general-purpose solution of sufficient accuracy has been found yet.

3.3.1 Exact Conditions

Though we do not know the exact functional form for the universal functional, we do know some facts about its behavior and the relationships between its components. Collections of these facts are called exact conditions. Some can be found by inspection of the formal definitions of the functionals and their variational properties. The correlation energy and its constituents are differences between functionals evaluated on the true and Kohn-Sham systems. As an example, consider the kinetic correlation:

$$T_c[n] = T[n] - T_s[n]. \tag{3.65}$$

Since the Kohn-Sham kinetic energy is the lowest kinetic energy of any wavefunction with density $n(\mathbf{r})$, we know T_c must be non-negative. Other inequalities follow similarly, as well as one from noting that the exchange functional is (by construction) never positive [17]:

$$E_x \leq 0,\ E_c \leq 0,\ U_c \leq 0,\ T_c \geq 0. \tag{3.66}$$

Some further useful exact conditions are found by uniform coordinate scaling [152]. In the ground state, this procedure requires scaling all the coordinates of the wavefunction[3] by a positive constant γ, while preserving normalization to N particles:

$$\Psi_\gamma(\mathbf{r_1}, \mathbf{r_2}, ..., \mathbf{r_N}) = \gamma^{3N/2}\Psi(\gamma\mathbf{r_1}, \gamma\mathbf{r_2}, ..., \gamma\mathbf{r_N}), \tag{3.67}$$

which has a scaled density defined as

$$n_\gamma(\mathbf{r}) = \gamma^3 n(\gamma\mathbf{r}). \tag{3.68}$$

Scaling by a factor larger than one can be thought of as squeezing the density, while scaling by $\gamma < 1$ spreads the density out. For more details on the many conditions that can be extracted using this technique and how they can be used in functional approximations, see Ref. [17].

Of greatest interest in our context are conditions involving exchange-correlation and other components of the universal functional. Through application of the foregoing definition of uniform scaling, we can write down some simple uniform scaling equalities. Scaling the density yields

$$T_s[n_\gamma] = \gamma^2 T_s[n] \tag{3.69}$$

for the non-interacting kinetic energy and

$$E_x[n_\gamma] = \gamma\ E_x[n] \tag{3.70}$$

[3]Here and in the remainder of the chapter, we restrict ourselves to square-integrable wavefunctions over the domain $\mathbb{R}^{3N}$.

for the exchange energy. Such simple conditions arise because these functionals are defined on the non-interacting Kohn-Sham Slater determinant. On the other hand, although the density from a scaled interacting wavefunction is the scaled density, the scaled wavefunction is not the ground-state wavefunction of the scaled density. This means correlation scales less simply and only inequalities can be derived for it.

Another type of scaling that is simply related to coordinate scaling is interaction scaling, the adiabatic change of the interaction strength [195]. In the latter, the electron-electron interaction in the Hamiltonian, V_{ee}, is multiplied by a factor, λ between 0 and 1, while holding n fixed. When $\lambda = 0$, interaction vanishes. At $\lambda = 1$, we return to the Hamiltonian for the fully interacting system. Due to the simple, linear scaling of V_{ee} with coordinate scaling, we can relate it to scaling of interaction strength. Combining this idea with some of the simple equalities above leads to one of the most powerful relations in ground-state functional development, the adiabatic connection formula [87, 143]:

$$E_{xc}[n] = \int_0^1 d\lambda U_{xc}[n](\lambda), \tag{3.71}$$

where

$$U_{xc}[n](\lambda) = V_{ee}[\Psi^{\lambda}[n]] - U[n] \tag{3.72}$$

and $\Psi^{\lambda}[n]$ is the ground-state wavefunction of density n for a given λ and

$$\Psi^{\lambda}[n](\mathbf{r_1}, \mathbf{r_2}, ..., \mathbf{r_N}) = \lambda^{3N/2}\Psi[n_{1/\lambda}](\lambda\mathbf{r_1}, \lambda\mathbf{r_2}, ..., \lambda\mathbf{r_N}). \tag{3.73}$$

Interaction scaling also leads to some of the most important exact conditions for construction of functional approximations, the best of which are based on the exchange-correlation hole. The exchange-correlation hole represents an important effect of an electron sitting at a given

position. All other electrons will be kept away from this position by exchange and correlation effects, due to the antisymmetry requirement and the Coulomb repulsion, respectively. This representation allows us to calculate V_{ee}, the electron-electron repulsion, in terms of an electron distribution function.[4]

To define the hole distribution function, we need first to introduce the pair density function. The pair density, $P(\mathbf{r}, \mathbf{r}')$ describes the distribution of the electron pairs. This is proportional to the the probability of finding an electron in a volume d^3r around position $\mathbf{r}$ *and* a second electron in the volume d^3r' around $\mathbf{r}'$. In terms of the electronic wavefunction, it is written as follows

$$P(\mathbf{r}, \mathbf{r}') = N(N-1) \int d^3r_3 \ldots \int d^3r_N \; |\Psi(\mathbf{r}, \mathbf{r}', \ldots, \mathbf{r}_N)|^2. \tag{3.74}$$

We then can define the conditional probability density of finding an electron in d^3r' after having already found one at $\mathbf{r}$, which we will denote $n_2(\mathbf{r}, \mathbf{r}')$. Thus

$$n_2(\mathbf{r}, \mathbf{r}') = P(\mathbf{r}, \mathbf{r}')/n(\mathbf{r}). \tag{3.75}$$

If the positions of the electrons were truly independent of one another (no electron-electron interaction and no antisymmetry requirement for the wavefunction) this would be just $\rho(\mathbf{r}')$, independent of $\mathbf{r}$. But this cannot be, as

$$\int d^3r' \; n_2(\mathbf{r}, \mathbf{r}') = N - 1. \tag{3.76}$$

The conditional density integrates to one fewer electron, since one electron is at the reference point. We therefore define a "hole" density:

$$n_2(\mathbf{r}, \mathbf{r}') = n(\mathbf{r}') + n_{\text{hole}}(\mathbf{r}, \mathbf{r}'). \tag{3.77}$$

[4]For a more extended discussion of these topics, see Ref. [195].

which is typically negative and integrates to -1 [195]:

$$\int d^3r' \; n_{\text{hole}}(\mathbf{r}, \mathbf{r}') = -1. \tag{3.78}$$

The exchange-correlation hole in DFT is given by the coupling-constant average:

$$n_{xc}(\mathbf{r}, \mathbf{r}') = \int_0^1 d\lambda \; n^{\lambda}_{\text{hole}}(\mathbf{r}, \mathbf{r}'), \tag{3.79}$$

where $n^{\lambda}_{\text{hole}}$ is the hole in Ψ^{λ}. So, via the adiabatic connection formula (Eq. 3.71), the exchange-correlation energy can be written as a double integral over the exchange-correlation hole:

$$E_{xc} = \frac{1}{2} \int d^3r \; n(\mathbf{r}) \int d^3r' \; \frac{n_{xc}(\mathbf{r}, \mathbf{r}')}{|\mathbf{r} - \mathbf{r}'|}. \tag{3.80}$$

By definition, the exchange hole is given by $n_x = n^{\lambda=0}_{\text{hole}}$ and the correlation hole, n_c, is everything *not* in n_x. The exchange hole may be readily obtained from the (ground-state) pair-correlation function of the Kohn-Sham system. Moreover $n_x(\mathbf{r}, \mathbf{r}) = 0$, $n_x(\mathbf{r}, \mathbf{r}') \leq 0$, and for one particle systems $n_x(\mathbf{r}, \mathbf{r}') = -n(\mathbf{r}')$. If the Kohn-Sham state is a single Slater determinant, then the exchange energy assumes the form of the Fock integral evaluated with occupied Kohn-Sham orbitals. It is straightforward to verify that the exchange-hole satisfies the sum rule

$$\int d^3r' \; n_x(\mathbf{r}, \mathbf{r}') = -1 \; ; \tag{3.81}$$

and thus

$$\int d^3r' \; n_c(\mathbf{r}, \mathbf{r}') = 0 \; . \tag{3.82}$$

The correlation hole is a more complicated quantity, and its contributions oscillate from negative to positive in sign. Both the exchange and the correlation hole decay to zero at large distances from the reference position $\mathbf{r}$.

These and other conditions on the exact hole are used to constrain exchange-correlation functional approximations. The seemingly unreasonable reliability of the simple LDA has been explained as the result of the "correctness" of the LDA exchange-correlation hole [53, 109]. Since the LDA is constructed from the uniform gas, which has many realistic properties, its hole satisfies many mathematical conditions on this quantity [20]. Many of the most popular improvements on LDA, including the PBE generalized gradient approximation, are based on models of the exchange-correlation hole, not just fits of exact conditions or empirical data [194]. In fact, the most successful approximations usually are based on models for the exchange-correlation hole, which can be explicitly tested [24]. Unfortunately, insights about the ground-state exchange-correlation hole do not simply generalize as temperatures increase, as will be discussed later.

3.4 Thermal DFT

Thermal DFT deals with statistical ensembles of quantum states describing the thermodynamical equilibrium of many-electron systems. The grand canonical ensemble is particularly convenient to deal with the symmetry of identical particles. In the limit of vanishing temperature, thermal DFT reduces to an equiensemble ground state DFT description [56], which, in turn, reduces to the standard pure-state approach for non-degenerate cases.

While in the ground-state problem the focus is on the ground state energy, in the statistical mechanical framework the focus is on the grand canonical potential. Here, the grand canonical Hamiltonian plays an analogous role as the one played by the Hamiltonian for the

ground-state problem. The former is written

$$\hat{\Omega} = \hat{H} - \tau\hat{S} - \mu\hat{N}, \tag{3.83}$$

where $\hat{H}$, $\hat{S}$, and $\hat{N}$ are the Hamiltonian, entropy, and particle-number operators. The crucial quantity by which the Hamiltonian differs from its grand-canonical version is the entropy operator:[5]

$$\hat{S} = -\, k_B \ln\hat{\Gamma} \ , \tag{3.84}$$

where

$$\hat{\Gamma} = \sum_{N,i} w_{N,i} |\Psi_{N,i}\rangle\langle\Psi_{N,i}| \ . \tag{3.85}$$

$|\Psi_{N,i}\rangle$ are orthonormal N-particle states (that are not necessarily eigenstates in general) and $w_{N,i}$ are normalized statistical weights satisfying $\sum_{N,i} w_{N,i} = 1$. $\hat{\Gamma}$ allows us to describe the thermal ensembles of interest.

Observables are obtained from the statistical average of Hermitian operators

$$O[\hat{\Gamma}] = \text{Tr } \{\hat{\Gamma}\hat{O}\} = \sum_N \sum_i w_{N,i} \langle\Psi_{N,i}|\hat{O}|\Psi_{N,i}\rangle \ . \tag{3.86}$$

These expressions are similar to Eq. (3.53), but here the trace is not restricted to the ground-state manifold.

In particular, consider the average of the $\hat{\Omega}$, $\Omega[\hat{\Gamma}]$, and search for its minimum at a given temperature, τ, and chemical potential, μ. The quantum version of the Gibbs Principle ensures that the minimum exists and is unique (we shall not discuss the possible complications

[5]Note that, we eventually choose to work in a system of units such that the Boltzmann constant is $k_B = 1$, that is, temperature is measured in energy units.

introduced by the occurrence of phase transitions). The minimizing statistical operator is the grand-canonical statistical operator, with statistical weights given by

$$w^0_{N,i} = \frac{\exp[-\beta(E^0_{N,i} - \mu N)]}{\sum_{N,i} \exp[-\beta(E^0_{N,i} - \mu N)]}. \tag{3.87}$$

$E^0_{N,i}$ are the eigenvalues of N-particle eigenstates. It can be verified that $\Omega[\hat{\Gamma}]$ may be written in the usual form

$$\Omega = E - \tau S - \mu N = -k_B \tau \ln Z_G, \tag{3.88}$$

where Z_G is the grand canonical partition function; which is defined by

$$Z_G = \sum_N \sum_j e^{-\beta(E^0_{N,i} - \mu N)} \, . \tag{3.89}$$

The statistical description we have outlined so far is the standard one. Now, we wish to switch to a density-based description and thereby enjoy the same benefits as in the ground-state problem. To this end, the minimization of Ω can be written as follows:

$$\Omega^\tau_{v-\mu} = \min_\rho \left\{ F^\tau[n] + \int d^3r \; n(\mathbf{r})(v(\mathbf{r}) - \mu) \right\} \tag{3.90}$$

with $n(\mathbf{r})$ an ensemble N-representable density and

$$F^\tau[n] := \min_{\hat{\Gamma} \to n} F^\tau[\hat{\Gamma}] = \min_{\hat{\Gamma} \to n} \left\{ T[\hat{\Gamma}] + V_{ee}[\hat{\Gamma}] - \tau S[\hat{\Gamma}] \right\}. \tag{3.91}$$

This is the constrained-search analog of the Levy functional [148, 185], Eq. (3.44). It replaces the functional originally defined by Mermin [169] in the same way that Eq. (3.44) replaces Eq. (3.21) in the ground-state theory. [6]

[6] The interested reader may find the extension of the Hohenberg-Kohn theorem to the thermal framework in Mermin's paper.

Eq. (3.91) defines the thermal universal functional. Universality of this quantity means that *it does not depend explicitly on the external potential nor on* μ. This is very appealing, as it hints at the possibility of widely applicable approximations.

We identify $\Gamma^\tau[n]$ as the minimizing statistical operator in Eq. (3.91). We can then define other interacting density functionals at a given temperature by taking the trace over the given minimizing statistical operator. For example, we have:

$$T^\tau[n] := T[\hat{\Gamma}^\tau[n]] \tag{3.92}$$

$$V_{ee}^\tau[n] := V_{ee}[\hat{\Gamma}^\tau[n]] \tag{3.93}$$

$$S^\tau[n] := S[\hat{\Gamma}^\tau[n]]. \tag{3.94}$$

In order to introduce the thermal Kohn-Sham system, we proceed analogously as in the zero-temperature case. We assume that there exists an ensemble of non-interacting systems with same average particle density *and* temperature of the interacting ensemble. Ultimately, this determines the one-body Kohn-Sham potential, which includes the corresponding chemical potential. Thus, the noninteracting (or Kohn-Sham) universal functional is defined as

$$F_s^\tau[n] := \min_{\hat{\Gamma}\to n} K^\tau[\hat{\Gamma}] = K^\tau[\hat{\Gamma}_s^\tau[n]] = K_s^\tau[n], \tag{3.95}$$

where $\hat{\Gamma}_s^\tau[n]$ is a statistical operator that describes the Kohn-Sham ensemble and $K^\tau[\hat{\Gamma}] := T[\hat{\Gamma}] - \tau S[\hat{\Gamma}]$ is a combination we have chosen to call the kentropy.

We can also write the corresponding Kohn-Sham equations at non-zero temperature, which are analogous to Eqs. (3.30) and (3.39) [132]:

$$\left[-\frac{1}{2}\nabla^2 + v_s(\mathbf{r})\right]\varphi_i(\mathbf{r}) = \epsilon_i^\tau \varphi_i(\mathbf{r}) \tag{3.96}$$

$$v_s(\mathbf{r}) = v_H[n](\mathbf{r}) + v_{xc}[n](\mathbf{r}) + v(\mathbf{r}). \tag{3.97}$$

The accompanying density formula is

$$n(\mathbf{r}) = \sum_i f_i |\varphi_i(\mathbf{r})|^2, \tag{3.98}$$

where

$$f_i = \left(1 + e^{\left(\epsilon_i^\tau - \mu\right)/\tau}\right)^{-1}. \tag{3.99}$$

Eqs. (3.96) and (3.97) look strikingly similar to the case of non-interacting Fermions. However, the Kohn-Sham weights, f_i, are not simply the familiar Fermi functions, due to the temperature dependence of the Kohn-Sham eigenvalues.

Through the series of equalities in Eq. (3.95), we see that the non-interacting universal density functional is obtained by evaluating the kentropy on a non-interacting, minimizing statistical operator which, at temperature τ, yields the average particle density n. The seemingly simple notation of Eq. (3.95) reduces the kentropy first introduced as a functional of the statistical operator to a finite-temperature functional of the density. From the same expression, we see that the kentropy plays a role in this framework analogous to that of the kinetic energy within ground-state DFT. Finally, we spell-out the components of $F_s^\tau[n]$:

$$F_s^\tau[n] = T_s^\tau[n] - \tau S_s^\tau[n] \,, \tag{3.100}$$

where $T_s^\tau[n] := T[\hat{\Gamma}_s^\tau[n]]$ and $S_s^\tau[n] := S[\hat{\Gamma}_s^\tau[n]]$.

Now we identify other fundamental thermal DFT quantities. First, consider the decompo-

sition of the interacting grand-canonical potential as a functional of the density given by

$$\Omega^{\tau}_{v-\mu}[n] = F^{\tau}_{s}[n] + U[n] + \mathcal{F}^{\tau}_{xc}[n] + \int d^3r \; n(\mathbf{r})\,(v(\mathbf{r}) - \mu) \;\; . \tag{3.101}$$

Here, $U[n]$ is the Hartree energy having the form in Eq. (3.34). The adopted notation stresses that temperature dependence of $U[n]$ enters only through the input equilibrium density. The exchange-correlation free-energy density functional is given by

$$\mathcal{F}^{\tau}_{xc}[n] = F^{\tau}[n] - F^{\tau}_{s}[n] - U[n] \; . \tag{3.102}$$

It is also useful to introduce a further decomposition:

$$\mathcal{F}^{\tau}_{xc}[n] := \mathcal{F}^{\tau}_{x}[n] + \mathcal{F}^{\tau}_{c}[n] \; . \tag{3.103}$$

This lets us analyze the two terms on the right hand side along with their components.

The exchange contribution is

$$\mathcal{F}^{\tau}_{x}[n] = V_{\mathrm{ee}}[\Gamma^{\tau}_{s}[n]] - U[n] \; . \tag{3.104}$$

Note that the average on the right hand side is taken with respect to the Kohn-Sham ensemble and that kinetic and entropic contributions do not contribute to exchange effects explicitly. Interaction enters in Eq. (3.104) in a fashion that is reminiscent of (but not the same as) finite-temperature Hartree-Fock theory. In fact, $\mathcal{F}^{\tau}_{x}[n]$ may be expressed in terms of the square modulus of the finite-temperature Kohn-Sham one-body density matrix. Thus $\mathcal{F}^{\tau}_{x}[n]$ has an explicit, known expression, just as does $\mathcal{F}^{\tau}_{s}[n]$. For the sake of practical calculations, however, approximations are still needed.

The fundamental theorems of density functional theory were proven for any ensemble with monotonically decreasing weights [238] and were applied to extract excitations [85, 159, 173]. But simple approximations to the exchange for such ensembles are corrupted by ghost interactions [73] contained in the ensemble Hartree term. The Hartree energy defined in Eq. (3.34) is defined as the electrostatic self-energy of the density, both for ground-state DFT and at non-zero temperatures. But the physical ensemble of Hartree energies is in fact the Hartree energy of each ensemble member's density, added together with the weights of the ensembles. Because the Hartree energy is quadratic in the density, it therefore contains ghost interactions [73], i.e., cross terms, that are unphysical. These must be canceled by the exchange energy, which must therefore contain a contribution:

$$\Delta E_X^{GI} = \sum_i w_i U[n_i] - U\left[\sum_i w_i n_i\right]. \tag{3.105}$$

Such terms appear only when the temperature is non-zero and so are missed by any ground-state approximation to E_x.

Consider, now, thermal DFT correlations. We may expect correctly that these will be obtained as differences between interacting averages and the noninteracting ones. The kinetic correlation energy density functional is

$$T_c^\tau[n] := T^\tau[n] - T_s^\tau[n], \tag{3.106}$$

and similar forms apply to $S_c^\tau[n]$ and $K_c^\tau[n]$. Another important quantity is the correlation potential density functional. At finite-temperature, this is defined by

$$U_c^\tau[n] := V_{\rm ee}[\Gamma^\tau[n]] - V_{\rm ee}[\Gamma_s^\tau[n]]\,. \tag{3.107}$$

Finally, we can write the correlation free energy as follows

$$\mathcal{F}_c^\tau[n] = K_c^\tau[n] + U_c^\tau[n] = E_c^\tau[n] - \tau S_c^\tau[n] \tag{3.108}$$

where

$$K_c^\tau[n] = T_c^\tau[n] - \tau S_c^\tau[n] \tag{3.109}$$

is the correlation kentropy density functional and

$$E_c^\tau[n] := T_c^\tau[n] + U_c^\tau[n] \tag{3.110}$$

generalizes the expression of the correlation energy to finite temperature. Above, we have noticed that entropic contributions do not enter explicitly in the definition of $\mathcal{F}_x^\tau[n]$. From Eq. (3.108), on the other hand, we see that the correlation entropy is essential for determining $\mathcal{F}_c^\tau[n]$. Further, it may be grouped together the kinetic contributions (as in the first identity) or separately (as in the second identity), depending on the context of the current analysis.

In the next section, we consider finite-temperature analogs of the exact conditions described earlier for the ground state functionals. This allow us to gain additional insights about the quantities identified so far.

3.5 Exact Conditions at Non-Zero Temperature

In the following, we review several properties of the basic energy components of thermal Kohn-Sham DFT [45, 202].

We start with some of the most elementary properties, their signs [202]:

$$\mathcal{F}_x^\tau[n] \leq 0,\ \mathcal{F}_c^\tau[n] \leq 0,\ U_c^\tau[n] \leq 0,\ K_c^\tau[n] \geq 0. \tag{3.111}$$

The sign of $\mathcal{F}_x^\tau[n]$ is evident from the definition given in terms of the Kohn-Sham one-body reduced density matrix [50]. The others may be understood in terms of their variational properties. For example, let us consider the case for $K_c^\tau[n]$. We know that the Kohn-Sham statistical operator minimizes the kentropy

$$K_s^\tau[n] = K^\tau[\hat{\Gamma}_s^\tau[n]]\ . \tag{3.112}$$

Thus, we also know that $K_s^\tau[n]$ must be less than $K^\tau[n] = K^\tau[\Gamma^\tau[n]]$, where $\Gamma^\tau[n]$ is the equilibrium statistical operator. This readily implies that

$$K_c^\tau[n] = K^\tau[\hat{\Gamma}^\tau[n]] - K^\tau[\hat{\Gamma}_s^\tau[n]] \geq 0. \tag{3.113}$$

An approximation for $K_c^\tau[n]$ that does not respect this inequality will not simply have the "wrong" sign. Much worse is that results from such an approximation will suffer from improper variational character.

A set of remarkable and useful properties are the scaling relationships. What follows mirrors the zero-temperature case, but an important and intriguing difference is the relationship between coordinate and temperature scaling.

We first introduce the concept of uniform scaling of statistical ensembles in terms of a particular scaling of the corresponding statistical operators. [7] Wavefunctions of each state in the ensemble can be scaled as in Eq. (3.67). At the same time, we require that the statistical mixing is not affected, so the statistical weights are held fixed under scaling (we

[7] Uniform coordinate scaling may be considered as (very) careful dimensional analysis applied to density functionals. Dufty and Trickey analyze non-interacting functionals in this way in Ref. [45].

shall return to this point in Section 3.6.1). In summary, the scaled statistical operator is

$$\hat{\Gamma}_\gamma := \sum_N \sum_i w_{N,i} |\Psi_{\gamma,N,i}\rangle\langle\Psi_{\gamma,N,i}|, \tag{3.114}$$

where (the representation free) Hilbert space element $|\Psi_\gamma\rangle$ is such that $\Psi_\gamma(\mathbf{r}_1, ..., \mathbf{r}_N) = \langle \mathbf{r}_1, ..., \mathbf{r}_N | \Psi_\gamma \rangle$. For sake of simplicity, we restrict ourselves to states of the type typically considered in the ground-state formalism.

Eq. (3.114) leads directly to scaling relationships for any observable. For instance, we find

$$N[\hat{\Gamma}_\gamma] = N[\hat{\Gamma}], \tag{3.115}$$

$$T[\hat{\Gamma}_\gamma] = \gamma^2 T[\hat{\Gamma}], \text{ and} \tag{3.116}$$

$$S[\hat{\Gamma}_\gamma] = S[\hat{\Gamma}] \, . \tag{3.117}$$

Combining these, we find

$$\hat{\Gamma}_s^\tau[n_\gamma] = \hat{\Gamma}_{\gamma,s}^{\tau/\gamma^2}[n] \text{ and } F_s^\tau[n_\gamma] = \gamma^2 F_s^{\tau/\gamma^2}[n]. \tag{3.118}$$

Eq. (3.118) states that the value of the non-interacting universal functional evaluated at a scaled density is related to the value of the same functional evaluated on the unscaled density at a scaled temperature. Eq. (3.118) constitutes a powerful statement, which becomes more apparent by rewriting it as follows [202]:

$$F_s^{\tau'}[n] = \frac{\tau'}{\tau} F_s^\tau[\rho_{\sqrt{\tau/\tau'}}]. \tag{3.119}$$

This means that, if we know $F_s^\tau[n]$ at some non-zero temperature τ, we can find its value at any other temperature by scaling its argument.

Scaling arguments allow us to extract other properties of the functionals, such as some of

their limiting behaviors. For instance, we can show that in the "high-density" limit, the kinetic term dominates [202]:

$$T_s^{\infty}[n] = \lim_{\gamma \to +\infty} F_s[n_\gamma]/\tau^2 \tag{3.120}$$

while in the "low-density" limit, the entropic term dominates:

$$S_s^{\infty}[n] = \lim_{\gamma \to 0} F_s[n_\gamma]\tau. \tag{3.121}$$

Also, we may consider the interacting universal functional for a system with coupling strength equal to λ

$$F^{\tau,\lambda}[n] = \min_{\hat{\Gamma} \to n} \left\{ T[\hat{\Gamma}] + \lambda V_{ee}[\hat{\Gamma}] - \tau S[\hat{\Gamma}] \right\}, \tag{3.122}$$

and note that in general,

$$\hat{\Gamma}^{\tau,\lambda}[n] \neq \hat{\Gamma}^{\tau}[n]. \tag{3.123}$$

We can relate these two statistical operators [202]. In fact, one can prove

$$\hat{\Gamma}^{\tau,\lambda}[n] = \hat{\Gamma}_{\lambda}^{\tau/\lambda^2}[n_{1/\lambda}] \text{ and } F^{\tau,\lambda}[n] = \lambda^2 F^{\tau/\lambda^2}[n_{1/\lambda}]. \tag{3.124}$$

In the expressions above, a single superscript implies full interaction [202]. Eq. (3.124) demands scaling of the coordinates, the temperature, and the strength of the interaction at once. This procedure connects one equilibrium state to another equilibrium state, that of a "scaled" system. Eq. (3.124) may be used to state other relations similar to those discussed above for the non-interacting case.

Scaling relations combined with the Hellmann-Feynman theorem allow us to generate the

thermal analog of one of the most important statements of ground-state DFT, the adiabatic connection formula [202]:

$$\mathcal{F}_{xc}^{\tau}[n] = \int_0^1 d\lambda \; U_{xc}^{\tau}[n](\lambda), \tag{3.125}$$

where

$$U_{xc}^{\tau}[n](\lambda) = V_{ee}[\hat{\Gamma}^{\tau,\lambda}[n]] - U[n] \tag{3.126}$$

and a superscript λ implies an electron-electron interaction strength equal to λ. The interaction strength runs between zero, corresponding to the noninteracting Kohn-Sham system, and one, which gives the fully interacting system. All this must be done while keeping the density constant. In thermal DFT, an expression like Eq. (3.125) offers the appealing possibility of defining an approximation for $\mathcal{F}_{xc}^{\tau}[n]$ *without* having to deal with kentropic contributions explicitly.

Another interesting relation generated by scaling connects the exchange-correlation to the exchange-only free energy [202]:

$$\mathcal{F}_{x}^{\tau}[n] = \lim_{\gamma\to\infty} \mathcal{F}_{xc}^{\gamma^2\tau}[n_\gamma]/\gamma. \tag{3.127}$$

This may be considered the definition of the exchange contribution in an xc functional, and so Eq. (3.127) may also be used to extract an approximation for the exchange free energy, if an approximation for the exchange-correlation free energy as a whole is given (for example, if obtained from Eq. (3.125)).

Despite decades of research [38, 199, 200, 201], thermal exchange-correlation GGAs have not been fully developed. The majority of the applications in the literatures have adopted two *practical* methods: one uses plain finite-temperature LDA, the other uses ground-state GGAs

within the thermal Kohn-Sham scheme. This latter method ignores any modification to the exchange-correlation free energy functional due to its non-trivial temperature dependence. As new approximations are developed, exact conditions such as those above are needed to define consistent and reliable thermal approximations.

3.6 Discussion

In this section, we discuss several aspects that may not have been fully clarified by the previous, relatively abstract sections. First, by making use of a simple example, we will illustrate in more detail the tie between temperature and coordinate scaling. Then, with the help of another example, we will show how scaling and other exact properties of the functionals can guide development and understanding of approximations. The last subsection notes some complications in importing tools directly from ground-state methods to thermal DFT.

3.6.1 Temperature and Coordinate Scaling

Here we give an illustration of how the scaling of the statistical operators introduced in the previous section is applicable to thermal ensembles. Our argument applies – with proper modifications and additions, such as the scaling of the interaction strength – to all Coulomb-interacting systems with all one-body external potentials. For sake of simplicity, we shall restrict ourselves to non-interacting fermions in a one-dimensional harmonic oscillator at thermodynamic equilibrium.

Let us start from the general expression of the Fermi occupation numbers

$$n_i(\tau, \mu\epsilon_i) = \left(1 + e^{\beta(\epsilon_i - \mu)}\right)^{-1}, \tag{3.128}$$

where ϵ_i is the i^{th} eigenvalue of the harmonic oscillator, $\epsilon_i = \omega(i + 1/2)$. For our system, the (time-independent) Schrödinger equation is:

$$\left\{-\frac{1}{2}\frac{d^2}{dx^2} + v(x)\right\}\phi_i(x) = \epsilon_i\phi_i(x)\ . \tag{3.129}$$

Now, we multiply the x-coordinates by γ

$$\left\{-\frac{1}{2\gamma^2}\frac{d^2}{dx^2} + v(\gamma x)\right\}\phi_i(\gamma x) = \epsilon_i\phi_i(\gamma x). \tag{3.130}$$

We then multiply both sides by γ^2:

$$\left\{-\frac{1}{2}\frac{d^2}{dx^2} + \gamma^2 v(\gamma x)\right\}\phi_i(\gamma x) = \gamma^2\epsilon_i\phi_i(\gamma x). \tag{3.131}$$

Substituting $\tilde{v}(x) = \gamma^2 v(\gamma x)$, $\tilde{\phi}_i(x) = \sqrt{\gamma}\phi_i(\gamma x)$ (to maintain normalization), and $\tilde{\epsilon}_i = \gamma^2\epsilon_i$ yields

$$\left\{-\frac{1}{2}\frac{d^2}{dx^2} + \tilde{v}(x)\right\}\tilde{\phi}_i(x) = \tilde{\epsilon}_i\tilde{\phi}_i(x). \tag{3.132}$$

The latter may be interpreted as the Schrödinger equation for a "scaled" system. In the special case of the harmonic oscillator,

$$\gamma^2 v(\gamma x) = \gamma^4 v(x), \tag{3.133}$$

the frequency scales quadratically, consistent with the scaling of the energies described just above. Now, let us look at the occupation numbers for the "scaled" system

$$n_i(\tau, \tilde{\mu}, \tilde{\epsilon}_i) = \left(1 + e^{\beta(\tilde{\epsilon}_i - \tilde{\mu})}\right)^{-1}, \tag{3.134}$$

where $\tilde{\mu} = \gamma^2\mu$ (in this way, the average number of particle is kept fixed too). These

occupation numbers are equal to those of the original system at a temperature τ/γ^2,

$$n_i(\tau, \tilde{\mu}, \tilde{\epsilon}_i) = n_i(\tau/\gamma^2, \mu, \epsilon_i). \tag{3.135}$$

Thus the statistical weights of the scaled system are precisely those of the original system, at a suitably scaled temperature.

3.6.2 Thermal-LDA for Exchange Energies

In ground-state DFT, uniform coordinate scaling of the exchange has been used to constrain the form of the exchange-enhancement factor in GGAs. In thermal DFT, a "reduction" factor, R_x, enters already in the expression of a LDA for the exchange energies. This lets us capture the reduction in exchange with increasing temperature, while keeping the zero-temperature contribution well-separated from the modification entirely due to non-vanishing temperatures.

The behavior of R_x can be understood using the basic scaling relation for the exchange free energy. Observe that, from the scaling of $\hat{\Gamma}_s^{\tau}$, U, and $V_{ee}[\Gamma_s^\tau[n]]$, one readily arrives at

$$\mathcal{F}_x^\tau[n_\gamma] = \gamma \mathcal{F}_x^{\tau/\gamma^2}[n]. \tag{3.136}$$

Since

$$\mathcal{F}_x^{\mathrm{LDA},\tau}[n] = \int d^3r \; f_x^\tau(n(r)), \tag{3.137}$$

Eq. (3.136) implies that a thermal-LDA exchange free energy density must have the form [202]

$$f_x^{\mathrm{unif},\tau}(n) = e_x^{\mathrm{unif}}(n) R_x(\Theta), \tag{3.138}$$

where $e_x^{\text{unif}}(n) = -A_x n^{4/3}$, $A_x = (3/4\pi)(3\pi^2)^{1/3}$, and R_x can only depend on τ and n through the electron degeneracy $\Theta = 2\tau/(3\pi^2 n(\mathbf{r}))^{2/3}$.

The LDA is exact for the uniform electron gas and so automatically satisfies many conditions. As such, it also reduces to the ground-state LDA as temperature drops to zero:

$$R_x \to 1 \text{ as } \tau \to 0. \tag{3.139}$$

Moreover, for fixed n, we expect

$$\mathcal{F}_x^\tau / U \to 0 \text{ as } \tau \to \infty \tag{3.140}$$

because the effect of the Pauli exclusion principle drops off as the behavior of the system becomes more classical. Moreover, since $U[n]$ does not depend explicitly on the temperature, fixing n also fixes U. We conclude that, the reduction factor must drop to zero:

$$R_x \to 0 \text{ as } \tau \to \infty. \tag{3.141}$$

Now, let us consider the parameterization of R_x for the uniform gas by Perrot and Dharma-Wardana [200]:

$$R_x^{\text{unif}}(\Theta) \approx \left(\frac{4}{3}\right) \frac{0.75 + 3.04363\Theta^2 - 0.092270\Theta^3 + 1.70350\Theta^4}{1 + 8.31051\Theta^2 + 5.1105\Theta^4} \text{tanh}\Theta^{-1} \,, \tag{3.142}$$

Here, $\Theta = \tau/\epsilon_F = 2\tau/k_F^2$ and k_F is the Fermi wavevector. Note the factor of $4/3$ that is not present in their original paper, which arises because we include a factor of $3/4$ in A_x they do not. Fig. 3.4 shows the plot of this reduction factor. From both Fig. 3.4 and Eq. (3.142), it is apparent that the parametrization satisfies all the exact behaviors discussed just above.

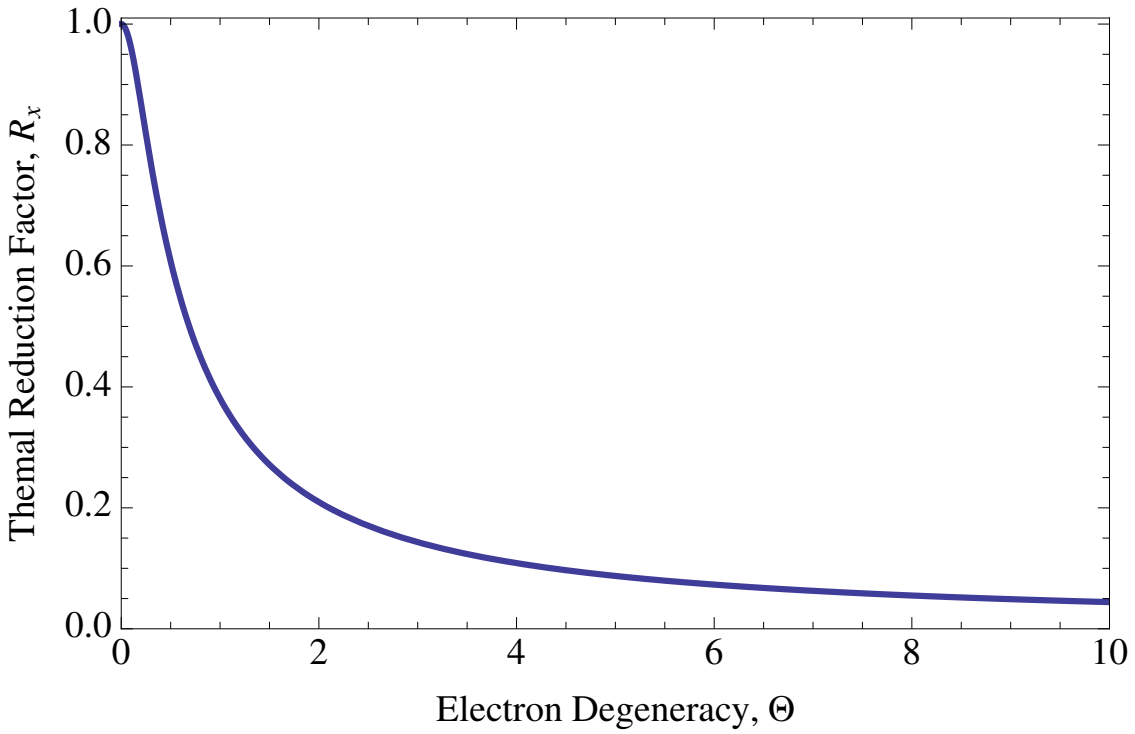

Figure 3.4: Perrot and Dharma-Wardana's parameterization [200] of the thermal reduction factor for the exchange free energy for the uniform gas is plotted versus the electron degeneracy parameter

3.6.3 Exchange-Correlation Hole at Non-Zero Temperature

Previously, we have emphasized that in ground-state DFT, the exchange-correlation hole function was vital for constructing reliable approximations. Therefore, it is important to reconsider this quantity in the context of thermal DFT. As we show below, this does not come without surprises.

In the grand canonical ensemble, the pair correlation function is a sum over statistically weighted pair correlation functions of each of the states in the ensemble labeled with collective index, ν (in this section, we follow notation and convention of Refs. [190] and [139]). A state $\Psi_{\lambda,\nu}$ has particle number N_ν, energy E_ν, and corresponds to λ-scaled interaction. If its weight in the ensemble is denoted as

$$w_{\lambda,\nu} = \frac{e^{-\beta(E_{\lambda,\nu}-\mu N_\nu)}}{\sum_\nu e^{-\beta(E_{\lambda,\nu}-\mu N_\nu)}}, \tag{3.143}$$

the ensemble average of the exchange-correlation hole density is

$$\left\langle n^\lambda_{xc}(\mathbf{r},\mathbf{r}')\right\rangle = \sum_\nu w_{\lambda,\nu} n^\lambda_{xc,\nu}(\mathbf{r},\mathbf{r}'). \tag{3.144}$$

However, the exchange-correlation hole function used to obtain $\mathcal{F}^\tau_{xc}$ through a λ integration requires the addition of more complicated terms [139]:

$$n^\lambda_{xc}(\mathbf{r},\mathbf{r}') = \left\langle n^\lambda_{xc}(\mathbf{r},\mathbf{r}')\right\rangle + \sum_\nu w_{\lambda,\nu}\frac{[n_{\lambda,\nu}(\mathbf{r})-n(\mathbf{r})]}{n(\mathbf{r})}[n_{\lambda,\nu}(\mathbf{r}')+n^\lambda_{xc,\nu}(\mathbf{r},\mathbf{r}')], \tag{3.145}$$

where $n^\lambda_{xc,\nu}$ is the usual exchange-correlation hole corresponding to $\Psi_{\lambda,\nu}$ with particle density $n_{\lambda,\nu}$.

Thus, the sum rule stated in the ground state gets modified as follows [191]

$$\int d^3r' \; n_{xc}^{\lambda}(\mathbf{r}, \mathbf{r}') = -1 + \sum_{\nu} w_{\lambda,\nu} \frac{n_{\lambda,\nu}(\mathbf{r})}{n(\mathbf{r})} [N_\nu - \langle N \rangle]. \tag{3.146}$$

The last expression shows that the sum rule for the thermal exchange-correlation hole accounts for an additional term due to particle number fluctuations. Worse still, this term carries along with it state-dependent, and therefore system-dependent, quantities. This is an important warning that standard methodologies for producing reliable ground-state functional approximations must be properly revised for use in the thermal context.

3.7 Conclusion

Thermal density functional theory is an area ripe for development in both fundamental theory and the construction of approximations because of rapidly expanding applications in many areas. Projects underway in the scientific community include construction of temperature-dependent GGAs [204], exact exchange methods for non-zero temperatures [82], orbital-free approaches at non-zero temperatures [121], and continued examination of the exact conditions that may guide both of these developments [204]. In the world of warm dense matter, simulations are being performed, often very successfully [203], generating new insights into both materials science and the quality of our current approximations [205]. As discussed above, techniques honed for zero-temperature systems should be carefully considered before being applied to thermal problems. Studying exact properties of functionals may guide efficient progress in application to warm dense matter. In context, thermal DFT emerges as as a clear and solid framework that provides users and developers practical and formal tools of general fundamental relevance.

We would like to thank the Institute for Pure and Applied Mathematics for organization of

Workshop IV: Computational Challenges in Warm Dense Matter and for hosting APJ during the Computational Methods in High Energy Density Physics long program. APJ thanks the U.S. Department of Energy (DE-FG02-97ER25308), SP and KB thank the National Science Foundation (CHE-1112442), and SP and EKUG thank European Community's FP7, CRONOS project, Grant Agreement No. 280879.

Part IV

Ensemble DFT

Chapter 4

Excitations and benchmark ensemble density functional theory for two electrons

written with Zeng-hui Yang, John R. Trail, Kieron Burke, Richard J. Needs, and Carsten A. Ullrich. Published in *J. Chem. Phys.* **140** 18A541 (2014).

Abstract: *A new method for extracting ensemble Kohn-Sham potentials from accurate excited state densities is applied to a variety of two electron systems, exploring the behavior of exact ensemble density functional theory. The issue of separating the Hartree energy and the choice of degenerate eigenstates is explored. A new approximation, spin eigenstate Hartree-exchange (SEHX), is derived. Exact conditions that are proven include the signs of the correlation energy components, the virial theorem for both exchange and correlation, and the asymptotic behavior of the potential for small weights of the excited states. Many energy components are given as a function of the weights for two electrons in a one-dimensional flat box, in a box with a large barrier to create charge transfer excitations, in a three-dimensional harmonic well*

(Hooke's atom), and for the He atom singlet-triplet ensemble, singlet-triplet-singlet ensemble, and triplet bi-ensemble.

4.1 Introduction and illustration

Ground-state density functional theory[99, 132] (DFT) is a popular choice for finding the ground-state energy of electronic systems,[18] and excitations can now easily be extracted using time-dependent DFT[32, 162, 214, 243] (TDDFT). Despite its popularity, TDDFT calculations have many well-known difficulties,[103, 160, 181, 245] such as double excitations[48] and charge-transfer excitations.[44, 242] Alternative DFT treatments of excitations[69, 77, 151] are always of interest.

Ensemble DFT (EDFT)[85, 86, 159, 238] is one such alternative approach. Unlike TDDFT, it is based on an energy variational principle.[86, 239] An ensemble of monotonically decreasing weights is constructed from the $M+1$ lowest levels of the system, and the expectation value of the Hamiltonian over orthogonal trial wavefunctions is minimized by the $M+1$ exact lowest eigenfunctions.[86] A one-to-one correspondence can be established between ensemble densities and potentials for a given set of weights, providing a Hohenberg-Kohn theorem, and application to non-interacting electrons of the same ensemble density yields a Kohn-Sham scheme with corresponding equations.[85] In principle, this yields the exact ensemble energy, from which individual excitations may be extracted.

But to make a practical scheme, approximations must be used.[68, 170, 173, 174, 225] These have been less successful for EDFT than those of ground-state DFT[13, 14, 112, 145, 194] and TDDFT,[107, 162] and their accuracy is not yet competitive with TDDFT transition frequencies from standard approximations. Some progress has been made in identifying some major sources of error.[73, 235, 236]

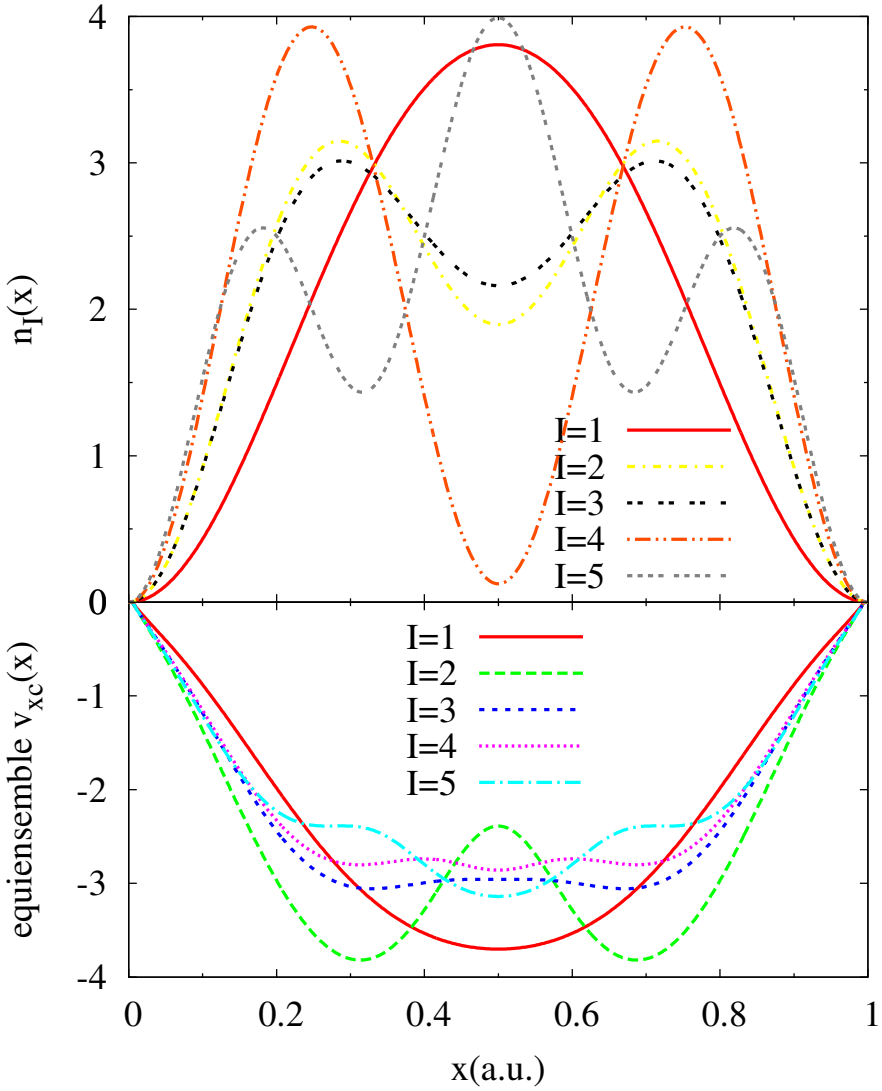

Figure 4.1: Exact densities and equiensemble exchange-correlation potentials of the 1D box with two electrons. The third excited state ($I = 4$) is a double excitation. See Sec. 4.6.1.

To help speed up that progress, we have developed a numerical algorithm to calculate ensemble Kohn-Sham (KS) quantities (orbital energies, energy components, potentials, etc.) essentially exactly,[257] from highly accurate excited-state densities. In the present paper, we provide reference KS calculations and results for two-electron systems under a variety of conditions. The potentials we find differ in significant ways from the approximations suggested so far, hopefully leading to new and better approximations.

To illustrate the essential idea, we perform calculations on simple model systems. For example, Sec. 4.6.1 presents two 'electrons' in a one-dimensional box, repelling one another via a (slightly softened) Coulomb repulsion. In Fig. 4.1, we show their ground- and excited-state densities, with I indicating the specific ground or excited state. We also plot the ensemble exchange-correlation potentials for equally weighted mixtures of the ground and excited states, which result from our inversion scheme. In this lower plot, $I = 1$ denotes the ground-state exchange-correlation potential, and $I > 1$ indicates the potential corresponding to an equal mixture of the ground state and all multiplets up to and including the I-th state. Excitation energies for all these states are extracted using the EDFT methods described below.

The paper is laid out as follows. In the next section, we briefly review the state-of-the-art for EDFT, introducing our notation. Then we give some formal considerations about how to define the Hartree energy. The naive definition, taken directly from ground-state DFT, introduces spurious unphysical contributions (which then must be corrected-for) called 'ghost' corrections.[73] We also consider how to make choices among KS eigenstates when they are degenerate, and show that such choices matter to the accuracy of the approximations. We close that section by showing how to construct symmetry-projected ensembles.

In the following section, we prove a variety of exact conditions within EDFT. Such conditions have been vital in constructing useful approximations in ground-state DFT.[152, 194] Following that, we describe our numerical methods in some detail.

The results section consists of calculations for quite distinct systems, but all with just two electrons. The one-dimensional flat box was used for the illustration here, which also gives rise to double excitations. A box with a high, asymmetric barrier produces charge-transfer excitations. Hooke's atom is a three-dimensional system, containing two Coulomb-repelling electrons in a harmonic oscillator external potential.[62] It has proven useful in the past to test ideas and approximations in both ground-state and TDDFT calculations.[97] We close the section reporting several new results for the He atom, using ensembles that include low-lying triplet states. Atomic units [$e = \hbar = m_e = 1/(4\pi\epsilon_0) = 1$] are used throughout unless otherwise specified.

4.2 Background

4.2.1 Basic theory

The ensemble variational principle[86] states that, for an ensemble of the lowest $M+1$ eigenstates $\Psi_0, \ldots, \Psi_M$ of the Hamiltonian $\hat{H}$ and a set of orthonormal trial functions $\tilde{\Psi}_0, \ldots, \tilde{\Psi}_M$,

$$\sum_{m=0}^{M} \mathtt{w}_m \left\langle \tilde{\Psi}_m \middle| \hat{H} \middle| \tilde{\Psi}_m \right\rangle \geq \sum_{m=0}^{M} \mathtt{w}_m E_m, \tag{4.1}$$

when the set of weights $\mathtt{w}_m$ satisfies

$$\mathtt{w}_0 \geq \mathtt{w}_1 \geq \ldots \geq \mathtt{w}_m \geq \ldots \geq 0, \tag{4.2}$$

and E_m is the eigenvalue of the mth eigenstate of $\hat{H}$. Equality holds only for $\tilde{\Psi}_m = \Psi_m$. The density matrix of such an ensemble is defined by

$$\hat{D}_{\mathcal{W}} = \sum_{m=0}^{M} \mathtt{w}_m |\Psi_m\rangle\langle\Psi_m|, \tag{4.3}$$

where w denotes the entire set of weight parameters. Properties of the ensemble are then defined as traces of the corresponding operators with the density matrix. The ensemble density $n_{\mathcal{W}}(\mathbf{r})$ is

$$n_{\mathcal{W}}(\mathbf{r}) = \mathrm{tr}\{\hat{D}_{\mathcal{W}}\hat{n}(\mathbf{r})\} = \sum_{m=0}^{M} \mathtt{w}_m n_m(\mathbf{r}), \tag{4.4}$$

and the ensemble energy $E_{\mathcal{W}}$ is

$$E_{\mathcal{W}} = \mathrm{tr}\{\hat{D}_{\mathcal{W}}\hat{H}\} = \sum_{m=0}^{M} \mathtt{w}_m E_m. \tag{4.5}$$

$n_{\mathcal{W}}(\mathbf{r})$ is normalized to the number of electrons, implying $\sum_{m=0}^{M} \mathtt{w}_m = 1$.

A Hohenberg-Kohn (HK)[99] type theorem for the one-to-one correspondence between $n_{\mathcal{W}}(\mathbf{r})$ and the potential in $\hat{H}$ has been proven,[85, 238] so all ensemble properties are functionals of $n_{\mathcal{W}}(\mathbf{r})$, including $\hat{D}_{\mathcal{W}}$. The ensemble HK theorem allows the definition of a non-interacting KS system, which reproduces the exact $n_{\mathcal{W}}(\mathbf{r})$. The existence of an ensemble KS system assumes ensemble v-representability. EDFT itself, however, only requires ensemble non-interacting N-representability, since a constrained-search formalism is available.[85, 91] Ensemble N- and v-representability are not yet proven, only assumed.

As in the ground-state case, only the ensemble energy functional is formally known, which is

$$E_{\mathcal{W}}[n] = F_{\mathcal{W}}[n] + \int \mathrm{d}^3 r \; n(\mathbf{r}) v(\mathbf{r}), \tag{4.6}$$

where $v(\mathbf{r})$ is the external potential. The ensemble universal functional $F_{\mathcal{W}}$ is defined as

$$F_{\mathcal{W}}[n] = \mathrm{tr}\{\hat{D}_{\mathcal{W}}[n](\hat{T} + \hat{V}_{\mathrm{ee}})\}, \tag{4.7}$$

where $\hat{T}$ and $\hat{V}_{\mathrm{ee}}$ are the kinetic and electron-electron interaction potential operators, respectively. The ensemble variational principle ensures that the ensemble energy functional evaluated at the exact ensemble density associated with $v(\mathbf{r})$ is the minimum of this functional, Eq. (4.5).

The ensemble KS system is defined as the non-interacting system that reproduces $n_{\mathcal{W}}(\mathbf{r})$ and satisfies the following non-interacting Schrödinger equation:

$$\left\{-\frac{1}{2}\nabla^2 + v_{\mathrm{s},\mathcal{W}}[n_{\mathcal{W}}](\mathbf{r})\right\}\phi_{j,\mathcal{W}}(\mathbf{r}) = \epsilon_{j,\mathcal{W}}\phi_{j,\mathcal{W}}(\mathbf{r}). \tag{4.8}$$

The ensemble KS system has the same set of $\mathtt{w}_m$ as the interacting system. This consistency has non-trivial implications even for simple systems. This will be explored more in Sec. 4.2.2.

The KS density matrix $\hat{D}_{\mathrm{s},\mathcal{W}}$ is

$$\hat{D}_{\mathrm{s},\mathcal{W}} = \sum_{m=0}^{M} \mathtt{w}_m |\Phi_m\rangle\langle\Phi_m|, \tag{4.9}$$

where Φ_m are non-interacting N-particle wavefunctions, usually assumed to be single Slater determinants formed by KS orbitals $\phi_{j,\mathcal{W}}$. We find that this choice can be problematic, and it will be discussed in Sec. 4.3.1. The ensemble density $n_{\mathcal{W}}(\mathbf{r})$ is reproduced by the KS system, meaning

$$n_{\mathcal{W}}(\mathbf{r}) = \sum_{m=0}^{M} \mathtt{w}_m n_m(\mathbf{r}) = \sum_{m=0}^{M} \mathtt{w}_m n_{\mathrm{s,m}}(\mathbf{r}), \tag{4.10}$$

where $n_m(\mathbf{r}) = \langle \Psi_m | \hat{n}(\mathbf{r}) | \Psi_m \rangle$, and $n_{\mathrm{S,m}}(\mathbf{r}) = \langle \Phi_m | \hat{n}(\mathbf{r}) | \Phi_m \rangle$. The KS densities of the individual states are generally not related to those of the interacting system; only their weighted sums are equal, as in Eq. (4.10).

$E_{\mathcal{W}}[n]$ is decomposed as in ground-state DFT,

$$\begin{aligned} E_{\mathcal{W}}[n] &= T_{\mathrm{S},\mathcal{W}}[n] + V[n] + E_{\mathrm{H}}[n] + E_{\mathrm{XC},\mathcal{W}}[n] \\ &= \mathrm{tr}\{\hat{D}_{\mathrm{S},\mathcal{W}}\hat{T}\} + \int \mathrm{d}^3 r \; n(\mathbf{r}) v(\mathbf{r}) \\ &\quad + E_{\mathrm{H}}[n] + E_{\mathrm{XC},\mathcal{W}}[n], \end{aligned} \tag{4.11}$$

where only the ensemble exchange-correlation (XC) energy $E_{\mathrm{XC},\mathcal{W}}$ is unknown. The form of $v_{\mathrm{S},\mathcal{W}}(\mathbf{r})$ is then determined according to the variational principle by requiring $\delta E_{\mathcal{W}}[n_{\mathcal{W}}]/\delta n_{\mathcal{W}}(\mathbf{r}) = 0$, resulting in

$$v_{\mathrm{S},\mathcal{W}}[n_{\mathcal{W}}](\mathbf{r}) = v(\mathbf{r}) + v_{\mathrm{H}}[n_{\mathcal{W}}](\mathbf{r}) + v_{\mathrm{XC},\mathcal{W}}[n_{\mathcal{W}}](\mathbf{r}), \tag{4.12}$$

where $v_{\mathrm{H}}[n](\mathbf{r}) = \delta E_{\mathrm{H}}[n]/\delta n(\mathbf{r})$, and $v_{\mathrm{XC},\mathcal{W}}[n](\mathbf{r}) = \delta E_{\mathrm{XC},\mathcal{W}}[n]/\delta n(\mathbf{r})$. E_{H} is generally defined to have the same form as the ground-state Hartree energy functional. Although this choice is reasonable, we find that it is more consistent to consider E_{HX}, the combined Hartree and exchange energy. This point will be discussed in Sec. 4.3.1.

The ensemble universal functional $F_{\mathcal{W}}[n]$ depends on the set of weights $\mathtt{w}_m$. Ref. [85] introduced the following set of weights, so that only one parameter $\mathtt{w}$ is needed:

$$\mathtt{w}_m = \begin{cases} \frac{1-\mathtt{w}g_I}{M_I - g_I} & m < M_I - g_I, \\ \mathtt{w} & m \geq M_I - g_I, \end{cases} \tag{4.13}$$

where $\mathtt{w} \in [0, 1/M_I]$. In this ensemble, here called GOK for the authors Gross, Oliveira, and Kohn,[73] I denotes the set of degenerate states (or 'multiplet') with the highest energy in

the ensemble, g_I is the multiplicity of the I-th multiplet, and M_I is the total number of states up to the I-th multiplet. GOK ensembles must contain full sets of degenerate states to be well-defined. The weight parameter $\mathtt{w}$ interpolates between two ensembles: the equiensemble up to the I-th multiplet ($\mathtt{w} = 1/M_I$) and the equiensemble up to the $(I-1)$-th multiplet ($\mathtt{w} = 0$). All previous studies of EDFT have been based on this type of ensemble.

The purpose of EDFT is to calculate excited-state properties, not ensemble properties. With the GOK ensemble, the excitation energy of multiplet I from the ground state, ω_I, is obtained using ensembles up to the I-th multiplet as

$$\omega_I = \frac{1}{g_I} \left.\frac{\partial E_{I,\mathtt{w}}}{\partial \mathtt{w}}\right|_{\mathtt{w}=\mathtt{w}_I} + \sum_{i=0}^{I-1} \frac{1}{M_i} \left.\frac{\partial E_{i,\mathtt{w}}}{\partial \mathtt{w}}\right|_{\mathtt{w}=\mathtt{w}_i}, \tag{4.14}$$

which simplifies to

$$\omega_1 = \omega_{\mathrm{s},1,\mathtt{w}} + \left.\frac{\partial E_{\mathrm{XC},\mathtt{w}}[n]}{\partial \mathtt{w}}\right|_{n=n_{\mathtt{w}}} \tag{4.15}$$

for the first excitation energy. Eq. (5.10) holds for any valid $\mathtt{w}_i$'s if the ensemble KS systems are exact, despite every term in Eq. (5.10) being $\mathtt{w}$-dependent. No existing $E_{\mathrm{XC},\mathtt{w}}$ approximations satisfy this condition.[159, 173]

Levy[150] pointed out that there is a special case for $\mathtt{w} \to 0$ of bi-ensembles ($I = 2$, with all degenerate states within a multiplet having the same density),

$$\begin{aligned} \Delta v_{\mathrm{XC}} &= \lim_{\mathtt{w}\to 0} \left.\frac{\partial E_{\mathrm{XC},\mathtt{w}}[n]}{\partial \mathtt{w}}\right|_{n=n_{\mathtt{w}}} \\ &= \left[\lim_{\mathtt{w}\to 0} v_{\mathrm{XC},\mathtt{w}}[n_{\mathtt{w}}](\mathbf{r})\right] - v_{\mathrm{xc},\mathtt{w}=0}[n_{\mathtt{w}=0}](\mathbf{r}) \end{aligned} \tag{4.16}$$

for finite r, where Δv_{XC} is the change in the KS highest-occupied-molecular-orbital (HOMO) energy between $\mathtt{w} = 0$ (ground state) and $\mathtt{w} \to 0_+$.[1] Δv_{XC} is a property of electron-number-neutral excitations, and should not be confused with the ground-state derivative discontinuity

Δ_{XC}, which is related to ionization energies and electron affinities.[43]

4.2.2 Degeneracies in the Kohn-Sham system

Taking the He atom as our example, the interacting system has a non-degenerate ground state, triply degenerate first excited state, and a non-degenerate second excited state. However, the KS system has a four-fold degenerate first excited state (corresponding to four Slater determinants), due to the KS singlet and triplet being degenerate (Fig. 4.2). Consider an ensemble of these states with arbitrary, decreasing weights, in order to work with the most general case. Represent the ensemble energy functional Eq. (4.5) as the KS ensemble energy, $E_{\mathrm{s},\mathcal{W}}$, plus a correction, $G_{\mathcal{W}}$. This correction then must encode the switch from depending only on the sum of the weights of the excited states as a whole in the KS case to depending on the sum of triplet weights and the singlet weight separately.

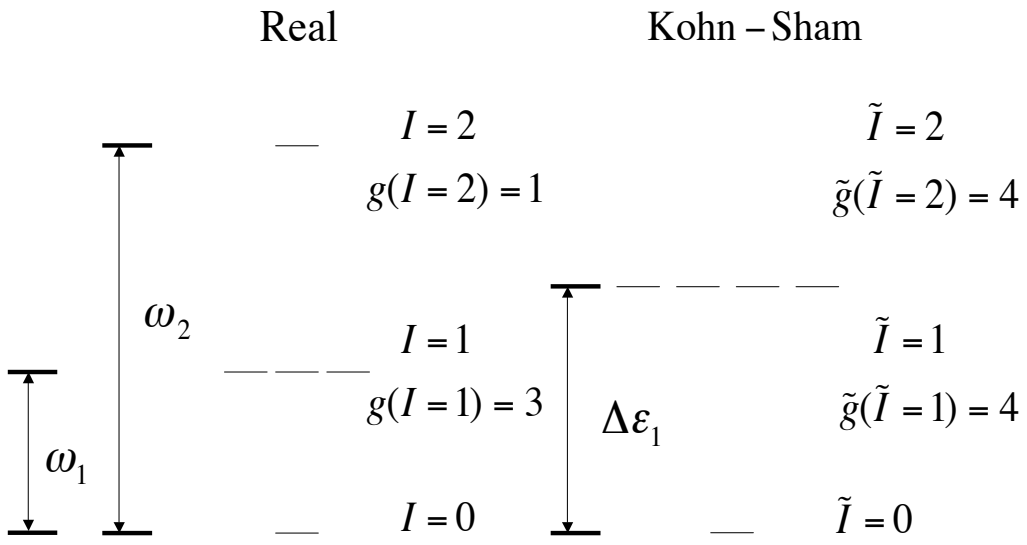

Figure 4.2: Diagram of the interacting and KS multiplicity structure for He. Degeneracy of the I-th multiplet is $g(I)$; tildes denote KS values. For instance, $\tilde{I} = 2$ refers to the KS multiplet used to construct the second (singlet) multiplet of the real system ($I = 2$), as is described in Sec. 4.3.2.

For the interacting system, the ensemble energy and density take the forms

$$\begin{aligned} E_{\mathcal{W}} &= E_0 + \mathtt{w}_{\mathrm{T}}\omega_1 + \mathtt{w}_{\mathrm{S}}\omega_2, \\ n_{\mathcal{W}}(\mathbf{r}) &= n_0(\mathbf{r}) + \mathtt{w}_{\mathrm{T}}\Delta n_1(\mathbf{r}) + \mathtt{w}_{\mathrm{S}}\Delta n_2(\mathbf{r}), \end{aligned} \tag{4.17}$$

where $\omega_i = E_i - E_0$, and so on, $\mathtt{w}_{\mathrm{T}}$ is the sum of the triplet weights, and $\mathtt{w}_{\mathrm{S}}$ is the singlet weight. On the other hand, for the KS system we have

$$\begin{aligned} E_{\mathrm{S},\mathcal{W}} &= E_{\mathrm{S},0} + \left(\mathtt{w}_{\mathrm{T}} + \mathtt{w}_{\mathrm{S}}\right)\Delta\epsilon_{1,\mathtt{w}}, \\ n_{\mathcal{W}}(\mathbf{r}) &= 2\left|\phi_{1s}\right|^2 + \left(\mathtt{w}_{\mathrm{T}} + \mathtt{w}_{\mathrm{S}}\right)\left(\left|\phi_{2s}\right|^2 - \left|\phi_{1s}\right|^2\right). \end{aligned} \tag{4.18}$$

Each of the weights must be the same for the non- interacting and interacting systems, in order to define an adiabatic connection, but $\mathtt{w}_{\mathrm{T}}$ may differ from $\mathtt{w}_{\mathrm{S}}$. If they are equal as in some ensemble treatments, variational principles for ensembles may be connected to statistical mechanics and one another more readily.[186]

The functional $G_{\mathcal{W}} = E_{\mathcal{W}} - E_{\mathrm{S},\mathcal{W}}$ in this case is

$$G_{\mathcal{W}}[n_{\mathcal{W}}] = E_0 - E_{\mathrm{s},0} + \mathtt{w}_{\mathrm{T}}\left(\omega_1 - \Delta\epsilon_1\right) + \mathtt{w}_{\mathrm{S}}\left(\omega_2 - \Delta\epsilon_1\right), \tag{4.19}$$

showing that, in its most general form, the exact ensemble energy functional (which can also be decomposed as in Eq. (4.11)) has to encode the change in the multiplet structure between non-interacting and interacting systems, even for a simple system like the He atom. Such information is unknown *a priori* for general systems, and can be very difficult to incorporate into approximations. In light of this difficulty, some researchers opt to use single-Slater-determinant states and equal weights for degenerate states.[186] However, we show that this problem can be alleviated if the degeneracies are the result of symmetry. This will be discussed in Sec. 4.3.3.

4.2.3 Approximations

Available approximations to the ensemble E_{XC} include the quasi-local-density approximation (qLDA) functional[131, 159] and the 'ghost'-corrected exact exchange (EXX) functional.[73, 173] The qLDA functional is based on the equiensemble qLDA,[131] and it interpolates between two consecutive equiensembles:[159]

$$E_{\mathrm{XC,I,w}}^{\mathrm{qLDA}}[n] = (1 - M_I\mathtt{w})E_{\mathrm{XC,I-1}}^{\mathrm{eqLDA}}[n] + M_I\mathtt{w}E_{\mathrm{XC,I}}^{\mathrm{eqLDA}}[n], \tag{4.20}$$

where $E_{\mathrm{XC}}^{\mathrm{eqLDA}}$ is the equiensemble qLDA functional defined in terms of finite-temperature LDA in Ref. [131].

The ensemble Hartree energy is defined analogously to the ground-state Hartree energy as shown in Eq. (4.11). Similarly, Nagy provides a definition of the exchange energy for bi-ensembles:[173]

$$E_{\mathrm{X,w}}^{\mathrm{Nagy}}[n_\uparrow, n_\downarrow] = -\frac{1}{2}\sum_\sigma \int \mathrm{d}^3r\mathrm{d}^3r' \, \frac{|n_\sigma(\mathbf{r},\mathbf{r}')|^2}{|\mathbf{r}-\mathbf{r}'|}, \tag{4.21}$$

where $n_\sigma(\mathbf{r},\mathbf{r}')$ is the reduced density matrix defined analogously to its ground-state counterpart, assuming a spin-up electron is excited in the first excited state:

$$n_{\sigma,\mathtt{w}}(\mathbf{r},\mathbf{r}') = \sum_{j=1}^{N_\sigma} n_{j,\sigma}(\mathbf{r},\mathbf{r}') + \delta_{\sigma,\uparrow}\mathtt{w}\left(n_{\mathrm{L}\uparrow}(\mathbf{r},\mathbf{r}') - n_{\mathrm{H}\uparrow}(\mathbf{r},\mathbf{r}')\right), \tag{4.22}$$

with $n_{j,\sigma}(\mathbf{r},\mathbf{r}') = \phi_{j,\sigma}(\mathbf{r})\phi_{j,\sigma}^*(\mathbf{r}')$, $L\uparrow = N_\uparrow + 1$ and $H\uparrow = N_\uparrow$, the spin-up lowest-unoccupied-molecular-orbital (LUMO) and HOMO, respectively. Both E_{H} in Eq. (4.11) and (4.21) contain 'ghost' terms,[73] which are cross-terms between different states in the ensemble due to the summation form of $n_{\mathtt{w}}(\mathbf{r})$ in Eq. (4.4) and $n_{\mathtt{w}}(\mathbf{r},\mathbf{r}')$ in Eq. (4.22). An EXX functional is obtained after such spurious terms are corrected. As an example of the GPG X energy functional[73] (named for its creators Gidopoulos, Papaconstinou, and Gross), take two-state

ensembles constructed as in the Nagy example above. For this simplified case, the GPG X energy functional is

$$E_{\mathrm{x},\mathtt{w}}^{\mathrm{GPG}}[n_\uparrow, n_\downarrow] = \int \frac{\mathrm{d}^3 r \mathrm{d}^3 r'}{|\mathbf{r}-\mathbf{r}'|} \left\{ -\frac{1}{2}\left(n_\sigma(\mathbf{r},\mathbf{r}')\right)^2 + \mathtt{w}\overline{\mathtt{w}}\left[n_{\mathrm{H}\uparrow}(\mathbf{r},\mathbf{r}')n_{\mathrm{L}\uparrow}(\mathbf{r},\mathbf{r}') - n_{\mathrm{H}\uparrow}(\mathbf{r}')n_{\mathrm{H}\uparrow}(\mathbf{r}')\right] \right\}, \tag{4.23}$$

where $\overline{\mathtt{w}} = 1 - \mathtt{w}$. These 'ghost' corrections are small compared to the Hartree and exchange energies. However, they are large corrections to the excitation energies, as Eq. (5.10) contains energy derivatives instead of energies. Table 4.1 shows a few examples.

With the help of the exact ensemble KS systems to be presented in this paper, we construct a new approximation, the motivation and justification of which will be explained in Secs. 4.3.1 and 4.3.2.

4.3 Theoretical considerations

In this section, we review important definitions and extend EDFT to improve the consistency and generality of the theory.

4.3.1 Choice of Hartree energy

The energy decomposition in Eq. (4.11) is analogous to its ground-state counterpart. However, unlike T_S and V, the choices for E_H and E_X and E_C are ambiguous; only their sum is uniquely determined. As shown in Eq. (4.11) and (4.21), definitions for E_H and E_X can introduce 'ghost' terms. Corrections can be considered either a part of E_H and E_X or a part of E_C. Such correction terms also take a complicated form when generalized to multi-state ensembles.

A more natural way of defining E_{H} and E_{XC} for ensembles can be achieved by considering the purpose of this otherwise arbitrary energy decomposition. In the ground-state case, the electron-electron repulsion reduces[154] to the Hartree energy for large Z, which is a simple functional of the density. The remaining unknown, E_{XC} (and its components E_{X} and E_{C}), is a small portion of the total energy, so errors introduced by approximations to it are small.

For ensembles, we review a slightly different energy decomposition proposed by Nagy.[174, 175] Instead of defining E_{H} and E_{X} in analogy to their ground-state counterparts, first define the combined Hartree-exchange energy E_{HX}, which is the more fundamental object in EDFT. E_{HX} can be explicitly represented as the trace of the KS density matrix:

$$E_{\text{HX},\mathcal{W}} = \text{tr}\{\hat{D}_{\text{S},\mathcal{W}}\hat{V}_{\text{ee}}\} = \sum_{m=0}^{M} \mathtt{w}_m \left\langle \Phi_m \middle| \hat{V}_{\text{ee}} \middle| \Phi_m \right\rangle . \tag{4.24}$$

For the ground state, both Hartree and exchange contributions are first-order in the adiabatic coupling constant, while correlation consists of all higher-order terms. According to the definition above, this property in the ensemble is retained. Eq. (4.24) contains no 'ghost' terms by definition, eliminating the need to correct them.[175] As a consequence, the correlation energy, E_{C}, is defined and decomposed as

$$E_{\text{C},\mathcal{W}} = E_{\text{HXC},\mathcal{W}} - E_{\text{HX},\mathcal{W}} = T_{\text{C},\mathcal{W}} + U_{\text{C},\mathcal{W}}, \tag{4.25}$$

where $E_{\text{HXC},\mathcal{W}} = E_{\mathcal{W}} - T_{\text{S},\mathcal{W}} - V$, $T_{\text{C},\mathcal{W}} = T_{\mathcal{W}} - T_{\text{S},\mathcal{W}}$ and $U_{\text{C},\mathcal{W}} = E_{\text{C},\mathcal{W}} - T_{\text{C},\mathcal{W}}$.

This form of E_{HX} reveals a deeper problem in EDFT. As demonstrated in Sec. 4.2.2, the multiplet structure of real and KS He atoms is different. Real He has a triplet state and a singlet state as the first and second excited states, but KS He has four degenerate single Slater determinants as the first excited states. Worse, the KS single Slater determinants are not eigenstates of the total spin operator $\hat{S}^2$, so their ordering is completely arbitrary. The KS system is constructed to yield only the real spin densities, not other quantities. KS wavefunc-

tions that are not eigenstates of $\hat{S}^2$ do not generally affect commonly calculated ground-state DFT properties,[196] but things are clearly different in EDFT. Consider the bi-ensemble of the ground state and the triplet excited state of He. Then $E_{\mathrm{HX},\mathtt{w}}[\rho_{\mathtt{w}}]$ depends on which three of the four KS excited-state Slater determinants are chosen, though it must be uniquely defined. Therefore, we choose the KS wavefunctions in EDFT to be linear combinations of the degenerate KS Slater determinants, preserving spatial and spin symmetries and eliminating ambiguity in E_{HX}. We note here that GPG allows use of spin eigenstates[73] as in their own atomic calculations, but we *require* it from our approximation. Such multi-determinant, spin eigenstates are also required for construction of symmetry-projected ensembles, as described in Sec. 4.3.3.

With E_{HX} fixed, the definitions of E_{H} and E_{X} depend on one another, but E_{C} does not. Defining a Hartree functional in the same form as the ground-state

$$U[n] = \frac{1}{2}\int \mathrm{d}^3r \int \mathrm{d}^3r' \, \frac{n(\mathbf{r})n(\mathbf{r})}{|\mathbf{r}-\mathbf{r}'|}, \tag{4.26}$$

we can examine different definitions for the GOK ensemble. A 'ghost'-free ensemble Hartree, $E_{\mathrm{H}}^{\mathrm{ens}}$, can be defined as

$$E_{\mathrm{H},\mathtt{w}}^{\mathrm{ens}} = \sum_{m=0}^{M} \mathtt{w}_m U[n_m], \tag{4.27}$$

i.e., the ensemble sum of the Hartree energies of the interacting densities, or as the slightly different

$$E_{\mathrm{H},\mathtt{w}}^{\mathrm{KS\ ens}} = \sum_{m=0}^{M} \mathtt{w}_m U[n_{\mathrm{s},m}], \tag{4.28}$$

i.e., the ensemble sum of the Hartree energies of the KS densities. The traditional Hartree

definition,

$$E_{\mathrm{H},\mathtt{w}}^{\mathrm{trad}} = U[n_{\mathtt{w}}], \tag{4.29}$$

introduces 'ghost' terms through the fictitious interaction of ground- and excited-state densities. Traditional and ensemble definitions differ in their production of 'ghosts,' as well as in their $\mathtt{w}$-dependence. The 'ghost'-corrected E_{H} in Ref. [73]

$$E_{\mathrm{H},\mathtt{w}}^{\mathrm{GPG}} = \sum_{m=0}^{M} \mathtt{w}_m^2 U[n_{\mathrm{s},m}] \tag{4.30}$$

has a different form from Eq. (4.28), which is also 'ghost'-free. Each of these definitions of E_{H} reduces to the ground-state E_{H} when $\mathtt{w}_0 = 1$ and satisfies simple inequalities such as $E_{\mathrm{H}} > 0$ and $E_{\mathrm{X}} < 0$. However, this ambiguity in the definition of E_{H} requires that an approximated ensemble E_{XC} be explicit about its compatible E_{H} definition.

The different flavors of $E_{\mathrm{H},\mathtt{w}}$ are compared for the He singlet ensemble[257] in Fig. 4.3. Even though $E_{\mathrm{H},\mathtt{w}}^{\mathrm{ens}}$ and $E_{\mathrm{H},\mathtt{w}}^{\mathrm{KS\ ens}}$ do not contain 'ghost' terms by definition, their magnitude is slightly bigger than that of $E_{\mathrm{H}}^{\mathrm{trad}}$, which is not 'ghost'-free. This apparent contradiction stems from $E_{\mathrm{H},\mathtt{w}}^{\mathrm{ens}}$ and $E_{\mathrm{H},\mathtt{w}}^{\mathrm{KS\ ens}}$ depending linearly on $\mathtt{w}$, while $E_{\mathrm{H},\mathtt{w}}^{\mathrm{trad}}$ depends on $\mathtt{w}$ quadratically. The quadratic dependence on $\mathtt{w}$ is made explicit with the 'ghost'-corrected $E_{\mathrm{H},\mathtt{w}}^{\mathrm{GPG}}$ of Ref. [73]. Comparing with the 'ghost'-free $E_{\mathrm{H},\mathtt{w}}^{\mathrm{ens}}$ and $E_{\mathrm{H},\mathtt{w}}^{\mathrm{KS\ ens}}$, it is clear that $E_{\mathrm{H}}^{\mathrm{GPG}}$ overcorrects in a sense, and is compensated by an over-correction of the opposite direction in $E_{\mathrm{X}}^{\mathrm{GPG}}$.

The traditional definition of Eq. (4.29) has the advantage that $v_{\mathrm{H}}(\mathbf{r})$ is a simple functional derivative with respect to the ensemble density. Any other definition requires solving an optimized effective potential (OEP)[223, 232]-type equation to obtain v_{H}. On the other hand, an approximated E_{XC} compatible with $E_{\mathrm{H}}^{\mathrm{trad}}$ requires users to approximate the corresponding 'ghost' correction as part of E_{XC}. Since the ghost correction is usually non-negligible, this is a major source of error for the qLDA functional.

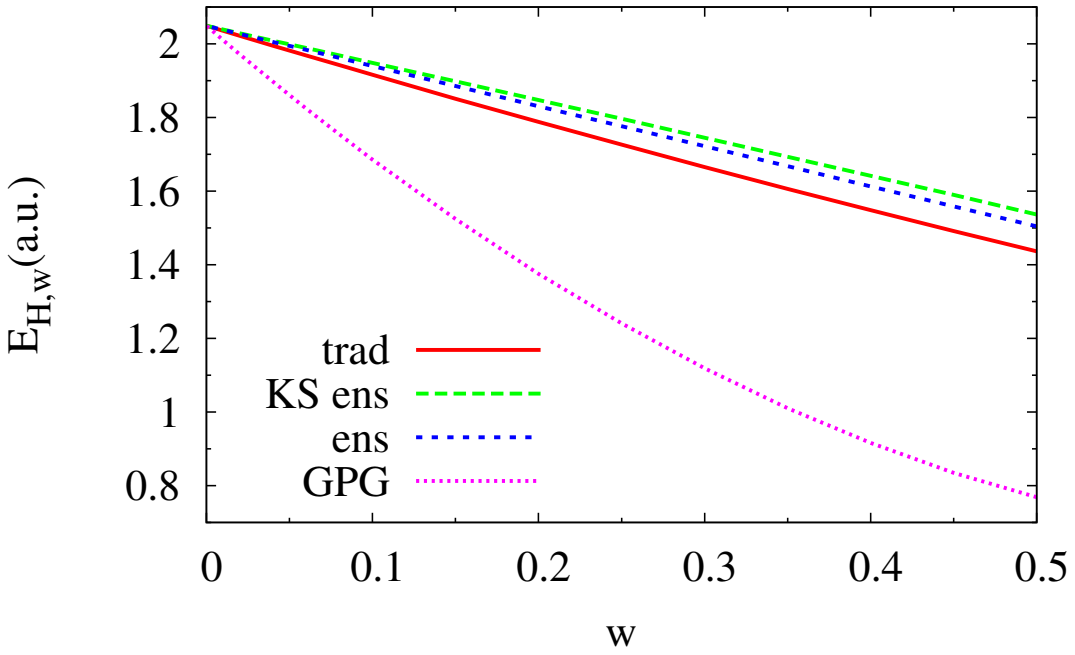

Figure 4.3: Behaviors of the different ensemble Hartree energy definitions for the singlet ensemble of He.

4.3.2 Symmetry-eigenstate Hartree-exchange (SEHX)

We have now identified E_{HX} as being more consistent with the EDFT formalism than E_{H} and E_{X}. Having also justified multi-determinant ensemble KS wavefunctions, we now derive a spin-consistent EXX potential, the symmetry-eigenstate Hartree-exchange (SEHX). Define the two-electron repulsion integral

$$(\mu\nu \mid \kappa\lambda) = \int \frac{\mathrm{d}^3 r \mathrm{d}^3 r'}{|\mathbf{r} - \mathbf{r}'|} \phi_\mu^*(\mathbf{r}) \phi_\nu^*(\mathbf{r}') \phi_\kappa(\mathbf{r}) \phi_\lambda(\mathbf{r}') \tag{4.31}$$

and

$$L_{\mu\nu\kappa\lambda} = (\mu\nu \mid \kappa\lambda)\, \delta_{\sigma_\mu,\sigma_\kappa} \delta_{\sigma_\nu,\sigma_\lambda}. \tag{4.32}$$

$\phi_\mu(\mathbf{r})$ denotes the μ-th KS orbital and σ_μ its spin state. If the occupation of the p-th Slater determinant of the μ-th KS orbital of the $\tilde{i}$-th multiplet of the KS system is $f_{p\mu}^{(\tilde{i})}$, define

$$\alpha_{\mu,\nu,\kappa,\lambda}^{(i,k)} = \sum_{p=1}^{\tilde{g}(\tilde{i})} C_p^{(i,k)} f_{p,\mu}^{(\tilde{i})} f_{p,\nu}^{(\tilde{i})} \prod_{\eta\neq\mu,\nu,\kappa,\lambda}^{\tilde{g}(\tilde{i})} \delta_{f_{p,\eta}^{\tilde{i}}, f_{q,\eta}^{\tilde{i}}} \tag{4.33}$$

for the q-dependent kth state of the ith multiplet of the exact system. $\tilde{g}(\tilde{i})$ is the KS multiplicity of the i-th multiplet, and C's are the coefficients of the multi-determinant wavefunctions defined by

$$\Psi_{\mathrm{s}}^{(i,k)}(\mathbf{r}_1,\ldots,\mathbf{r}_N) = \sum_{p=1}^{\tilde{g}(\tilde{i})} C_p^{(i,k)} \tilde{\Psi}_{\mathrm{s},p}^{\tilde{i}}(\mathbf{r}_1,\ldots,\mathbf{r}_N). \tag{4.34}$$

$\tilde{\Psi}_{\mathrm{s}}$ is a KS single Slater determinant. Note the numbering of the KS multiplets, $\tilde{i}$, depends on i, the numbering of the exact multiplet structure. The C coefficients are chosen according to the spatial and spin symmetries of the exact state. Now, with p and q KS single Slater determinants of the KS multiplet, define

$$h_{\mu\nu\kappa\lambda}^{(i,k)} = \sum_{q=1}^{\tilde{g}(\tilde{i})} \left(\alpha_{\mu,\nu,\kappa,\lambda}^{(i,k)} \alpha_{\kappa,\lambda,\mu,\nu}^{(i,k)} - \left(C_q^{(i,k)}\right)^2 f_{q,\mu}^{(\tilde{i})} f_{q,\nu}^{(\tilde{i})} f_{q,\kappa}^{(\tilde{i})} f_{q,\lambda}^{(\tilde{i})} \right), \tag{4.35}$$

in order to write

$$H^{(i,k)} = \sum_{\substack{\mu,\nu>\mu \\ \kappa,\lambda>\kappa}} \left(L_{\mu\nu\kappa\lambda} - L_{\mu\nu\lambda\kappa}\right) h_{\mu\nu\kappa\lambda}^{(i,k)}. \tag{4.36}$$

Then, if

$$G^{(i,k)} = \sum_{\mu,\nu>\mu} \left(L_{\mu\mu\nu\nu} - \Re L_{\mu\nu\mu\nu}\right) \sum_{p=1}^{\tilde{g}(\tilde{i})} \left|C_p^{(i,k)}\right|^2 f_{p,\mu}^{\tilde{i}} f_{p,\nu}^{\tilde{i}}, \tag{4.37}$$

the Hartree-exchange energy for up to the I-th multiplet is

$$E_{\mathrm{HX},\mathcal{W}}^{\mathrm{SEHX}} = \sum_{i=1}^{I} \sum_{k=1}^{g(i)} \mathtt{w}^{(i,k)} \left\{ G^{(i,k)} + H^{(i,k)} \right\}, \tag{4.38}$$

where $g(i)$ is the exact multiplicity of the i-th multiplet. The $v_{\mathrm{HX},\mathcal{W}}$ potential is then

$$\begin{aligned} v_{\mathrm{HX},\mathcal{W},\sigma}^{\mathrm{SEHX}}(\mathbf{r}) &= \frac{\delta E_{\mathrm{HX},\mathcal{W}}}{\delta n_{\mathcal{W},\sigma}(\mathbf{r})} \\ &= \int \mathrm{d}^3 r' \sum_j \frac{\delta E_{\mathrm{HX},\mathcal{W}}}{\delta \phi_{j,\sigma}(\mathbf{r}')} \frac{\delta \phi_{j,\sigma}(\mathbf{r}')}{\delta n_{\mathcal{W},\sigma}(\mathbf{r})} + \mathrm{c.c.}, \end{aligned} \tag{4.39}$$

which yields an OEP-type equation for $v_{\mathrm{HX},\mathcal{W}}(\mathbf{r})$.

The $v_{\mathrm{HX},\mathcal{W}}(\mathbf{r})$ of Eq. (4.39) produces no 'ghost' terms. For closed-shell systems, Eq. (4.39) yields $v_{\mathrm{HX},\mathcal{W},\uparrow}(\mathbf{r}) = v_{\mathrm{HX},\mathcal{W},\downarrow}(\mathbf{r})$. An explicit $v_{\mathrm{HX},\mathcal{W}}(\mathbf{r})$ can be obtained by applying the usual Krieger-Li-Iafrate(KLI)[137] approximation. Here we provide the example of the singlet bi-ensemble studied in our previous paper.[257] E_{HX} for a closed-shell, singlet ensemble is

$$E_{\mathrm{HX},\mathtt{w}}^{\mathrm{SEHX}} = \int \frac{\mathrm{d}^3 r \mathrm{d}^3 r'}{|\mathbf{r}-\mathbf{r}'|} \left\{ n_1^{\mathrm{orb}}(\mathbf{r}) n_1^{\mathrm{orb}}(\mathbf{r}') + \mathtt{w} \left[n_1^{\mathrm{orb}}(\mathbf{r}) \left(n_2^{\mathrm{orb}}(\mathbf{r}') - n_1^{\mathrm{orb}}(\mathbf{r}') \right) + \phi_1^*(\mathbf{r}) \phi_2^*(\mathbf{r}') \phi_1(\mathbf{r}') \phi_2(\mathbf{r}) \right] \right\}, \tag{4.40}$$

where $n_j^{\mathrm{orb}}(\mathbf{r}) = |\phi_j(\mathbf{r})|^2$ is the KS orbital density. Spin is not explicitly written out because the system is closed-shell. After applying the KLI approximation, we obtain

$$v_{\mathrm{HX},\mathtt{w}}(\mathbf{r}) = \frac{1}{n_{\mathtt{w}}(\mathbf{r})} \left\{ (2-\mathtt{w}) n_1^{\mathrm{orb}}(\mathbf{r}) \left[v_1(\mathbf{r}) + \bar{v}_{\mathrm{HX1}} - \bar{v}_1 \right] + \mathtt{w}\, n_2^{\mathrm{orb}}(\mathbf{r}) \left[v_2(\mathbf{r}) + \bar{v}_{\mathrm{HX2}} - \bar{v}_2 \right] \right\}, \tag{4.41}$$

with

$$v_1(\mathbf{r}) = \frac{1}{(2-\mathtt{w})} \int \frac{\mathrm{d}^3 r'}{|\mathbf{r}-\mathbf{r}'|} \left[2(1-\mathtt{w}) n_1^{\mathrm{orb}}(\mathbf{r}') + \mathtt{w} \left(n_2^{\mathrm{orb}}(\mathbf{r}') + \phi_1^*(\mathbf{r}') \phi_2^*(\mathbf{r}) \phi_2(\mathbf{r}') / \phi_1^*(\mathbf{r}) \right) \right], \tag{4.42}$$

$$v_2(\mathbf{r}) = \int \frac{\mathrm{d}^3 r'}{|\mathbf{r}-\mathbf{r}'|}\left[n_1^{\mathrm{orb}}(\mathbf{r}') + \frac{\phi_1^*(\mathbf{r})\phi_2^*(\mathbf{r}')\phi_1(\mathbf{r}')}{\phi_2^*(\mathbf{r})}\right], \tag{4.43}$$

and

$$\bar{v}_j = \int \mathrm{d}^3 r \; v_j(\mathbf{r}) n_j^{\mathrm{orb}}(\mathbf{r}). \tag{4.44}$$

Eq. (4.41) is an integral equation for $v_{\mathrm{HX}}(\mathbf{r})$ that can be easily solved.

To fully understand the performance of $v_{\mathrm{HX}}(\mathbf{r})$, self-consistent EDFT calculations would be needed at different values of $\mathtt{w}$, which is beyond the scope of this paper. Ideally these self-consistent calculations would be compared to the symmetry-eigenstate form of GPG used in Table I of Ref. [73]. In this work, we demonstrate the performance of SEHX at $\mathtt{w} = 0$ in Sec. 4.4.3.

4.3.3 Symmetry-projected Hamiltonian

The ensemble variational principle holds for any Hamiltonian. If the Hamiltonian $\hat{H}$ commutes with another operator $\hat{O}$, one can apply to $\hat{H}$ a projection operator formed by the eigenvectors of $\hat{O}$. One obtains a new Hamiltonian, and the ensemble variational principle holds for this subspace of $\hat{H}$, allowing an EDFT to be formulated.

An example would be the total spin operator $\hat{S}^2$, where

$$S^2 = \sum_{S=0}^{\infty} (2S+1)|S\rangle\langle S| \tag{4.45}$$

and $|S\rangle$ are its eigenvectors. Define a new Hamiltonian $\hat{H}_1$ as

$$\hat{H}_1 = |S\rangle\langle S|\hat{H}. \tag{4.46}$$

$\hat{H}_1$ has the same set of eigenvectors as $\hat{H}$, but the eigenvalues are 0 for the eigenvectors not having spin S. Since one can change the additive constant in $\hat{H}$ arbitrarily, it is always possible to make the eigenvalues of any set of spin-S eigenvectors negative and thus ensure that they are the lowest energy states of $\hat{H}_1$. The ensemble variational principle holds for ensembles of spin-S states. We have employed this symmetry argument in our previous paper[257] for a purely singlet two-state ensemble of the He atom.

A similar statement is available in ground-state DFT, allowing direct calculation of the lowest state of a certain symmetry.[76, 88] The differences between the subspace and full treatments are encoded in the differences in their corresponding E_{XC}. Thus the lowest two states within each spatial and spin symmetry category can be treated in EDFT in a two-state-ensemble fashion, which is vastly simpler than the multi-state formalism.

Since the multiplet structures of the interacting system and the KS system must be compatible, a symmetry-projected ensemble also requires a symmetry-projected KS system, which is impossible if KS wavefunctions are single Slater determinants, as discussed in Sec. 4.3.1.

4.4 Exact conditions

Here we prove some basic relations for the signs of various components of the KS scheme and construct an energy density from the virial. We describe a feature of the ensemble derivative discontinuity and extraction of excited properties from the ground state.

4.4.1 Inequalities and energy densities

Simple exact inequalities of the energy components (such as $E_{\mathrm{C}} < 0$) have been proven in ground-state DFT.[43] If these are true in EDFT, experiences designing approximated E_{XC} in ground-state DFT may be transferrable to EDFT. Here we show that inequalities related to the correlation energy are still valid in EDFT.

Due to the variational principle,[86] the wavefunctions that minimize the ensemble energy Eq. (4.5) are the interacting wavefunctions Ψ_m. Thus

$$E_{\mathrm{C},\mathcal{W}} = \mathrm{tr}\{\hat{D}_{\mathcal{W}}\hat{H}\} - \mathrm{tr}\{\hat{D}_{\mathrm{S},\mathcal{W}}\hat{H}\} \leq 0. \tag{4.47}$$

The existence of a non-interacting KS system[85] means $T_{\mathrm{S},\mathcal{W}}$ is the smallest possible kinetic energy for a given density $n_{\mathcal{W}}(\mathbf{r})$, resulting in

$$T_{\mathrm{C},\mathcal{W}} = T_{\mathcal{W}} - T_{\mathrm{S},\mathcal{W}} \geq 0. \tag{4.48}$$

From Eq. (4.47) and (4.48) we immediately obtain

$$U_{\mathrm{C},\mathcal{W}} = E_{\mathrm{C},\mathcal{W}} - T_{\mathrm{C},\mathcal{W}} \leq 0, \tag{4.49}$$

and

$$|U_{\mathrm{C},\mathcal{W}}| \geq |T_{\mathrm{C},\mathcal{W}}|\,. \tag{4.50}$$

These inequalities are later verified with exact ensemble KS calculations.

Since EDFT is a variational method, one expects that the virial theorem holds. This was first proven by Nagy[171, 175] and later extended to excited states.[176] Here, we use the theorem to construct energy densities, which have been important interpretation tools in ground-state

DFT. The virial theorem provides an expression for kinetic correlation in terms of HXC,

$$T_{\mathrm{C},\mathcal{W}}[n] = -E_{\mathrm{HXC},\mathcal{W}}[n] - \int d^3r\; n(\mathbf{r})\mathbf{r}\cdot\nabla v_{\mathrm{HXC},\mathcal{W}}(\mathbf{r}), \tag{4.51}$$

for Hartree-exchange in terms of its potential,

$$E_{\mathrm{HX},\mathcal{W}}[n] = -\int d^3r\; n(\mathbf{r})\mathbf{r}\cdot\nabla v_{\mathrm{HX},\mathcal{W}}(\mathbf{r}). \tag{4.52}$$

and one relating correlation energies through the correlation potential.

$$T_{\mathrm{C},\mathcal{W}}[n] = -E_{\mathrm{C},\mathcal{W}}[n] - \int d^3r\; n(\mathbf{r})\mathbf{r}\cdot\nabla v_{\mathrm{C},\mathcal{W}}(\mathbf{r}). \tag{4.53}$$

The integrand of Eq. (4.51) can be interpreted as an energy density, since integrating over all space gives

$$\begin{aligned} E_{\mathrm{HXC},\mathcal{W}} + T_{\mathrm{C},\mathcal{W}} &= \int d^3r\,(e_{\mathrm{HXC},\mathcal{W}} + t_{\mathrm{C},\mathcal{W}}) \\ &= -\int d^3r\; n(\mathbf{r})\mathbf{r}\cdot\nabla v_{\mathrm{HXC},\mathcal{W}}(\mathbf{r}), \end{aligned} \tag{4.54}$$

which can easily be converted to an "unambiguous" energy density.[19]

4.4.2 Asymptotic behavior

Ref. [150] derived the ensemble derivative discontinuity of Eq. (4.16) for bi-ensembles, in the limit of $\mathtt{w} \to 0$. For finite $\mathtt{w}$ of an atomic system, as shown in our previous paper,[257] Δv_{XC} is close to a finite constant for small r, and jumps to 0 at some position denoted by r_{C}. We provide the derivation of the location of r_{C} as a function of $\mathtt{w}$ here.

For atoms, the HOMO wavefunction and LUMO wavefunctions have the following behavior:

$$\begin{aligned}\phi_{\text{HOMO}}(\mathbf{r}) &\sim A r^{\beta} e^{-\alpha r} \\ \phi_{\text{LUMO}}(\mathbf{r}) &\sim A' r^{\beta'} e^{-\alpha' r},\end{aligned} \tag{4.55}$$

with $\alpha \geq \alpha'$. For the bi-ensemble of the ground state and the first excited state, the ensemble density is

$$n_{\mathtt{w}}(\mathbf{r}) \sim 2 \sum_{n=1}^{\text{HOMO}} |\phi_n(\mathbf{r})|^2 + \mathtt{w}\left(A'^2 r^{2\beta'} e^{-2\alpha' r} - A^2 r^{2\beta} e^{-2\alpha r}\right), \quad r \to \infty, \tag{4.56}$$

assuming that the HOMO is doubly-occupied. The behavior of the density at large r is dominated by the density of the doubly-occupied HOMO and the second term. In order to see where the density decay switches from that of the HOMO to the LUMO, we find the r-value at which the two differently decaying contributions are equal:

$$(2 - \mathtt{w})\, A^2 r^{2\beta} e^{-2\alpha r} = \mathtt{w} A'^2 r^{2\beta'} e^{-2\alpha r}. \tag{4.57}$$

As $\mathtt{w} \to 0$, r_{C} is then

$$r_{\text{C}} \to -\frac{\ln \mathtt{w}}{2\Delta\alpha}, \tag{4.58}$$

with $\Delta\alpha = \alpha - \alpha'$.

The ionization energies are available for the He ground state and singlet excited state. Since

$$n(\mathbf{r}) \sim e^{-2\alpha r} \approx e^{-2\sqrt{2I} r}, \tag{4.59}$$

we obtain

$$r_{\rm C} \to -0.621 \ln \mathtt{w}, \quad \mathtt{w} \to 0. \tag{4.60}$$

for the He singlet bi-ensemble with $\mathtt{w}$ close to 0.

4.4.3 Connection to ground-state DFT

With weights as in Eq. (4.13), calculation of the excitation energies is done recursively: for the Mth excited state, one needs to perform an EDFT calculation with the Mth state highest in the ensemble, and another EDFT calculation with the $(M-1)$th as the highest state, and so on. Thus for the Mth state, one needs to perform M separate EDFT calculations for its excitation energy.

For bi-ensembles, however, the calculation of the excitation energy can be greatly simplified. Eq. (5.10) holds for $\mathtt{w} = 0$, so one can work with ground-state data only and obtain the first-excited state energy, without the need for an explicit EDFT calculation of the two-state ensemble.

We calculate the first excitation energies of various atoms and ions with Eq. (5.10) at $\mathtt{w} = 0$ with both qLDA[131, 159] (based on LDA ground states), EXX,[173] GPG,[73] and SEHX, with the last three based on OEP-EXX (KLI) ground states.[137] In order to ensure the correct symmetry in the end result, SEHX must be performed on spin-restricted ground states. However, for closed-shell systems, these results coincide with those of spin-unrestricted calculations. We use these readily available results when possible in this paper. The $\mathtt{w}$-derivatives of the $E_{\rm XC}$'s for qLDA and GPG required in Eq. (5.10) are (considering Eq. (4.65))

$$\lim_{\mathtt{w}\to 0} \frac{\partial E^{\rm qLDA}_{{\rm XC},\mathtt{w}}[n]}{\partial \mathtt{w}}\bigg|_{n=n_{\mathtt{w}}} = M_I \left(E^{\rm eqLDA}_{\rm XC}[I=2,n] - E^{\rm LDA}_{\rm XC}[n] \right), \tag{4.61}$$

where $E_{\rm XC}^{\rm LDA}$ is the ground-state LDA functional, and

$$\lim_{\mathtt{w}\to 0}\left.\frac{\partial E_{\rm X,\mathtt{w}}^{\rm GPG}[n]}{\partial \mathtt{w}}\right|_{n=n_{\mathtt{w}}} = \iint \frac{{\rm d}^3r{\rm d}^3r'}{|\mathbf{r}-\mathbf{r}'|}\Bigg\{\left[\sum_{j=1}^{N_{\rm H}} n_j(\mathbf{r},\mathbf{r}')\right][n_{\rm H}(\mathbf{r},\mathbf{r}')-n_{\rm L}(\mathbf{r},\mathbf{r}')] - n_{\rm H}(\mathbf{r})n_{\rm L}(\mathbf{r}')+n_{\rm H}(\mathbf{r},\mathbf{r}')n_{\rm L}(\mathbf{r},\mathbf{r}')\Bigg\} + \int {\rm d}^3r\; v_{\rm XC}(\mathbf{r})[n_{\rm H}(\mathbf{r})-n_{\rm L}(\mathbf{r})], \tag{4.62}$$

where j sums over the spin-up densities. Only ground state properties are needed to evaluate Eq. (4.62). The results are listed in Table 4.1. Note that the single-determinant form of GPG performs well here, despite not being designed for this method. SEHX improves calculated excitation energies for systems where single-determinant GPG has large errors with this method, such as Be and Mg atoms.

	He	Li	Li^+	Be	Be^+	Mg	Ca	Ne	Ar
Exp.	20.62	1.85	60.76	5.28	3.96	4.34	2.94	16.7	11.6
qLDA	-	1.93	53.85	3.71	4.30	3.58	1.79	14.2	10.7
EXX	27.30	6.34	72.26	10.22	12.38	8.25	9.89	26.0	18.2
GPG	20.67	1.84	60.40	3.53	4.00	3.25	3.25	18.2	12.1
SEHX	21.29	2.08*	61.64	5.25	4.06*	4.39	3.55	18.4	12.2

Table 4.1: First non-triplet excitation energies (in eV) of various atoms and ions calculated with qLDA, EXX, GPG, and SEHX functionals. qLDA calculations were performed upon LDA (PW92)[198] ground states; EXX[173] ground states were used for the rest. Asterisks indicate use of spin-restricted ground states. qLDA relies on ground-state LDA orbital energy differences; it cannot be used with the single bound orbital of LDA He. GPG is used with single-determinant states and performs well, though GPG allows the choice of multi-determinant states.

4.5 Numerical procedure

We invert the ensemble KS equation with exact densities to obtain the exact KS potential. We describe the numerical inversion procedure in Ref. [257]. For ease in obtaining the

Hartree potential, E_{H} is always chosen to be $E_{\mathrm{H}}^{\mathrm{trad}}$. The resulting KS potential, being exact, does not depend on the choice of E_{H}, but E_{XC} and $v_{\mathrm{XC}}(\mathbf{r})$ reported in later sections are those compatible with $E_{\mathrm{H}}^{\mathrm{trad}}$ and $v_{\mathrm{H}}^{\mathrm{trad}}(\mathbf{r})$, respectively. For simplicity, only GOK-type ensembles [Eq. (4.13)] are considered, though there is no difficulty adapting the method to other types of ensembles. With this numerical procedure, $v_{\mathrm{XC},\mathtt{w}}(\mathbf{r})$ is determined up to an additive constant.

We implemented the numerical procedure on a real-space grid. The ensemble KS equation (4.8) is solved by direct diagonalization of the discrete Hamiltonian. The grid is in general nonuniform, which complicates the discretization of the KS kinetic energy operator. We tested two discretization schemes, details of which are available in the Supplemental Material. Based on these tests, all results presented in this paper have been obtained using the finite-difference representation

$$-\frac{1}{2}\frac{d^2\phi(x)}{dx^2} \approx \frac{\phi(x_i)}{(x_i - x_{i-1})(x_{i+1} - x_i)} - \frac{\phi(x_{i-1})}{(x_i - x_{i-1})(x_{i+1} - x_{i-1})} - \frac{\phi(x_{i+1})}{(x_{i+1} - x_i)(x_{i+1} - x_{i-1})}. \tag{4.63}$$

4.5.1 Derivative Corrections

Exactness of the inversion process can be verified by calculating the excitation energies with Eq. (5.10) at different $\mathtt{w}$ values. Eq. (5.10) requires calculating $E_{\mathrm{XC},\mathtt{w}}$ of the exact ensemble KS system,

$$E_{\mathrm{XC},\mathtt{w}}[n_{\mathtt{w}}] = E_{\mathtt{w}} - E_{\mathrm{s},\mathtt{w}} + \int \mathrm{d}^3 r \; n_{\mathtt{w}}(\mathbf{r}) \left[\frac{v_{\mathrm{H}}[n_{\mathtt{w}}](\mathbf{r})}{2} + v_{\mathrm{XC},\mathtt{w}}[n_{\mathtt{w}}](\mathbf{r}) \right]. \tag{4.64}$$

Since we do not have a closed-form expression for the exact E_{XC}, its derivative can only be calculated numerically. However, the numerical derivative of E_{XC}, $\partial E_{\mathrm{XC},\mathtt{w}}[n_{\mathtt{w}}]/\partial \mathtt{w}$, is not the

quantity required in Eq. (5.10). It is related to the true derivative through

$$\left.\frac{\partial E_{\mathrm{XC},\mathtt{w}}[n]}{\partial \mathtt{w}}\right|_{n=n_{\mathtt{w}}} = \frac{\partial E_{\mathrm{XC},\mathtt{w}}[n_{\mathtt{w}}]}{\partial \mathtt{w}} - \int \mathrm{d}^3 r \; v_{\mathrm{XC},\mathtt{w}}[n_{\mathtt{w}}](\mathbf{r}) \frac{\partial n_{\mathtt{w}}(\mathbf{r})}{\partial \mathtt{w}}. \tag{4.65}$$

The correction to the numerical derivative of $E_{\mathrm{XC},\mathtt{w}}$ adjusts for the $\mathtt{w}$-dependence of the ensemble density, which is not inherent to $E_{\mathrm{XC},\mathtt{w}}$. All our calculations show that the two terms on the right hand side of Eq. (4.65) are of the same order of magnitude. This shows that the exact $E_{\mathrm{XC},\mathtt{w}}[n]$ changes more slowly than $n_{\mathtt{w}}(\mathbf{r})$ as $\mathtt{w}$ changes. Though the calculations of $E_{\mathrm{XC},\mathtt{w}}$ and $\partial E_{\mathrm{XC},\mathtt{w}}[n]/\partial \mathtt{w}|_{n=n_{\mathtt{w}}}$ both involve integrations containing $v_{\mathrm{XC},\mathtt{w}}(\mathbf{r})$, they are independent of the additive constant.

4.6 Results

We apply the numerical procedure described in Sect. 4.5 to both 1D and 3D model systems in order to further demonstrate our method for inverting ensemble densities.

4.6.1 1D flat box

The external potential of the 1D flat box is

$$v(x) = \begin{cases} 0, & 0 < x < L, \\ \infty, & x \leq 0 \text{ or } x \geq L. \end{cases} \tag{4.66}$$

The exact wavefunctions can be solved numerically for two electrons with the following soft-Coulomb interaction:

$$v_{\mathrm{SC}}(x, x') = \frac{1}{\sqrt{(x - x')^2 + a^2}}, \tag{4.67}$$

where we choose $a = 0.1$.

I	E	T
0 (singlet)	15.1226	10.0274
1 (triplet)	27.5626	24.7045
2 (singlet)	30.7427	24.7696
3 (singlet)	43.9787	39.6153
4 (triplet)	52.8253	49.3746

Table 4.2: Total and kinetic energies in a.u. for a unit-width box, including a doubly-excited state ($I = 3$).

Table 4.2 shows the total and kinetic energies of the exact ground state and first four excited states for $L = 1$ a.u., calculated on a 2D uniform grid with 1000 points for each position variable. The third excited state is a doubly-excited state corresponding to both electrons occupying the second orbital of the box. Fig. 4.1 shows the exact densities of the ground state and first four excited states, together with the XC potential of equiensembles containing 1 to 5 multiplets. Table 4.3 lists calculated excitation energies, showing that the excitation energy is independent of $\mathtt{w}$, no matter how many states are included in the ensemble. This is a non-trivial exact condition for the ensemble $E_{\rm XC}$.

Double excitations are generally difficult to calculate. It has been shown that adiabatic TDDFT cannot treat double or multiple excitations.[48] Table 4.3 shows that there is no fundamental difficulty in treating double excitations with EDFT. Fig. 4.1 shows that $v_{\rm XC,\mathtt{w}}(\mathbf{r})$ for the 4-multiplet equiensemble resembles the potentials of other ensembles. The exact two-multiplet ensemble XC potentials at different $\mathtt{w}$ are plotted in Fig. 4.4. The bump up near the center of the box in these potentials ensures that the ensemble KS density matches that of the real ensemble density. Increasing the proportion of the excited state density (see Fig. 4.1) included in the ensemble density requires a corresponding increase in the height of this bump (see Supplemental Material). With no asymptotic region, there is no derivative discontinuity for the box, and $v_{\rm XC,\mathtt{w}\to 0}(\mathbf{r})$ is equal to the ground-state $v_{\rm XC}(\mathbf{r})$. Energy components for the bi-ensemble of the 1D box satisfy the inequalities shown in Sec. 4.4.1 and are reported in

the Supplemental Material.

2-multiplet: $\omega_1 = 12.4399$ hartree			
$\mathtt{w}_2$	0.25	0.125	0.03125
$E^{\mathrm{KS}}_{1,\mathtt{w}_2} - E^{\mathrm{KS}}_{0,\mathtt{w}_2}$	13.9402	13.9201	13.8932
$\partial E_{\mathrm{xc},\mathtt{w}_2}[I=2,n]/\partial \mathtt{w}_2\vert_{n=n_{\mathtt{w}_2}}$	-4.5010	-4.4407	-4.3598
$(E_1 - E_0)_{\mathtt{w}_2}$	12.4399	12.4399	12.4399
3-multiplet: $\omega_2 = 15.6202$ hartree			
$\mathtt{w}_3$	0.2	0.1	0.025
$E^{\mathrm{KS}}_{2,\mathtt{w}_3} - E^{\mathrm{KS}}_{0,\mathtt{w}_3}$	14.2179	14.0757	13.9735
$\partial E_{\mathrm{xc},\mathtt{w}_3}[I=3,n]/\partial \mathtt{w}_3\vert_{n=n_{\mathtt{w}_3}}$	2.7358	2.7713	2.7969
$(E_2 - E_0)_{\mathtt{w}_2,\mathtt{w}_3}$	15.6202	15.6201	15.6202
4-multiplet: $\omega_3 = 28.8561$ hartree (double)			
$\mathtt{w}_4$	0.166666	0.083333	0.020833
$E^{\mathrm{KS}}_{3,\mathtt{w}_4} - E^{\mathrm{KS}}_{0,\mathtt{w}_4}$	28.7534	28.5826	28.4706
$\partial E_{\mathrm{xc},\mathtt{w}_4}[I=4,n]/\partial \mathtt{w}_4\vert_{n=n_{\mathtt{w}_4}}$	1.1061	1.1186	1.1858
$(E_3 - E_0)_{\mathtt{w}_2,\mathtt{w}_3,\mathtt{w}_4}$	28.8561	28.8561	28.8561
5-multiplet: $\omega_4 = 37.7028$ hartree			
$\mathtt{w}_5$	0.111111	0.055555	0.013888
$E^{\mathrm{KS}}_{4,\mathtt{w}_5} - E^{\mathrm{KS}}_{0,\mathtt{w}_5}$	38.8375	38.8602	38.8746
$\partial E_{\mathrm{xc},\mathtt{w}_5}[I=5,n]/\partial \mathtt{w}_5\vert_{n=n_{\mathtt{w}_5}}$	-1.1279	-1.2205	-1.2787
$(E_4 - E_0)_{\mathtt{w}_2,\mathtt{w}_3,\mathtt{w}_4,\mathtt{w}_5}$	37.7028	37.7027	37.7028

Table 4.3: Excitation energies of the 1D box calculated at different $\mathtt{w}$ values using the exact ensemble KS systems and Eq. (5.10). The double excitation (4-multiplet) shows accuracy comparable to that of the single excitation (2-multiplet). All energies are in Hartree. See Supplemental Material for the full table.

4.6.2 Charge-transfer excitation with 1D box

Charge-transfer (CT) excitations are difficult to treat with approximate TDDFT, due to the lack of overlap between orbitals.[71] With common approximations, the excitation energy calculated by TDDFT is much smaller than experimental values.[243] Here we provide a 1D example of an excited state with CT character, showing that there is no fundamental difficulty in treating CT excitations with EDFT. Since EDFT calculations do not involve transition densities, they do not suffer from the lack-of-orbital-overlap problem in TDDFT.

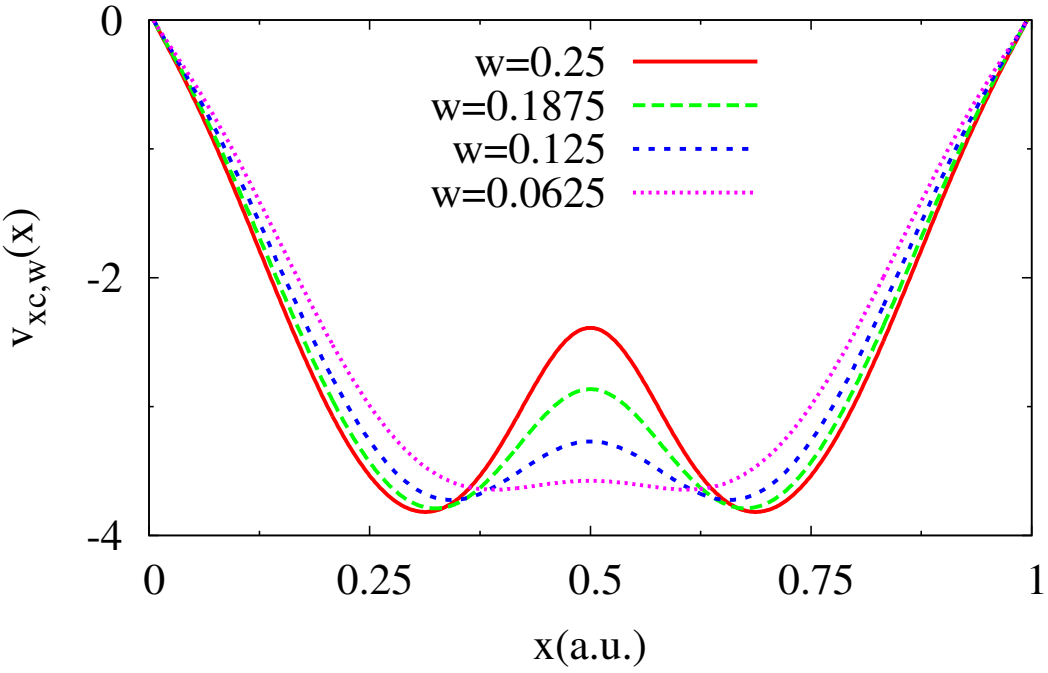

Figure 4.4: Exact ensemble XC potentials of the 1D box with two electrons. The ensemble contains the ground state and the first (triplet) excited state.

The external potential for the CT box is

$$v(x) = \begin{cases} 0 & x \in [0,1] \cup [2,4] \\ 20 & x \in (1,2) \\ \infty & x < 0 \text{ or } x > 4, \end{cases} \tag{4.68}$$

with the barrier dimensions chosen for numerical stability of the inversion process. The lowest two eigenstate densities are given in the top of Fig. 4.5. The ground-state and first-excited-state total and kinetic energies of the CT system described are

$$\begin{aligned} E_0 &= 138.254\,\text{eV}, \quad T_0 = 63.4617\,\text{eV (singlet)}, \\ E_1 &= 140.652\,\text{eV}, \quad T_1 = 112.141\,\text{eV (triplet)}. \end{aligned} \tag{4.69}$$

This significant increase in kinetic energy together with a small total energy change designate the CT character of the first excited state. The electrons become distributed between the

two wells of the potential, instead of being confined in one well.

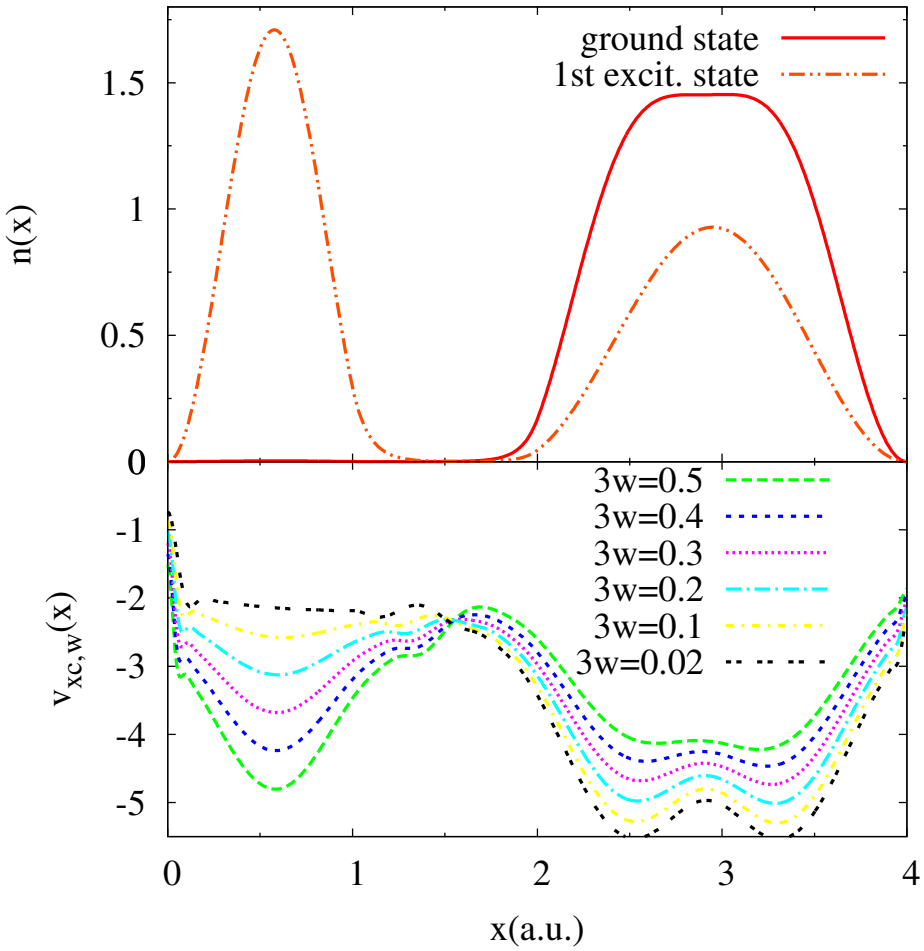

Figure 4.5: Exact densities and ensemble xc potentials of the 1D charge-transfer box.

The ground- and first-excited-state densities and ensemble XC potentials are plotted in Fig. 4.5. The potentials show the characteristic step-like structures of charge-transfer excitations, which align the chemical potentials of the two wells.[95, 96] Table 4.4 lists the ensemble energies of the CT box. Excitation energies have larger errors than those for the 1D flat box due to greater numerical instability, but they are still accurate to within 0.01 eV.

$3\mathtt{w}$	0.5	0.1	0.02
$E^{\mathrm{KS}}_{1,\mathtt{w}} - E^{\mathrm{KS}}_{0,\mathtt{w}}$	2.2048	2.4092	2.4317
$\partial E_{\mathrm{XC},\mathtt{w}}[n]/\partial n\vert_{n=n_{\mathtt{w}}}/3$	0.1993	-0.0108	-0.0334
$\omega_{1,\mathtt{w}}$	2.4042	2.3983	2.3983

Table 4.4: First excitation energy and energy decomposition of the two-multiplet ensemble of the 1D charge-transfer box at different $\mathtt{w}$ values, calculated using Eq. (5.10). All energies are in eV. The exact first excitation energy is $E_1 - E_0 = 2.3983$ eV. See Supplemental Material for additional data.

4.6.3 Hooke's atom

Hooke's atom is a popular model system[63, 144] with the following external potential:

$$v(\mathbf{r}) = \frac{k}{2} |\mathbf{r}|^2 . \tag{4.70}$$

For our calculation, $k = 1/4$. Though the first excited state has cylindrical symmetry, we use a spherical grid, as it has been shown that the error due to spherical averaging is small.[141] As a closed-shell system, the spatial parts, and therefore the densities, of the spin-up and spin-down ensemble KS orbitals have to be the same, so we treat this system as a bi-ensemble.

The magnitude of the external potential of the Hooke's atom is smallest at $r = 0$, and becomes larger as r increases. This is completely different from the Coulomb potential of real atoms. Since the electron-electron interaction is still coulombic, $v_{\mathrm{XC}}(\mathbf{r})$ can be expected to have a $-1/r$ behavior as $r \to \infty$, which is negligibly small compared to $v(\mathbf{r})$. Combined with a density that decays faster than real atomic densities, $n(\mathbf{r}) \sim \exp(-ar^2)$ versus $n(\mathbf{r}) \sim \exp(-br)$, convergence of the Hooke's atom $v_{\mathrm{XC}}(\mathbf{r})$ is difficult in the asymptotic region. Additionally, $v_{\mathrm{XC}}(\mathbf{r}) \gg v(\mathbf{r})$ for small r, so larger discretization errors in this region also contribute to poorer inversion performance. Despite these challenges, we still obtain highly accurate excitation energies.

A logarithmic grid with 550 points ranging from $r = 10^{-5}$ a.u. to 10 a.u. is used for all the Hooke's atom calculations. On this grid, the exact ground- and first excited-state energies are

$$E_1 = 54.42\,\text{eV}, \quad E_2 = 64.19\,\text{eV}. \tag{4.71}$$

Calculated ω_2 was 9.786 eV for all values of $\mathtt{w}$ tested (see Supplemental Material). Unlike the He atom and the 1D flat box, the $n_{\mathtt{w}}(\mathbf{r})$ and $v_{\text{XC},\mathtt{w}}(\mathbf{r})$ show little variation with $\mathtt{w}$ (see Supplemental Material). The second KS orbital of the Hooke's atom is a p-type orbital, which has no radial node and a radial shape similar to that of the first KS orbital. Consequently, the changes in the KS and xc potentials are also smaller.

4.6.4 He

Using the methods in Ref. [257], we employ a Hylleraas expansion of the many-body wavefunction[41] to calculate highly accurate densities of the first few states of the He atom. We report the exact ensemble XC potentials for He singlet ensemble in that paper. Table 4.5 shows accurate excitation energies calculated from mixed symmetry, three-multiplet, and strictly triplet ensembles, demonstrating the versatility of EDFT. Fig. 4.6 compares $v_{\text{XC},\mathtt{w}}(\mathbf{r})$ for four types of He equiensembles, highlighting their different features. The characteristic bump up in these potentials is shifted left in the 2-multiplet case, relative to the others shown. This shift has little impact on the first "shell" of the ensemble density's shell-like structure, but the second is shifted left and has sharper decay, noticeably different from that of the singlet ensemble.[257]

The inequalities shown in Sec. 4.4.1 and the virial theorem Eq. (4.53) are verified by the exact results. Behaviors of the energy components for the singlet ensemble versus $\mathtt{w}$ are plotted in Fig. 4.7. Correlation energies show strong non-linear behavior in $\mathtt{w}$. According to

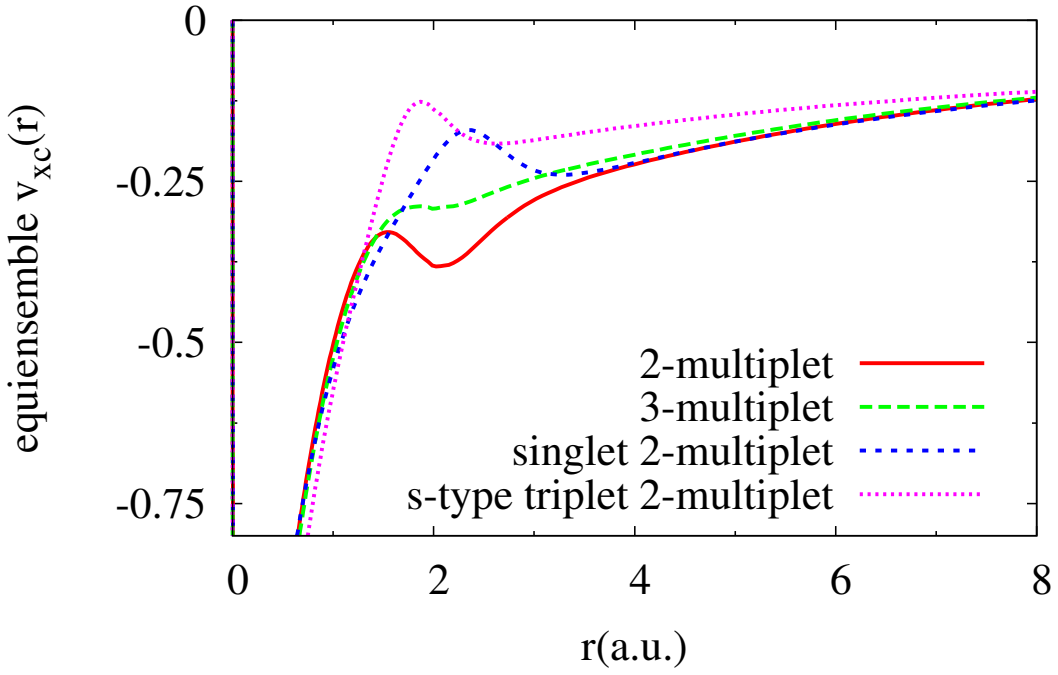

Figure 4.6: Ensemble XC potentials of the singlet-triplet, singlet-triplet-singlet, strictly singlet, and strictly triplet He equiensembles.

2-multiplet ensemble: $\omega_1 = 19.8231$ eV			
$\mathtt{w}_2$	0.25	0.125	0.03125
$E^{\rm KS}_{1,\mathtt{w}_2} - E^{\rm KS}_{0,\mathtt{w}_2}$	25.1035	22.4676	21.6502
$\partial E_{{\rm xc},\mathtt{w}_2}[n]/\partial \mathtt{w}_2\vert_{n=n_{\mathtt{w}_2}}$	-15.8099	-7.9358	-5.4351
$(E_1 - E_0)_{\mathtt{w}_2}$	19.8336	19.8224	19.8385
3-multiplet ensemble: $\omega_2 = 20.6191$ eV			
$\mathtt{w}_3$	0.2	0.1	0.025
$E^{\rm KS}_{2,\mathtt{w}_3} - E^{\rm KS}_{0,\mathtt{w}_3}$	26.8457	25.8895	25.2853
$\partial E_{{\rm xc},\mathtt{w}_3}[n]/\partial \mathtt{w}_3\vert_{n=n_{\mathtt{w}_3}}$	-0.9596	-0.7207	-0.5696
$(E_2 - E_0)_{\mathtt{w}_2,\mathtt{w}_3}$	20.6270	20.6184	20.6306
triplet ensemble: $\omega_1 = 2.8991$ eV			
$\mathtt{w}$	0.16667	0.08333	0.02083
$E^{\rm KS}_1 - E^{\rm KS}_0$	2.8928	2.8956	2.8967
$\partial E_{{\rm XC},\mathtt{w}}[n]/\partial \mathtt{w}\vert_{n=n_{\mathtt{w}}}$	0.0187	0.0104	0.0074
$(E_1 - E_0)_{\mathtt{w}}$	2.8990	2.8990	2.8992

Table 4.5: He atom excitation energies, calculated using Eq. (5.10) and various ensemble types: singlet-triplet (2-multiplet), singlet-triplet-singlet (3-multiplet), and strictly triplet. All energies are in eV. $\mathtt{w}_2$ dependency of the 3-multiplet excitation energies is noted explicitly, though $\mathtt{w}_2 = (1 - \mathtt{w}_3)/4$ for the GOK ensemble. See Supplemental Material for additional data and figures.

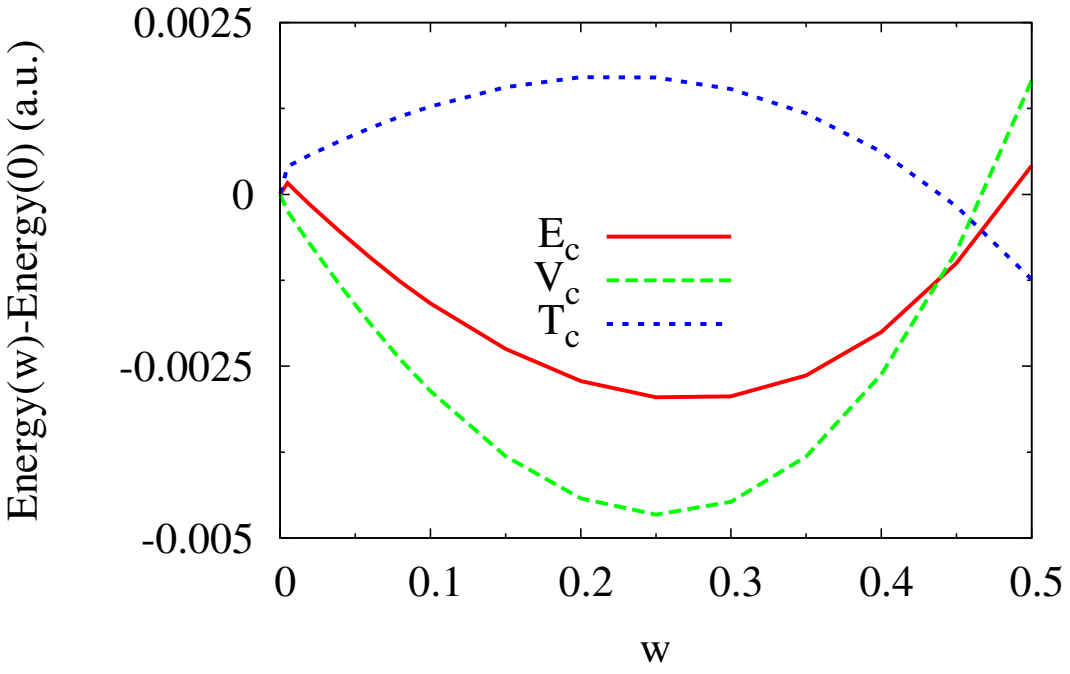

Figure 4.7: Behaviors of the various energy components for the singlet ensemble of He. The ground state ($\mathtt{w} = 0$) values are taken from Ref. [102]. The small kinks near $\mathtt{w} = 0$ are due to the difference in the numerical approaches of this work and Ref. [102].

Eq. (5.10), the excitation energies are related to the derivative of $E_{\rm XC}$ versus $\mathtt{w}$. Therefore, $E_{\rm C}$ is crucial for accurate excitation energies, even though its absolute magnitude is small.

4.7 Conclusion

This paper is an in-depth exploration of ensemble DFT, an alternative to TDDFT for extracting excitations from DFT methodology. Unlike TDDFT, EDFT is based on a variational principle, and so one can expect that the failures and successes of approximate functionals should occur in different systems than those of TDDFT.

Apart from exploring the formalism and showing several new results, the main result of this work is to apply a new algorithm to highly-accurate densities of eigenstates to explore the exact EDFT XC potential. We find intriguing characteristic features of the exact potentials that can be compared against the performance of old and new approximations. We also extract the weight-dependence of the KS eigenvalues, which are needed to extract accurate transition frequencies, and find that a large cancellation of weight-dependence occurs in the exact ensemble. Many details of these calculations are reported in the supplemental information.

From the original works of Gross, Oliviera, and Kohn, ensemble DFT has been slowly developed over three decades by a few brave pioneering groups, most prominently that of Nagy. We hope that the insight these exact results bring will lead to a plethora of new ensemble approximations and calculations and, just possibly, a competitive method to treating excitations within DFT.

Z.-H.Y. and C.U. are funded by National Science Foundation Grant No. DMR-1005651. A.P.J. is supported by DOE grant DE-FG02-97ER25308. J.R.T. and R.J.N. acknowledge financial support from the Engineering and Physical Sciences Research Council (EPSRC) of

the UK. K.B. is supported by DOE grant DE-FG02-08ER46496.

Chapter 5

Exact and approximate Kohn-Sham potentials in ensemble density-functional theory

written with Zeng-hui Yang, John R. Trail, Kieron Burke, Richard J. Needs, and Carsten A. Ullrich. Published in *Phys. Rev. A* **90** 042501 (2014).

Abstract: *We construct exact Kohn-Sham potentials for the ensemble density-functional theory (EDFT) from the ground and excited states of helium. The exchange-correlation (XC) potential is compared with the quasi-local-density approximation and both single determinant and symmetry eigenstate ghost-corrected exact exchange approximations. Symmetry eigenstate Hartree-exchange recovers distinctive features of the exact XC potential and is used to calculate the correlation potential. Unlike the exact case, excitation energies calculated from these approximations depend on ensemble weight, and it is shown that only the symmetry eigenstate method produces an ensemble derivative discontinuity. Differences in asymptotic and near-ground-state behavior of exact and approximate XC potentials are discussed in the*

context of producing accurate optical gaps.

5.1 Introduction

The balance of useful accuracy with computational efficiency makes density-functional theory (DFT) popular for finding ground-state electronic properties of a wide range of systems and materials [18]. While exact conditions [194] and fitting to chemical data sets [14] are often used to construct approximations, another major source of inspiration has been highly accurate calculations of Kohn-Sham (KS) quantities for simple systems, such as the He atom [246]. The exact KS potential, orbitals, energies, and energy components have been enormously useful in illustrating basic theorems of DFT and testing approximations. Many algorithms now exist for extracting the KS potential from accurate densities [79, 142, 188].

Time-dependent density-functional theory (TDDFT) [162, 243] has become the standard DFT method for calculating excitation energies, at least for molecules, with typical accuracies and efficiency comparable to what can be achieved in ground-state DFT [106]. Once again, accurate KS energies, of both occupied and unoccupied orbitals, play a vital role [3]. But alternative density-functional approaches for excitation energies can be valuable, both as practical tools and for gaining physical insight [78, 151]. The ensemble density-functional theory (EDFT) formalism for excited states [85, 86, 91, 159, 238, 239] is based on a variational principle of ensembles comprising the ground state and a chosen number of excited states. Despite its rigorous formal framework and appealing physical motivation[73, 170, 173, 174, 186, 187], the EDFT excited-state formalism has seen only limited practical success. The lack of good approximate exchange-correlation (XC) functionals for EDFT leads to inaccurate transition frequencies. Better approximations are needed for EDFT to become more useful.

Here, we describe an algorithm that extracts the ensemble KS and XC potentials from

the various eigenstate densities, and apply that algorithm to highly accurate densities of the helium atom. We use the exact results to analyze errors in approximations that have been designed for use in EDFT, plot various potentials, and check the virial theorem for the ensemble correlation potential. We demonstrate the weight-independence of transition frequencies in the exact case, but also find a strong weight-dependence in the individual elements contributing to the exact expression, all of which cancels in the final excitation energy. We show that approximations all yield (incorrectly) weight-dependent transition frequencies, and demonstrate how this is related to the ensemble derivative discontinuity.

5.2 Theory

An ensemble in EDFT consists of the ground state and M excited states. For the lowest $M+1$ eigenstates Ψ_m of the many-body Hamiltonian $\hat{H}$, sorted by energy in ascending order, each state is assigned a weight $\mathtt{w}_M$. EDFT states that for

$$\mathtt{w}_0 \geq \mathtt{w}_1 \geq \mathtt{w}_2 \geq \cdots \geq \mathtt{w}_M \geq 0, \tag{5.1}$$

there is a one-to-one correspondence between the ensemble density

$$n(\mathbf{r}) = \sum_{m=0}^{M} \mathtt{w}_m \langle \Psi_m | \hat{n}(\mathbf{r}) | \Psi_m \rangle \tag{5.2}$$

and the external potential [85, 86]. A Kohn-Sham (KS) scheme can then be constructed in the usual way [85].

We consider only bi-ensembles of the ground and first-excited states. For a non-degenerate

ground state,

$$n_{\mathtt{w}}(\mathbf{r}) = \overline{\mathtt{w}}\; n_0(\mathbf{r}) + g\;\mathtt{w}\; n_1(\mathbf{r}), \qquad \mathtt{w} \leq 1/(1+g) \tag{5.3}$$

$$E_{\mathtt{w}}[n_{\mathtt{w}}] = \overline{\mathtt{w}}\; E_0 + g\;\mathtt{w}\; E_1, \tag{5.4}$$

where g is the degeneracy of the excited state, $\overline{\mathtt{w}} = 1 - g\,\mathtt{w}$, and subscripts 0 and 1 refer to the ground and excited states. EDFT also holds for ensembles of states that share a symmetry-projected Hamiltonian [109]. For helium, the ground state is a singlet, the first excited state is a triplet, and the second excited state is again a singlet, shown in Fig. 5.1. The (unprojected) bi-ensemble always includes the ground state and the first excited state. Here we focus on calculations in the spin-projected ensemble to find the transition to the lowest singlet.

The corresponding ensemble KS potential $v_{s,\mathtt{w}}[n_{\mathtt{w}}](\mathbf{r})$ is defined as the potential of the non-interacting system

$$\left\{-\frac{1}{2}\nabla^2 + v_s(\mathbf{r})\right\}\phi_j(\mathbf{r}) = \epsilon_j\phi_j(\mathbf{r}), \tag{5.5}$$

which reproduces the exact ensemble density as

$$n_{\mathtt{w}}(\mathbf{r}) = (1+\overline{\mathtt{w}})\,|\phi_1(\mathbf{r})|^2 + g\,\mathtt{w}\;|\phi_2(\mathbf{r})|^2\,, \tag{5.6}$$

where $\phi_j(\mathbf{r})$ are KS orbitals. Atomic units ($e = \hbar = m_e = 1/4\pi\epsilon_0 = 1$) are used throughout, and all KS quantities are $\mathtt{w}$-dependent. Then

$$E_{\mathtt{w}}[n] = T_{s,\mathtt{w}}[n] + \int \mathrm{d}^3r\; n(\mathbf{r})v(\mathbf{r}) + E_{\mathrm{HXC},\mathtt{w}}[n], \tag{5.7}$$

where $T_{s,\mathtt{w}}[n] = (1+\overline{\mathtt{w}})\,t_1 + g\,\mathtt{w}\,t_2$ is the ensemble KS kinetic energy, with t_j the kinetic energy

of ϕ_j. $v(\mathbf{r})$ is the external potential of the interacting system.

$$E_{\text{HX}} = \overline{\mathtt{w}} \left\langle \Phi_{0,\mathtt{w}}[n] \left| |\mathbf{r} - \mathbf{r}'|^{-1} \right| \Phi_{0,\mathtt{w}}[n] \right\rangle + g\ \mathtt{w} \left\langle \Phi_{1,\mathtt{w}}[n] \left| |\mathbf{r} - \mathbf{r}'|^{-1} \right| \Phi_{1,\mathtt{w}}[n] \right\rangle \tag{5.8}$$

is the ensemble Hartree-exchange energy, and the ensemble correlation energy $E_{\text{C}} = E_{\text{HXC}} - E_{\text{HX}}$. $\Phi_{i,\mathtt{w}}[n]$ is the KS many-body wavefunction, with $i = 0$ or 1 again indicating the ground or excited state. Here we choose E_{H} to be the Hartree energy of the ensemble density, although it contains "ghost" interactions[73]. The exchange energy is then defined as the expectation of the electron-electron repulsion on the KS ensemble minus the Hartree energy. This definition of E_{HXC} is consistent with our choice of spin eigenstates that are necessarily multi-determinant. The ensemble KS potential is

$$v_{s,\mathtt{w}}[n](\mathbf{r}) = v(\mathbf{r}) + v_{\text{HXC},\mathtt{w}}[n](\mathbf{r}), \tag{5.9}$$

where $v_{\text{HXC},\mathtt{w}}[n](\mathbf{r}) = \delta E_{\text{HXC},\mathtt{w}}[n]/\delta n(\mathbf{r})$. The excitation energy is then independent of $\mathtt{w}$:

$$\omega = E_1 - E_0 = \Delta\epsilon_{\mathtt{w}} + \partial E_{\text{HXC},\mathtt{w}}[n]/\partial \mathtt{w}|_{n=n_{\mathtt{w}}}, \tag{5.10}$$

where $\Delta\epsilon_{\mathtt{w}} = \epsilon_{2,\mathtt{w}} - \epsilon_{1,\mathtt{w}}$.

The $\mathtt{w}$-dependence of the HXC energy comes from both the $\mathtt{w}$-dependence of $n_{\mathtt{w}}(\mathbf{r})$ and from the HXC energy functional. Eq. (5.10) shows that the correction to the KS gap originates from the $\mathtt{w}$-dependence of XC, not from $n_{\mathtt{w}}(\mathbf{r})$. Using a ground-state XC functional in EDFT yields no correction to the KS excitation energy. EDFT is a more general theory encompassing ground-state DFT, and the ground-state XC functional is only a special case ($\mathtt{w} = 0$) of the ensemble XC functional. However, the excitation energies can also be obtained from the difference of two consecutive equiensemble energies. In contrast to Eq. (5.10), the density-based $\mathtt{w}$-dependence of $E_{\text{HXC},\mathtt{w}}$ does not drop out in that approach, and using ground-state XC functionals would yield finite corrections. These two approaches for the excitation energy

yield the same result using the *exact* functional, but no known approximations can achieve such consistency.

5.3 Inversion Method

The only unknown in the ensemble KS procedure is the XC functional. Without this functional, an inversion method for EDFT is needed to extract XC potentials from accurate densities. Ref. [170] presented an inversion scheme for EDFT similar to the van Leeuwen-Baerends (LB) algorithm in ground-state DFT[142], but we found its numerical stability unsatisfactory. Ref. [188] observed that a LB-type algorithm cannot change the local sign of the KS potential during the iteration. While not a fundamental problem, it makes the algorithm less stable. Also, it can be hard to obtain the $-1/r$ asymptotic behavior of $v_{\rm XC}$ using the LB algorithm without having to build it in the initial guess. Ref. [188] suggested an alternative ground-state density-inversion algorithm, where the xc potential is updated iteratively by

$$v_{\rm XC}^{(i+1)}(r) = v_{\rm XC}^{(i)}(r) + \alpha r^{\beta}[n_{\rm KS}^{(i)}(r) - n(r)] + [I_{\rm KS}^{(i)} - I]\left[\theta(1-r)r^{\gamma} + \frac{\theta(r-1)}{r^{\delta}}\right], \qquad (5.11)$$

where α, β, γ, δ are parameters controlling the speed of convergence, and I is the ionization energy. In the asymptotic region, the density difference in the second term of Eq. (5.11) is very small, so the convergence needs to be accelerated by the use of the r^{β} in front of this term. Even so, the $-1/r$ asymptotic behavior of $v_{\rm XC}$ can be hard to obtain, and the third term of Eq. (5.11) is there to ensure this asymptotic behavior.

Our scheme for EDFT is based on the ground-state density-inversion method of Ref. [188] and Eq. (5.11), producing the ensemble XC potential from any given ensemble density. For

simplicity, we describe the scheme for spherical systems, but it can be extended to other systems easily. We modify the ground-state Eq. (5.11) for EDFT usage as

$$v_{\mathrm{xc},\mathtt{w}}^{(i+1)}(r) = v_{\mathrm{xc},\mathtt{w}}^{(i)}(r) + \alpha r^{\beta}[n_{\mathrm{KS},\mathtt{w}}^{(i)}(r) - n_{\mathtt{w}}(r)]/h(r), \tag{5.12}$$

where $h(r)$ is described below. Since the ionization energies of Eq. (5.11) are not defined for an ensemble, a double-loop scheme is used to ensure the correct $-1/r$ asymptotic behavior.

In the first iterative loop, we update the ensemble xc potential with Eq. (5.12) and set $h(r) = 1$. Convergence is reached when

$$\int \mathrm{d}^3 r \ \left| n_{KS,\mathtt{w}}^{(i)}(\mathbf{r}) - n_{\mathtt{w}} \right| < \Delta_1, \tag{5.13}$$

for a chosen accuracy Δ_1. Even if large β values are used to accelerate convergence in the large-r region, this first loop is usually insufficient to produce the $-1/r$ asymptotic behavior in the ensemble xc potential, due to the exponential asymptotic decay of the density. To compensate for this, we use a second iterative loop. Starting from the result of the first loop, the ensemble xc potential is updated using Eq. (5.12) with $h(r) = n_{\mathtt{w}}(r)$ and new values of α and β. The convergence of the second loop is also checked with Eq. (5.13), but with a smaller Δ_2. This second loop updates the ensemble xc potential with the relative error in the ensemble density, so the correction in the large-r region for each iteration is larger than in the first loop. The second loop is therefore more sensitive to the initial guess than the first loop, so it cannot be used independently. We consistently obtain $-1/r$ asymptotic behavior in the ensemble XC potentials produced by this double-loop procedure, without having to build it in the algorithm or in the initial guess. This double loop scheme guarantees both numerical stability and good convergence in the asymptotic region.

For ensembles of the helium atom, we found that parameters $\alpha \in [0, 2]$ and $\beta \in [0, 2]$ guarantee convergence of the first loop. For the second loop, $\alpha \in [0, 0.0001]$ and $\beta \in [0, 2]$

guarantee convergence, if `w` is not close to 0. As `w` approaches 0, the value of α needs to be smaller to prevent the second loop from becoming unstable. The double-loop scheme has had good numerical performance in all types of grids and discretizations of the Hamiltonian tested thus far.

5.4 Exact results for He atom

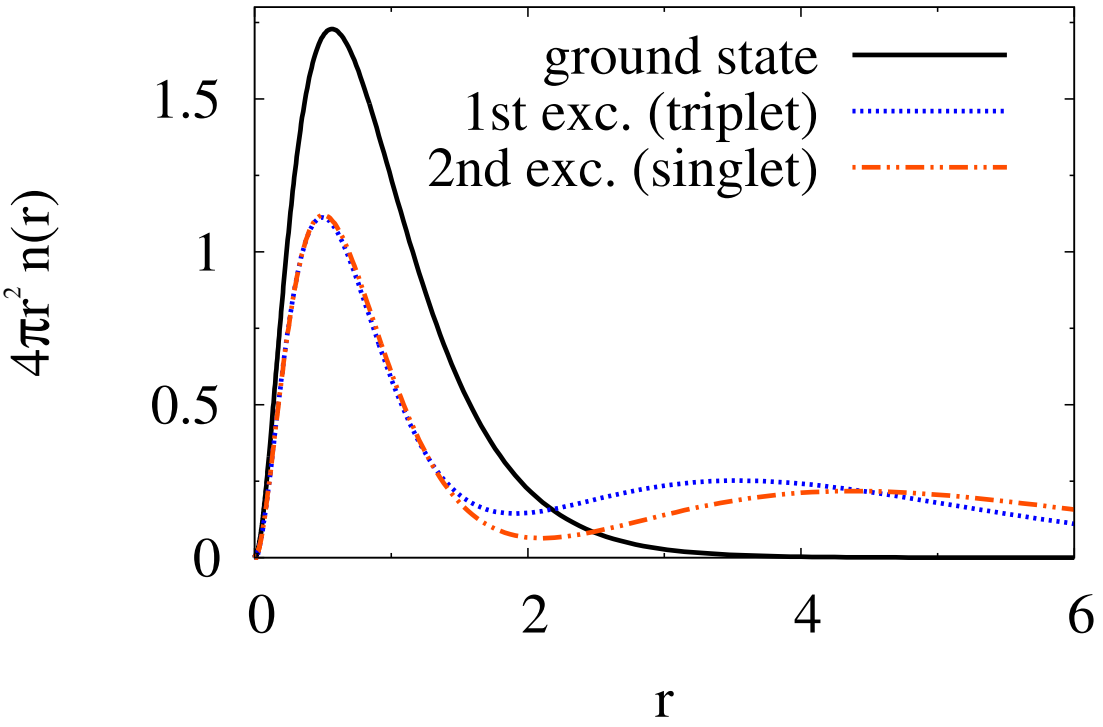

Figure 5.1: Radial densities for the three lowest eigenstates of helium. Color online.

We apply this scheme to highly accurate helium densities. Fig. 5.1 shows the ground and first two excited state densities for helium, which are essentially numerically exact. Two-body electronic wave functions were obtained by optimizing an expansion in Hylleraas functions[41]. Analytic integration of the density matrix associated with the optimum wave function provides an accurate spherically averaged charge density at each radius as a sum of terms. Basis sets composed of 376 and 406 Hylleraas functions for the singlet and triplet

states, respectively, result in total energies within 10^{-11} a.u. of accurate estimates[178]. The errors in the virial are below 10^{-12} a.u. for the ground state and 10^{-8} a.u. for the first singlet excited state, used in the singlet bi-ensemble. Our calculation for $\mathtt{w} = 0$ agrees with the known exact ground-state DFT quantities of helium [246].

The exact equiensemble density and potential are plotted in Fig. 5.2, along with those resulting from an equal mixture of orbitals from the ground-state KS potential. The subtle shell-like structure in the ensemble density corresponds to the cross-over between the ground-state density and the first singlet excited-state density. The upward bump near $r = 2.5$ in the ensemble KS potential ensures its ensemble density matches the interacting one, unlike the ensemble of orbitals from the ground-state KS potential. This bump is shifted left in the XC potential for the unprojected bi-ensemble (Fig. 5.3).

Fig. 5.4 shows the exact ensemble XC potentials at various $\mathtt{w}$ values, which have been found by subtracting the Hartree potential of the ensemble density from the KS potential. The bump near $r = 2.5$ develops as $\mathtt{w}$ increases. Even when $\mathtt{w}$ is close to 0, $v_{\mathrm{XC},\mathtt{w}}(r)$ differs from the $\mathtt{w} = 0$ (ground-state) XC potential in Fig. 5.4. The potentials shift further and further from the ground-state curve in the small-r region as $\mathtt{w}$ increases.

This discrepancy between small-$\mathtt{w}$ and $\mathtt{w} = 0$ potentials is due to the ensemble derivative discontinuity[150]. For any nonzero $\mathtt{w}$, the asymptotic behavior of the ensemble density is dominated by that of the excited state. Levy [150] proved an analog of the derivative discontinuity of ground-state DFT: the ensemble KS highest-occupied-molecular-orbital (HOMO) energy has a finite change as $\mathtt{w}$ changes from 0 (ground state) to 0_+:

$$\Delta v_{\mathrm{XC}}(\mathbf{r}) = \lim_{\mathtt{w}\to 0} v_{\mathrm{HXC},\mathtt{w}}[n_{\mathtt{w}}](\mathbf{r}) - v_{\mathrm{HXC}}[n](\mathbf{r}) \tag{5.14}$$

$$= \lim_{\mathtt{w}\to 0} \partial E_{\mathrm{HXC},\mathtt{w}}[n]/\partial \mathtt{w}|_{n=n_{\mathtt{w}}}. \tag{5.15}$$

This is an exact property of number-conserving excitations[1]. According to Eq. (5.10) and

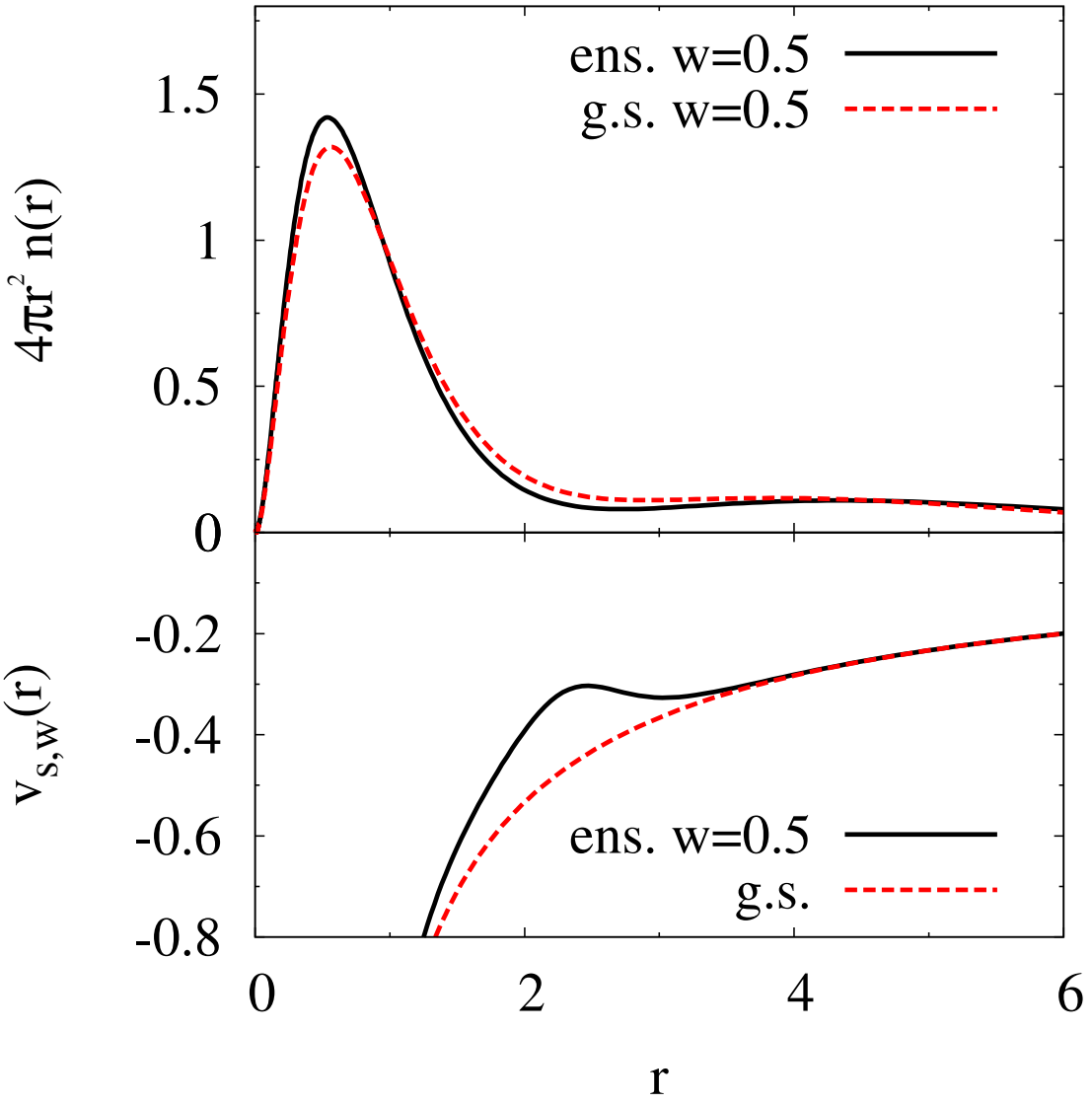

Figure 5.2: Radial densities and KS potentials for helium in singlet EDFT. The black solid lines are equiensemble properties. The red dashed line in the upper panel shows an equiensemble density constructed from orbitals of the ground-state KS potential; the red dashed line in the lower panel shows the exact ground-state KS potential.

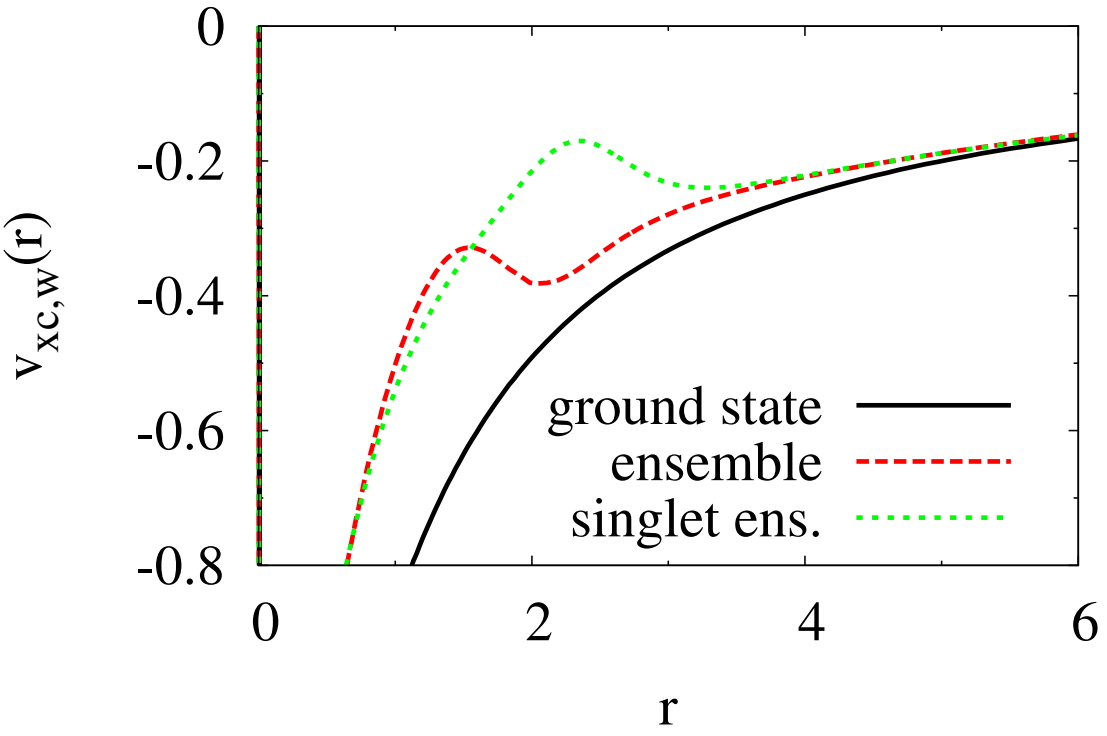

Figure 5.3: XC potentials for the helium ground state, bi-ensemble, and symmetry-projected singlet ensemble, produced by inverting ensemble densities constructed from the states shown in Fig. 5.1.

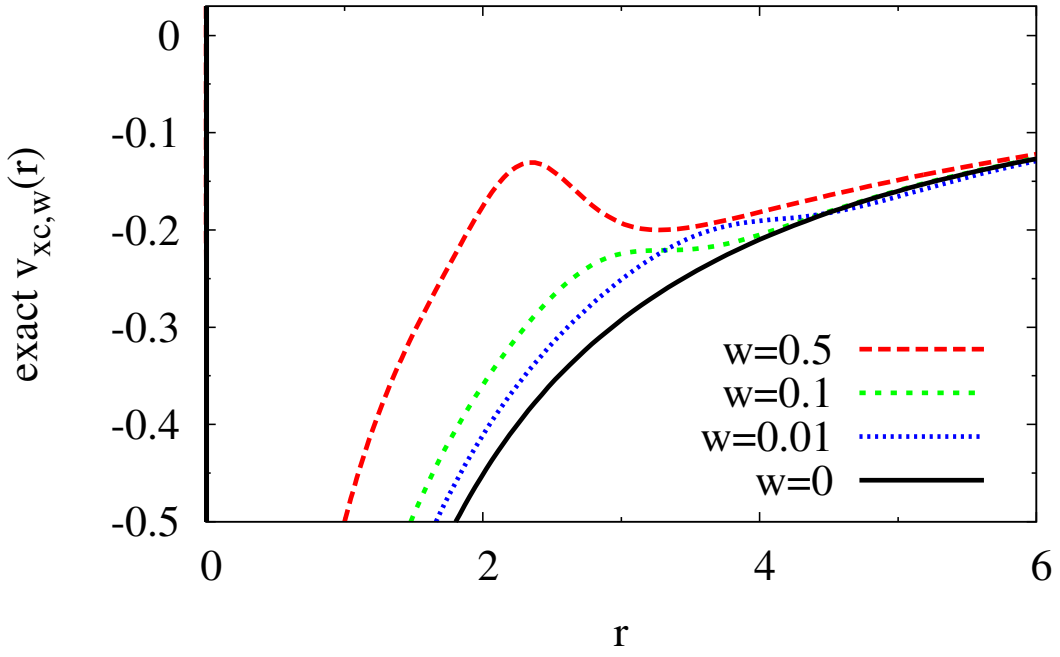

Figure 5.4: The exact XC potential for the helium singlet ensemble at various ensemble weights.

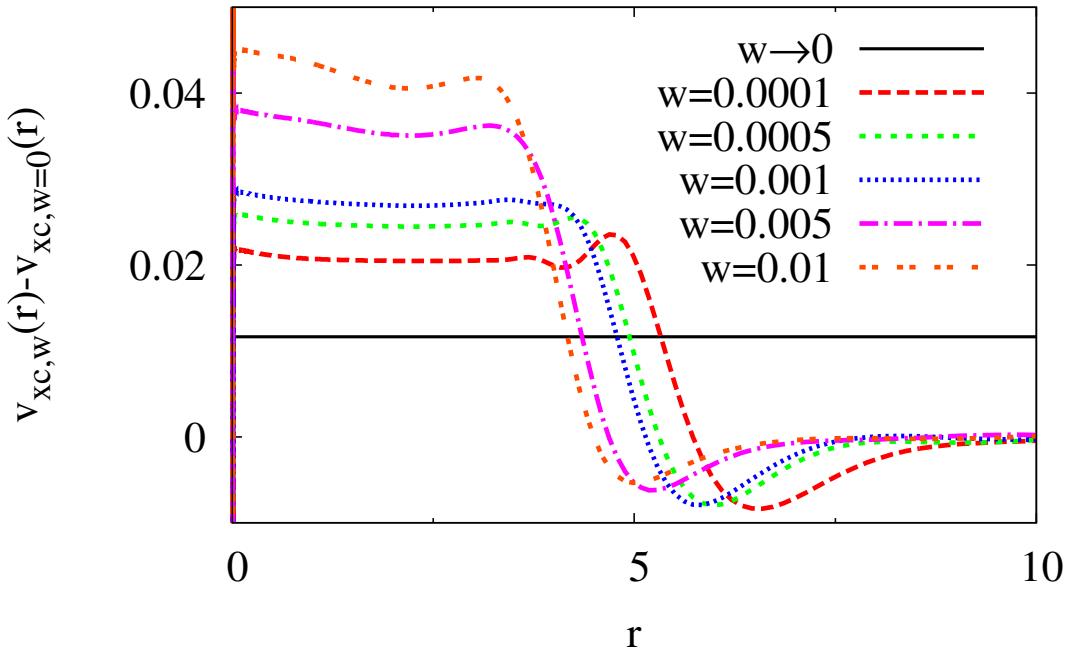

Figure 5.5: The exact potential jump Δv_{XC} as $\mathtt{w} \to 0$. The location of the step depends logarithmically on $\mathtt{w}$. As $\mathtt{w} \to 0$, the drop-off to the $\mathtt{w} = 0$ value moves infinitely far from the origin.

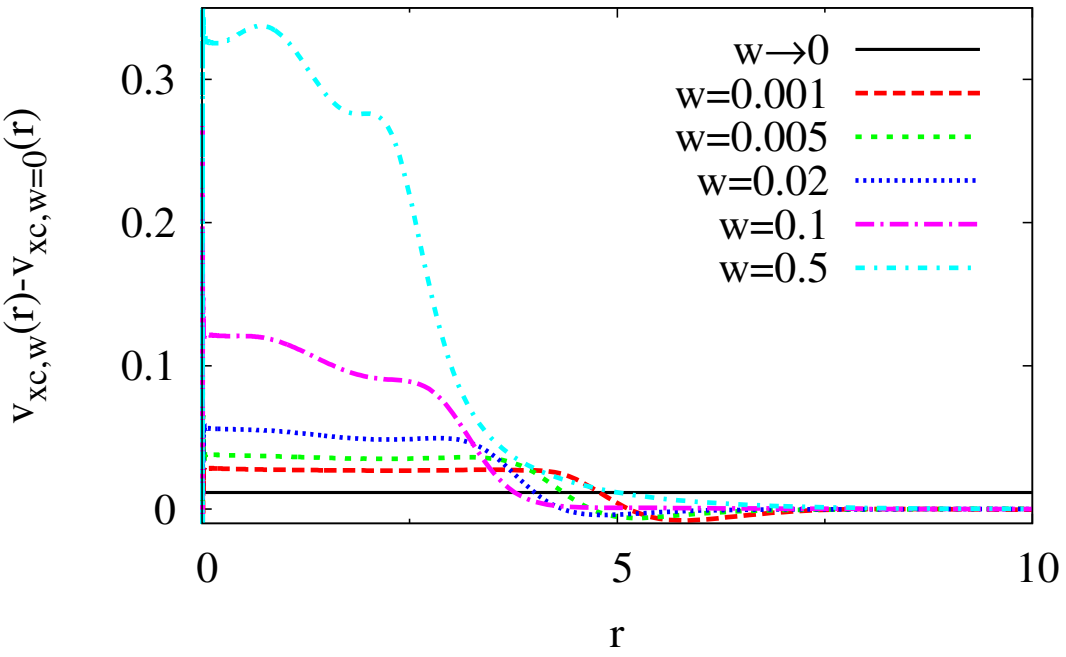

Figure 5.6: The exact potential jump $\Delta v_{\rm XC}$, showing the shoulder in the XC potential developing from the small-w step as w increases. Since w is no longer near zero, the asymptotic formula for the position of the drop-off no longer holds.

(5.15), we obtain $\Delta v_{\rm XC} = 0.0116$ a.u. for the singlet bi-ensemble.

Fig. 5.5 shows the exact XC potential jump for small w values. A step structure occurs since the ensemble density at small r is dominated by the HOMO density, and at large r the dominating behavior switches to the lowest-unoccupied-molecular-orbital (LUMO) density, which decays more slowly than the HOMO density. As w decreases, the switching point $r_{\rm C}$ moves to the right. In the limit of $\mathtt{w} \to 0$, the HOMO density dominates $n_{\mathtt{w}}(r)$ for finite r, so $\Delta v_{\rm XC}(r)$ becomes a constant. The ground-state limit is thus recovered since an additional constant on a potential has no physical effect. Though this difference is not close to a constant in the small-r region for larger w (Fig. 5.6), evidence of the step down remains in the shoulder present before the sharp decrease to the ground-state potential. We showed[207] that the switching point $r_{\rm C}$ for small values of w depends on $\log \mathtt{w}$, so the $\mathtt{w} \to 0$ limit is achieved slowly as w decreases. The large-w difference between the ground-state and

ensemble XC potentials (Fig. 5.4) appears to emerge continuously from the step-like small-$\mathtt{w}$ behavior, suggesting that the derivative discontinuity is crucial for replication of the bump in $v_{\mathrm{XC}}(\mathbf{r})$.

With the exact ensemble XC potentials available, we can numerically verify exact conditions of EDFT, such as the virial theorem[171, 175]. With traditionally defined Hartree, its form is similar to its ground-state counterpart[152]:

$$T_{\mathrm{C},\mathtt{w}}[n] = -E_{\mathrm{XC},\mathtt{w}}[n] - \int \mathrm{d}^3 r \; n(\mathbf{r})\mathbf{r}\cdot\nabla v_{\mathrm{XC},\mathtt{w}}(\mathbf{r}). \tag{5.16}$$

The virial as defined by Nagy yields the same results as directly calculated kinetic correlation to within 1%.

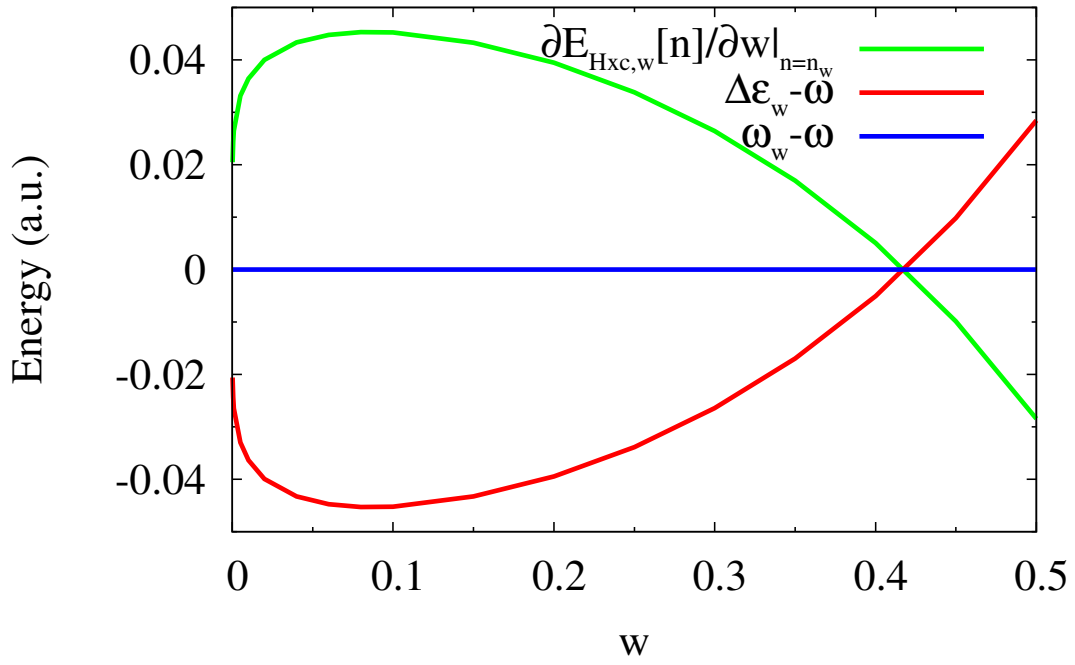

Figure 5.7: Eq. (5.10) applied to the exact helium singlet ensemble, demonstrating the exact cancellation of all $\mathtt{w}$-dependence in KS gaps (red) and corrections to the KS gap (green), leading to no $\mathtt{w}$ dependence in the calculated optical gap (blue). Gaps are shifted by the true optical gap ω for ease of comparison. Color online.

Eq. (5.10) converts the $\mathtt{w}$-dependent KS transition energies, $\Delta\epsilon_{\mathtt{w}}$, into the exact, $\mathtt{w}$-independent

transition frequency. The last term in Eq. (5.10) is significant for all values of $\mathtt{w}$ and is strongly $\mathtt{w}$-dependent. Fig. 5.7 shows the exact cancellation of the $\mathtt{w}$-dependence as required by Eq. (5.10). If this cancellation is incomplete, as it is in existing approximations, $\mathtt{w}$-dependent excitation energies will result.

The strong $\mathtt{w}$-dependence in the exact KS gap $\Delta\epsilon_{\mathtt{w}}$ is related to the bumps in the exact XC potentials (Fig. 5.4). The bump near $r = 2.5$ creates a local confinement effect near the nucleus, shifting the KS eigenvalues upward from the ground-state values. The effect is smaller for the 1s orbital because the 1s orbital density is already small and monotonically decaying at the position of the bump. The KS gap becomes larger as the bump is more prominent, as can be seen in the large-$\mathtt{w}$ region of Fig. 5.7. The sharp change of $\Delta\epsilon_{\mathtt{w}}$ in the small-$\mathtt{w}$ region of Fig. 5.7 is due to the ensemble derivative discontinuity, since $\Delta v_{\mathrm{XC}}(r)$ effectively creates a bump in the XC potential in the small-r region.

5.5 Approximations

To illustrate the usefulness of these results, we test the few existing approximations to EDFT, including the quasi-local-density approximation (qLDA)[131, 159], the single-Slater-determinant ghost-corrected exact exchange (SD)[73, 173], and the symmetry eigenstate Hartree-exchange (SEHX)[73, 207]. Both SD and SEHX are approximations falling under the overarching work on ghost interactions by Gidopoulos, Papaconstantinou, and Gross[73], which we denote here as GPG. The flexibility of GPG lies in its general approach to the description and elimination of ghost interactions introduced by the exchange and traditionally defined Hartree energies. These ghosts occur when one uses the ensemble density as input into these terms, as there are spurious interactions between the ground and excited states. If one uses the ensemble definition of Hartree-exchange in Eq. (5.8), these ghosts are avoided.

As a general methodology, GPG can be used in various forms. When faced with degenerate states, one always has choices about which states to use to describe the system of interest. Two obvious choices are single- and multi-determinant descriptions. When the GPG methodology is applied to ensemble Hartree-exchange using symmetry eigenstates with the Krieger-Li-Iafrate approximation[137], one produces the SEHX approximation. Alternatively, one may choose to use single-determinant states within the GPG methodology. We show this SD approach alongside the SEHX approximation to clarify the effect of using full eigenstates to describe ensemble ghosts, since previous calculations[37, 133, 174, 187, 236] can be reevaluated in light of these comparisons.

The general equation of the SEHX energy for an ensemble up to the I-th group of degenerate states('multiplet') is[207]

$$
\begin{aligned}
&E_{\mathrm{HX}}^{\mathrm{SEHX}} = \\
&\int \frac{\mathrm{d}^3 r \mathrm{d}^3 r'}{|\mathbf{r}-\mathbf{r}'|} \Bigg\{ \sum_{\mu,\nu>\mu} \left\{ n_\mu^{\mathrm{orb}}(\mathbf{r}) n_\nu^{\mathrm{orb}}(\mathbf{r}') - \Re[n_\mu^{\mathrm{orb}}(\mathbf{r}',\mathbf{r}) n_\nu^{\mathrm{orb}}(\mathbf{r},\mathbf{r}')] \delta_{\sigma_\mu,\sigma_\nu} \right\} \sum_{i=1}^{I} \sum_{k=1}^{g_i} \mathtt{w}_{i,k} \sum_{p=1}^{\tilde{g}_{\tilde{i}}} |C_{i,k,p}|^2 f_{\tilde{i},p,\mu} f_{\tilde{i},p,\nu} \\
&+ \sum_{\substack{\mu,\nu>\mu \\ \kappa,\lambda>\kappa}} [\phi_\mu^*(\mathbf{r}) \phi_\nu^*(\mathbf{r}') \phi_\kappa(\mathbf{r}) \phi_\lambda(\mathbf{r}') \delta_{\sigma_\mu,\sigma_\kappa} \delta_{\sigma_\nu,\sigma_\lambda} - \phi_\mu^*(\mathbf{r}) \phi_\nu^*(\mathbf{r}') \phi_\lambda(\mathbf{r}) \phi_\kappa(\mathbf{r}') \delta_{\sigma_\mu,\sigma_\lambda} \delta_{\sigma_\nu,\sigma_\kappa}] \\
&\times \sum_{i=1}^{I} \sum_{k=1}^{g_i} \mathtt{w}_{i,k} \sum_{p,q\neq p}^{\tilde{g}_{\tilde{i}}} C_{i,k,p}^* C_{i,k,q} f_{\tilde{i},p,\mu} f_{\tilde{i},p,\nu} f_{\tilde{i},q,\kappa} f_{\tilde{i},q,\lambda} \prod_{\eta\neq\mu,\nu,\kappa,\lambda} \delta_{f_{\tilde{i},p,\eta}, f_{\tilde{i},q,\eta}} \Bigg\},
\end{aligned}
\tag{5.17}
$$

where i denotes a multiplet; k denotes a specific state in the i-th multiplet; g_i is the degeneracy of the i-th multiplet; $\tilde{g}_{\tilde{i}}$ is the degeneracy of the corresponding Kohn-Sham (KS) multiplet; p, q denote specific KS single Slater determinants; $\mu, \nu, \kappa, \lambda, \eta$ denote KS orbitals; $\mathtt{w}_{i,k}$ is the weight of the k-th state in the i-th multiplet; $C_{i,k,p}$ is the mixing coefficient of the p-th determinant to make up the k-th state in the i-th multiplet; $f_{\tilde{i},p,\mu}$ is the occupation number of the μ-th orbital in the p-th determinant of the $\tilde{i}$-th KS multiplet; σ denotes spin, ϕ denotes KS orbitals; $n_\mu^{\mathrm{orb}}(\mathbf{r})$ is the orbital density of the μ-th orbital; and $n_\mu^{\mathrm{orb}}(\mathbf{r},\mathbf{r}') = \phi_\mu(\mathbf{r})\phi_\mu^*(\mathbf{r}')$.

This form is more explicit than the one given in our previous work[207], in order to facilitate use of the SEHX version of GPG. Ref. [73] presents the general framework and a single-determinant example based on the exact exchange OEP formalism of Nagy[172, 173]. However, the authors use the ensemble Hartree-exchange definition of Eq. (5.8) and symmetry eigenstates to calculate their reported results. We have denoted such a procedure as SEHX. SEHX, as written out here and in Ref. [207], yields self-consistent results that agree to within 0.03 eV with those presented in Table I of Ref. [73], with this difference assumed to be due to numerical differences in implementation.

5.6 Approximate Results

Comparison of exact and approximate quantities exposes differences in single- and multi-determinant approximations, as well as the shortcomings both share. Fig. 5.8 shows exact and approximate XC potentials using the exact ensemble density. Both the SD and the SEHX are OEPs, which guarantees their correct $-1/r$ asymptotic behavior in the XC potential (Fig. 5.8). However, only the SEHX potential shows the large $\mathtt{w}$ bump and recovers the general shape of the exact $v_{\mathrm{XC},\mathtt{w}}(r)$.

The correlation potential $v_{\mathrm{C},\mathtt{w}}(r)$ displays two distinct bumps, shown in Fig. 5.9. The $w = 0$ correlation potential matches perfectly with the exact ground-state correlation potential in Ref. [246]. The first bump at about $r = 1$ also exists in the ground-state $v_{\mathrm{C}}(r)$, while the second bump at about $r = 2.5$, which vanishes rapidly as $\mathtt{w}$ decreases, is unique to EDFT.

Fig. 5.10 shows that, in the small $\mathtt{w}$ region, only SEHX generates a step-like form for the ensemble derivative discontinuity. The SEHX XC potential is also the only approximation that has the characteristic bump of the exact XC potential. Both SEHX and SD are OEP methods, but the former satisfies the exact condition of the ensemble derivative disconti-

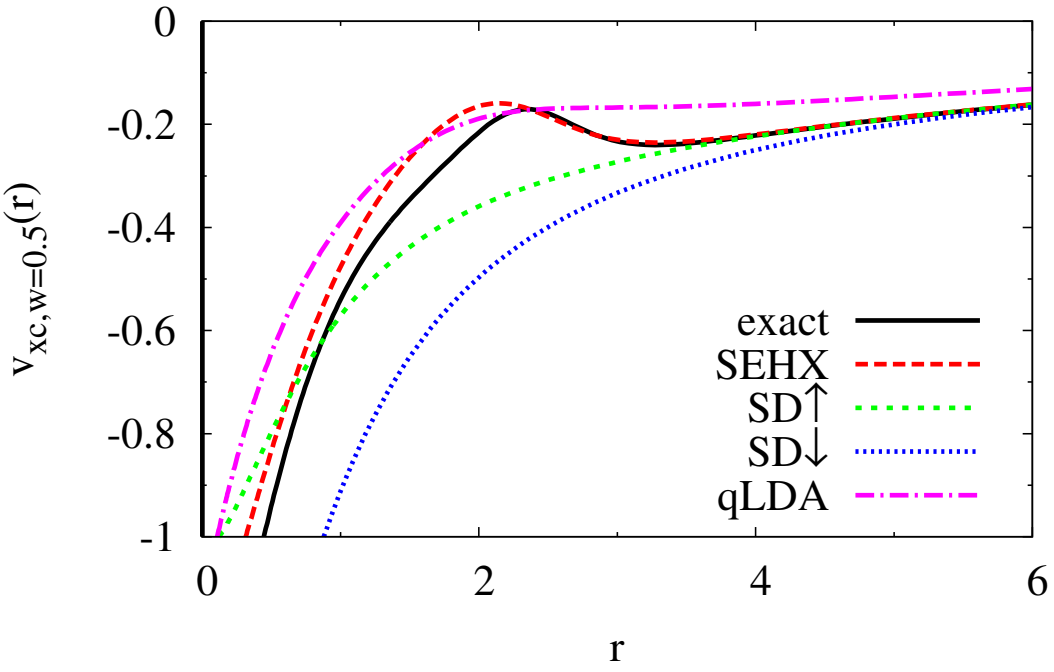

Figure 5.8: The exact and approximated $v_{\rm XC}(\mathbf{r})$ for the helium singlet equiensemble. The approximated $v_{\rm XC}$'s are evaluated using the exact ensemble density as input.

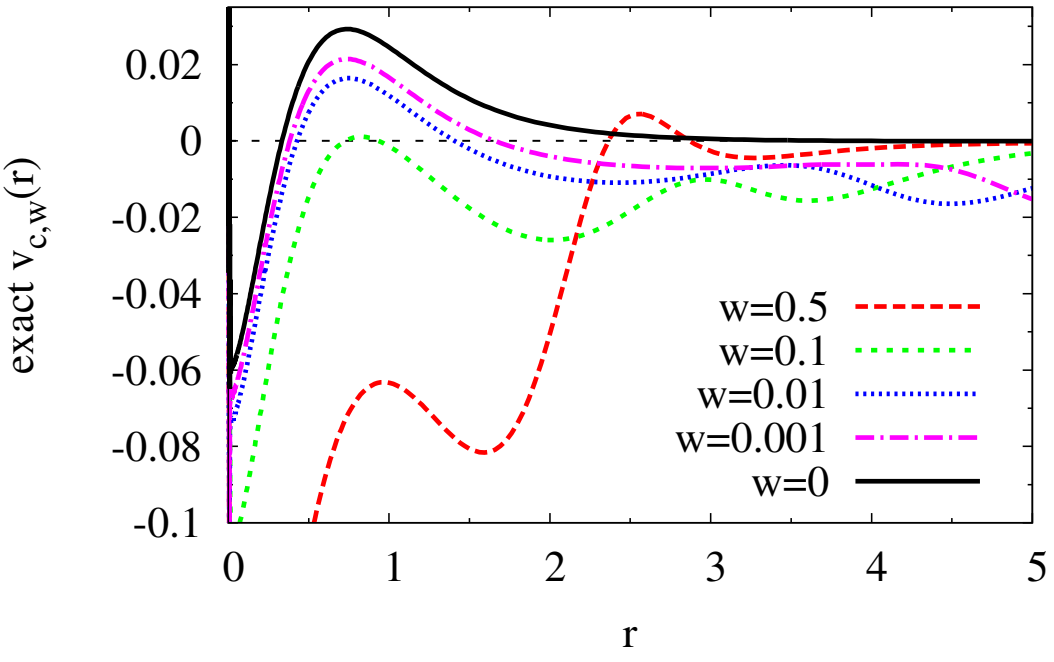

Figure 5.9: The exact $v_{\rm C}(r)$ for the helium singlet equiensemble shows two upward bumps and does not depend on the definition of the Hartree potential used. These are obtained by subtracting SEHX $v_{\rm X,w}(r)$ of the exact ensemble density from the exact $v_{\rm XC,w}(r)$.

nuity, while the latter does not. The SEHX potential is obtained by applying the KLI approximation[137] to the optimized effective potential (OEP) equation[173]. Equations for $v^{\mathrm{SEHX}}_{\mathrm{HX},\mathtt{w}}(\mathbf{r})$ of the helium singlet bi-ensemble are given in Eqs. 41 - 43 of Ref. [207].

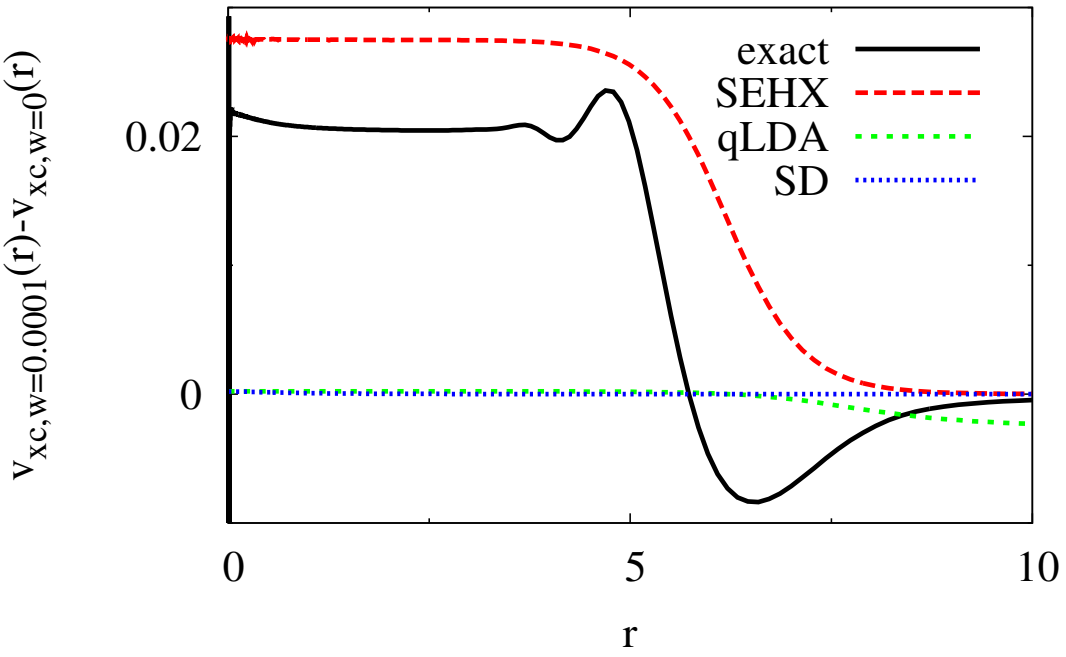

Figure 5.10: Self-consistent $\Delta v_{\mathrm{XC}}(r)$ of various approximations at $\mathtt{w} = 0.0001$. Only SEHX (dotted red) replicates a shift similar to that of the exact curve (solid black). Color online.

To understand the absence of the derivative discontinuity in SD, we compare the small-$\mathtt{w}$ behavior of both SD and SEHX[207]. The SD potential for the spin-up electron is

$$\begin{aligned} v^{\mathrm{SD}}_{\mathrm{HX}\uparrow,\mathtt{w}}(\mathbf{r}) = &\Big\{(1-\mathtt{w})n^{\mathrm{orb}}_{1\uparrow}(\mathbf{r})[v_{1\uparrow}(\mathbf{r}) + \bar{v}_{\mathrm{HX}1\uparrow,\mathtt{w}} - \bar{v}_{1\uparrow}] \\ &+ \mathtt{w}n^{\mathrm{orb}}_{2\uparrow}(\mathbf{r})[v_{2\uparrow}(\mathbf{r}) + \bar{v}_{\mathrm{HX}2\uparrow,\mathtt{w}} - \bar{v}_{2\uparrow}]\Big\}/n_{\uparrow,\mathtt{w}}(\mathbf{r}), \end{aligned} \tag{5.18}$$

where $n_{\uparrow,\mathtt{w}}(\mathbf{r}) = (1-\mathtt{w})n^{\mathrm{orb}}_{1\uparrow}(\mathbf{r}) + \mathtt{w}n^{\mathrm{orb}}_{2\uparrow}(\mathbf{r})$, and

$$v_{1\uparrow}(\mathbf{r}) = v_{2\uparrow}(\mathbf{r}) = \int \frac{\mathrm{d}^3 r'}{|\mathbf{r}-\mathbf{r}'|} n^{\mathrm{orb}}_{1\downarrow}(\mathbf{r}'). \tag{5.19}$$

Barred quantities are defined

$$\bar{v}_j = \int \mathrm{d}^3 r \; v_j(\mathbf{r}) n_j^{\mathrm{orb}}(\mathbf{r}), \tag{5.20}$$

so that $\bar{v}_{\mathrm{HX1}\uparrow,\mathtt{w}}$, for instance, is the expectation value of the spin-up HX potential with respect to $n_{1\uparrow}^{\mathrm{orb}}(\mathbf{r})$.

Comparing the SEHX[207] and SD expressions for the HX potentials makes the disappearance of the derivative discontinuity in the SD approximation clear. When $\mathtt{w}$ is very small, in the region where r is smaller than a certain r_{C}, $n_{\mathtt{w}}(\mathbf{r})$ is dominated by the $(2-\mathtt{w})n_1^{\mathrm{orb}}(\mathbf{r})$ term (see Eq. 41 of Ref. [207]). In the $r > r_{\mathrm{C}}$ region, however, it is dominated by the $wn_2^{\mathrm{orb}}(\mathbf{r})$ term due to the slower decay of $n_2^{\mathrm{orb}}(\mathbf{r})$. Thus, when $\mathtt{w}$ is very small, we have

$$v_{\mathrm{HX},\mathtt{w}\approx 0}^{\mathrm{SEHX}}(\mathbf{r}) \approx \begin{cases} v_1(\mathbf{r}) + \bar{v}_{\mathrm{HX1}} - \bar{v}_1, & r < r_{\mathrm{C}}, \\ v_2(\mathbf{r}) + \bar{v}_{\mathrm{HX2}} - \bar{v}_2, & r > r_{\mathrm{C}}, \end{cases} \tag{5.21}$$

and

$$v_{\mathrm{HX}\uparrow,\mathtt{w}\approx 0}^{\mathrm{SD}}(\mathbf{r}) \approx \begin{cases} v_{1\uparrow}(\mathbf{r}) + \bar{v}_{\mathrm{HX1}\uparrow,\mathtt{w}} - \bar{v}_{1\uparrow}, & r < r_{\mathrm{C}}, \\ v_{2\uparrow}(\mathbf{r}) + \bar{v}_{\mathrm{HX2}\uparrow,\mathtt{w}} - \bar{v}_{2\uparrow}, & r > r_{\mathrm{C}}, \end{cases} \tag{5.22}$$

For any $\mathtt{w}$, $v_{1\uparrow}(\mathbf{r}) = v_{2\uparrow}(\mathbf{r})$, so the SD approximation yields the same behavior at large or small $\mathtt{w}$. In contrast, when $\mathtt{w}$ is very small within the SEHX approximation,

$$v_1(\mathbf{r}) \approx \int \frac{\mathrm{d}^3 r'}{|\mathbf{r} - \mathbf{r}'|} n_1(\mathbf{r}'), \tag{5.23}$$

and

$$\begin{aligned} v_2(\mathbf{r}) &= \int \frac{\mathrm{d}^3 r'}{|\mathbf{r}-\mathbf{r}'|}\left[n_1^{\mathrm{orb}}(\mathbf{r}') + \frac{\phi_1^*(\mathbf{r})\phi_2^*(\mathbf{r}')\phi_1(\mathbf{r}')}{\phi_2^*(\mathbf{r})}\right] \\ &= v_1(\mathbf{r}) + f(\mathbf{r}). \end{aligned} \tag{5.24}$$

$v_1(\mathbf{r})$ and $v_2(\mathbf{r})$ therefore have a finite difference even at $\mathtt{w} = 0$. We have shown that $r_{\mathrm{C}} \approx -0.621\ln\mathtt{w}$ in Ref. [207], so the constant terms in Eq. (5.21) are

$$\begin{aligned} \bar{v}_{\mathrm{HX1}}(\mathbf{r}) - \bar{v}_1(\mathbf{r}) &= \int \mathrm{d}^3 r\; n_1^{\mathrm{orb}}(\mathbf{r})[v_{\mathrm{HX},\mathtt{w}\approx 0}^{\mathrm{SEHX}}(\mathbf{r}) - v_1(\mathbf{r})] \\ &\approx \int \mathrm{d}\Omega \int_{r_{\mathrm{C}}}^{\infty} \mathrm{d}r\; n_1^{\mathrm{orb}}(\mathbf{r}) f(\mathbf{r}), \end{aligned} \tag{5.25}$$

because the integrand vanishes when $r < r_{\mathrm{C}}$ and $\mathtt{w}$ is small. Similarly,

$$\bar{v}_{\mathrm{HX2}}(\mathbf{r}) - \bar{v}_2(\mathbf{r}) \approx -\int \mathrm{d}\Omega \int_0^{r_{\mathrm{C}}} \mathrm{d}r\; n_2^{\mathrm{orb}}(\mathbf{r}) f(\mathbf{r}). \tag{5.26}$$

Eq. 5.24 shows that $f(\mathbf{r})$ decreases rapidly as $\mathbf{r}$ increases, since $\phi_1(\mathbf{r})$ decays faster asymptotically than $\phi_2(\mathbf{r})$. Since $f(\mathbf{r})$ is a part of $v_2(\mathbf{r})$, which only dominates the large-r behavior of $v_{\mathrm{HX},\mathtt{w}\approx 0}^{\mathrm{SEHX}}(\mathbf{r})$, the difference between the large-r and small-r behaviors of $v_{\mathrm{HX},\mathtt{w}\approx 0}^{\mathrm{SEHX}}(\mathbf{r})$ is due to the constant terms in Eqs. (5.25) and (5.26). In the $w \to 0$ limit, Eq. (5.25) vanishes, and Eq. (5.26) approaches a finite negative value. The additive constant in the HX potential obtained needs to be determined by matching with the known $1/r$ behavior, and the resulting potential would show the upward ensemble derivative discontinuity step illustrated in Fig. 5.5. Since both $\bar{v}_{\mathrm{HX1}\uparrow,\mathtt{w}} - \bar{v}_{1\uparrow}$ and $\bar{v}_{\mathrm{HX2}\uparrow,\mathtt{w}} - \bar{v}_{2\uparrow}$ vanish in the $\mathtt{w} \to 0$ limit, there is no ensemble derivative discontinuity for SD.

Figs. 5.11, 5.12, and 5.13 demonstrate that qLDA, SD, and SEHX approximations are unable to generate $\mathtt{w}$-independent excitation energies. The less severe $\mathtt{w}$-dependence of the SEHX KS gap is due to its closer replication of the exact ensemble derivative discontinuity, though the SEHX cancellation of excitation energy $\mathtt{w}$-dependence is not exact. Fig. 5.8

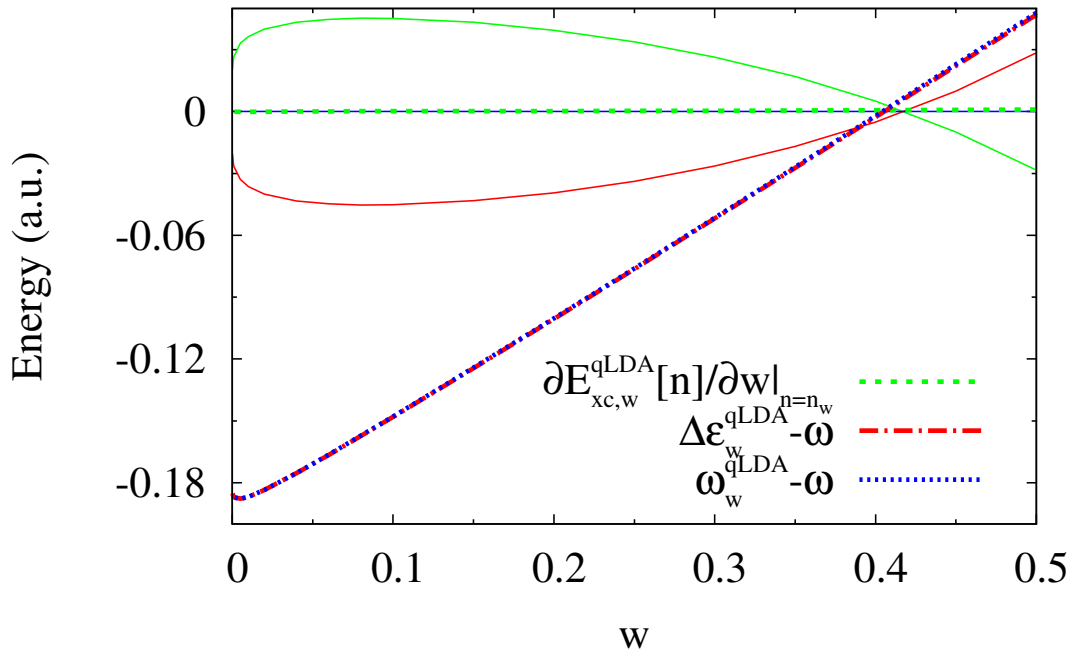

Figure 5.11: Eq. (5.10) applied to self-consistent quasi-LDA results. The correction to the quasi-LDA KS gap (dashed green) is not 0, but it is too small to be noticed on this scale. This correction is inadequate to cancel the w-dependence in the qLDA KS gap (dashed red), resulting in inaccurate, w-dependent calculated optical gaps (dashed blue). The gaps have been shifted in this figure by the optical gap ω for easier comparison, and the exact results of Fig. 5.7 are also shown for context. Color online.

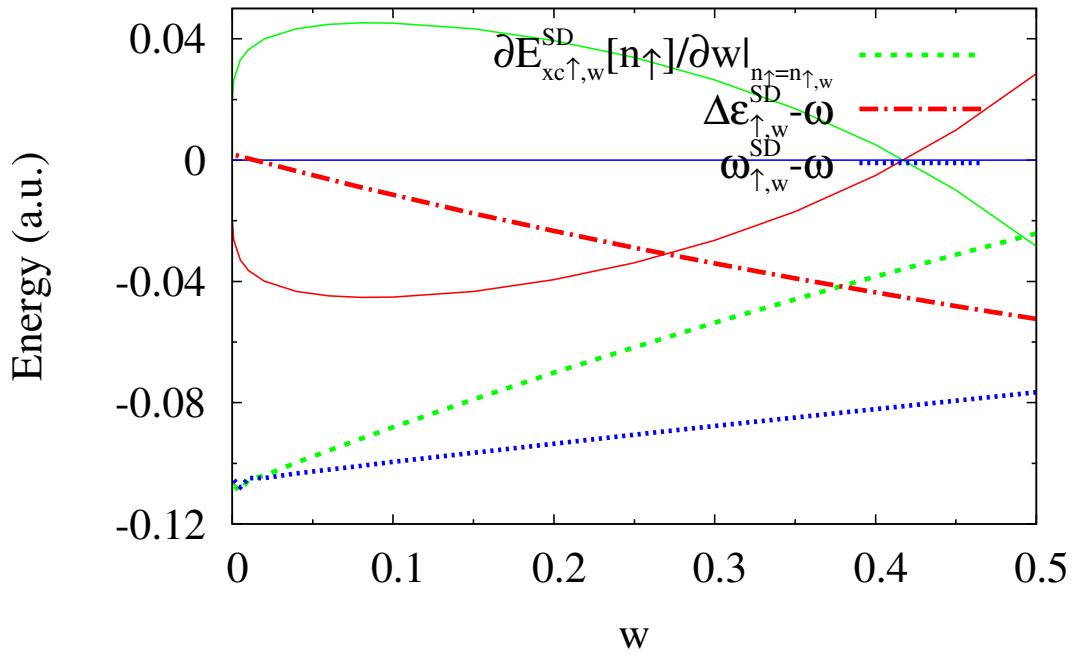

Figure 5.12: Eq. (5.10) applied to self-consistent SD results. The spin-up SD KS gap (dashed red) is insufficiently corrected by the SD corrections to the KS gap (dashed green), yielding calculated optical gaps that are too small (dashed blue). Though the w-dependence is less severe than for qLDA, it is still non-negligible. The gaps have been shifted in this figure by the optical gap ω for easier comparison, and the exact results of Fig. 5.7 are also shown for context. Color online.

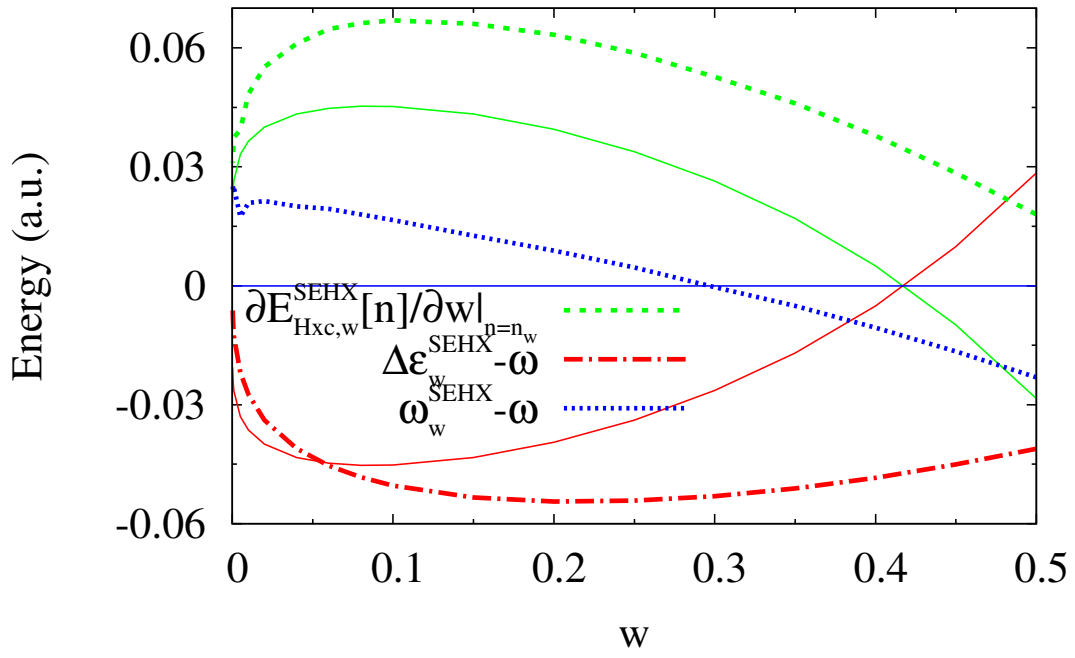

Figure 5.13: Eq. (5.10) applied to approximate self-consistent SEHX results. SEHX produces far less variation in calculated excitation energies with `w` (dashed blue), which appears to be the result of its ensemble derivative discontinuity. This produces approximate KS gaps (dashed red) and KS gap corrections (dashed green) that most closely resemble the exact curves in overall shape. The exact results (as in Fig. 5.7) are also shown for context. The gaps have been shifted in this figure by the optical gap ω for easier comparison, and the exact results of Fig. 5.7 are also shown for context. Color online.

shows that the position of the large w bump of SEHX is at smaller r values than the exact one. This agrees with the less rapid change of the SEHX KS gap in the large-w region. In Fig. 5.13, the sharp change of the SEHX KS gap in the small-w region is similar to that of the exact ensemble, which is due to the bump created by the step in $\Delta v_{\rm XC}$. qLDA and SD potentials have neither the large-w bump nor the small-w derivative discontinuity step, so the w-dependencies of their KS gaps are very different from the exact one. Comparing to Figs. 5.4 and 5.8, the $r = 2.5$ bump in the correlation potential (Fig. 5.9) fixes the position of the bump in the exchange-only (SEHX) potential, and thereby sets the w-dependence of the KS gap and its correction.

5.7 Conclusion

This work provides a method for inverting ensemble densities, so that the resulting exact ensemble KS systems can be used as references for developing approximated EDFT functionals. We show the density-inversion method for spherically-symmetric systems in this paper, but it is not difficult to generalize the method for other types of systems. We have tested the density-inversion method in cylindrically-symmetric systems and it also yields good results[207]. For systems with lower symmetry, the real-space approach shown in this paper would not yield accurate results without a massive grid point set. Though expression in a basis set may solve this problem, further study is required to determine the effect this would have on the density-inversion method's stability and performance.

We applied the density-inversion method on the helium singlet bi-ensemble for its simplicity. This exposes the continuous emergence of the exact XC potential bump from the ensemble derivative discontinuity and facilitates comparison with approximations. The singlet bi-ensemble is by no means the limit of the applicability of the density-inversion method, however. In Ref. [207], we apply the method to ensembles of various real and model 2-

electron systems, in which it retains the numerical stability and accuracy seen in this paper. This work illustrates that EDFT properties deviate from ground-state DFT ones in previously unseen ways. Also, some exact conditions, such as Eq. (5.10), do not suggest obvious methods for their satisfaction by approximations. Of the approximations we tested, the SEHX version of GPG, the only one with an ensemble derivative discontinuity, generated the most accurate XC potentials and excitation energies. These complications make developing a good EDFT functional considerably harder than in ground state, and we hope the exact results shown in this work can alleviate some burden on EDFT developers.

We thank Nikitas Gidopoulos for providing very helpful clarifications regarding Ref. [73]. Z.-H.Y. thanks Yu Zhang and Daniel Jensen for very helpful discussions on density inversion problems. Z.-H.Y. and C.A.U. are supported by NSF grant No. DMR-1005651. A.P.J. is supported by DOE grant DE-FG02-97ER25308. J.R.T. and R.J.N. acknowledge financial support from the Engineering and Physical Sciences Research Council (EPSRC) of the UK. K.B. supported by DOE grant DE-FG02-08ER46496.

Part V

Finite Temperature Potential Functional Theory

Chapter 6

Foundations of Finite Temperature PFT

6.1 Potential Functional Theory (PFT)

In DFT calculations, the computational bottleneck involves solving the Kohn-Sham equations. One way around this costly step is formulating an orbital-free method, which requires a direct approximation of the kinetic energy functional. As shown by Cangi et al.[27, 28], the kinetic energy can be expressed as a functional of the density or of the potential, due to the one-to-one correspondence of density and potential as shown by the Hohenberg-Kohn Theorem in 1964.[99] Unreasonable accuracy for box boundary conditions can be achieved at zero temperature by use of an approximate density formula and coupling-constant expression for the non-interacting kinetic energy[28]:

$$T_{\mathrm{S}}^{cc}[v] = \int d^3r \; \{\bar{n}_{\mathrm{S}}^{A}[v](\mathbf{r}) - n_{\mathrm{S}}^{A}[v](\mathbf{r})\} \; v(\mathbf{r}). \tag{6.1}$$

Here, $n_{\mathrm{S}}^{A}[v](\mathbf{r})$ is an approximation to the non-interacting density as a functional of the potential, and

$$\bar{n}_{\mathrm{S}}^{A}[v](\mathbf{r}) = \int_0^1 d\lambda \; n_{\mathrm{S}}^{A}[v^{\lambda}](\mathbf{r}), \tag{6.2}$$

where $v^{\lambda}(\mathbf{r}) = (1-\lambda)v_0(\mathbf{r}) + \lambda v(\mathbf{r})$ and v_0 is chosen to be zero. The coupling constant, λ, in our formula connects two potentials:

$$v^{\lambda}(\mathbf{r}) = (1-\lambda)v_0(\mathbf{r}) + \lambda v(\mathbf{r}), \tag{6.3}$$

where v_0 is some reference potential and $v(\mathbf{r})$ is our potential of interest. One may think of it as a dial: as λ increases from 0 to 1, our system moves smoothly from a reference potential to our potential of interest, passing through a weighted mixture of the two. For instance, a coupling constant could be used to move gradually from a flat box potential to a box with a dip in the middle.

By defining both the kinetic energy and density as functionals of the potential, a general approximation to the kinetic energy is automatically generated, eliminating the need for a separate kinetic energy approximation. It will be shown that a similar kinetic energy approximation can be generated at finite temperature.

6.2 Derivation of Formalism at Finite Temperature

Cangi et al. have shown PFT to be highly accurate at zero temperature and that inclusion of leading corrections to the local density approximation improves the accuracy of functionals.[27, 28, 49] Since these corrections are built into semiclassical methods, pursuit of finite temperature PFT (FT PFT) is a natural progression. The first step is to derive a potential functional expression for the non-interacting kentropy in terms of the coupling

constant.

In general, a universal potential functional can be defined in order to establish the grand potential at finite temperature as a functional of the potential. For a non-interacting system,

$$\Omega_{\rm S}^{\tau}[v] \quad = F_{\rm S}^{\tau}[v] + \int d^3r \; n^{\tau}[v](\mathbf{r}) \;\; (v(\mathbf{r}) - \mu) \tag{6.4}$$

$$= K_{\rm S}^{\tau}[v] + \int d^3r \; n^{\tau}[v](\mathbf{r}) \;\; (v(\mathbf{r}) - \mu)\,. \tag{6.5}$$

Using $v^{\lambda} = (1-\lambda)v_0 + \lambda \; v(\mathbf{r})$, we can also write

$$\Omega_{\rm S}^{\tau}[v] = \Omega_0^{\tau}[v] + \int_0^1 d\lambda \;\; \left(\frac{\partial \Omega_{\rm S}^{\tau}[v^{\lambda}]}{\partial \lambda}\right) \tag{6.6}$$

$$= \Omega_{\rm S}^{\tau}[v_0] + \int d^3r \int_0^1 d\lambda \, (-v_0(\mathbf{r}) + v(\mathbf{r})) \;\; n^{\tau}[v^{\lambda}](\mathbf{r}) \tag{6.7}$$

where $\Omega_{\rm S}^{\tau}[v_0] = K_{\rm S}^{\tau}[v_0] + V^{\tau}[v_0] - \mu^{\tau} N$ is the non-interacting grand potential of a system in a reference potential at temperature τ. By setting v_0 as the infinite square well potential, we can write the non-interacting kentropy in terms of a reference kentropy and the density as a potential functional:

$$K_{\rm S}^{\tau}[v] = K_{\rm S}^{\tau}[v_0] + \int d^3r \left\{ \int_0^1 d\lambda \; n^{\tau}[v^{\lambda}](\mathbf{r}) - n^{\tau}[v](\mathbf{r}) \right\} v(\mathbf{r}). \tag{6.8}$$

Labeling the reference kentropy to clarify its dependence on the box boundary conditions, the coupling constant expression for the non-interacting kentropy is written

$$K_{\rm S}^{\tau}[v] = K_{\rm box}^{\tau} + \int d^3r \, \{\bar{n}^{\tau}[v](\mathbf{r}) - n^{\tau}[v](\mathbf{r})\} \, v(\mathbf{r}), \tag{6.9}$$

where $\bar{n}^{\tau}[v](\mathbf{r}) = \int_0^1 d\lambda \; n^{\tau}[v^{\lambda}](\mathbf{r})$ and we've dropped the *cc* superscript for simplicity of notation. Thus, by this method, one needs only select an approximation to the density and

calculate the reference kentropy to calculate the approximate non-interacting kentropy.

To summarize, we have used the idea of the coupling constant to derive an exact expression that feeds the potential into a functional that then yields the density, and then uses that density to generate the exact universal functional at finite temperature. The universal functional is a combination of free energy and electron-electron interaction energy that is the same for any system of electrons at finite temperature. If we have the exact density written in terms of the potential, we will get out the exact universal functional value. If we have a very good approximation to the density, we will get out a very good approximation to it. This formalism is exact and applies to all systems. It can be used with interacting or non-interacting density expressions. To leverage the huge body of work in XC approximations and to simplify the task of finding highly accurate density approximations, our formalism uses it with non-interacting densities, as discussed in the next section.

Chapter 7

An Efficient Formalism for Warm Dense Matter Simulations

written with Attila Cangi. Submitted to *Phys. Rev. B* (2015).

Abstract: *Simulation of warm dense matter requires computational methods that capture both quantum and classical behavior efficiently under high-temperature, high-density conditions. Currently, density functional theory molecular dynamics is used to model electrons and ions, but this method's computational cost skyrockets as temperatures and densities increase. We propose finite-temperature potential functional theory as an in-principle-exact alternative that suffers no such drawback. We derive an orbital-free free energy approximation through a coupling-constant formalism. Our density approximation and its associated free energy approximation demonstrate the method's accuracy and efficiency.*

7.1 Introduction

Warm dense matter (WDM) is a highly energetic phase of matter with characteristics of both solids and plasmas[80]. The high temperatures and pressures necessary for creation of WDM are present in the centers of giant planets and on the path to ignition of inertial confinement fusion capsules[5, 180]. The high cost of experiments in this region of phase space has led to renewed interest and great progress in its theoretical treatment[81, 167, 218]. Traditional plasma and condensed matter theoretical approaches exhibit serious shortcomings[80], leading to the WDM regime's characterization as the "malfunction junction." Since both quantum and classical effects are crucial to accurate WDM simulations[128], density functional theory (DFT) molecular dynamics has been used with increasing frequency[101]. This method relies on Kohn-Sham (KS) DFT, which simplifies solving the interacting problem of interest by mapping it onto a non-interacting system[99, 132]. While the agreement between these calculations and experimental results is excellent[123, 213], the calculations remain incredibly expensive[163, 164]. The computational bottleneck in these calculations is the solution of the KS equations, a step that becomes increasingly expensive as temperatures and fractional occupations rise. In fact, the cost exhibits nearly exponential scaling with temperature due to the KS cycle including many states at WDM temperatures[120].

A solution to this problem is orbital-free DFT[250], which avoids this costly step using non-interacting kinetic energy approximations that depend directly on the electronic density. Because the kinetic energy is such a large fraction of the total energy, however, these approximations must be highly accurate to be of practical use. Though much progress has been made for WDM[116, 121, 226], approximations are complicated by temperature effects. The KS kentropy, the free energy consisting of the non-interacting kinetic energy and entropy, must be approximated directly, greatly complicating the production of useful, efficient approximations.

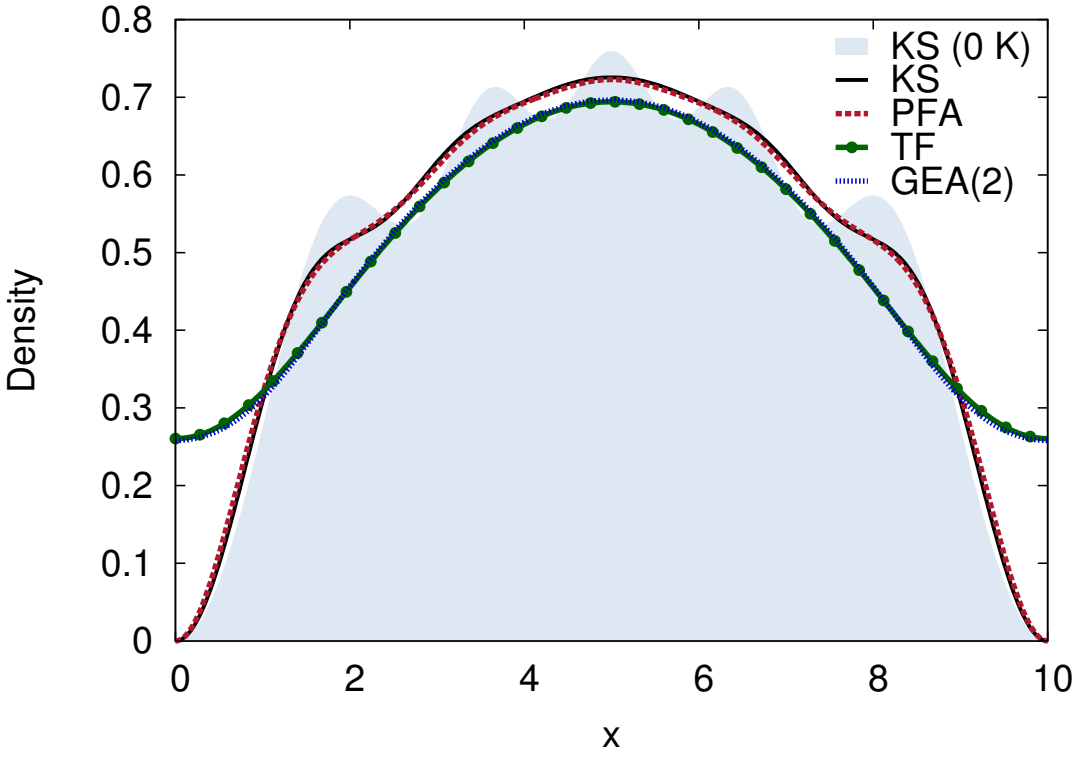

Figure 7.1: Shortcomings of the TF approximation in the WDM regime: Total density of five particles in the potential $v(x) = -2\sin^2(\pi x/10)$ within a box (of size 10 a.u.) at $\Lambda = \tau/\mu = 0.93$. Compare the exact density (solid black curve) with our PFA (dashed red curve) derived in Eq. (7.12), which is basically on top of the exact result. On the other hand, the TF approximation (dotted green curve) and conventional (second-order) gradient expansion (dotted purple) capture the general qualitative features, but completely miss the quantum oscillations. We also show the corresponding exact density at zero temperature (light blue shaded area), with its pronounced oscillations that smooth as temperatures rise.

At zero temperature, potential functional theory (PFT) is a promising approach to the electronic structure problem[26, 28]. It is also orbital-free, but skirts the troublesome issue of separately approximating the KS kinetic energy. PFT's coupling-constant formalism automatically generates a highly accurate kinetic energy potential functional approximation (PFA) for any density PFA[28]. In this way, one needs only find a sufficiently accurate density approximation[27]. Approximations to the non-interacting density have been derived in various semiclassical[27, 49, 212], and stochastic approaches[6]. Most closely related to this work is the pioneering path-integral formalism of Yang[255, 256] which goes beyond the gradient expansion at finite temperature. An advantage of PFT is that it generates leading corrections to zero-temperature local approximations[27], which become exact in the well-known Lieb limit[154]. Finite-temperature Thomas-Fermi theory[61, 240] becomes relatively exact for non-zero temperatures under similar scaling[177]. In this way, our method provides a pathway to systematic improvements to approximations, something generally missing from DFT approaches.

The particular scaling conditions under which TF becomes exact for all temperatures is related to the breakdown of purely quantum or classical behavior as both temperatures and particle numbers increase[80]. The importance of both these effects in the WDM regime underlies its theoretical complexity[206]. It is useful to represent the influences of temperature and density with a single electron degeneracy parameter defined by $\Lambda = \tau/\mu$, which depends on the system temperature τ and temperature-dependent chemical potential μ. Then, the WDM regime can be defined as where $\Lambda \approx 1$. At these conditions, KS-DFT is hugely expensive, while traditional plasma methods miss critical electronic structure features. In Fig. 7.1, density oscillations still present at WDM conditions are neglected by the smooth, classical TF approximation and its conventional gradient correction, but are captured by our method.

In this work, we (i) derive PFT for thermal ensembles, (ii) give an explicit equation for the kentropy relying solely on the temperature-dependent density, (iii) derive and implement

a highly accurate density approximation in one dimension to illustrate our general result, and (iv) perform (orbital-free) PFT calculations in the WDM regime. Our method generates highly accurate density and kentropy approximations, skirts the need for separate kentropy approximations, provides a roadmap for systematically improved approximations, and converges more quickly as temperatures increase while maintaining accuracy at low temperatures. At the same time, it bridges low and high temperature methods, and so is uniquely suited to WDM.

7.2 Theory

At non-zero temperature, the energy is replaced by the grand canonical potential as the quantity of interest[56, 169]. The grand canonical Hamiltonian is written

$$\hat{\Omega} = \hat{H} - \tau\hat{S} - \mu\hat{N}, \tag{7.1}$$

where $\hat{H}$, $\hat{S}$, and $\hat{N}$ are the Hamiltonian, entropy, and particle-number operators. In electronic structure theory, we typically deal with non-relativistic electrons, most commonly within the Born-Oppenheimer approximation. The electronic Hamiltonian (in atomic units here and thereafter) reads

$$\hat{H} = \hat{T} + \hat{V}_{\text{ee}} + \hat{V}\,, \tag{7.2}$$

where $\hat{T}$ denotes the kinetic energy operator, $\hat{V}_{\text{ee}}$ the interelectronic repulsion, and $v(\mathbf{r})$ the static external potential in which the electrons move. (We suppress spin for simplicity of notation.) The grand canonical potential can be written in terms of potential functionals

(denoted by square brackets) as follows:

$$\Omega^{\tau}_{v-\mu} = F^{\tau}[v] + \int d^3r\ n^{\tau}[v](\mathbf{r})(v(\mathbf{r}) - \mu). \tag{7.3}$$

Here, $F^{\tau}[v] = F^{\tau}[\hat{\Gamma}^0_{v-\mu}] = T[\hat{\Gamma}^0_{v-\mu}] + V_{ee}[\hat{\Gamma}^0_{v-\mu}] - \tau S[\hat{\Gamma}^0_{v-\mu}]$ denotes the universal functional in terms of the equilibrium statistical operator $\hat{\Gamma}^0_{v-\mu}$, which captures all system-independent behavior in thermal DFT[202].

In practice, approximating this expression would require two separate approximate potential functionals, one for the universal finite-temperature functional and one for the density:

$$\breve{\Omega}^{\tau}_{v-\mu} = \breve{F}^{\tau}[v] + \int d^3r\ \breve{n}^{\tau}[v](\mathbf{r})(v(\mathbf{r}) - \mu). \tag{7.4}$$

However, we can generate an approximation (denoted by a breve above the approximated quantity) to the universal functional that corresponds to any chosen density approximation. In analogy to the zero-temperature case[28], we introduce a coupling constant λ in the one-body potential, $v^{\lambda}(\mathbf{r}) = (1-\lambda)v_0(\mathbf{r}) + \lambda v(\mathbf{r})$, where v_0 is some reference potential. Via the Hellmann-Feynman theorem, we rewrite the grand potential,

$$\Omega^{\tau}_{v-\mu} = \Omega^{\tau}_0 + \int_0^1 d\lambda \int d^3r\ n^{\tau}[v^{\lambda}](\mathbf{r})\Delta v(\mathbf{r}), \tag{7.5}$$

where $\Delta v(\mathbf{r}) = v(\mathbf{r}) - v_0(\mathbf{r})$ and Ω^{τ}_0 is the reference system grand potential. Setting $v_0 = 0$ and defining $\bar{n}^{\tau}[v](\mathbf{r}) = \int_0^1 d\lambda\, n^{\tau}[v^{\lambda}](\mathbf{r})$, we now write the exact finite-temperature universal functional in terms of the density written as a potential functional:

$$F^{\tau}[v] = \int d^3r\ \left\{\bar{n}^{\tau}[v](\mathbf{r}) - n^{\tau}[v](\mathbf{r})\right\} v(\mathbf{r}). \tag{7.6}$$

This defines an approximate functional, $\breve{F}^{\tau}[v]$, corresponding to the chosen density approximation $\breve{n}^{\tau}$ and is the generalization of PFT to thermal ensembles. The coupling-constant ap-

proach differentiates the present formalism from previous groundbreaking work in Refs. [256] and [9].

Practical use of this formula as written would require sufficiently accurate approximations to the interacting electron density. These are likely unavailable, so we instead apply it to the non-interacting electrons of the KS system. In DFT, the KS system is a clever way of approximating the exact F^τ by mapping the interacting system to a non-interacting system with the same electronic density and temperature. This determines the one-body KS potential and corresponding chemical potential. Through this mapping, the non-interacting, finite-temperature universal density functional is defined[202]

$$\tilde{F}^\tau_{\rm S}[n] := \min_{\hat{\Gamma}\to n} K^\tau[\hat{\Gamma}] = K^\tau[\hat{\Gamma}^\tau_{\rm s}[n]] = \tilde{K}^\tau_{\rm s}[n] \ . \tag{7.7}$$

The non-interacting kentropy $\tilde{K}_{\rm S}[n] = \tilde{T}_{\rm S}[n] - \tau\tilde{S}_{\rm S}[n]$ generates the KS equations and the KS orbitals, and tildes denote density functionals. The orbitals are implicit functionals of the density via the KS equations, and the average density is constructed by Fermi-weighted summing of the orbitals. Solution of these equations at every time-step is the most costly step of DFT molecular dynamics.

The KS potential is defined[26, 28]

$$v_{\rm S}(\mathbf{r}) = v(\mathbf{r}) + \tilde{v}_{\rm H}[n^\tau_{\rm S}[v_{\rm S}]](\mathbf{r}) + \tilde{v}_{\rm XC}[n^\tau_{\rm S}[v_{\rm S}]](\mathbf{r}) \, , \tag{7.8}$$

where, in contrast to KS-DFT, the density is posed as a *potential* functional. All many-body interactions among the electrons are captured in the usual KS-DFT sense, via the (traditionally defined) Hartree and XC potentials[43]. The difference from a usual KS-DFT calculation is that Eq. (7.8) in conjunction with an approximation to the non-interacting density *bypasses* the hugely expensive iterative solution of the KS equations for WDM. Choosing a *potential* functional approximation to the non-interacting density automatically

generates an approximated KS potential, as illustrated in the Supplemental Materials. Once the self-consistent KS potential is determined, the KS kentropy is computed from

$$K_{\rm S}^{\tau}[v_{\rm S}] = \int d^3r \;\; \{\bar{n}_{\rm S}^{\tau}(\mathbf{r}) - n_{\rm S}^{\tau}[v_{\rm S}](\mathbf{r})\}\, v_{\rm S}(\mathbf{r})\,, \tag{7.9}$$

which is the analog of Eq. (7.6) for KS electrons. Again, Eq. (7.9) defines a coupling-constant approximation, $\breve{K}_{\rm S}^{\tau}[v_{\rm S}]$, when evaluated on any chosen approximation to the non-interacting density $\breve{n}_{\rm S}^{\tau}$. Finally, the grand potential expressed in terms of KS quantities[202],

$$\Omega_{v-\mu}^{\tau} = K_{\rm S}^{\tau}[v_{\rm S}] + \tilde{U}[n_{\rm S}^{\tau}[v_{\rm S}]] + \tilde{\mathcal{F}}_{xc}^{\tau}[n_{\rm S}^{\tau}[v_{\rm S}]] + \int d^3r \; n^{\tau}[v_{\rm S}](\mathbf{r})\,(v(\mathbf{r}) - \mu) \;\;, \tag{7.10}$$

can be evaluated via Eq. (7.9). Through this result, we leverage the body of time-proven XC approximations and eliminate the need to construct separate approximations to the KS kentropy for use in orbital-free (and thereby computationally inexpensive) schemes. Only an approximation to the non-interacting density is required. A general, systematic, non-empirical route to improved kentropy approximations is now available.

7.3 Numerical Demonstration

To illustrate the significance of our main result in Eq. (7.9), we consider a simple, yet useful, numerical demonstration: Non-interacting, spinless fermions in an arbitrary potential $v(x)$ confined to a box of size L obeying vanishing Dirichlet boundary conditions. (In a practical realization, this would be the self-consistent KS potential of the given many-body problem.) A starting point for deriving an approximation to the non-interacting density at finite temperature is the semiclassical propagator, which can be written as a convolution of the zero-temperature propagator with a factor carrying all temperature dependence[9].

From the propagator, we extract the density via an inverse Laplace transformation.

$$\breve{n}_{\rm S}^{\tau}[v_{\rm S}](\mathbf{r}) = \lim_{\mathbf{r}'\to\mathbf{r}} \frac{1}{2\pi i} \int_{\eta-\infty}^{\eta+\infty} d\alpha \, \frac{e^{\mu\alpha}}{\alpha} \, G^{\tau}[v_{\rm S}](\mathbf{r},\mathbf{r}';\alpha) \; . \tag{7.11}$$

Recently, a highly accurate PFA to the density was derived for this model using the path integral formalism and semiclassical techniques[30]. Here we extend this result to finite temperature and obtain:

$$\breve{n}_{\rm S}^{\tau}(x) = \lim_{x'\to x} \sum_{\alpha=1}^{4} \sum_{j=0}^{\infty} \breve{\gamma}_{\rm S}^{\tau}(x,x';\alpha,j) \, , \tag{7.12}$$

a PFA to the density at a given temperature and chemical potential, where

$$\breve{\gamma}_{\rm S}^{\tau}(x,x';\alpha,j) = \frac{\tau \sin\Theta_{\mu}^{\alpha}(x,x';j) \mathrm{csch}[\pi\tau\mathcal{T}_{\mu}^{\alpha}(x,x';j)]}{(-1)^{\alpha+1}\sqrt{k_{\mu}(x)k_{\mu}(x')}} \; . \tag{7.13}$$

Here we define generalized classical phases $\Theta_{\mu}^{1}(x,x';j) = \theta_{\mu}^{-}(x,x') + 2j\theta_{\mu}(L)$, $\Theta_{\mu}^{2}(x,x';j) = \theta_{\mu}^{+}(x,x') + 2j\theta_{\mu}(L)$, $\Theta_{\mu}^{3}(x,x';j) = \theta_{\mu}^{-}(x,x') - 2(j+1)\theta_{\mu}(L)$, $\Theta_{\mu}^{4}(x,x';j) = \theta_{\mu}^{+}(x,x') - 2(j+1)\theta_{\mu}(L)$ and generalized classical traveling times $\mathcal{T}_{\mu}^{\alpha}(x,x';j) = d\Theta_{\mu}^{\alpha}(x,x';j)/d\mu$. Furthermore, $\theta^{\pm}(x,x') = \theta(x) \pm \theta(x')$, where $\theta_{\mu}(x) = \int_0^x dy \, k_{\mu}(y)$ and $k_{\mu}(x) = \sqrt{2(\mu - v(x))}$ at a given chemical potential μ, which is determined by normalization of the density.

The physical interpretation of our result in Eq. (7.12) is instructive: For a given chemical potential there are infinitely many classical paths that contribute to the total density. The paths are classified into four primitives (identified by α) onto which an integral number of periods (labelled by j) is added. The first primitive is special, in that it yields the TF density. However, higher-order terms in j do not yield the conventional gradient expansion. All other primitives and additional periods carry phase information about reflections from the boundaries, producing quantum density oscillations that greatly improve upon the TF result[30]. For more details, we refer to Ref. [30].

Our result in Eq. (7.12) can be evaluated numerically for a given temperature by truncating the infinite sum at an upper limit at which the sum has converged. Importantly for WDM applications, the higher the temperature, the lower the upper limit required for convergence of the sum. In fact, in the WDM regime only the leading term ($j = 1$) in the sum needs to be kept. Similar results have also been recently found at zero temperature[30, 211], so this may be a universal feature due to the approximation's semiclassical nature.

However, the stationary phase approximation used to derive Eq. (7.12) yields the TF density at zero temperature as the leading term, i.e., $\lim_{x'\to x} \breve{\gamma}^{\tau}_{\mathrm{S}}(x, x'; 1, 0) = k_{\mu}(x)/\pi = \breve{n}^{0}_{\mathrm{TF}}(x)$, instead of the finite-temperature TF density $\breve{n}^{\tau}_{\mathrm{TF}}(x) = \sqrt{\tau/(2\pi)}\, F_{-1/2}(z)$, where $F_{\nu}(z) = \int_0^{\infty} da\, a^{\nu}[1 + \exp(a - z)]^{-1}$ and $z = k^2_{\mu}(x)/2\tau$. We fix this problem with an ad-hoc correction and ensure the correct boundary conditions. To do so, we replace the density from the first primitive $\lim_{x'\to x} \breve{\gamma}^{\tau}_{\mathrm{S}}(x, x'; 1, 0)$ with a Gaussian interpolation of $\breve{n}^{0}_{\mathrm{TF}}(x)$ and $\breve{n}^{\tau}_{\mathrm{TF}}(x)$. In this way, we cope with the density approaching the high-temperature limit (under which TF theory becomes exact) differently in two distinct regions, the interior of the box and the edge regions near the walls. These two distinct boundary layers have different asymptotic expansions in the high-temperature limit. The size of the edge-region boundary layers shrinks as the limit is approached. Our Gaussian interpolation is a crude version of the asymptotic matching used in boundary-layer theory[100].

In Fig. 7.1, we plot a typical density of five particles in the WDM regime ($\Lambda \approx 1$) in the potential $v(x) = -2\sin^2(\pi x/10)$ within a ten-unit box, along with approximate densities. The black curve is the exact result, the red dashed curve is our approximation, the green dotted curve is the TF density, and the purple dotted curve is the second-order gradient-corrected TF[9] density with the second-order gradient correction given by $-\partial_x^2 v(x)/\sqrt{512\pi\tau^3}F_{-5/2}(z) - 5(\partial_x v)^2/\sqrt{8192\pi\tau^5}F_{-7/2}(z)$. In addition, the light-blue shaded area denotes the corresponding density at zero temperature. Quantum oscillations in the density persist in the WDM regime, and TF theory completely fails to capture them. On

the other hand, our PFA – derived to include quantum effects – is able to describe them properly and is therefore highly accurate. This mimics the results for cold densities seen in Fig. 1 of Ref. [27].

Table 7.1: Residual kentropy of five particles in the same potential as in Fig. 7.1. We list the error of the conventional TF approach, its gradient correction, and of our PFA (given in Eq. (7.14)) far below and above where WDM is typically encountered.

Λ	$K^\tau_{\mathrm{S},0}$	$\Delta K^\tau_{\mathrm{S}}$	error $\times$ 10^2		
			TF	GEA(2)	PFA
0.16	3.94	0.462	6.39	8.93	-0.32
0.31	3.87	0.461	7.16	9.85	-0.28
0.47	3.76	0.459	7.91	10.11	-0.31
0.62	3.64	0.456	8.39	10.01	-0.29
0.78	3.50	0.452	8.61	9.78	-0.30
0.93	3.34	0.448	8.65	9.52	-0.37
1.09	3.16	0.444	8.58	9.24	-0.50
1.40	2.77	0.435	8.21	8.63	-0.87
1.71	2.36	0.425	7.69	7.99	-1.27
2.02	1.92	0.414	7.13	7.35	-1.61
2.48	1.25	0.396	6.34	6.46	-1.86
2.94	0.58	0.378	5.64	5.69	-1.80
3.41	-0.10	0.360	5.04	5.04	-1.45
4.03	-0.99	0.338	4.37	4.33	-0.63

Next, we demonstrate the accuracy of our approach for kentropies. For our example, Eq. (7.9) simplifies to

$$\breve{K}^\tau_{\mathrm{S}}[v] = K^\tau_{\mathrm{S},0} + \int dx \ \left\{\breve{\tilde{n}}^\tau_{\mathrm{S}}(x) - \breve{n}^\tau_{\mathrm{S}}[v](x)\right\} v(x) \ . \tag{7.14}$$

In this case the reference potential is not zero, but an infinite square well. Hence, a kentropic contribution $K^\tau_{\mathrm{S},0} = T^\tau_{\mathrm{S},0} - \tau S^\tau_{\mathrm{S},0}$ of the reference system appears, which we compute exactly. The kinetic energy of the infinite square well is $T^\tau_{\mathrm{S},0} = \sum_j^N f^\tau_j \, \epsilon_{j,0}$, and the entropy is $S^\tau_{\mathrm{S},0} = -\sum_j f^\tau_j \ln(f^\tau_j) + (1-f^\tau_j)\ln(1-f^\tau_j)$, with $f^\tau_j = 1/(1.0 + \exp\left[(\epsilon_{j,0} - \mu_0)/\tau\right])$ denoting Fermi functions and $\epsilon_{j,0}$ and μ_0 the j^{th} eigenvalue and chemical potential. We avoid temperature-dependent KS eigenvalues[206] by choosing a purely non-interacting reference system, not a

KS system associated with a specific interacting system. Evaluating Eq. (7.14) for the same potential as in Fig. 7.1 yields the results in Tab. 7.1. We measure the error of TF theory, its gradient correction, and our PFA with respect to the residual kentropy $\Delta K_{\mathrm{S}}^{\tau} = K_{\mathrm{S}}^{\tau} - K_{\mathrm{S},0}^{\tau}$, because this is the only approximated piece of the kentropy. From cold temperatures up to the WDM regime ($\Lambda \approx 1$), our PFA yields kentropies that are significantly more accurate than either TF theory or the gradient expansion, improving them by roughly an order of magnitude. In fact, the gradient correction worsens the results, though it may improve them in other systems. In any case, the gradient correction is small, while our PFA yields dramatic improvements. Far beyond the WDM regime, the entropic contribution dominates, and the errors of all methods become comparable. In Tab. 7.1, N is fixed as temperature increases. If instead N scales with increasing temperature, the system will approach a Lieb-like limit and TF accuracy is less than one percent for $\Lambda > 2$.

We can better understand the advantage of our PFA over the conventional TF approach by analyzing both in real space. We compute residual kentropic densities (the integrand of Eq. (7.14)) for the example in Fig. 7.1. As illustrated in Fig. 7.2, the TF approach (dotted green curve) and its gradient correction (dotted purple) only reproduce the qualitative trends of the exact result (black curve). Errors due to an overestimation in the interior are balanced by underestimation in the outer regions of the system. Our PFA, on the other hand, not only yields accurate integrated kentropies (area under the curve in Fig. 7.2), but is also highly accurate in real space. As such, and unlike TF, our PFA does not rely on cancellation of errors in the kentropy density for its accurate kentropy values.

7.4 Conclusion

The finite-temperature PFA approach outlined here offers several advantages over other methods, particularly for WDM, where solution of the KS equations for numerous occu-

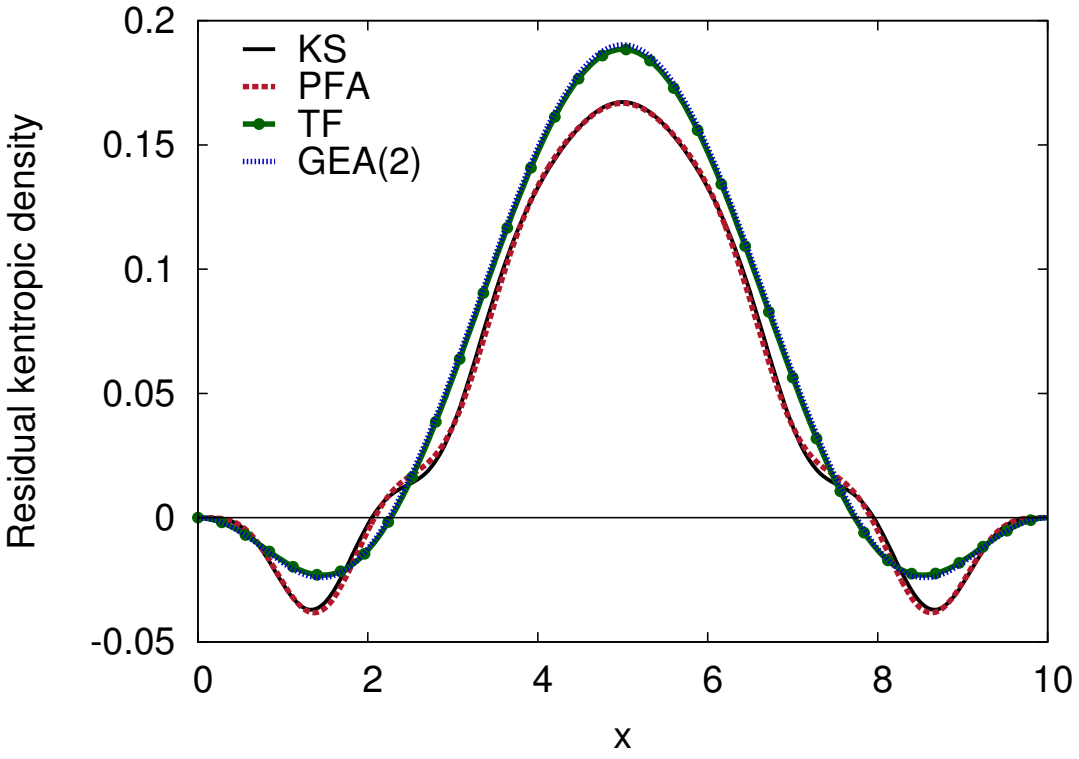

Figure 7.2: Residual kentropic density of five particles in the same potential as in Fig. 7.1 in the WDM regime. Our PFA (solid red curve) derived in Eq. (7.12) is on top of the exact result (solid black curve). TF (dotted green curve) and its gradient correction (dotted purple), on the other hand, follow the general trend as expected, but miss quantitative details.

pied states becomes especially daunting. We retain the advantages of the KS system while avoiding the costly, repetitive solution of eigenvalue problems by isolating a piece of the kentropy to approximate through the coupling-constant formalism. Combined with our density approximation, this improves approximate kentropies by up to an order of magnitude in the WDM regime and produces highly accurate kentropic densities. This accuracy relies on inclusion of quantum oscillations beyond the minor corrections of the conventional gradient expansion. The density approximation derived in this paper is computationally efficient because only the leading term is needed for convergence at WDM temperatures.

The path integral method used to derive this approximation[30] invites use of successful zero-temperature approximations to the propagator, and it is a promising approach for extension to three dimensional systems. Furthermore, combining finite-temperature PFT with semiclassical methods offers prospects for a systematic route to exchange energy approximations, instead of relying on existing, zero-temperature density functional approximations. Work in this direction is currently in development. With these advantages, finite-temperature PFT is poised to bridge the "malfunction junction" of WDM by providing computationally efficient, semiclassical methods at high temperatures and densities.

We acknowledge Hardy Gross and Kieron Burke for providing an atmosphere facilitating independent research. We are grateful to Rudy Magyar for useful discussion. A.C. has been partially supported by NSF grant CHE-1112442. A.P.J. is supported by DOE grant DE-FG02-97ER25308.

Part VI

Conclusions

Chapter 8

Summary and Future Work

Warm dense matter, with its physical complexity and idiosyncratic behavior, offers many challenges to theorists, whether they begin from the chilly regime of condensed matter or the sizzling perspective of traditional plasma physics. We are driven to face these challenges by the huge rewards doing so would offer in fields as diverse as astronomy, materials science, and the quest for fusion energy. In this thesis, I've begun to address some of them, namely, how to include temperature dependence in DFT approximations and how to overcome the computational inefficiency of KS-DFT.

In Chapters 6 and 7, I presented a novel method for calculating the electronic structure of finite-temperature systems that avoids solution of the Kohn-Sham equations. The formalism is valid in three dimensions, and we demonstrated it using a highly accurate semiclassical density approximation. This orbital-free method, when combined with our path-integral-based approximation, is well-suited to WDM simulations because it works well across a wide range of phase space and becomes more efficient as temperatures rise.

Finite-temperature DFT was explained as a specific case of ensemble DFT in Chapter 3, and the importance of derivative discontinuities in approximations was demonstrated in

Chapters 4 and 5. These chapters also showed that inclusion of ghost interactions and using only single determinant states reduces the accuracy of ensemble DFT energy calculations and Kohn-Sham potentials.

Future work related to that presented here could proceed on a multitude of paths. Some projects that are already in progress or planned in the near future include:

- exact conditions of DFT at finite temperature, such as
  - the FT Lieb-Oxford bound
  - limits of the correlation free energy from perturbation theory
  - relations between different components of the correlation energy
- using methods from strongly correlated physics to examine how FT KS-DFT is used in practice
- developing weight-dependent XC approximations for ensemble DFT
- developing non-empirical, temperature-dependent GGA XC approximations
- rigorously extending TDDFT to finite temperatures within linear response
- deriving tied temperature-time-interaction scaling relationships
- testing of our density PFA with different potentials and developing new PFAs
- extending FT PFT to realistic, three-dimensional systems and implementing PFT-MD

Work in density functional theory and potential functional theory for WDM will continue, in hopes that the challenges of this wonderfully troublesome region can be met. Doing so will surely continue to expose new avenues for improvement and drive further investigation.

Bibliography

[1] There appears to be a sign error in Eq. (16) of Ref. [150]: the two terms on the right-hand side should be swapped.

[2] Y. Andersson, D. Langreth, and B. Lunqvist. van der Waals Interactions in Density-Functional Theory. *Phys. Rev. Lett.*, 76:102, 1996.

[3] H. Appel, E. K. U. Gross, and K. Burke. Excitations in time-dependent density-functional theory. *Phys. Rev. Lett.*, 90(4):043005, Jan 2003.

[4] R. Armiento and A. Mattsson. Functional designed to include surface effects in self-consistent density functional theory. *Phys. Rev. B*, 72:085108, 2005.

[5] S. Atzeni and J. Meyer-ter Vehn. *The Physics of Inertial Fusion: Beam-Plasma Interaction, Hydrodynamics, Hot Dense Matter*. Clarendon Press, 2004.

[6] R. Baer, D. Neuhauser, and E. Rabani. Self-Averaging Stochastic Kohn-Sham Density-Functional Theory. *Phys. Rev. Lett.*, 111:106402, Sep 2013.

[7] E. J. Baerends, O. V. Gritsenko, and R. van Meer. The Kohn-Sham gap, the fundamental gap and the optical gap: the physical meaning of occupied and virtual Kohn-Sham orbital energies. *Phys. Chem. Chem. Phys.*, 15:16408–16425, 2013.

[8] T. A. Barnes, J. D. Goodpaster, F. R. Manby, and T. F. Miller. Accurate basis set truncation for wavefunction embedding. *The Journal of Chemical Physics*, 139(2), 2013.

[9] J. Bartel, M. Brack, and M. Durand. Extended thomas-fermi theory at finite temperature. *Nuclear Physics A*, 445(2):263 – 303, 1985.

[10] R. J. Bartlett and M. Musial. Coupled-cluster theory in quantum chemistry. *Rev. Mod. Phys.*, 79:291–352, Feb 2007.

[11] A. Becke. Density-functional thermochemistry .5. Systematic optimization of exchange-correlation functionals. *Journal Of Chemical Physics*, 107(20):8554–8560, Nov 22 1997.

[12] A. Becke and E. Johnson. Exchange-hole dipole moment and the dispersion interaction: High-order dispersion coefficients. *J. Chem. Phys.*, 124:014104, 2006.

[13] A. D. Becke. Density-functional exchange-energy approximation with correct asymptotic behavior. *Phys. Rev. A*, 38(6):3098–3100, Sep 1988.

[14] A. D. Becke. Density-functional thermochemistry. III. The role of exact exchange. *The Journal of Chemical Physics*, 98(7):5648–5652, 1993.

[15] A. D. Becke and E. R. Johnson. Exchange-hole dipole moment and the dispersion interaction revisited. *The Journal of Chemical Physics*, 127(15), 2007.

[16] A. D. Becke and E. R. Johnson. A unified density-functional treatment of dynamical, nondynamical, and dispersion correlations. *The Journal of Chemical Physics*, 127(12), 2007.

[17] K. Burke. The ABC of DFT, 2007. Available online.

[18] K. Burke. Perspective on density functional theory. *J. Chem. Phys.*, 136, 2012.

[19] K. Burke, F. G. Cruz, and K.-C. Lam. Unambiguous exchange-correlation energy density. *The Journal of Chemical Physics*, 109(19):8161–8167, 1998.

[20] K. Burke, J. Perdew, and D. Langreth. Is the local spin density approximation exact for short-wavelength fluctuations? *Phys. Rev. Lett.*, 73:1283, 1994.

[21] K. Burke, J. P. Perdew, and Y. Wang. *Derivation of a generalized gradient approximation: The PW91 density functional*, page 81. Plenum, NY, 1997.

[22] K. Burke and L. O. Wagner. DFT in a nutshell. *Int. J. Quant. Chem.*, 2012.

[23] K. Burke and L. O. Wagner. Dft in a nutshell. *Int. J. Quant. Chem.*, 113:96–101, 2013.

[24] A. Cancio, C. Fong, and J. Nelson. Exchange-correlation hole of the Si atom: A quantum Monte Carlo study. *Phys. Rev. A*, 6206:2507, 2000.

[25] A. C. Cancio and C. Y. Fong. Scaling properties of exchange and correlation holes of the valence shell of second-row atoms. *Phys. Rev. A*, 85:042515, Apr 2012.

[26] A. Cangi, E. K. U. Gross, and K. Burke. Potential functionals versus density functionals. *Phys. Rev. A*, 88(6), 2013.

[27] A. Cangi, D. Lee, P. Elliott, and K. Burke. Leading corrections to local approximations. *Phys. Rev. B*, 81(23):235128, Jun 2010.

[28] A. Cangi, D. Lee, P. Elliott, K. Burke, and E. K. U. Gross. Electronic structure via potential functional approximations. *Phys. Rev. Lett.*, 106:236404, Jun 2011.

[29] A. Cangi and A. Pribram-Jones. Bypassing the malfunction junction in warm dense matter simulations. *ArXiv e-prints*, 2014.

[30] A. Cangi, E. Sim, and K. Burke, 2014. in preparation.

[31] R. Car and M. Parrinello. Unified approach for molecular dynamics and density-functional theory. *Phys. Rev. Lett.*, 55(22):2471–2474, Nov 1985.

[32] M. E. Casida. Time-dependent density functional response theory of molecular systems: theory, computational methods, and functionals. In J. M. Seminario, editor, *Recent developments and applications in density functional theory*. Elsevier, Amsterdam, 1996.

[33] A. J. Cohen, P. Mori-Sánchez, and W. Yang. Insights into current limitations of density functional theory. *Science*, 321(5890):792–794, 2008.

[34] M. Cohen and A. Wasserman. On hardness and electronegativity equalization in chemical reactivity theory. *Journal of Statistical Physics*, 125:1121–1139, 2006. 10.1007/s10955-006-9031-0.

[35] M. H. Cohen and A. Wasserman. On the foundations of chemical reactivity theory. *The Journal of Physical Chemistry A*, 111(11):2229–2242, 2007.

[36] F. E. S. A. Committee. Advancing the science of high energy density laboratory plasmas. Technical report, U.S. Department of Energy, January 2009.

[37] J. Cullen, M. Krykunov, and T. Ziegler. The formulation of a self-consistent constricted variational density functional theory for the description of excited states. *Chemical Physics*, 391(1):11 – 18, 2011. Open problems and new solutions in time dependent density functional theory.

[38] R. G. Dandrea, N. W. Ashcroft, and A. E. Carlsson. Electron liquid at any degeneracy. *Phys. Rev. B*, 34(4):2097–2111, Aug 1986.

[39] M. Dion, H. Rydberg, E. Schröder, D. C. Langreth, and B. I. Lundqvist. Van der Waals density functional for general geometries. *Phys. Rev. Lett.*, 92(24):246401, Jun 2004.

[40] P. A. M. Dirac. Note on exchange phenomena in the Thomas atom. *Mathematical Proceedings of the Cambridge Philosophical Society*, 26(03):376–385, 1930.

[41] G. W. F. Drake and Z.-C. Yan. Variational eigenvalues for the S states of helium. *Chem. Phys. Lett.*, 229:486, 1994.

[42] R. Dreizler, J. da Providência, and N. A. T. O. S. A. Division, editors. *Density Functional Methods in Physics*. NATO ASI B Series. Springer Dordrecht, 1985.

[43] R. M. Dreizler and E. K. U. Gross. *Density Functional Theory: An Approach to the Quantum Many-Body Problem*. Springer–Verlag, Berlin, 1990.

[44] A. Dreuw, J. L. Weisman, and M. Head-Gordon. Long-range charge-transfer excited states in time-dependent density functional theory require non-local exchange. *J. Chem. Phys.*, 119:2943, 2003.

[45] J. W. Dufty and S. B. Trickey. Scaling, bounds, and inequalities for the noninteracting density functionals at finite temperature. *Phys. Rev. B*, 84:125118, Sep 2011.

[46] P. Elliott and K. Burke. Non-empirical derivation of the parameter in the B88 exchange functional. *Can. J. Chem. Ecol.*, 87(10):1485–1491, Oct 2009.

[47] P. Elliott, K. Burke, M. H. Cohen, and A. Wasserman. Partition density-functional theory. *Phys. Rev. A*, 82(2):024501, Aug 2010.

[48] P. Elliott, S. Goldson, C. Canahui, and N. T. Maitra. Perspectives on double-excitations in TDDFT. *Chemical Physics*, 391(1):110 – 119, 2011.

[49] P. Elliott, D. Lee, A. Cangi, and K. Burke. Semiclassical origins of density functionals. *Phys. Rev. Lett.*, 100(25):256406, Jun 2008.

[50] E. Engel and R. M. Dreizler. *Density Functional Theory: An Advanced Course*. Springer, Berlin, 2011.

[51] H. Englisch and R. Englisch. Hohenberg-Kohn theorem and non-V-representable densities. *Physica A: Statistical Mechanics and its Applications*, 121(1-2):253 – 268, 1983.

[52] M. Ernzerhof, K. Burke, and J. Perdew. Long-range asymptotic behavior of ground-state wavefunctions. *J. Chem. Phys.*, 105:2798, 1996.

[53] M. Ernzerhof, K. Burke, and J. P. Perdew. Density functional theory, the exchange hole, and the molecular bond. In J. M. Seminario, editor, *Recent Developments and Applications in Density Functional Theory*. Elsevier, Amsterdam, 1996.

[54] M. Ernzerhof and J. Perdew. Generalized gradient approximation to the angle- and system-averaged exchange hole. *J. Chem. Phys.*, 109:3313, 1998.

[55] M. Ernzerhof and G. E. Scuseria. Assessment of the Perdew–Burke–Ernzerhof exchange-correlation functional. *J. Chem. Phys*, 110:5029, 1999.

[56] H. Eschrig. $T > 0$ ensemble-state density functional theory via Legendre transform. *Phys. Rev. B*, 82:205120, Nov 2010.

[57] H. Eshuis and F. Furche. A parameter-free density functional that works for noncovalent interactions. *The Journal of Physical Chemistry Letters*, 2(9):983–989, 2011.

[58] H. Eshuis, J. Yarkony, and F. Furche. Fast computation of molecular random phase approximation correlation energies using resolution of the identity and imaginary frequency integration. *The Journal of Chemical Physics*, 132(23):234114, 2010.

[59] F. W. Averill and G. S. Painter. *Phys. Rev. B*, 15:2498, 1992.

[60] E. Fermi. *Rend. Acc. Naz. Lincei*, 6, 1927.

[61] E. Fermi. Eine statistische Methode zur Bestimmung einiger Eigenschaften des Atoms und ihre Anwendung auf die Theorie des periodischen Systems der Elemente (A statistical method for the determination of some atomic properties and the application of this method to the theory of the periodic system of elements). *Zeitschrift für Physik A Hadrons and Nuclei*, 48:73–79, 1928.

[62] C. Filippi, C. J. Umrigar, and M. Taut. Comparison of exact and approximate density functionals for an exactly soluble model. *The Journal of Chemical Physics*, 100(2):1290–1296, 1994.

[63] C. Filippi, C. J. Umrigar, and M. Taut. Comparison of exact and approximate density functionals for an exactly soluble model. *J. Chem. Phys.*, 100:1290, 1994.

[64] C. Fiolhais, F. Nogueira, and M. Marques. *A Primer in Density Functional Theory*. Springer-Verlag, New York, 2003.

[65] C. Fischer. A multi-configuration Hartree-Fock program. *Computer Physics Communications*, 1(3):151 – 166, 1969.

[66] C. Fischer. *Hartree–Fock method for atoms. A numerical approach*. Wiley, Jan 1977.

[67] V. Fock. Näherungsmethode zur lösung des quantenmechanischen mehrkörperproblems. *Z. Phys.*, 61:126–148, 1930.

[68] O. Franck and E. Fromager. Generalised adiabatic connection in ensemble density-functional theory for excited states: example of the h2 molecule. *Molecular Physics*, pages 1–18, 2013.

[69] I. Frank, J. Hutter, D. Marx, and M. Parrinello. Molecular dynamics in low-spin excited states. *The Journal of Chemical Physics*, 108(10):4060–4069, 1998.

[70] M. Fuchs, Y.-M. Niquet, X. Gonze, and K. Burke. Describing static correlation in bond dissociation by Kohn–Sham density functional theory. *The Journal of Chemical Physics*, 122(9):094116, 2005.

[71] J. I. Fuks, A. Rubio, and N. T. Maitra. Charge transfer in time-dependent density-functional theory via spin-symmetry breaking. *Phys. Rev. A*, 83:042501, Apr 2011.

[72] F. Furche. Developing the random phase approximation into a practical post-Kohn–Sham correlation model. *The Journal of Chemical Physics*, 129(11), 2008.

[73] N. Gidopoulos, P. Papaconstantinou, and E. Gross. Spurious interactions, and their correction, in the ensemble-kohn-sham scheme for excited states. *Phys. Rev. Lett.*, 88:033003, 2002.

[74] G. F. Giuliani and G. Vignale, editors. *Quantum Theory of the Electron Liquid*. Cambridge University Press, 2008.

[75] J. D. Goodpaster, T. A. Barnes, F. R. Manby, and T. F. Miller. Accurate and systematically improvable density functional theory embedding for correlated wavefunctions. *The Journal of Chemical Physics*, 140(18), 2014.

[76] A. Görling. Symmetry in density-functional theory. *Phys. Rev. A*, 47:2783, 1993.

[77] A. Görling. Density-functional theory for excited states. *Phys. Rev. A*, 54:3912, 1996.

[78] A. Görling. Density-functional theory beyond the hohenberg-kohn theorem. *Phys. Rev. A*, 59:3359, 1999.

[79] A. Görling and M. Levy. Dft ionization formulas and a dft perturbation theory for exchange and correlation, through adiabatic connection. *Int. J. Quant. Chem.*, 29:93, 1995.

[80] F. Graziani, M. P. Desjarlais, R. Redmer, and S. B. Trickey, editors. *Frontiers and Challenges in Warm Dense Matter*, volume 96 of *Lecture Notes in Computational Science and Engineering*. Springer International Publishing, 2014.

[81] F. R. Graziani, V. S. Batista, L. X. Benedict, J. I. Castor, H. Chen, S. N. Chen, C. A. Fichtl, J. N. Glosli, P. E. Grabowski, A. T. Graf, S. P. Hau-Riege, A. U. Hazi, S. A. Khairallah, L. Krauss, A. B. Langdon, R. A. London, A. Markmann, M. S. Murillo, D. F. Richards, H. A. Scott, R. Shepherd, L. G. Stanton, F. H. Streitz, M. P. Surh, J. C. Weisheit, and H. D. Whitley. Large-scale molecular dynamics simulations of dense plasmas: The cimarron project. *High Energy Density Physics*, 8(1):105 – 131, 2012.

[82] M. Greiner, P. Carrier, and A. Görling. Extension of exact-exchange density functional theory of solids to finite temperatures. *Phys. Rev. B*, 81(15):155119, Apr 2010.

[83] S. Grimme. Semiempirical GGA-type density functional constructed with a long-range dispersion correction. *Journal of Computational Chemistry*, 27(15):1787–1799, 2006.

[84] E. Gross, J. Dobson, and M. Petersilka. Density functional theory of time-dependent phenomena. *Topics in Current Chemisty*, 181:81, 1996.

[85] E. Gross, L. Oliveira, and W. Kohn. Density-functional theory for ensembles of fractionally occupied states. i. basic formalism. *Phys. Rev. A*, 37:2809, 1988.

[86] E. Gross, L. Oliveira, and W. Kohn. Rayleigh-ritz variational principle for ensembles of fractionally occupied states. *Phys. Rev. A*, 37:2805, 1988.

[87] O. Gunnarsson and B. Lundqvist. Exchange and correlation in atoms, molecules, and solids by the spin-density-functional formalism. *Phys. Rev. B*, 13:4274, 1976.

[88] O. Gunnarsson and B. I. Lundqvist. Exchange and correlation in atoms, molecules, and solids by the spin-density-functional formalism. *Phys. Rev. B*, 13:4274, 1976.

[89] H. Englisch and R. Englisch. *Phys. Stat. Solidi B*, 123:711, 1984.

[90] H. Englisch and R. Englisch. *Phys. Stat. Solidi B*, 124:373, 1984.

[91] N. Hadjisavvas and A. Theophilou. *Phys. Rev. A*, 32:720, 1985.

[92] N. C. Handy and A. J. Cohen. Left-right correlation energy. *Molecular Physics*, 99(5):403–412, 2001.

[93] J. Harriman. *Phys. Rev. A*, 24:680, 1981.

[94] D. R. Hartree and W. Hartree. Self-consistent field, with exchange, for beryllium. *Proceedings of the Royal Society of London. Series A - Mathematical and Physical Sciences*, 150(869):9–33, 1935.

[95] M. Hellgren and E. K. U. Gross. Discontinuities of the exchange-correlation kernel and charge-transfer excitations in time-dependent density-functional theory. *Phys. Rev. A*, 85:022514, Feb 2012.

[96] M. Hellgren and E. K. U. Gross. Discontinuous functional for linear-response time-dependent density-functional theory: The exact-exchange kernel and approximate forms. *Phys. Rev. A*, 88:052507, 2013.

[97] P. Hessler, N. T. Maitra, and K. Burke. Correlation in time-dependent density-functional theory. *The Journal of Chemical Physics*, 117(1):72–81, 2002.

[98] J. Heyd, G. E. Scuseria, and M. Ernzerhof. Hybrid functionals based on a screened coulomb potential. *The Journal of Chemical Physics*, 118(18):8207–8215, 2003.

[99] P. Hohenberg and W. Kohn. Inhomogeneous electron gas. *Phys. Rev.*, 136(3B):B864–B871, Nov 1964.

[100] M. H. Holmes. *Introduction to Perturbation Methods*. Springer, 2013.

[101] B. Holst, R. Redmer, and M. P. Desjarlais. Thermophysical properties of warm dense hydrogen using quantum molecular dynamics simulations. *Phys. Rev. B*, 77:184201, May 2008.

[102] C.-J. Huang and C. J. Umrigar. Local correlation energies of two-electron atoms and model systems. *Phys. Rev. A*, 56:290–296, Jul 1997.

[103] M. Huix-Rotllant, A. Ipatov, A. Rubio, and M. E. Casida. Assessment of dressed time-dependent density-functional theory for the low-lying valence states of 28 organic chromophores. *Chemical Physics*, 391(1):120 – 129, 2011.

[104] R. Iftimie, P. Minary, and M. E. Tuckerman. Ab initio molecular dynamics: Concepts, recent developments, and future trends. *Proceedings of the National Academy of Sciences of the United States of America*, 102(19):6654–6659, 2005.

[105] J. T. Chayes, L. Chayes, and M. B. Ruskai. *J. Stat. Phys*, 38:497, 1985.

[106] D. Jacquemin, E. A. Perpète, I. Ciofini, C. Adamo, R. Valero, Y. Zhao, and D. G. Truhlar. On the performances of the m06 family of density functionals for electronic excitation energies. *Journal of Chemical Theory and Computation*, 6(7):2071–2085, 2010.

[107] D. Jacquemin, V. Wathelet, E. A. Perpète, and C. Adamo. Extensive td-dft benchmark: Singlet-excited states of organic molecules. *Journal of Chemical Theory and Computation*, 5(9):2420–2435, 2009.

[108] E. R. Johnson and A. D. Becke. Van der waals interactions from the exchange hole dipole moment: Application to bio-organic benchmark systems. *Chemical Physics Letters*, 432(4 - 6):600 – 603, 2006.

[109] R. Jones and O. Gunnarsson. The density functional formalism, its applications and prospects. *Rev. Mod. Phys.*, 61:689, 1989.

[110] R. O. Jones. Density functional theory: A personal view. In A. Avella and F. Mancini, editors, *Strongly Correlated Systems*, volume 171 of *Springer Series in Solid-State Sciences*, pages 1–28. Springer Berlin Heidelberg, 2012.

[111] A. Z. J.P. Perdew, S. Kurth and P. Blaha. Accurate density functional with correct formal properties: A step beyond the generalized gradient approximation. *Phys. Rev. Lett.*, 82:2544, 1999.

[112] K. B. J.P. Perdew and M. Ernzerhof. Perdew, Burke, and Ernzerhof reply. *Phys. Rev. Lett.*, 80:891, 1998.

[113] S. V. K. J. M. P. D. S. J.P. Perdew, J.A. Chevary and C. Fiolhais. Atoms, molecules, solids, and surfaces: Applications of the generalized gradient approximation for exchange and correlation. *Phys. Rev. B*, 46:6671, 1992.

[114] P. Jurecka, J. Sponer, J. Cerny, and P. Hobza. Benchmark database of accurate (MP2 and CCSD(T) complete basis set limit) interaction energies of small model complexes, DNA base pairs, and amino acid pairs. *Phys. Chem. Chem. Phys.*, 8:1985–1993, 2006.

[115] V. Karasiev and S. Trickey. Issues and challenges in orbital-free density functional calculations. *Computer Physics Communications*, 183(12):2519 – 2527, 2012.

[116] V. V. Karasiev, D. Chakraborty, O. A. Shukruto, and S. B. Trickey. Nonempirical generalized gradient approximation free-energy functional for orbital-free simulations. *Phys. Rev. B*, 88:161108, Oct 2013.

[117] V. V. Karasiev, R. S. Jones, S. B. Trickey, and F. E. Harris. Properties of constraint-based single-point approximate kinetic energy functionals. *Phys. Rev. B*, 80:245120, Dec 2009.

[118] V. V. Karasiev, R. S. Jones, S. B. Trickey, and F. E. Harris. Erratum: Properties of constraint-based single-point approximate kinetic energy functionals [Phys. Rev. B 80, 245120 (2009)]. *Phys. Rev. B*, 87:239903, Jun 2013.

[119] V. V. Karasiev, R. S. Jones, S. B. Trickey, and F. E. Harris. Erratum: Properties of constraint-based single-point approximate kinetic energy functionals [phys. rev. b 80, 245120 (2009)]. *Phys. Rev. B*, 87:239903, Jun 2013.

[120] V. V. Karasiev, T. Sjostrom, D. Chakraborty, J. W. Dufty, K. Runge, F. E. Harris, and S. Trickey. Innovations in finite-temperature density functionals. In F. Graziani, M. P. Desjarlais, R. Redmer, and S. B. Trickey, editors, *Frontiers and Challenges in Warm Dense Matter*, volume 96 of *Lecture Notes in Computational Science and Engineering*, pages 61–85. Springer International Publishing, 2014.

[121] V. V. Karasiev, T. Sjostrom, and S. B. Trickey. Generalized-gradient-approximation noninteracting free-energy functionals for orbital-free density functional calculations. *Phys. Rev. B*, 86:115101, Sep 2012.

[122] M. Karplus. Spinach on the ceiling: A theoretical chemist's return to biology. *Annual Review of Biophysics and Biomolecular Structure*, 35(1):1–47, 2006.

[123] A. Kietzmann, R. Redmer, M. P. Desjarlais, and T. R. Mattsson. Complex behavior of fluid lithium under extreme conditions. *Phys. Rev. Lett.*, 101:070401, Aug 2008.

[124] M.-C. Kim, E. Sim, and K. Burke. Understanding and reducing errors in density functional calculations. *Phys. Rev. Lett.*, 111:073003, Aug 2013.

[125] M.-C. Kim, E. Sim, and K. Burke. Ions in solution: Density corrected density functional theory (DC-DFT). *The Journal of Chemical Physics*, 140(18):18A528, 2014.

[126] G. Knizia and G. K.-L. Chan. Density matrix embedding: A simple alternative to dynamical mean-field theory. *Phys. Rev. Lett.*, 109:186404, Nov 2012.

[127] G. Knizia and G. K.-L. Chan. Density matrix embedding: A strong-coupling quantum embedding theory. *arXiv:1212.2679*, 2013.

[128] M. D. Knudson and M. P. Desjarlais. Shock Compression of Quartz to 1.6 TPa: Redefining a Pressure Standard. *Phys. Rev. Lett.*, 103:225501, Nov 2009.

[129] M. D. Knudson, M. P. Desjarlais, R. W. Lemke, T. R. Mattsson, M. French, N. Nettelmann, and R. Redmer. Probing the interiors of the ice giants: Shock compression of water to 700 gpa and 3.8 $\mathbf{g}/\mathrm{cm}^3$. *Phys. Rev. Lett.*, 108:091102, Feb 2012.

[130] W. Koch and M. C. Holthausen. *A Chemist's Guide to Density Functional Theory*. Wiley-VCH, Weinheim, second edition, 2002.

[131] W. Kohn. *Phys. Rev. A*, 34:5419, 1986.

[132] W. Kohn and L. J. Sham. Self-consistent equations including exchange and correlation effects. *Phys. Rev.*, 140(4A):A1133–A1138, Nov 1965.

[133] E. Kraisler and L. Kronik. Piecewise linearity of approximate density functionals revisited: Implications for frontier orbital energies. *Phys. Rev. Lett.*, 110:126403, Mar 2013.

[134] G. Kresse and J. Furthmüller. Efficient iterative schemes for ab initio total-energy calculations using a plane-wave basis set. *Phys. Rev. B*, 54(16):11169–11186, Oct 1996.

[135] G. Kresse and J. Hafner. Ab initio molecular dynamics for liquid metals. *Phys. Rev. B*, 47(1):558–561, Jan 1993.

[136] G. Kresse and J. Hafner. Ab initio molecular-dynamics simulation of the liquid-metal–amorphous-semiconductor transition in germanium. *Phys. Rev. B*, 49(20):14251–14269, May 1994.

[137] J. Krieger, Y. Li, and G. Iafrate. *Phys. Lett. A*, 146:256, 1990.

[138] L. Kronik, T. Stein, S. Refaely-Abramson, and R. Baer. Excitation gaps of finite-sized systems from optimally tuned range-separated hybrid functionals. *Journal of Chemical Theory and Computation*, 8(5):1515–1531, 2012.

[139] S. Kurth and J. P. Perdew. In G. J. Kalman, J. M. Rommel, and K. Blagoev, editors, *Strongly Coupled Coulomb Systems*. Plenum Press, New York, NY, 1998.

[140] S. Kurth and J. P. Perdew. Role of the exchange-correlation energy: Nature's glue. *International Journal of Quantum Chemistry*, 77(5):814–818, 2000.

[141] F. W. Kutzler and G. S. Painter. *Phys. Rev. Lett.*, 59:1285, 1987.

[142] K. Laidig. Density functional methods of the spatial distribution of electronic charge. *Chem. Phys. Lett.*, 225:285, 1994.

[143] D. Langreth and J. Perdew. The exchange-correlation energy of a metallic surface. *Solid State Commun.*, 17:1425, 1975.

[144] P. M. Laufer and J. B. Krieger. Test of density-functional approximations in an exactly soluble model. *Phys. Rev. A*, 33:1480, 1986.

[145] C. Lee, W. Yang, and R. G. Parr. Development of the Colle-Salvetti correlation-energy formula into a functional of the electron density. *Phys. Rev. B*, 37(2):785–789, Jan 1988.

[146] K. Lee, A. K. Kelkkanen, K. Berland, S. Andersson, D. C. Langreth, E. Schröder, B. I. Lundqvist, and P. Hyldgaard. Evaluation of a density functional with account of van der Waals forces using experimental data of H_2 physisorption on Cu(111). *Phys. Rev. B*, 84:193408, Nov 2011.

[147] M. Levitt. The birth of computational structural biology. *Nature Structural Biology*, 8:392–393, 2001.

[148] M. Levy. Universal variational functionals of electron densities, first-order density matrices, and natural spin-orbitals and solution of the v-representability problem. *Proceedings of the National Academy of Sciences of the United States of America*, 76(12):6062–6065, 1979.

[149] M. Levy. Electron densities in search of hamiltonians. *Phys. Rev. A*, 26:1200–1208, Sep 1982.

[150] M. Levy. Excitation energies from density-functional orbital energies. *Phys. Rev. A*, 52:R4313, 1995.

[151] M. Levy and A. Nagy. Variational density functional theory for an individual excited state. *Phys. Rev. Lett.*, 83:4361, 1999.

[152] M. Levy and J. Perdew. Hellmann-feynman, virial, and scaling requisites for the exact universal density functionals. shape of the correlation potential and diamagnetic susceptibility for atoms. *Phys. Rev. A*, 32:2010, 1985.

[153] M. Levy and J. P. Perdew. Tight bound and convexity constraint on the exchange-correlation-energy functional in the low-density limit, and other formal tests of generalized-gradient approximations. *Phys. Rev. B*, 48:11638–11645, Oct 1993. *ibid.* **55**, 13321(E) (1997).

[154] E. Lieb and B. Simon. Thomas-Fermi theory revisited. *Phys. Rev. Lett.*, 31:681, 1973.

[155] E. H. Lieb. Thomas-fermi and related theories of atoms and molecules. *Rev. Mod. Phys.*, 53:603–641, Oct 1981.

[156] E. H. Lieb. Density functionals for coulomb systems. *Int. J. Quantum Chem.*, 24(3):243–277, 1983.

[157] E. H. Lieb and B. Simon. The Thomas-Fermi theory of atoms, molecules and solids. *Advances in Mathematics*, 23(1):22 – 116, 1977.

[158] H. Lin and D. Truhlar. QM/MM: what have we learned, where are we, and where do we go from here? *Theoretical Chemistry Accounts*, 117(2):185–199, 2007.

[159] E. G. L.N. Oliveira and W. Kohn. Density-functional theory for ensembles of fractionally occupied states. ii. application to the helium atom. *Phys. Rev. A*, 37:2821, 1988.

[160] N. T. Maitra, F. Zhang, R. J. Cave, and K. Burke. Double excitations within time-dependent density functional theory linear response. *The Journal of Chemical Physics*, 120(13):5932–5937, 2004.

[161] F. R. Manby, M. Stella, J. D. Goodpaster, and T. F. Miller. A simple, exact density-functional-theory embedding scheme. *Journal of Chemical Theory and Computation*, 8(8):2564–2568, 2012.

[162] M. A. L. Marques, N. T. Maitra, F. M. S. Nogueira, E. K. U. Gross, and A. Rubio, editors. *Fundamentals of Time-Dependent Density Functional Theory*. Number 837 in Lecture Notes in Physics. Springer, Heidelberg, 2012.

[163] D. Marx and J. Hutter. Ab initio molecular dynamics: Theory and implementation. In J. Grotendorst, editor, *Modern Methods and Algorithms of Quantum Chemistry*, volume 1 of *NIC Series*, pages 301–449. J ulich, 2000.

[164] D. Marx and J. Hutter. *Ab Initio Molecular Dynamics: Basic Theory and Advanced Methods*. Cambridge University Press, 2009.

[165] A. E. Mattsson and R. Armiento. Implementing and testing the AM05 spin density functional. *Phys. Rev. B*, 79:155101, Apr 2009.

[166] A. E. Mattsson and R. Armiento. The subsystem functional scheme: The Armiento-Mattsson 2005 (AM05) functional and beyond. *International Journal of Quantum Chemistry*, 110(12):2274–2282, 2010.

[167] T. R. Mattsson and M. P. Desjarlais. Phase diagram and electrical conductivity of high energy-density water from density functional theory. *Phys. Rev. Lett.*, 97:017801, Jul 2006.

[168] A. J. Medford, J. Wellendorff, A. Vojvodic, F. Studt, F. Abild-Pedersen, K. W. Jacobsen, T. Bligaard, and J. K. Norskøv. Assessing the reliability of calculated catalytic ammonia synthesis rates. *Science*, 345(6193):197–200, 2014.

[169] N. D. Mermin. Thermal properties of the inhomogenous electron gas. *Phys. Rev.*, 137:A: 1441, 1965.

[170] A. Nagy. *Int. J. Quantum Chem. Symp.*, 29, 1995.

[171] Á. Nagy. Coordinate scaling and adiabatic connection formula for ensembles of fractionally occupied excited states. *International Journal of Quantum Chemistry*, 56(4):225–228, 1995.

[172] Á. Nagy. Excited states in density functional theory. *International Journal of Quantum Chemistry*, 70(4-5):681–691, 1998.

[173] A. Nagy. Kohn-sham equations for multiplets. *Phys. Rev. A*, 57:1672, 1998.

[174] Á. Nagy. An alternative optimized potential method for ensembles of excited states. *Journal of Physics B: Atomic, Molecular and Optical Physics*, 34(12):2363, 2001.

[175] Á. Nagy. Virial theorem in the density functional ensemble theory. *Acta Phys. Chim. Debrecina*, 34-35:99, 2002.

[176] Á. Nagy. Local virial theorem for ensembles of excited states. In S. K. Ghosh and P. K. Chattaraj, editors, *Concepts and Methods in Modern Theoretical Chemistry: Electronic Structure and Reactivity*. CRC Press, 2013.

[177] H. Narnhofer and W. Thirring. Asymptotic exactness of finite temperature thomas-fermi theory. *Annals of Physics*, 134(1):128 – 140, 1981.

[178] R. A. Nistor. Improved strategies for variational calculations for helium. M.Sc. Thesis, University of Windsor, Canada, 2004.

[179] U. S. D. of Energy. Basic research needs for high energy density laboratory physics: Report of the workshop on high energy density laboratory physics research needs. Technical report, Office of Science and National Nuclear Security Administration, 2009.

[180] N. R. C. C. on High Energy Density Plasma Physics Plasma Science Committee. *Frontiers in High Energy Density Physics: The X-Games of Contemporary Science*. The National Academies Press, 2003.

[181] G. Onida, L. Reining, and A. Rubio. Electronic excitations: density-functional versus many-body green's-function approaches. *Rev. Mod. Phys.*, 74(2):601–659, Jun 2002.

[182] A. Otero-de-la Roza, B. H. Cao, I. K. Price, J. E. Hein, and E. R. Johnson. Predicting the relative solubilities of racemic and enantiopure crystals by density-functional theory. *Angewandte Chemie International Edition*, 53(30):7879–7882, 2014.

[183] P. R. T. Schipper, O. V. Gritsenko, and E. J. Baerends. *Theor. Chem. Acc.*, 99:4056, 1998.

[184] P. R. T. Schipper, O. V. Gritsenko, and E. J. Baerends. *J. Chem. Phys.*, 111:4056, 1999.

[185] R. G. Parr and W. Yang. *Density Functional Theory of Atoms and Molecules*. Oxford University Press, 1989.

[186] E. Pastorczak, N. I. Gidopoulos, and K. Pernal. Calculation of electronic excited states of molecules using the Helmholtz free-energy minimum principle. *Phys. Rev. A*, 87:062501, Jun 2013.

[187] E. Pastorczak and K. Pernal. Ensemble density variational methods with self- and ghost-interaction-corrected functionals. *J. Chem. Phys.*, 140:18A514, 2014.

[188] K. Peirs, D. Van Neck, and M. Waroquier. Algorithm to derive exact exchange-correlation potentials from correlated densities in atoms. *Phys. Rev. A*, 67:012505, 2003.

[189] D. Peng, S. N. Steinmann, H. van Aggelen, and W. Yang. Equivalence of particle-particle random phase approximation correlation energy and ladder-coupled-cluster doubles. *The Journal of Chemical Physics*, 139(10), 2013.

[190] J. Perdew. What do the kohn-sham orbital energies mean? how do atoms dissociate? In R. Dreizler and J. da Providencia, editors, *Density Functional Method in Physics, vol. 123 of NATO Advanced Study Institute, Series B: Physics*. Plenum, New York, 1985.

[191] J. Perdew. *What do the Kohn-Sham orbitals mean? How do atoms dissociate?*, page 265. Plenum, NY, 1985.

[192] J. Perdew. Density functional approximation for the correlation energy of the inhomogeneous gas. *Phys. Rev. B*, 33:8822, 1986.

[193] J. Perdew, J. Chevary, S. Vosko, K. Jackson, M. Pederson, D. Singh, and C. Fiolhais. Atoms, molecules, solids, and surfaces - applications of the generalized gradient approximation for exchange and correlation (vol 46, pg 6671, 1992). *Physical Review B*, 48(7):4978, Aug 15 1993.

[194] J. P. Perdew, K. Burke, and M. Ernzerhof. Generalized gradient approximation made simple. *Phys. Rev. Lett.*, 77(18):3865–3868, Oct 1996. *ibid.* **78**, 1396(E) (1997).

[195] J. P. Perdew and S. Kurth. *Density Functionals for Non-relativistic Coulomb Systems in the New Century*, pages 1–55. Springer, Berlin / Heidelberg, 2003.

[196] J. P. Perdew, A. Ruzsinszky, L. A. Constantin, J. Sun, and G. I. Csonka. Some fundamental issues in ground-state density functional theory: A guide for the perplexed. *Journal Of Chemical Theory and Computation*, 5(4):902–908, Apr 2009.

[197] J. P. Perdew and K. Schmidt. In V. E. V. Doren, K. V. Alsenoy, and P. Geerlings, editors, *Density Functional Theory and Its Applications to Materials*. American Institute of Physics, Melville, NY, 2001.

[198] J. P. Perdew and Y. Wang. Accurate and simple analytic representation of the electron-gas correlation energy. *Phys. Rev. B*, 45(23):13244–13249, Jun 1992.

[199] F. Perrot. Gradient correction to the statistical electronic free energy at nonzero temperatures: Application to equation-of-state calculations. *Phys. Rev. A*, 20:586–594, Aug 1979.

[200] F. Perrot and M. W. C. Dharma-wardana. Exchange and correlation potentials for electron-ion systems at finite temperatures. *Phys. Rev. A*, 30:2619–2626, Nov 1984.

[201] F. Perrot and M. W. C. Dharma-wardana. Spin-polarized electron liquid at arbitrary temperatures: Exchange-correlation energies, electron-distribution functions, and the static response functions. *Phys. Rev. B*, 62(24):16536–16548, Dec 2000.

[202] S. Pittalis, C. R. Proetto, A. Floris, A. Sanna, C. Bersier, K. Burke, and E. K. U. Gross. Exact conditions in finite-temperature density-functional theory. *Phys. Rev. Lett.*, 107:163001, Oct 2011.

[203] K.-U. Plagemann, P. Sperling, R. Thiele, M. P. Desjarlais, C. Fortmann, T. Döppner, H. J. Lee, S. H. Glenzer, and R. Redmer. Dynamic structure factor in warm dense beryllium. *New Journal of Physics*, 14(5):055020, 2012.

[204] A. Pribram-Jones, S. Pittalis, and K. Burke. In preparation.

[205] A. Pribram-Jones, S. Pittalis, and K. Burke. In preparation.

[206] A. Pribram-Jones, S. Pittalis, E. Gross, and K. Burke. Thermal density functional theory in context. In F. Graziani, M. P. Desjarlais, R. Redmer, and S. B. Trickey, editors, *Frontiers and Challenges in Warm Dense Matter*, volume 96 of *Lecture Notes in Computational Science and Engineering*, pages 25–60. Springer International Publishing, 2014.

[207] A. Pribram-Jones, Z.-H. Yang, J. R. Trail, K. Burke, R. J. Needs, and C. A. Ullrich. Excitations and benchmark ensemble density functional theory for two electrons. *J. Chem. Phys.*, 140:18A541, 2014.

[208] D. Rappoport, N. R. M. Crawford, F. Furche, and K. Burke. Which functional should I choose? In E. Solomon, R. King, and R. Scott, editors, *Computational Inorganic and Bioinorganic Chemistry*. Wiley, John & Sons, Inc., 2009.

[209] M. Reed and B. Simon. *I: Functional Analysis (Methods of Modern Mathematical Physics)*. Academic Press, 1981.

[210] S. Refaely-Abramson, S. Sharifzadeh, M. Jain, R. Baer, J. B. Neaton, and L. Kronik. Gap renormalization of molecular crystals from density-functional theory. *Phys. Rev. B*, 88:081204, Aug 2013.

[211] J. Roccia and M. Brack. Closed-orbit theory of spatial density oscillations in finite fermion systems. *Phys. Rev. Lett.*, 100:200408, May 2008.

[212] J. Roccia, M. Brack, and A. Koch. Semiclassical theory for spatial density oscillations in fermionic systems. *Phys. Rev. E*, 81:011118, Jan 2010.

[213] S. Root, R. J. Magyar, J. H. Carpenter, D. L. Hanson, and T. R. Mattsson. Shock Compression of a Fifth Period Element: Liquid Xenon to 840 GPa. *Phys. Rev. Lett.*, 105(8):085501, Aug 2010.

[214] E. Runge and E. K. U. Gross. Density-functional theory for time-dependent systems. *Phys. Rev. Lett.*, 52(12):997, Mar 1984.

[215] S. G. Wang and W. H. E. Scharz. *J. Chem. Phys.*, 105:4641, 1996.

[216] S. V. Valone. *J. Chem. Phys.*, 73:1344, 1980.

[217] J. J. Sakurai. *Modern Quantum Mechanics (Revised Edition)*. Addison Wesley, 1993.

[218] K. Y. Sanbonmatsu, L. E. Thode, H. X. Vu, and M. S. Murillo. Comparison of molecular dynamics and particle-in-cell simulations for strongly coupled plasmas. *J. Phys. IV France*, 10(PR5):Pr5–259–Pr5–262, 2000.

[219] E. Schrödinger. An undulatory theory of the mechanics of atoms and molecules. *Phys. Rev.*, 28:1049–1070, Dec 1926.

[220] G. Schusteritsch and E. Kaxiras. Sulfur-induced embrittlement of nickel: a first-principles study. *Modeling and Simulation in Materials Science and Engineering*, 20:065007, 2012.

[221] F. Schwabl. *Quantum Mechanics*. Springer-Verlag, 2007.

[222] J. Schwinger. Thomas-Fermi model: The second correction. *Phys. Rev. A*, 24(5):2353–2361, Nov 1981.

[223] R. Sharp and G. Horton. A variational approach to the unipotential many-electron problem. *Phys. Rev.*, 90:317, 1953.

[224] C. D. Sherrill. Frontiers in electronic structure theory. *The Journal of Chemical Physics*, 132(11):110902, 2010.

[225] R. Singh and B. M. Deb. Developments in excited-state density functional theory. *Phys. Rep.*, 311:47, 1999.

[226] T. Sjostrom and J. Daligault. Nonlocal orbital-free noninteracting free-energy functional for warm dense matter. *Phys. Rev. B*, 88:195103, Nov 2013.

[227] J. C. Slater. A Simplification of the Hartree-Fock Method. *Phys. Rev.*, 81:385–390, Feb 1951.

[228] J. C. Snyder, M. Rupp, K. Hansen, L. Blooston, K.-R. Mller, and K. Burke. Orbital-free bond breaking via machine learning. *The Journal of Chemical Physics*, 139(22), 2013.

[229] J. C. Snyder, M. Rupp, K. Hansen, K.-R. Mueller, and K. Burke. Finding density functionals with machine learning. *Phys. Rev. Lett.*, 108:253002, 2012.

[230] J. M. Soler, E. Artacho, J. D. Gale, A. García, J. Junquera, P. Ordejón, and D. Sánchez-Portal. The SIESTA method for ab initio order-N materials simulation. *Journal of Physics: Condensed Matter*, 14(11):2745, 2002.

[231] J. Sun, R. Haunschild, B. Xiao, I. W. Bulik, G. E. Scuseria, and J. P. Perdew. Semilocal and hybrid meta-generalized gradient approximations based on the understanding of the kinetic-energy-density dependence. *The Journal of Chemical Physics*, 138(4), 2013.

[232] J. Talman and W. Shadwick. Optimized effective atomic central potential. *Phys. Rev. A*, 14:36, 1976.

[233] R. Tang, J. Nafziger, and A. Wasserman. Fragment occupations in partition density functional theory. *Phys. Chem. Chem. Phys.*, 14:7780–7786, 2012.

[234] J. Tao, J. P. Perdew, V. N. Staroverov, and G. E. Scuseria. Climbing the density functional ladder: Nonempirical meta–generalized gradient approximation designed for molecules and solids. *Phys. Rev. Lett.*, 91(14):146401, Sep 2003.

[235] F. Tasnádi and Á. Nagy. An approximation to the ensemble Kohn-Sham exchange potential for excited states of atoms. *The Journal of Chemical Physics*, 119(8):4141–4147, 2003.

[236] F. Tasnádi and Á. Nagy. Ghost- and self-interaction-free ensemble calculations with local exchange-correlation potential for atoms. *Journal of Physics B: Atomic, Molecular and Optical Physics*, 36(20):4073, 2003.

[237] E. Teller. On the stability of molecules in the Thomas-Fermi theory. *Rev. Mod. Phys.*, 34(4):627–631, Oct 1962.

[238] A. Theophilou. The energy density functional formalism for excited states. *J. Phys. C*, 12:5419, 1979.

[239] A. K. Theophilou. In N. H. March and B. M. Deb, editors, *The Single-Particle Density in Physics and Chemistry*. Academic press, London, 1987.

[240] L. H. Thomas. The calculation of atomic fields. *Math. Proc. Camb. Phil. Soc.*, 23(05):542–548, 1927.

[241] A. Tkatchenko and M. Scheffler. Accurate Molecular Van Der Waals Interactions from Ground-State Electron Density and Free-Atom reference data. *Phys. Rev. Lett.*, 102:073005, Feb 2009.

[242] D. Tozer. Relationship between long-range charge-transfer excitation energy error and integer discontinuity in kohn-sham theory. *J. Chem. Phys.*, 119:12697, 2003.

[243] C. A. Ullrich. *Time-Dependent Density-Functional Theory*. Oxford University Press, Oxford, 2012.

[244] C. A. Ullrich and W. Kohn. Kohn-sham theory for ground-state ensembles. *Phys. Rev. Lett.*, 87:093001, Aug 2001.

[245] C. A. Ullrich and Z.-H. Yang. A brief compendium of time-dependent density-functional theory. *Brazilian J. Phys.*, 44:154, 2014.

[246] C. J. Umrigar and X. Gonze. Accurate exchange-correlation potentials and total-energy components for the helium isoelectronic series. *Phys. Rev. A*, 50(5):3827–3837, Nov 1994.

[247] H. van Aggelen, Y. Yang, and W. Yang. Exchange-correlation energy from pairing matrix fluctuation and the particle-particle random phase approximation. *The Journal of Chemical Physics*, 140(18), 2014.

[248] R. van Leeuwen. Density functional approach to the many-body problem: Key concepts and exact functionals. volume 43 of *Advances in Quantum Chemistry*, pages 25 – 94. Academic Press, 2003.

[249] W. Kohn. In F. Bassani, F. Fumi, and M. P. Tosi, editors, *Highlight of Condensed Matter Theory*, page 1, Amsterdam, 1985. North-Holland.

[250] Y. A. Wang and E. A. Carter. Orbital-free kinetic-energy density functional theory. In S. D. Schwartz, editor, *Theoretical Methods in Condensed Phase Chemistry*, chapter 5, page 117. Kluwer, Dordrecht, 2000.

[251] A. Warshel and M. Levitt. Theoretical studies of enzymic reactions: Dielectric, electrostatic and steric stabilization of the carbonium ion in the reaction of lysozyme. *Journal of Molecular Biology*, 103(2):227 – 249, 1976.

[252] S. R. White. Density matrix formulation for quantum renormalization groups. *Phys. Rev. Lett.*, 69(19):2863–2866, Nov 1992.

[253] S. R. White. Density-matrix algorithms for quantum renormalization groups. *Phys. Rev. B*, 48:10345–10356, Oct 1993.

[254] S. D. Wong, M. Srnec, M. L. Matthews, L. V. Liu, Y. Kwak, K. Park, C. B. Bell III, E. E. Alp, J. Zhao, Y. Yoda, S. Kitao, M. Seto, C. Krebs, J. M. Bollinger, and E. I. Solomon. Elucidation of the Fe(iv)=O intermediate in the catalytic cycle of the halogenase SyrB2. *Nature*, 499(7458):320–323, 07 2013.

[255] W. Yang. Ab initio approach for many-electron systems without invoking orbitals: An integral formulation of density-functional theory. *Phys. Rev. A*, 38(11):5494–5503, Dec 1988.

[256] W. Yang. Thermal properties of many-electron systems: An integral formulation of density-functional theory. *Phys. Rev. A*, 38:5504, 1988.

[257] Z.-H. Yang, J. R. Trail, A. Pribram-Jones, K. Burke, R. J. Needs, and C. A. Ullrich. Exact and approximate Kohn-Sham potentials in ensemble density-functional theory. *Phys. Rev. A*, 90:042501, 2014.

[258] A. Zangwill. The education of Walter Kohn and the creation of density functional theory. *Archive for History of Exact Sciences*, pages 1–74, 2014.

[259] G.-X. Zhang, A. Tkatchenko, J. Paier, H. Appel, and M. Scheffler. van der Waals Interactions in Ionic and Semiconductor Solids. *Phys. Rev. Lett.*, 107:245501, Dec 2011.